Modelling and Design of Ultra-Reliable and Low Latency communications for UAV-IoT Networks in 5G and beyond

by

Ali Nawaz RANJHA

MANUSCRIPT-BASED THESIS PRESENTED TO ÉCOLE DE TECHNOLOGIE SUPÉRIEURE IN PARTIAL FULFILLMENT FOR THE DEGREE OF DOCTOR OF PHILOSOPHY
Ph.D.

MONTREAL, NOVEMBER 8, 2021

ÉCOLE DE TECHNOLOGIE SUPÉRIEURE
UNIVERSITÉ DU QUÉBEC

BOARD OF EXAMINERS

THIS THESIS HAS BEEN EVALUATED

BY THE FOLLOWING BOARD OF EXAMINERS

M. Georges Kaddoum, Thesis Supervisor
Department of electrical engineering, École de technologie supérieure

M. Kaiwen Zhang, President of the board of examiners
Department of software engineering and IT, École de technologie supérieure

M. Frédéric Nabki, Member of the jury
Department of electrical engineering, École de technologie supérieure

Mme. Gunes Karabulut Kurt, External examiner
Department of electrical engineering, Polytechnique Montréal

THIS THESIS WAS PRESENTED AND DEFENDED

IN THE PRESENCE OF A BOARD OF EXAMINERS AND THE PUBLIC

ON "JANUARY 27, 2022"

AT ÉCOLE DE TECHNOLOGIE SUPÉRIEURE

ACKNOWLEDGEMENTS

Firstly, I would like to express my sincere gratitude to my advisor, Professor Kaddoum for his continuous support and efforts in helping me complete my Ph.D. and this dissertation. None of my scholarly publications made in my Ph.D. would have been possible without his inputs and professional comments. I have considered him my guru during my Ph.D. journey.

Afterwards, I would like to thank my near and dear friends, including Zeeshan, Danish, Hassan, Ahmed, Janet, Bharat, Yi, and Yongfei, for their unwavering support and encouragement. The love and motivation I have given to them have always been reciprocated back to me over the years. I am blessed to have such amazing friends in my life.

Finally, I would like to thank my parents for all the sacrifices they have made for me. I love you, mom and dad; you are the most amazing individuals. Thank you for being there for me when I needed you the most in my life.

Modélisation et conception de communications à faible latence très fiables pour les réseaux UAV-IoT en 5G et au-delà

Ali Nawaz RANJHA

RÉSUMÉ

Les futurs systèmes de communication sans fil 5G vont fournir trois types de services, à savoir le haut débit mobile amélioré (eMBB), les communications massives de type machine (mMTC) et les communications très fiables à faible latence (URLLC). Pour la plupart des applications, le niveau de fiabilité requis est de 99,999 % avec des exigences de latence variables. Atteindre un niveau de fiabilité et de latence sans précédent n'est pas possible dans les systèmes sans fil actuels, à savoir la 4G LTE, et exige que la communauté de recherche et l'industrie s'éloignent de la conception de systèmes de communication conventionnels pour se tourner vers d'autres alternatives. Une de ces alternatives disponibles est la communication assistée par véhicule aérien sans pilote (UAV), qui gagne beaucoup d'attention en raison de son déploiement rapide et favorable. De plus, la maniabilité des drones permet de meilleures performances en ajustant dynamiquement l'état de l'UAV pour mieux répondre aux besoins de la communication. De plus, les hautes altitudes des UAV permettent une communication en ligne direct (LoS), ce qui atténue les effets de blocage du signal. Par conséquent, dans notre recherche, nous visons à concevoir de nouveaux schémas pour réaliser l'URLLC dans les réseaux d'UAV.

À cet égard, le deuxième chapitre de cette thèse présente un modèle de simulation et une analyse détaillée de la distribution des ressources, c'est-à-dire la longueur de bloc et la distance dans un plan bidimensionnel (2-D) pour les systèmes URLLC utilisant des paquets courts communications assistés par des UAVs pour l'Internet des objets (IoT). Des outils issus de la théorie de l'optimisation sont utilisés pour modéliser le problème, où le récepteur est situé à une certaine distance de l'émetteur desservi par un système de relais UAV à sauts multiples. La métrique de performance clé considérée est la probabilité d'erreur de décodage en tant que problème de minimisation soumis aux contraintes de distribution de la longueur de bloc et de la distance entre l'émetteur et le récepteur pour un placement optimal des drones. Les résultats des simulation démontrent l'efficacité du schéma proposé pour de tels scénarios de déploiement.

Le troisième chapitre de cette thèse présente une analyse des performances d'un scénario de communication montante entre plusieurs utilisateurs au sol et une station de base (BS) aérienne sur UAV. L'objectif global est de minimiser la puissance totale de la liaison montante pour activer l'URLLC verte pour les communications IoT avec des paquets courts dans le contexte d'une BS UAV. La nouveauté du problème d'optimisation formulé est qu'il s'adapte à diverses contraintes, y compris la hauteur de l'UAV, la largeur de faisceau de l'UAV, l'emplacement de l'UAV et la distribution de la longueur de bloc sur les liaisons de communication entre les utilisateurs au sol et l'UAV. Au meilleur de nos connaissances, il s'agit du premier cadre d'optimisation qui étudie de manière exhaustive l'URLLC verte pour les communications avec des paquets courts. Par conséquent, le cadre d'optimisation proposé peut nous aider à comprendre les limites de performance de ces réseaux UAV-IoT pour divers scénarios de déploiement pratiques.

Le quatrième chapitre répond à la question: Comment une surface intelligente réfléchissante (RIS) peut-elle activer l'URLLC dans un scénario de communication assistée par UAV? L'optimisation est formulée comme un problème de minimisation de la probabilité d'erreur de décodage, et les contraintes comprennent la position de l'UAV, la distribution de la longueur de bloc et les déphasages pour les éléments RIS. Ici, un algorithme d'optimisation bien connu appelé *Nelder-Mead Simplex* (NMS) de la classe d'algorithmes directs est utilisé. De plus, NMS est choisi pour résoudre le problème car il a démontré des performances supérieures à la méthode dite *Gradient-Descent* en termes de nombre d'itérations requises pour évaluer la fonction objective. De plus, pour le problème donné, NMS a des performances équivalentes à la recherche exhaustive. Par conséquent, dans le chapitre quatre, une nouvelle conception pour la formation de faisceaux passifs, la longueur de bloc et le positionnement d'UAV est proposée.

Le chapitre 5 étudie la quasi-optimisation de la longueur de bloc, la puissance de transmission, l'emplacement, et la largeur de faisceau des systèmes de relais URLLC assistés par UAV avec de multiples robots mobiles. Encore une fois, l'optimisation est formulée comme un problème de minimisation de la probabilité d'erreur de décodage globale du scénario donné. Les utilisateurs ou les robots sont situés à une certaine distance du contrôleur ou de l'émetteur; par conséquent, ils sont desservis par un système de relais UAV décoder et transmettre. (DF). La technique d'optimisation proposée est basée sur la théorie des perturbations et a des performances comparables à la méthode de recherche exhaustive intelligente dans laquelle quelques paramètres sont fixés. De plus, la technique d'optimisation proposée a de meilleures performances que les méthodes à points fixes dans lesquelles une ou plusieurs contraintes sont fixées. Enfin, les résultats de simulation du chapitre 5 démontrent la nécessité d'optimiser conjointement divers paramètres, y compris la longueur de bloc, la localisation des drones, la puissance et la largeur du faisceau, pour faciliter l'URLLC dans de tels systèmes.

De même, le chapitre 6 traite: comment charger un UAV dans les airs à l'aide de faisceaux laser pour faciliter l'URLLC? L'un des problèmes les plus importants concernant les UAV est la capacité limitée de la batterie à bord. Par conséquent, ce chapitre étudie la minimisation de la probabilité d'erreur de décodage pour un scénario de communication IoT soumis à des contraintes de longueur de bloc et de trajectoire d'UAV. Encore une fois, l'algorithme proposé est basé sur la théorie des perturbations. l'UAV termine son vol d'une position initiale à une position finale en récoltant avec succès l'énergie laser. À notre connaissance, il s'agit du premier travail qui étudie et propose une conception quasi-optimale d'allocation des ressources, de planification de trajectoire et de récupération d'énergie pour des scénarios de communication URLLC assistés par UAV.

Enfin, le chapitre 7 étudie un système de multidiffusion activé par UAV à voilure fixe pour fournir des paquets communs de courte longueur de bloc URLLC aux nœuds terrestres (GN) en utilisant un chemin de trajectoire *Snake Traversal*. Pour accomplir cette tâche, nous considérons le protocole de vol et de communication pour l'UAV, où l'UAV balaie une grande zone rectangulaire pour disperser un fichier commun aux GN avec des positions obscures. Dans cette veine, nous étudions les problèmes de minimisation du temps et de l'énergie en présentant une conception quasi-optimale de la vitesse de vol, de l'altitude et de la largeur de faisceau de l'antenne de l'UAV.

Les résultats de simulation du chapitre 7 révèlent l'altitude optimale et la largeur de faisceau à mi-puissance, qui minimisent respectivement le temps de réalisation et la consommation d'énergie. De plus, pour une largeur de faisceau optimisée, la vitesse de l'UAV augmente de manière monotone avec l'altitude, tandis que le temps de réalisation et la consommation d'énergie diminuent de manière monotone avec l'altitude. Nous analysons également les effets de la longueur de bloc et de la probabilité d'erreur de décodage sur la vitesse optimale de l'UAV, le temps d'achèvement et la consommation d'énergie.

Mots-clés: URLLC, UAV multi-sauts, IoT, quasi-optimisation, probabilité d'erreur de décodage, paquets courts, allocation de ressources.

Modelling and Design of Ultra-Reliable and Low Latency communications for UAV-IoT Networks in 5G and beyond

Ali Nawaz RANJHA

ABSTRACT

The upcoming 5G wireless communication systems are going to provide three types of services, namely enhanced Mobile Broadband (eMBB), massive machine type communications (mMTC) and ultra-reliable low latency communication (URLLC). For most applications, the required level of reliability is 99.999% with varying latency requirements. Achieving such an unprecedented level of reliability and latency is not possible in current wireless systems, i.e., 4G LTE and will require the research community and industry to find alternatives to conventional communication system designs. One available alternative is the use of unmanned aerial vehicle (UAV) assisted communication, which is gaining increasing attention due to its fast and favourable deployment. Moreover, the UAVs' maneuverability can increase the system's performance by dynamically adjusting the UAV state to suit the communication needs. Additionally, UAVs' high altitudes enable line of sight (LoS) communication, which mitigates shadowing and signal blockage. Therefore, in our research, we aim to conceive new schemes to achieve URLLC in UAV networks.

In this regard, the second chapter of this thesis presents a simulation model and detailed analysis of the distribution of resources, i.e. blocklength and distance in a two-dimensional (2-D) plane for URLLC-assisted UAV systems for short packet internet of things (IoT) communications. Optimization theory tools are utilized to model the problem, where the receiver is located at a certain distance from the transmitter serviced by a multi-hop UAV relay system. The key performance metric considered is the minimization of the decoding error probability subject to the constraints on the distribution of blocklength and distance between the transmitter and receiver for optimal UAVs placement. Simulation results demonstrate the efficacy of the proposed scheme for such deployment scenarios.

The third chapter of this thesis presents a performance analysis of uplink communication between multiple ground users and a UAV flying base station (BS). The overall goal is to minimize the sum uplink power to enable green URLLC for short packet IoT communications in the context of a UAV BS. The novelty of the formulated optimization problem is that it accommodates various constraints, including the UAV's height, beamwidth, location, and the distribution of the blocklength on the communication links between ground users and the UAV. To the best of our knowledge, it is the first optimization framework that comprehensively studies green URLLC for short packet communications. Hence, the proposed optimization framework contributes to understanding the performance limits of such UAV-IoT networks for diverse practical deployment scenarios. The fourth chapter answers the question: How can a reflective intelligent surface (RIS) enable URLLC in UAV assisted communication scenarios? The optimization is formulated as a decoding error probability minimization problem, and the constraints considered are the UAV's position, the blocklength distribution, and the phase shifts of the RIS elements. Hereof, a well-known optimization algorithm called *Nelder-Mead Simplex* (NMS) from a class of direct

algorithms is employed. Additionally, NMS is chosen to solve the problem as it demonstrated superior performance over the so-called *Gradient-Descent* method by requiring a lower number of iterations to evaluate the objective function. Furthermore, NMS, performance is equivalent to that of exhaustive search for the given problem. Hence, in chapter four, a novel design for passive beamforming, blocklength and UAV positioning is proposed.

Chapter 5 studies the quasi-optimization of the blocklength, transmit power, location and beamwidth of URLLC-assisted UAV relay systems with multiple-mobile robots. Once again, the optimization is formulated as a minimization problem of the given scenario's overall decoding error probability. The users or the robots are located a certain distance away from the controller or the transmitter; hence they are served by a decode-and-forward (DF) UAV relay system. The proposed optimization technique is based on perturbation theory, and has comparable performance to the smart exhaustive search method in which a few parameters are fixed. Moreover, the optimization technique has better performance than fixed points methods in which one or more constraints are fixed. Finally, simulation results from chapter 5 highlight the need to jointly optimize various parameters, including blocklength, power, UAV location, and beamwidth, to facilitate URLLC under such systems.

Similarly, chapter 6 discusses: how to charge UAVs in the air using laser beams to facilitate URLLC? One of the most significant issues pertaining to UAVs is the limited-on board battery capacity. Hence, this chapter studies the minimization of the decoding error probability for an IoT communication scenario subject to blocklength and UAV trajectory constraints. Once again, the proposed algorithm is based on perturbation theory. The UAV completes its flight from an initial position to a final position by successfully harvesting energy from the laser transmitter. To the best of our knowledge, this is the first work that studies and proposes a quasi-optimal design of resource allocation, trajectory planning, and energy harvesting for URLLC assisted UAV communication scenarios.

Lastly, chapter 7 studies a fixed-wing UAV-enabled multicasting system to deliver common short blocklength URLLC packets to the ground nodes (GNs) using a *Snake Traversal* trajectory path. To accomplish this task, we consider the fly-and-communicate protocol for the UAV, where the UAV sweeps a large rectangular area to disperse a common file to GNs with obscure positions. In this vein, we investigate the dual time and energy minimization problems by presenting a quasi-optimal design of the UAV's flying speed, altitude, and antenna beamwidth. Simulation results of chapter 7 reveal the optimal altitude and half-power beamwidth, which minimize the completion time and energy consumption, respectively. Moreover, for optimized beamwidth, the UAV speed monotonically increases with the altitude, whereas both the completion time and energy consumption monotonically decrease with the altitude. We also analyze the effects of the blocklength and decoding error probability on optimal UAV speed, completion time and energy consumption.

Keywords: URLLC, multihop UAV, IoT, quasi-optimization, decoding error probability, short packets, resource allocation.

TABLE OF CONTENTS

Page

LIST OF TABLES

Page

LIST OF FIGURES

Page

LIST OF ALGORITHMS

LIST OF ABBREVIATIONS

1G	First Generation
2G	Second Generation
3G	Third Generation
4G	Fourth Generation
5G	Fifth Generation
3GPP	Third Generation Partnership Project
E2E	End to End
MCS	Modulation and Coding Schemes
IoT	Internet of Things
SMS	Short Message Service
URLLC	Ultra Reliable and Low Latency Communications
PER	Packet Error Rate
MC	Multi Connectivity
mMTC	Massive Machine type Communications
SNR	Signal to Noise Ratio
TDD	Time Division Duplexing
MIMO	Multi Input Multi Output
LTE	Long Term Evolution
NR	New Radio

eMBB	Enhanced Mobile Broadband
BER	Bit Error Rate
SoC	System on Chip
DC	Dual Connectivity
CQI	Channel Quality Indicator
BLER	Block Error Rate
FEC	Forward Error Correction
MN	Master Node
AR	Augmented Reality
VR	Virtual Reality
UAV	Unmanned Air Vehicle
SN	Secondary Node
URC	Ultra Reliable Communications
UE	User Equipment
RAN	Radio Access Network
RTT	Round Trip Time
NFV	Network Function Virtualization
CSI	Channel State Information
TTI	Transmit Time Interval
ICN	Information Centric Networks

RRC	Radio Resource Connection
ML	Machine Learning
AI	Artificial Intelligence
HARQ	Hybrid Automatic Repeat Request
EHARQ	Early Hybrid Automatic Repeat Request
CCQ	Clenshaw Curtis Quadrature
GCQ	Gaussian Chebyshev Quadrature
LOS	Line of Sight
NLOS	Non Line of Sight
PER	Packet Error Rate
BLER	Block Error Rate
QoS	Quality of Service
V2V	Vehicle to Vehicle Communication
AADR	Average Achievable Data Rate

LIST OF SYMBOLS AND UNITS OF MEASUREMENTS

x	Scalar variable
$\mathbb{Z}$	Set of integers
$\mathbf{H}$	Hermitian matrix
Δx	change in scalar variable
T_{x_k}	Set of transmitter nodes referring to IoT devices/users
R_{x}	Receiver node referring to UAV flying base station
$\boldsymbol{y}$	Position of UAV
$\boldsymbol{x_k}$	Position of each IoT devices/users
$\mathbb{R}^2$	Real coordinate space or a plane
Θ	Half-power beamwidth of UAV antenna
θ, ϕ	Azimuth, and elevation angles for UAV antenna gain
$G(\theta, \phi)$	Gain of UAV antenna in direction of (θ, ϕ)
h_k	Channel gain of the k^{th} IoT device/user
$\|\boldsymbol{y} - \boldsymbol{x}_k\|^2$	Euclidean distance between each T_{x_k} and R_{x}
H	Height of UAV
$\bar{r}$	Area covered by UAV antenna
R_k	Data rate of the k^{th} IoT device/user
γ_k	Signal to noise ratio of the k^{th} IoT device/user
V_k	Channel dispersion of the k^{th} IoT device/user

m_k	Blocklength allocated for the k^{th} IoT device/user
P_k	Transmit power of the k^{th} IoT device/user
$Q(x)$	Gaussian Q-function for variable x
$\mathbb{N}$	Set of natural numbers
λ	Lagrange multiplier
$\max\{.\}$	A function to return maximum of an argument
κ_m	Penalty coefficient updated at m^{th} iteration
$\mathbb{R}_+$	Set of positive real numbers
η_n	Step size chosen by Barzilai-Borwein method for **Algorithm 3.1**
`tol`	Tolerance value chosen for **Algorithms**
$\nabla \tilde{f}_1(\boldsymbol{y})$	The gradient of $\tilde{f}_1$ with respect to $\boldsymbol{y}$
$\mathcal{L}(m_k, \lambda)$	Lagrangian function of m_k and λ
$\lfloor . \rfloor$	A function to return floor of an argument
a_0, b_0	The initial points selected for golden section search
σ	Reduction factor for golden section search
ϵ	Accuracy of golden section search
$\mathcal{O}(.)$	Big-O notation to characterize time-complexity
L	Number of iterations of **Algorithm 3.2**
m	Each iteration of **Algorithm 3.1**
Δ_n	n^{th} principal minor of the Hessian matrix

$\mathbf{H}(P_k)$	Hessian matrix of P_k
$\vec{g}$	Vector representing ground transmitter's coordinates
$\vec{a}(t)$	Vector representing UAV's coordinates
$\vec{a}_0(t)$	Vector representing the mean location of UAV
$\vec{r}$	Vector representing RIS coordinates
$\vec{u}$	Vector representing ground user's coordinates
$M_\theta(t)$	Phase shift matrix for RIS
h_0	LoS channel between ground transmitter and UAV
h_2	LoS channel between UAV and RIS array
h_3	LoS channel between RIS array and ground user
$h_{s,1}$	Scattering channel between ground transmitter and ground user
$h_{s,2}$	Scattering channel between UAV and ground user
$d_0(t)$	Euclidean distance between ground transmitter and UAV
s_1	Euclidean distance from ground user to UAV
s_2	Euclidean distance from the ground user to the ground transmitter
$h_2(t,m)$	Channel gain between the UAV and RIS
d_2	Euclidean distance between UAV and RIS
ϕ_2	Cosine of the angle of arrival of the signal from the UAV to RIS
$h_3(t,m)$	Channel gain between RIS and ground user
d_3	Euclidean distance between ground user and RIS

$h_3(m)$	Deterministic LoS component of $h_3(t, m)$
$\tilde{h}_{m,3}(t)$	Non-deterministic LoS component of $h_3(t, m)$
β	Rician fading factor
$h(t)$	Total channel gain from ground transmitter to UAV to RIS to ground user
$\gamma_1(\vec{a})$	SNR of the path from ground transmitter to UAV
$\gamma_2(\vec{a}, \theta_m)$	SNR of the path from UAV to RIS to ground user
θ_m	Phase shift of the m^{th} RIS element
σ^2	Environmental noise variance
ε_t	Total decoding error rate between ground transmitter and ground user
L_{tot}	Total blocklength to be allocated
$\vec{a}_0$	Initial position of UAV
D	Operation region of the UAV around its initial position
$\boldsymbol{q}$	Location of the UAV
$\boldsymbol{w_k}(t)$	Location of the k^{th} robot
Θ	Half-power beamwidth of the UAV antenna
h_{UAV}	Channel gain of the UAV
$h_k(t)$	Channel gain of the k^{th} robot at arbitrary time t
β_0	Channel power gain at a reference distance of $d_0 = 1$ m
M	Overall blocklength allocated for the communication system
$\varepsilon_{UAV}(t)$	Decoding error probability of the UAV at arbitrary time t

$\varepsilon_k(t)$	Decoding error probability of the k^{th} robot at arbitrary time t
$\varepsilon(t)$	Overall decoding error probability from the controller to robots at arbitrary time t
$P_C(t)$	Power allocated for the controller at arbitrary time t
$P_D(t)$	Power allocated for the UAV at arbitrary time t
E_{tot}	Total energy consumption for the communication system
$\|\boldsymbol{q} - \boldsymbol{w}_k(t)\|^2$	Euclidean distance between the UAV and the k^{th} robot
γ_{UAV}	Signal to noise ratio of the UAV
V_{UAV}	Channel dispersion of the UAV
m_{UAV}	Blocklength allocated for the UAV
$\mathbf{H}(C_1)$	**Hessian** matrix of C_1
$\mathbf{H}(Q_{UAV})$	**Hessian** of $Q(f(\gamma_{UAV}))$
Δ_w	Total width of UAV coverage area
A_{b}	User located at the sweep border of the UAV
T	Completion time
P_m	Power consumption of the UAV
E_t	Total energy consumption of the UAV

INTRODUCTION

Motivations

The world today is impacted by continuously evolving technologies that shape human lives. With the emergence of the internet of things (IoT), unmanned aerial vehicles (UAVs), and mission-critical systems, the global demand for data traffic has increased tremendously. The IoT is an emerging technology where machines are embedded with sensors that allow them to relay small data packets to each other with little to no human involvement. Moreover, smartphone adoption is also growing linearly, where smartphones can now be used to control, monitor, and interact with such devices. In this regard, big businesses are also investing a huge capital in the research and development of IoT. A typical example is CISCO, which acquired an IoT company called Jasper for 1.4 billion, and now is branded as CISCO Jasper. Hence, it is evident that emerging technologies, such as IoT and UAVs, have a new set of communication requirements as well as new constraints for the next generation of wireless communication systems, formally known as the fifth generation the fifth-generation (5G) new radio (NR).

The research, development, and deployment of 5G wireless communication systems is presently a very hot topic. First generation (1G) and second generation (2G) systems were voice-centric, whereas third generation (3G) systems combined packet-switched and circuit-switched data and offered voice services. Fourth-generation (4G) systems offered higher throughputs and many significant architectural improvements and expanded the services offered by previous generations of cellular technology. A common point among all these generations is that they were throughput centric. Hence, the main goal of their design was to improve throughput. As for 5G NR, it will drop the traditional human-centric approach from previous generations designed to satisfy capacity and throughput solely. Unlike previous wireless technologies, 5G wireless systems aim to provide a broader and wider range of services, such as enhanced mobile

broadband (eMBB), ultra-reliable and low latency communications (URLLC), and massive machine type communications (mMTC).

The main aim of 5G is the massive connectivity of all the mobile devices, nodes and terminals. There are stringent requirements of reliability and latency in URLLC for 5G systems; as such traditional base stations (BSs) with stationary positions cannot meet these requirements. As a result, UAVs recently emerged as a promising candidate to fulfil these requirements. UAVs have added degrees of freedom and can establish line of sight communication links. Additionally, UAVs can serve as both flying relays and flying BSs in a 5G environment.

Problem Statement

The key service for future 5G systems is URLLC, and its key enabling technology is UAVs. Since the inception of wireless communication systems, a fixed BS has been utilized for both uplink and downlink communications. The basic idea of using UAVs to facilitate communications challenges the optimality of employing fixed BS in the context of URLLC. Hence, it is worth investigating UAVs acting as relays and flying BSs for future UAV-IoT networks. Moreover, as mentioned earlier, URLLC systems utilize short packets to reduce latency. Such short length packets adversely affect the channel gain and do not obey the Shannonian capacity formula based on the so-called *Strong law of large numbers*. Therefore, the idea of utilizing UAVs to facilitate URLLC has recently came to the limelight. Presently, only a few works in the literature discuss URLLC-enabled UAV communications, as outlined in (She, Liu, Quek, Yang & Li, 2019; Ren, Pan, Wang, Deng, Elkashlan & Nallanathan; Pan, Ren, Deng, Elkashlan & Nallanathan, 2019; Ren, Pan, Wang, Xu, Elkashlan & Nallanathan, 2020c). In the seminal work in (She *et al.*, 2019), authors study a framework to facilitate URLLC in control and non-payload communication (CNPC) links of the UAVs. The authors, aim to exploit the macro-diversity gain of multi-antenna systems by considering three distinct scenarios, namely distributed multi-antenna systems (DAS), centralized multi-antenna systems (CAS), and a modified DAS (M-DAS). Moreover, the authors

jointly optimize the antenna configuration, altitude of UAVs, and the duration of uplink and downlink phases with a goal to maximize the available range. The range is the maximum horizontal communication distance within which the round-trip delay and the overall packet loss probability can be ensured with a required probability. The problem of the average achievable data rate (AADR) for URLLC-enabled UAV systems is studied in (Ren *et al.*). The authors use the so-called *Gaussian-Chebyshev quadrature* method to derive an expression of achievable data rate in a system considering short packet delivery from a ground station to a UAV. Their approach supposedly provides insights about packet design in such communication systems. In (Pan *et al.*, 2019), the authors study the problem of joint blocklength allocation and UAV location to enable ultra-high reliability in single-hop UAV relay systems. In (Ren *et al.*, 2020c), the authors study URLLC enabled by a UAV serving as an amplify-and-forward (AF) relay. The authors propose low complexity algorithms to jointly optimize the UAV placement and power in a three-dimensional (3-D) channel to guarantee a minimum decoding error probability.

Research Objectives

In this thesis, we focus on (i) the development of an optimization framework to study resource allocation including blocklength, distance, and transmit power as well as UAV height and beamwidth in URLLC-enabled UAV systems, (ii) the study of uplink power optimization and energy efficiency in URLLC-enabled UAV systems, (iii) the study of passive beamforming and UAV positioning in three-dimensional (3D) space for hybrid URLLC-enabled UAV supported RIS systems, and (iv) the development of a mechanism to support *over-the-air* charging of URLLC-enabled UAV systems using a laser transmitter.

To accomplish these goals, we choose a reference channel model, namely the free space model. We aim to optimize the resource allocation for randomly distributed user(s) across a circular disk where a UAV is serving as a flying base station (BS). After that, we formulate an energy-efficient maximization problem, where we further consider power control, active user(s), blocklength

allocation, UAV's location including its height, and UAV's beamwidth as constraints in our problem. The decoding error probability is also an important design parameter to solve these problems. Afterwards, we try to find the globally optimal solution for our resource allocation problem, where our QoS constraints are non-convex due to the maximal achievable data rate in the short blocklength regime. We also derive a simplified expression for the short blocklength data rate in the considered UAV assisted URLLC scenario to reduce the complexity of our problem. Lastly, we achieve energy-efficient resource allocation, by optimizing the blocklength, distance and transmit power, UAV positioning, and *over-the-air* charging in such URLLC assisted UAV systems.

Contributions and Outline

For convenience, the big picture of this thesis is shown using a Venn diagram in Fig. 0.1.

Chapter 1 presents the background and comprehensive literature review of 5G and its services. More specifically, it highlights the URLLC goals, targets, and use cases. It also discusses the two aspects of URLLC, including latency and reliability. Afterwards, it presents the enablers of low latency and high reliability and discusses the underlying trade-offs in URLLC systems. A detailed discussion on UAV communications and URLLC-enabled UAV communications is presented, and the recent related works in this field are presented. Moreover, research gaps are identified; to fill in the research gaps, each of the following five chapters discusses a novel framework in URLLC assisted UAV communications.

Chapter 2 presents an optimization framework for achieving ultra-high reliability for short packets in future wireless communication systems, as current systems are designed only to transmit long packets based on classical information-theoretic principles. This chapter relies on multi-hop UAV relay links to deliver short URLLC instruction packets between ground IoT devices to tackle this challenge. To accomplish this task, we perform non-linear optimization to minimize the overall decoding error probability by finding the optimal values of the distance and

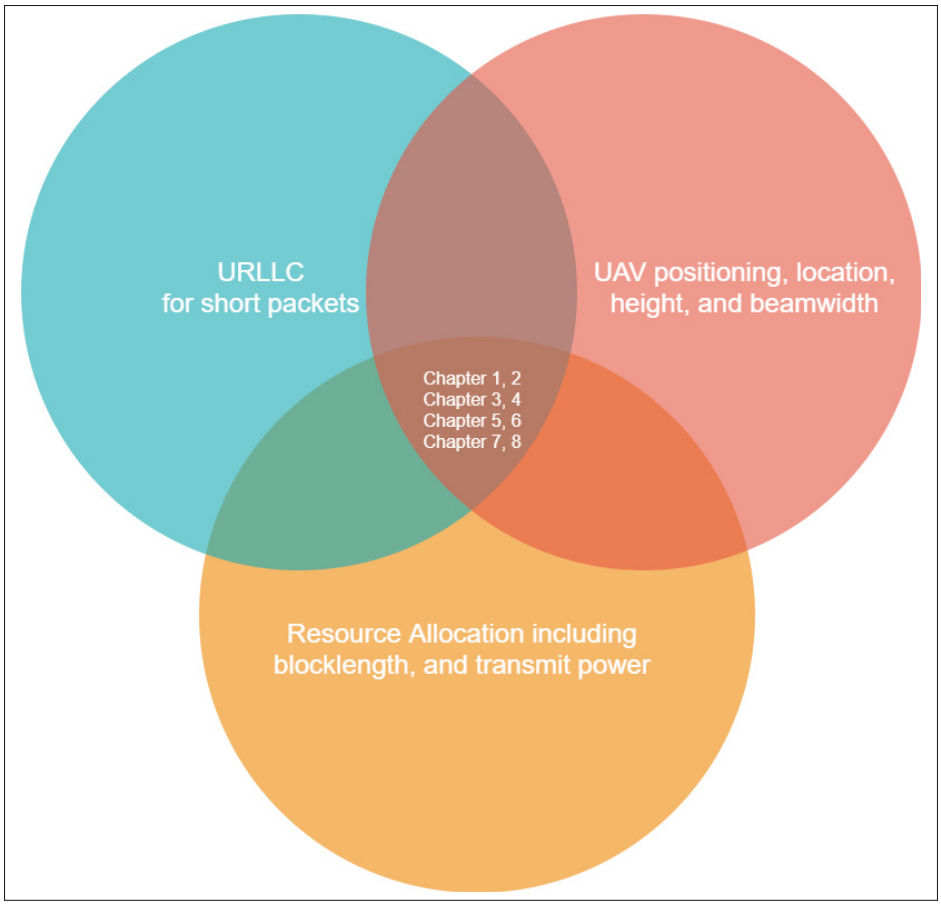

Figure 0.1 Paradigm of the thesis contributions using Venn diagram

the blocklength. In this vein, a novel, semi-empirical non-iterative algorithm is proposed to solve the quasi-optimization problem. The algorithm executes in quasilinear time and converges to a globally optimal/sub-optimal solution based on the chosen parameters. This chapter's simulation results demonstrate that our algorithm allows operation under the ultra-reliable regime (URR) and yields the same performance as the exhaustive search algorithms. It is worth mentioning that Chapter 2 only considers UAV-assisted URLLC for a single ground user. The more general multi-user scenario is presented in Chapter 3.

Chapter 3 discusses an efficient resource allocation to maximize the power efficiency, which is an important performance metric in future 5G communications. The minimization of the

sum uplink power to enable green communications while concurrently fulfilling the strict demands of ultra-reliability for short packets is an essential and central challenge that needs to be addressed in designing 5G wireless communication systems. To address this challenge, this chapter analyzes the joint optimization of various UAV systems parameters, including the UAV's position, height, beamwidth, and the resource allocation for uplink communications between ground IoT devices and a UAV employing short, URLLC data packets. Towards achieving the aforesaid task, we propose a perturbation-based iterative optimization to minimize the sum uplink power to determine the optimal position for the UAV, its height, beamwidth of its antenna, and the blocklength allocated for each IoT device. It is shown that the proposed algorithm has lower time complexity, yields a better performance than other benchmark algorithms, and achieves a similar performance to exhaustive search. Moreover, the results also demonstrate that Shannon's formula is not an optimum choice for modelling sum power for short packets. This is due to the fact that it can significantly underestimate the sum power, where our calculations show that there is an average difference of 47.51% for the given parameters between our proposed approach and Shannon's formula. Lastly, this chapter's simulation results confirm that the proposed algorithm allows ultra-high reliability for all the users and converges rapidly. Chapter 3 introduces an important metric called sum power saving for evaluating the system-level performance of 5G systems. However, the discussion lacks the usage of emergent technology such as reconfigurable intelligent surfaces (RIS), which could provide favourable channel gains to UAV-assisted URLLC systems. In this regard, Chapter 4 discusses URLLC facilitated by hybrid UAV-RIS systems.

Chapter 4 relies on a UAV and a RIS to deliver short URLLC instruction packets between ground Internet of Things (IoT) devices. In this context, we perform passive beamforming of RIS antenna elements as well as non-linear and non-convex optimization to minimize the total decoding error rate and find the UAV's optimal position and blocklength. In this chapter, a novel, polytope-based method from the class of direct search methods (DSM) named *Nelder-Mead Simplex* (NMS) is used to solve the optimization problem. The proposed approach yields better

convergence performance than the traditional gradient descent optimization algorithm and a lower computation time and equivalent performance for the blocklength variable as the exhaustive search. Moreover, the proposed approach allows ultra-high reliability, which can be attained by increasing the number of antenna elements in RIS and increasing the allocated blocklengths. This chapter's simulations demonstrate the RIS's performance gain and conclusively show that the UAV's position is crucial for achieving ultra-high reliability in short packet transmission. Although Chapter 4 invokes RIS in the context of URLLC facilitated by a UAV relay, it does not cater to the mobility of the ground users. Thus, a more robust resource allocation design for enabling URLLC in UAV systems with mobility considerations is discussed in Chapter 5.

Chapter 5 presents the importance of URLLC as an essential service to empower real-time wireless systems, smart grids, and intelligent transport systems. In this context, this paper considers a UAV acting as a decode-and-forward (DF) relay to communicate short URLLC control packets between a controller and multiple-mobile robots in a cell. Moreover, this paper employs perturbation theory and studies the quasi-optimization of the UAV's location, height, beamwidth, and resource allocation, including time-varying power and blocklength for the two phases of transmission from the controller to the UAV and from the UAV to the robots. In this regard, we propose an iterative optimization method to find the optimal UAV height, UAV location, antenna beamwidth, and the variable power and blocklength allocated to each robot inside the circular cell to minimize the average overall decoding error. It is demonstrated that the proposed algorithm provides a better performance than other benchmark algorithms based on fixed parameters and yields an almost equivalent performance to that of the smart exhaustive search. Lastly, this chapter's simulation results emphasize the need to jointly optimize all of the above-mentioned UAV's system parameters and resource allocation for the two phases of transmission to achieve ultra-reliable communication (URC) for multiple-mobile robots. Even though Chapter 5 discusses URLLC in UAV systems with multiple-mobile robots, it does not examine UAVs' limited operational duration in an area to provide communications. Therefore,

to tackle this challenge, Chapter 6 introduces a laser transmitter to charge UAV in the air to avoid communication disruptions.

Chapter 6 discusses a URLLC scenario involving infrastructure-less UAV-assisted communications. Moreover, one of the most significant issues of UAV is the limited battery capacity of these devices. To resolve these issues, we consider URLLC-enabled *over-the-air* charging of UAV relay system using a laser transmitter. Furthermore, we formulate a non-convex optimization problem to minimize the total decoding error rate subject to optimal resource allocation, including blocklength allocation, power control, trajectory planning, and energy harvesting to facilitate URLLC in such systems. In this regard, given its lower complexity, a novel perturbation-based iterative method is proposed to solve the optimization problem. The proposed method yields optimal blocklength allocation and power control for the two transmission phases, i.e., from the source node to the UAV and from the UAV to the robot acting as a ground station. It also maps the UAV trajectory from the initial position to the final position, and the UAV completes the flight using the laser's harvested energy. It is shown that the proposed algorithm and fixed baseline scheme, named fixed blocklength (FB), yield a similar performance as the exhaustive search in terms of UAV energy consumption. In contrast, fixed trajectory (FT) delivers the worst performance. Simultaneously, the proposed method yields the best performance in terms of the lowest average overall decoding error compared to fixed baseline schemes, including FB and FT, showing the efficacy of the proposed technique.

Chapter 7 relies on a fixed-wing UAV-enabled multicasting system to deliver common short blocklength ultra-reliable and low-latency (URLLC) packets to the ground nodes (GNs) using a *Snake Traversal* trajectory path. To accomplish this task, we consider the fly-and-communicate protocol for the UAV, where the UAV sweeps a large rectangular area to disperse a common file to GNs with obscure positions. In this vein, we investigate the dual time and energy minimization problems by presenting a quasi-optimal design of the UAV's flying speed, altitude,

and antenna beamwidth. Simulation results of numerical search reveal the optimal altitude and half-power beamwidth, which minimize the completion time and energy consumption, respectively. Moreover, for optimized beamwidth, the UAV speed monotonically increases with the altitude, whereas both the completion time and energy consumption monotonically decrease with the altitude. We also analyze the effects of the blocklength and decoding error probability on optimal UAV speed, completion time and energy consumption. Additionally, simulation results show for the completion time the percentage difference at minimum UAV altitude $h_{\min}$ and maximum UAV altitude $h_{\max}$ is 195.252 %, whereas for the energy consumption the percentage difference at $h_{\min}$ and $h_{\max}$ is 196.912 %. Similarly, for the completion time the percentage difference at minimum UAV antenna beamwidth $\theta_{\min}$ and maximum UAV antenna beamwidth $\theta_{\max}$ is 181.586 %, whereas for the energy consumption the percentage difference at $\theta_{\min}$ and $\theta_{\max}$ is 189.269 %. This demonstrates the efficacy of the proposed technique is almost two times in reducing the completion time and the energy consumption effectively between the minimum and the maximum values of the UAV altitude and the UAV antenna beamwidth. Lastly, the results demonstrate that for both the blocklength and decoding error probability, the UAV speed monotonically increases while completion time and energy consumption monotonically decrease.

CHAPTER 1

BACKGROUND AND LITERATURE REVIEW

The rapidly growing demand for IoT systems is moving the world towards the fourth industrial revolution, where all the devices will be talking to each other. Simultaneously, the number of human users at the mobile end terminals will be lower than the number of devices that need to transmit/receive data. The sensors in IoT devices produce small data packets, which contain critical information that needs to be transmitted with low latency and ultra-high reliability. Current wireless communication systems focus on transmitting large packets of data, where both 4G long term evolution (LTE) and wireless fidelity (Wi-Fi) were designed around this requirement. Thus they are not ideal for massive machine type communications (mMTC). Meanwhile, URC does not require high data rates but has strict latency and reliability requirements. According to (Polyanskiy, Poor & Verdú, 2010), the short blocklength capacity or rate is given by

$$\begin{aligned} R_k &\approx \log_2(1+\gamma_k) - \sqrt{\frac{V_k}{m_k}}\frac{Q^{-1}(\varepsilon_k)}{\ln 2}, \\ V_k &= 1-(1+\gamma_k)^{-2}, \\ \gamma_k &= P_k h_k. \end{aligned} \tag{1.1}$$

where $R_k, m_k, \varepsilon_k, P_k, \gamma_k$ and V_k denote the rate, blocklength, decoding error probability, power, signal to noise ratio (SNR), and channel dispersion of the k^{th} user or device, respectively. The short blocklength capacity has additional terms like channel dispersion and inverse Q-function, which result from the short packet size. As the packet size increases, the second term in equation 1.1 disappears, and the equation is reduced to Shannonian capacity. Additionally, stringent latency and reliability requirements cannot be satisfied with fixed position static BS. Therefore, dynamic BSs with an added degree of freedom, such as UAVs, are required. It is worth mentioning here that short packets are utilized for establishing CNPC links for UAVs. Hence, today one of the real challenges for researchers is to evaluate the performance of a wireless systems when short packet communication is considered. Since the norm is to consider long packets bounded by Shannonian capacity for the analysis and simulations of such systems,

this assumption cannot be more wrong; unlike Shannon's capacity, the short blocklength capacity is not bounded by the *Strong law of large numbers*. It is a non-trivial task to retrieve useful information from a small data packet in 5G NR systems. Therefore, the performance analysis of URLLC for short packets in UAV communications with pragmatic assumptions will be the main theme of this research.

1.0.1 5G Overview and services

As discussed above, every generation of wireless networks delivers faster speed and more functionalities than the previous ones. 1G introduced the very first cell phone, while 2G enabled the short message service (SMS), 3G brought users online, whereas 4G introduced high-speed internet and multimedia services. Finally, 5G new NR will drastically change the system design by moving from a throughput centric design to a latency and reliability centric design. Precisely, 5G NR will provide three broad and different service categories, including eMBB, mMTC, and URLLC. The first category is designed for mobile end users that want higher throughputs to, for instance use interactive entertainment services with a very good internet connection. The second category is IoT communication, where thousands of machines are talking to each other. And lastly, we have URLLC, which is going to be beneficial for such systems that are delay intolerant and require high levels of reliability.

1.0.2 URLLC goals and targets

URLLC basically has three goals

1. Maintaining an end to end (E2E) radio latency target of less than 1ms. In practice, 10-12ms is now achievable.
2. Reaching the ultra-high reliability target, which means that the packet error rate (PER)/ block error rate (BLER) or decoding error probability is less than or equal to 10^{-5}.
3. Ensuring zero-mobility interruption.

1.1 URLLC usecases

With the emergence of new technologies, like augmented reality (AR) / virtual reality (VR), autonomous vehicles, e-gaming systems, online and multi-player competitive modes in video games, the demand for ultra-high reliability and low latency has increased. Meanwhile, when the previous generations of wireless communication systems were developed, the major concern was to improve the throughput, while very little attention was drawn on the latency. However, for mission-critical applications, latency is as important as throughput. For instance, as shown in Figure 1.1, autonomous vehicles require a continuous data stream to function properly and guarantee the users' safety. If the latency or delay is high, the situation can be catastrophic for both the self-driving car and the passenger.

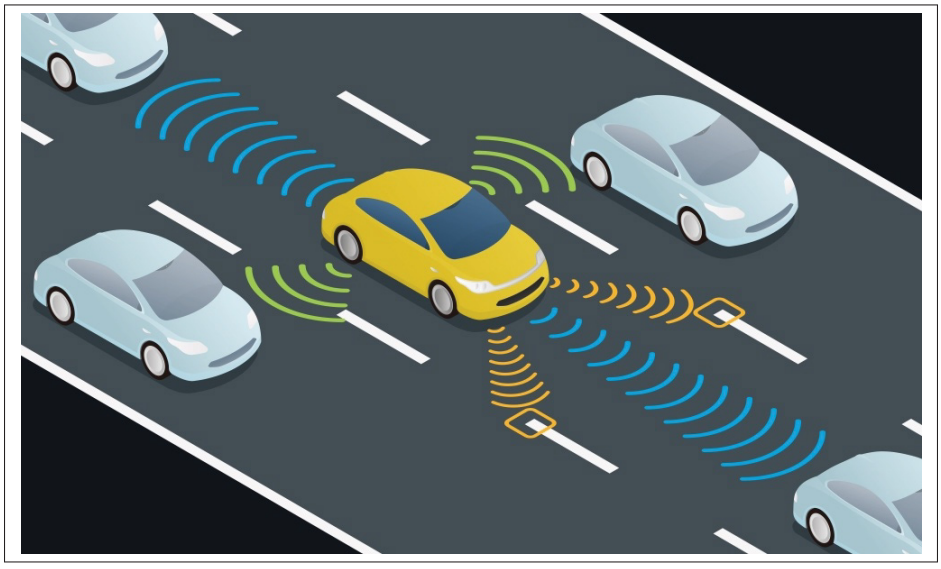

Figure 1.1 Functioning of an autonomous vehicle
Taken from Mimoso (2016)

Moreover, VR includes a haptic virtual environment where single or multiple users perform tasks via a simulation tool while perceiving objects by visuals and by sense of touch. Nowadays, VR is being used by surgeons to virtually train young doctors to perform surgery. This training allows young professionals to handle surgical equipment with more precision and achieve the skills required to operate on real patients. To make their hospital experience more pleasant, VR is also

used by doctors to soothe kids when they get vaccinated (Simsek, Aijaz, Dohler, Sachs & Fettweis, 2016). AR is slightly different from VR since it includes real and computer-generated content in the user field of view (Simsek *et al.*, 2016). In other words, in AR, the computer-generated graphics are superimposed on the real-world environment view via the AR headset. AR also has numerous use cases, for instance, as illustrated in Figure 1.2, unmanned aerial vehicles (UAV) controlled by a person wearing an AR headset are currently being deployed. These provide the user with a bird's eye view of the environment in which the drone is operating or flying while providing information like altitude and speed on the AR headset. Since the user is controlling the drone in real-time, any significant delay could cause the drone to crash. In addition, recently

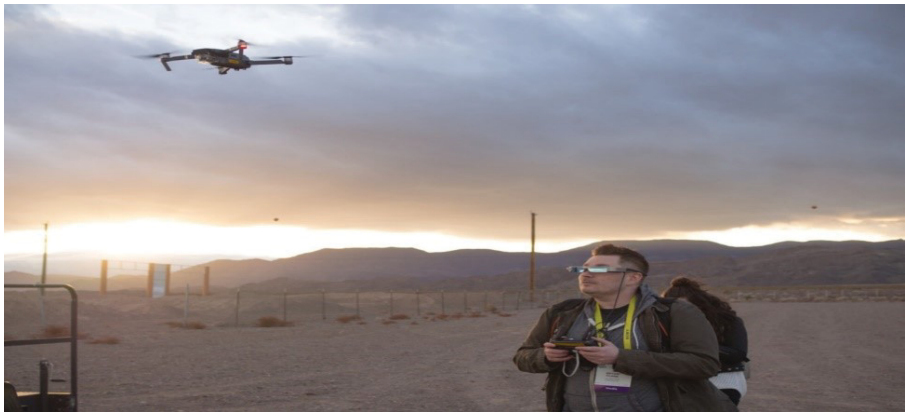

Figure 1.2 Epson UAV being controlled by the user with an AR headset
Taken from Wagner (2018)

e-gaming has evolved as a new kind of sport with games like DOTA and League of Legends where matches are taking place in huge arenas with a price pool of millions of dollars. In the context of e-gaming or online gaming, there is a lag problem which can be defined as the time it takes for the player to send certain commands to his/her character on the screen plus the time it takes for that character to respond to those commands. Such lag occurs due to current network limitations. These all are latency-sensitive applications which cannot afford to have any delay. According to (Wagner, 2018; OrCAD, 2018), the specific latency and reliability targets of these applications are presented in Table 1.1.

Table 1.1 Application specific targets

Application	Latency	Reliability
VR systems	< 20 ms	99.999%
AR systems	<= 5 ms	99.999%
Autonomous vehicles	<= 1 ms	99.999%

1.2 Latency and Reliability

The latency can be defined as the delay between a specific input and its corresponding output. There are two types of latencies in a cellular network: the User Plane Latency and Control Plane Latency. The user plane latency is the time taken by a data packet to reach from the source to the IP layer of its destination. As for the control plane latency, it can be defined as the UE's time to switch from its idle state to an active state. An idle state is a state where no resources are allocated to the UE. As illustrated in Figure 1.3 in an LTE system for one-way transmission of data packets, the latency is given by

$$Latency = T_{Radio} + T_{Backhaul} + T_{Core} + T_{Transport} \tag{1.2}$$

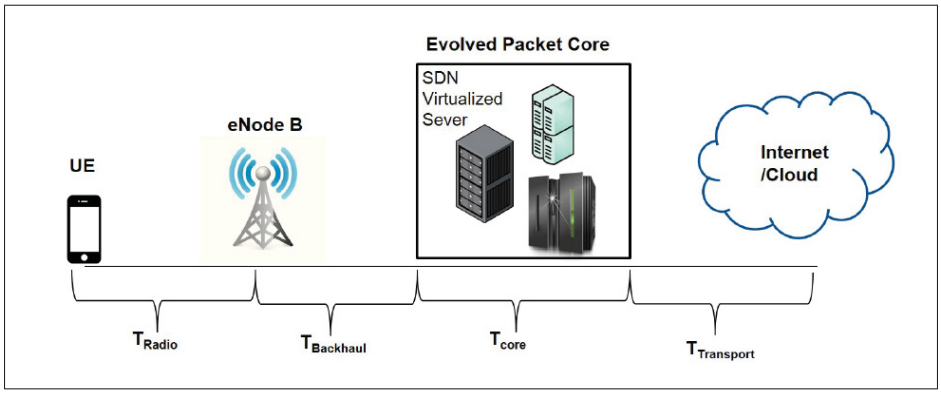

Figure 1.3 Main contributors to latency in an LTE system
Taken from Parvez, Rahmati, Guvenc, Sarwat & Dai (2018)

T_{Radio} denotes the physical layer latency, which is the time delay between the UE and eNode B or BS. $T_{Backhaul}$ is the time taken to build a connection between the BS and the core network

(Parvez *et al.*, 2018). The processing time at the core network is given by T_{Core}. Lastly, the time delay in establishing the connection between the Internet/cloud and the core network is $T_{Transport}$. T_{Radio} and T_{core} contribute significantly to the overall latency.

On the other hand, reliability can be defined as the probability of successfully transmitting a data packet from the source to the destination within a given time frame. Latency and reliability are tightly coupled. In wireless communication theory, the Shannon capacity theorem relates data rate, bandwidth, and SNR, where it dictates that it is possible to achieve a certain level of error free transmission or reliability given enough bandwidth and a certain level of SNR. At the physical layer, reliability can be achieved by link adaption, interference mitigation, diversity schemes, robust transmission of channel state information (CSI) signalling, error control coding, and MIMO, to name a few.

1.2.1 Enablers of low latency

1.2.1.1 Multiplexing URLLC and eMBB traffic

The third generation partnership project (3GPP) has recently standardized URLLC and eMBB multiplexing for downlink (DL) in 5G systems using the framework of superposition or puncturing (Anand, De Veciana & Shakkottai, 2018). As shown in Figure 1.4 in such systems, time is divided into slots, and each slot is divided into mini-slots. Each slot has a proposed duration of 1ms, and each mini-slot has a proposed duration of 0.125ms; therefore, each slot contains eight mini-slots. These time slots are occupied by eMBB traffic since URLLC traffic is sporadic and can arrive at any time, so it is scheduled in mini-slots using either superposition or puncturing (Anand *et al.*, 2018). Superposition refers to when the BS allocates non-zero transmission powers for both eMBB and URLLC traffic. On the other hand, in puncturing, eMBB traffic is given zero transmission power by the BS when URLLC traffic arrives. This is because, in those mini-slots, the eMBB data is not present (Anand *et al.*, 2018). For the uplink (UL) case, RAN1, which is based on the principle of pause and resume, is a popular scheme proposed. In this scheme, URLLC requests are prioritized, and a URLLC UE can take a resource that has already

been allocated to an eMBB user. Prioritization of URLLC traffic can reduce the queuing delay and thus improve latency.

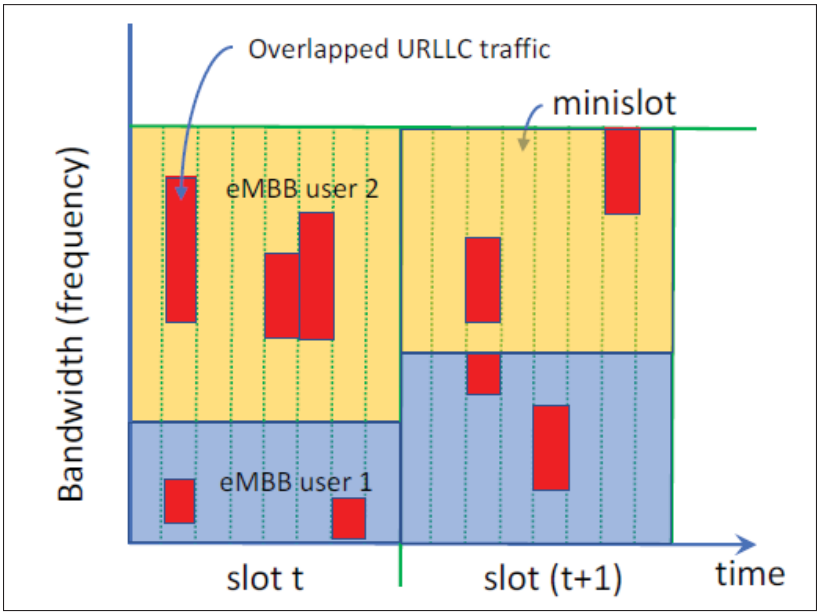

Figure 1.4 A puncturing/superposition approach for multiplexing eMBB and URLLC traffic in a 5G systems
Taken from Anand *et al.* (2018)

1.2.1.2 Shorter TTI and modified frame structure

In the current LTE standard, the frame structure is not flexible. Each resource block, which corresponds to 180 KHz in the frequency domain, i.e., 12 sub-carriers of f 15 KHz each has seven orthogonal frequency-division multiplexing (OFDM) symbols in the time domain. Thus, the time duration of one OFDM symbol is

$$T_{OFDM} = \frac{1}{15\ KHz} = 66.7\mu s \tag{1.3}$$

To reduce the transmit time interval (TTI), since there is an inversely proportional relationship between time and frequency, we can increase Δf. If Δf=60 KHz, we have

$$T_{OFDM} = \frac{1}{60\ KHz} = 16.7\mu\text{s} \tag{1.4}$$

For this reason, 3GPP proposed a very flexible frame structure with configurable carrier spacings that can operate in different frequency bands to shorten the TTI in 5G NR.

1.2.1.3 Network caching and new internet architecture

Future network architectures like information-centric networks (ICN) have a name-based operation, which means that the data packets are moved using their names instead of their location or IP addresses (Awais & Shah, 2017). This enables receiving data driven delivery where the user requests the data from the network, which then comes to him/her from the server or an intermediate cache. Assuming a scenario where two users request the same data at about the same time window, network caching will be useful, and the data would be stored somewhere close to the requester on a certain cache. This can reduce backhaul latency as ICN can function without any communication with the network core.

1.2.1.4 Grant free uplink transmission

Grant free access implies data transmission without the need for requests for any radio resource. Grant-free UL transmission can satisfy low latency requirements because it can avoid delays due to handshake in a radio environment. As illustrated in Figure 1.5, during a handshake process, a radio resource is requested, and then a specific time is required until a UL resource is allocated. Additionally, grant free access can also satisfy the reliability requirements imposed on control channels (Li, Uusitalo, Shariatmadari & Singh, 2018).

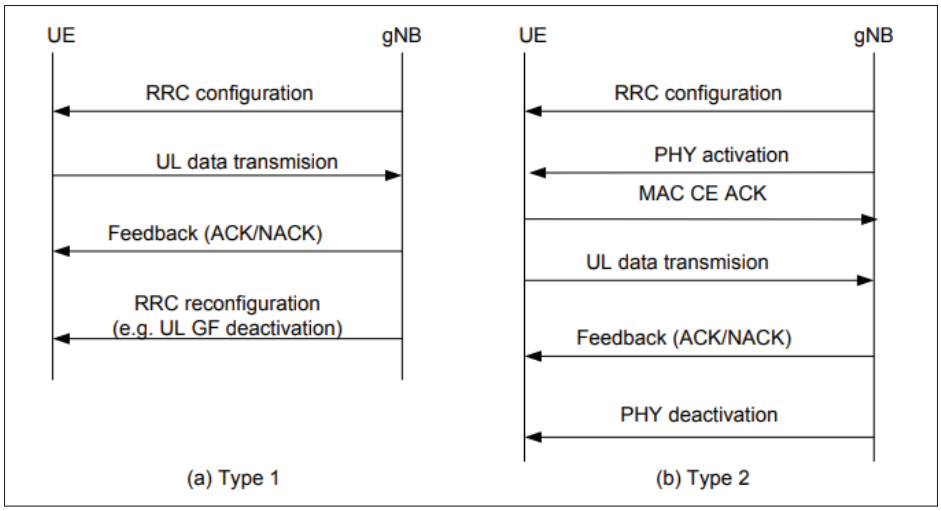

Figure 1.5 Two different types of uplink grantfree transmissions
Taken from Parvez *et al.* (2018)

1.2.1.5 Distributed machine learning at network edge and on device machine learning

In the context of wireless communication systems, a traditional approach for machine learning (ML) radio networks is the case where powerful BS that collects all the data samples performs classification or prediction tasks. Such approaches are not suitable for low latency applications where a more distributed ML framework is required. In such applications, the training data is required to be stored in a distributed fashion across numerous interconnected nodes, including small BSs. Thus the optimization problem should be solved collectively. (Bennis, Debbah & Poor, 2018). Therefore, this approach can help reduce radio latency. One such ML framework is called federated learning.

1.2.2 Enablers of ultra-reliability

1.2.2.1 Dual-connectivity

Upper layer solutions can also be implemented with high-reliability targets. These solutions focus on the layers above the physical layer. One such solution is based on the concept of dual connectivity (DC) in LTE systems. In DC, users can send or receive data from two different

base stations (BSs) simultaneously. In 4G systems, DC improves the throughput by splitting the data. In 5G NR, there is an emerging concept, i.e., multi-connectivity (MC), as illustrated in Figure 1.6. MC is an extension of DC, where DC only focuses on throughput, MC has additional constraints related to the latency and reliability. There are two types of nodes in MC setups, namely master node (MN) and secondary node (SN). The interface between MN and SN is Xn-U. When the MN establishes a radio resource connection (RRC) with a user equipment (UE), it asks the UE to report backchannel measurements and cell information. This helps the MN in selecting a SN with optimal channel measurements. MN requests the SN to allocate resources for the UE. If the SN accepts the allocation request then data from the core network is transmitted to the UE by either MN or SN.

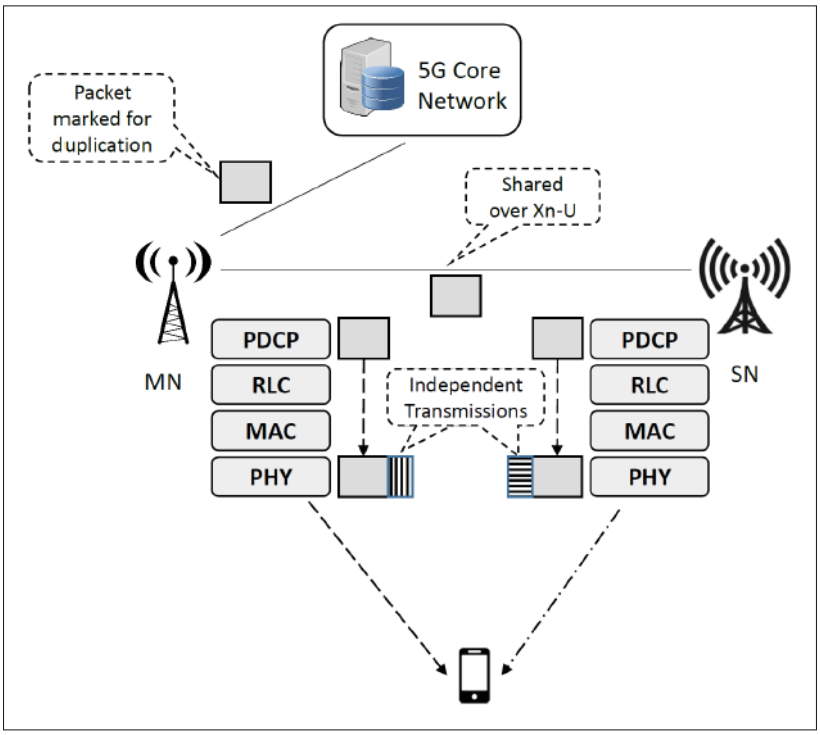

Figure 1.6 Schematic of MC setups in a 5G system
Taken from Mahmood, Lopez, Laselva, Pedersen & Berardinelli (2018)

While the UE is receiving data from two nodes or BSs, the data is split at the packet data convergence protocol (PDCP) layer at the transmitter side, and it is accumulated at the same layer at the receiver side. Additionally, the MN is duplicated and sent to the SN through an

Xn-U connection before being transmitted to the UE through two different radio path links, thus improving the reliability. The improved reliability comes at the cost of reduced spectral efficiency. Hence, this approach has its own limitations (Mahmood *et al.*, 2018).

1.2.2.2 Network slicing

Network slicing is the process of dividing a physical network into several slices. Each slice corresponds to a logical sub-network. Dedicated resources are allocated to each of these sub-networks, which are associated with specific applications, as shown in Figure 1.7. For example, a network slice can be used for high-speed video transmission between a doctor remotely operating on a patient using precision robots, while another slice can be used for ultra-reliable data transmission from sensors or controllers.

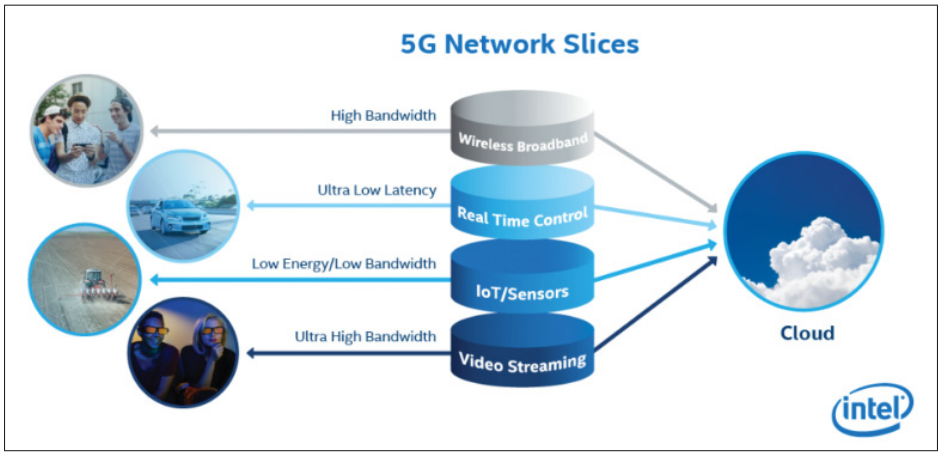

Figure 1.7 Example of how the different slices of 5G networks can be used for different applications
Taken from Chan (2016)

It is challenging to construct a network slice that satisfies the latency requirements of IoT sensors because it is difficult to accurately model and predict queuing delays (Bennis *et al.*, 2018).

1.2.2.3 Micro-diversity

In wireless environments, the time-varying multipath fading is what makes reliable communications difficult. An improvement in the signal to noise ratio (SNR) is required to reduce the bit error rate (BER). Micro-diversity refers to the idea of having multiple antennas at the transmitter side, receiver side or both, in order to provide an SNR improvement. For ultra-reliable applications, a single user with a single stream is preferred. As illustrated in Figure 1.8 URLLC links require MIMO configurations of at least 2x2 antennas. Therefore, transmission schemes that provide an improved diversity for a single user single stream should be adopted (Li *et al.*, 2018).

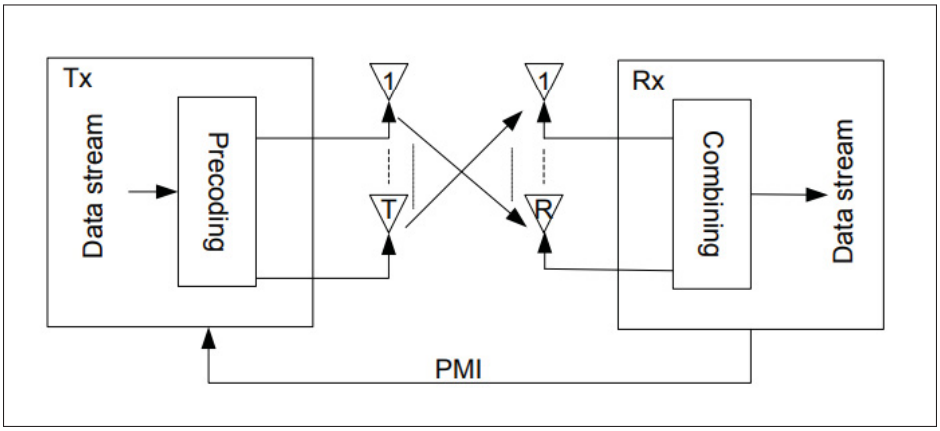

Figure 1.8 Micro diversity example for a single stream transmission
Taken from Li *et al.* (2018)

1.2.2.4 Network coding and relaying

When there is a stringent low latency target, diversity cannot be relied upon in case there is extreme fading. In most cases, the latency target is smaller than the channel coherence time. Thus, time diversity cannot be utilized. Contrarily, the usage of frequency diversity where the carriers are separated by the coherence bandwidth is also obsolete since this approach does not scale to many users. When two diversity schemes cannot be applied, network coding using

simultaneous relaying can enable two-way communications (Bennis *et al.*, 2018). Such a scheme can cater to time constraints, channel dynamics, and can ensure high reliability.

1.2.2.5 Highly reliable control channels

The overall communication system's reliability can be improved if control channels are made more reliable. A UE sends delay budget information to the BS on a control channel. This information includes the channel quality indicator (CQI) report and the remaining latency budget. Afterwards, based on the CQI report, the BS selects the optimal modulation and coding scheme (MCS). If the CQI value is wrongly decoded as a higher value, then the BS will employ a higher MCS, reducing the overall communication system's reliability. Increasing the reliability of control channels can be achieved by employing additional radio resources or reducing the payload of the CQI report (Li *et al.*, 2018). As discussed, the key enablers for latency and reliability are illustrated in Figure 1.9.

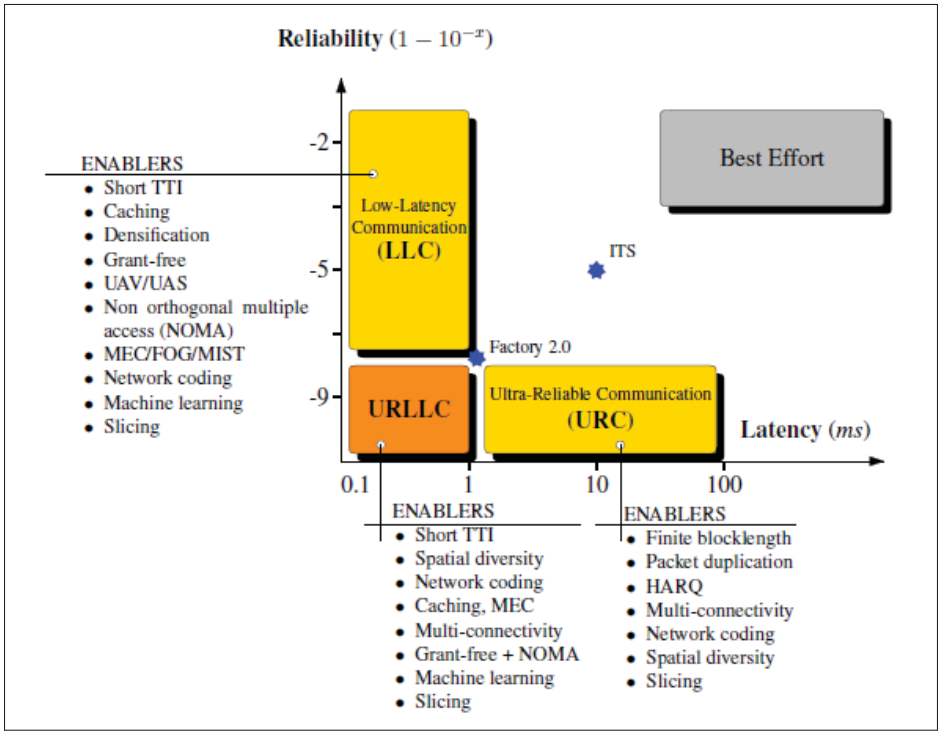

Figure 1.9 Enablers of URLLC
Taken from Bennis *et al.* (2018)

1.3 UNDERLYING TRADE-OFFS IN URLLC

1.3.1 Energy consumption of a device versus latency

In a radio environment, the devices are in active or sleep mode. The active mode is when the devices are transmitting/receiving, while the sleep mode is when no transmission/reception is taking place, and they are saving their battery to prolong the usage time. The devices switch from sleep mode to active mode to check the data packets sent by the network applications. The frequency with which the device receives the data packets determines the latency of those packets. More frequent reception of low latency data packets leads to a higher battery consumption in these devices. This case corresponds to traffic, which is bursty and sporadic.

1.3.2 Transmission energy vs reliability

High reliability requires having several low power transmissions at the physical layer instead of one highly reliable high-power transmission. There is an underlying trade-off between transmission energy and reliability.

1.3.3 Latency versus spectral efficiency

For low latency applications, the spectrum is not utilized efficiently because of shorter TTI and HARQ. Despite instability issues that might arise due to large traffic loads, the slotted ALOHA works well with cellular traffic (Sharma & Wang, 2019). For the UL case in low latency traffic, one-shot slotted ALOHA can be used to send the data packets almost immediately where the delay associated with the resource request and allocation can be avoided (Bennis *et al.*, 2018).

1.3.4 Latency versus reliability

It is well known that reliability in a communication system comes at a latency cost due to the retransmissions involved. HARQ (Hybrid Automatic Repeat Request), a physical layer mechanism based on a feedback mechanism of ACK/ NACK, provides robustness and reliability

in a radio link. HARQ RTT imposes an additional delay, where for 1ms latency (E2E) applications, i.e. URLLC, this mechanism becomes useless and needs to be modified. E-HARQ or early HARQ is an example of a modified HARQ that employs a classification algorithm for feedback and can provide the received signal's decodability ahead of the end of transmission, reducing the overall RTT (Strodthoff, Göktepe, Schierl, Hellge & Samek, 2018).

1.4 Can URLLC be supported by 4G networks?

As evidenced earlier in this chapter, future mobile broadband can no longer rely solely on increasing capacity and throughput. Latency will also play an important role in designing the next generation of wireless communication systems. Traditionally the latency requirements are relaxed to achieve a more reliable connection, where the design of a system that can provide ultra-reliability with low latency is an extremely challenging task. URLLC is one of the key enabling technology of the next generations of mobile broadband, i.e., 5G and beyond.

Table 1.2 Key differences between 4G LTE and 5G NR

Parameters	**4G**	**5G**
Metadata	important	crucial
Packet size	Long (MBB)	Short (URLLC)- Long (eMBB)
Design	Throughput-centric	Latency and reliability centric/ tails MATTER
Reliability	95% or less	$1 - 10^{-x}, x = [3, 4, 5, 6, 8, 9]$
Rate	Shannonian (long packets)	Rate loss due to short packets
Delay violation	Exponential decay	Faster decay than exponential
Latency	15ms RTT	1ms and less, shorter TTI, HARQ RTT
Queue size	unbounded	bounded
Frequency bands	sub-6GHz	Above-and sub-6GHz (URLLC at sub-6GHz)
Scale	A few users/ devices	billion devices

Table 1.2 shows the key differences between 4G LTE systems and 5G NR for different system parameters. As it is evident from Table 1.2, packet size, design, rate, latency/reliability requirements, and queue size, make 4G LTE technology an obsolete choice for supporting URLLC applications (Bennis *et al.*, 2018).

1.5 UAV communications: An overview

UAVs are a rising technology that can be fully exploited for civil, public, and military applications; the world has seen the high profile of advanced UAVs for military purposes, such as Predator and Global hawk (Khan, Heurtefeux, Mohamed, Harras & Hassan, 2017a). The past couple of years have also been vital in bringing UAVs closer to personal drones, such as the Phantom, Mavic and Inspire from DJI, the Solo from 3D Robotics, and the AR and Bebop from Parrot (Gupta, Jain & Vaszkun, 2015). UAVs can provide fast disaster warnings and assist in speeding up search and recovery operations when the public communication network is down. They can also carry medical supplies to inaccessible areas and can save precious lives. Without risking the life of the personnel involved in situations like wildfires, poisonous gas infiltration, and wildlife conservation, UAVs could be used to cover the danger in large areas swiftly. From aerial photography to package delivery; the use cases of consumer UAVs (a.k.a. drones) are booming. UAVs come in all shapes and sizes. Large UAVs can be used individually in missions, while small ones can be used in formations/ swarms. The latter ones are proving to be quite handy in civil applications. Generally, high-altitude platforms (HAPs) consist of large UAVs, balloons, and airships, while low-altitude platforms (LAPs) consists of cooperative small drones (Yan, Fu, Zhang & Wang, 2019).

The technical advances in electronics, artificial intelligence, computing, and sensor technology have broadened the horizon of UAV network applications to include use cases as diverse as traffic monitoring, wind estimation, and remote sensing (Bekmezci, Sahingoz & Temel, 2013). In this context, it is worth mentioning that according to a report by Federal Aviation Administration (FAA), the fleet of drones will be increased from 1.1 million vehicles in 2017 to 2.4 million units by 2022 (Fotouhi, Qiang, Ding, Hassan, Giordano, Garcia-Rodriguez & Yuan, 2019). As control and communications are an essential part of UAV systems, it is expected to bring promising new business opportunities for cellular operators. It is worth mentioning that UASs (Unmanned Aerial Systems) comprises both data links and ground control stations.

The 3GPP has recently undertaken a study to explore the potential opportunities and challenges for employing UAVs as a new UE, referred to as aerial UE (Meredith, 2017). This study's essential finding is that the enhanced line-of-sight (LOS) communication links are present between aerial UE and ground base stations (BSs) subject to the considered environment. Simultaneously a disadvantage would be an increase of interference in the system, which calls for new strategies to seamlessly mitigate interference and accommodate both aerial and ground UEs in the same system (Lin, Yajnanarayana, Muruganathan, Gao, Asplund, Maattanen, Bergstrom, Euler & Wang, 2018). More recently, as a part of Google Project Loon, in place of traditional terrestrial eNodeBs, new large-scale high-altitude UAV LTE eNodeBs were proposed (Fotouhi *et al.*, 2019).

A variety of novel techniques have already been proposed to address such interference issues, which show promising results. While 3GPP is mainly concerned with connecting UAVs to cellular networks, industry and academia are advancing to the next level of research and development that promises to harness UAVs communications' full potential. They are exploring this unique, unparalleled opportunity to realize UAV-mounted flying relays and BSs that can dynamically reposition themselves and boost coverage, spectral efficiency, and user quality of service (QoS). Many vendors have already field-trialled their prototypes to demonstrate the proof-of-concept of such UAV-mounted flying BSs (web, 2016), (web, 2018). Moreover, a number of papers have already been published in recent years proposing novel algorithms to optimize positioning, node placement, and mobility of flying relays and BSs (Pan *et al.*, 2019; Jiang & Swindlehurst, 2012).

1.6 URLLC and UAV: A natural wedlock

UAV-assisted communications have attracted extensive attention due to their fast deployment and favourable channel gains. Much research is currently undertaken in this field to enhance the overall system performance. The research efforts dedicated to UAV communications issues like latency and reliability have drawn little attention, which motivates us to solve the UAV-assisted communication system's ultra-high reliability problem.

1.6.1 Uplink power optimization and energy efficiency

A reduction of the energy consumption, despite significantly increased data rate demands, is one of the tasks with paramount importance in the realization of future 5G communication networks (Andrews, Buzzi, Choi, Hanly, Lozano, Soong & Zhang, 2014). This requires a consideration for advanced packet scheduling techniques that maintain certain QoS, i.e., packet error probabilities, arrival and delay constraints while reducing the overall transmission energy to achieve green communications. The topic of energy-efficient packet scheduling has already been studied extensively in the literature, as outlined in (Uysal-Biyikoglu, Prabhakar & El Gamal, 2002; Chen, Neely & Mitra, 2007), and (Wang & Li, 2013). The authors in (Uysal-Biyikoglu *et al.*, 2002) have studied energy-efficient packet scheduling where all the packets have the same deadline in additive white gaussian noise (AWGN) channels. The work in (Chen *et al.*, 2007) extended (Uysal-Biyikoglu *et al.*, 2002) by considering a FIFO system where the delay constraints bound packets. In (Uysal-Biyikoglu *et al.*, 2002; Chen *et al.*, 2007), the authors studied the optimization of the packet blocklength problem, the works (Chen, Mitra & Neely, 2009), (Wang & Li, 2013), and (Zafer & Modiano, 2009) have focused on optimizing packet transmission rates in quasi-static block fading channels while minimizing the transmission energy.

A common assumption made in the aforementioned works is that the power and data rate obey the Shannon capacity formula, which is based on the *Strong law of large numbers*, and is only valid when the channel code is extremely long (Polyanskiy *et al.*, 2010). However, as discussed before, next-generation 5G systems are expected to support a variety of services for different applications under stringent reliability and delay constraints, where the blocklength is expected to be short (Boccardi, Heath, Lozano, Marzetta & Popovski, 2014). This prohibits system designers from using the Shannon capacity formula for the performance analysis. Therefore, it is important to investigate the energy-efficient packet scheduling problems for short blocklength codes.

It is essential to examine the UAV mobility in three-dimensional space to fully exploit the degrees of freedom of UAV-enabled communications. In this regard, the problem of joint trajectory and power optimization for multi-hop UAVs was studied in (Zhang, Yan, Zeng, Cui & Liu, 2018). In (Sharma, Sabatini & Ramasamy, 2016), a study of the optimal UAV placement and distribution to minimize delays in in heterogeneous networks. Similarly, in (Jiang & Swindlehurst, 2012), the authors studied the optimization of UAV heading to provide enhanced uplink communication to the ground users. Moreover, the problem of joint optimization of blocklength and location for single-hop URLLC systems was studied in (Pan *et al.*, 2019). Recently, the authors in (Yang, Pan, Shikh-Bahaei, Xu, Chen, Elkashlan & Nallanathan, 2018) presented a joint sum uplink power optimization considering various system parameters, such as the antenna beamwidth, allocated bandwidth, transmit power, UAV location, and altitude. However, in these works, the energy efficiency was not optimized in the context of URLLC-enabled UAV communication systems. It is worth mentioning that the energy efficiency metric is essential as both UAV and IoT ground transmitters have limited batteries. Therefore, the total energy expenditure must be optimized in either uplink or downlink communications. Consequently, sum uplink power saving can provide a longer operational duration for communications in UAV-IoT networks.

1.6.2 Resource allocation in URLLC-enabled UAV communications

Resource allocation can maximize the spectrum and energy efficiency (EE), which are two important metrics in 5G communications. Resource allocation has been extensively studied in the literature for real-time services and systems. As mentioned earlier, the required E2E delay for URLLC services is 1ms, which is shorter than the channel coherence time. According to (Berry, 2013), the transmit power required to ensure the QoS requirements becomes unbounded when the delay bound exceeds the coherence time. Consequently, URLLC systems EE is lower than that of the traditional real-time systems with longer delay requirements. Recently, the resource allocation problem for short packet communication in URLLC systems has been studied in (Sun, Yan, Yang, Ding, Shen & Zhong, 2018b; She, Yang & Quek, 2018; Hu, Zhu, Gursoy & Schmeink, 2018). Specifically, (Sun *et al.*, 2018b) considered a non-orthogonal multiple access (NOMA)

system to optimize the throughput of user 1 given the throughput requirements of user 2 in short packet transmission. However, user 2's decoding error probability requirements have not been considered. The authors in (She *et al.*, 2018) derived a simplified rate expression for short packet transmission and studied the joint optimization of UL and DL blocklengths based on the CSI. In (Hu *et al.*, 2018), the authors studies the reliability performance of wireless information and power transfer (SWIPT) in relay-assisted URLLC systems. However, in this work, a fixed power assumption was made, and no guarantee for the decoding error probability at the relay was provided. According to (Hu *et al.*, 2018), mobile and IoT devices in many mission-critical applications have limited battery. To enhance the battery life, transmit power optimization for short packet UL transmission was studied in (López, Alves, Souza & Fernández, 2017), (Khan *et al.*, 2017a). However, to ensure E2E delay and overall reliability in URLLC systems, the UL and DL resources should be jointly allocated (Aijaz, 2016), which is a challenging task. In (Ren, Pan, Deng, Elkashlan & Nallanathan, 2020b), the authors considered resource allocation problem for secure URLLC in mission-critical IoT scenarios. The authors aimed to optimize both the secrecy date rate and transmission power, where they employed the secrecy capacity formula under a finite blocklength as the performance metric in their study. Similarly, in (Ren, Pan, Deng, Elkashlan & Nallanathan, 2020b), the authors studied URLLC in the context of mission-critical industrial applications under the umbrella of the fourth industrial revolution (Industrial 4.0). In this context, the authors employed massive multiple-input multiple-output (MIMO) systems to provide wireless connectivity comparable to wired lines, which provided deterministic communications thanks to its channel hardening effects. The authors aimed to optimize both the pilot and data power allocation by proposing novel low complexity algorithms to maximize the sum-rate under maximum-ratio combining (MRC) and zero-forcing (ZF) receivers. Similarly, the idea of using intelligent surfaces for communications recently came into limelight on the dissecting table of wireless communications researchers, as outlined in (Liang, Long, Zhang, Chen, Cheng & Guo, 2019b; Wu & Zhang, 2019; He & Yuan, 2019; Basar, Di Renzo, De Rosny, Debbah, Alouini & Zhang, 2019). The authors in (Liang *et al.*, 2019b) studied the fundamentals and implementation of large intelligent surfaces/antennas (LISA), which is a variant of intelligent surfaces. The authors aimed to provide the necessary

details associated to the use of LISA for backscatter communication as well as reflective relaying. In (Wu & Zhang, 2019), Wu *et al.* studied a communication scenario employing an intelligent surface assisting the communication between multiple users equipped with a single antenna and a multiantenna access point (AP). The authors sought to minimize the total transmit power at the AP subject to the users' individual signal-to-interference-plus-noise ratio (SINR) constraints. In (He & Yuan, 2019), the authors studied and laid the general framework for estimating the channel between MIMO systems assisted by a large intelligent metasurface (LIM). Similarly, in (Basar *et al.*, 2019), the authors studied the theoretical performance limits of RIS and identified potential use cases for RIS in 5G and beyond wireless networks. The seminal work in (Pan, Ren, Wang, Xu, Elkashlan, Nallanathan & Hanzo, 2020b), considered intelligent reflective surfaces (IRS) at the cell boundary to mitigate cell-edge users' inter-cell interference in downlink communication channels. To accomplish the goal mentioned above, the authors jointly optimized the active precoding matrices at the BSs and the phase shifts of the IRS subject to the constrained BS's power to maximize the weighted sum rate (WSR) of all users. Similarly, in (Pan, Ren, Wang, Elkashlan, Nallanathan, Wang & Hanzo, 2020a), the authors invoked an IRS to improve the energy harvesting performance of a simultaneous wireless information and power transfer (SWIFT) system. As mentioned earlier in the system, a multi-antenna assisted BS communicates with several multi-antenna aided information receivers (IRs). The authors aimed to jointly optimize the transmit precoding matrices of the BS as well as the passive precoding matrices of the IRS to maximize the WSR of the IRs. Recently, in (Bai, Pan, Deng, Elkashlan, Nallanathan & Hanzo, 2020), the authors considered an IRS to mitigate propagation induced impairments to fully exploit the benefits of mobile edge computing (MEC) systems for offloading computational tasks. Moreover, the authors considered single antenna devices for offloading part of their computational tasks to edge computing nodes employing a multi-antenna access point facilitated by an IRS. The authors formulated latency minimization problems for both single and multi-device scenarios subject to the constraints of mobile edge computing capability and IRS phase shift design. In (Zhou, Pan, Ren, Wang, Di Renzo & Nallanathan, 2020), the authors considered an IRS-aided multi-user multi-input single-output (MU-MISO) system with an assumption of imperfect CSI. The authors aimed to minimize the transmit power

while guaranteeing each user's QoS requirements subject to unit modulus and rate constraints. Similarly, in (Zhou, Pan, Ren, Wang & Nallanathan, 2020), the authors studied the problem of robust beamforming based on the imperfect cascaded BS-IRS user channels at the transmitter end (CBIUT). Moreover, the authors formulated the transmit power minimization problems subject to worst-case rate constraints under the bounded CSI error model and the rate outage probability constraints under the statistical CSI error model. Nonetheless, the resource allocation study for UAV-assisted URLLC or hybrid UAV-assisted URLLC-RIS systems was not considered in these works, which provides limited insights. From our previous discussion, it is evident that the resource allocation problems for URLLC assisted UAV relaying systems and flying BS for UL and DL communications scenarios are largely missing from the literature. These problems can be studied in the context of multi-hop UAV relay systems, dual UAV-RIS relay systems, single-input multi-output (SIMO) UAV relays, and UAV flying BS for UL and DL, respectively. Thus, the five problems mentioned above comprises a chapter of the thesis that is either a published or submitted work.

1.6.3 Time-complexity of resource allocation algorithms in URLLC-enabled UAV communications

Time-complexity is a simplified analysis of the algorithm's efficiency. Moreover, it gives the algorithm's complexity in terms of input variables. On the other hand, it is machine-independent such that it provides us a way to extract the algorithm's efficiency without accounting for the system specifications on which the algorithm is running. Additionally, time-complexity can be expressed as Big-O notation, which denotes the worst-case time-complexity. In this regard, it is worth mentioning that we shall use Big-O notation in the subsequent chapters to express the computational efficiency of our proposed resource allocation algorithms in URLLC-enabled UAV communications.

CHAPTER 2

QUASI-OPTIMIZATION OF DISTANCE AND BLOCKLENGTH IN URLLC AIDED MULTI-HOP UAV RELAY LINKS

Ali Nawaz Ranjha[1] , Georges Kaddoum[1]

[1] Department of Electrical Engineering, École de Technologie Supérieure,
1100 Notre-Dame Ouest, Montréal, Québec, Canada H3C 1K3

Paper published in *IEEE Wireless Communication Letters*, Volume: 9, Issue: 3, March 2020.

2.1 Abstract

Achieving ultra-high reliability for short packets is a core challenge for future wireless communication systems, as current systems are designed only to transmit long packets based on classical information-theoretic principles. To tackle this challenge, this letter relies on multi-hop UAV relay links to deliver short URLLC instruction packets between ground IoT devices. To accomplish this task, we perform non-linear optimization to minimize the overall decoding error probability in order to find the optimal values of the distance and the blocklength. In this vein, a novel, semi-empirical based non-iterative algorithm is proposed to solve the quasi-optimization problem. The algorithm executes in quasilinear time and converges to a globally optimal/sub-optimal solution based on the chosen parameters. Simulation results demonstrate that our algorithm allows operation under the URR, and yields the same performance as exhaustive search algorithms.

2.2 Introduction

Ultra-reliable and low-latency communications are among the key differentiators in the upcoming 5G networks. Mission critical applications require URLLC to support important use cases such as remote control of robots, vehicle to vehicle (V2V) communications, tactile internet, industrial automation, etc. (Bennis *et al.*, 2018). URLLC produces short packets that have strict latency and reliability constraints. In the URR of URLLC, the packet error rate (PER) should be 10^{-5}

or lower. Shannon capacity bound is inapplicable here as it assumes coding is performed over an infinite blocklength. For finite blocklenghs, channel coding rate and capacity bounds were studied and reviewed in (Polyanskiy *et al.*, 2010).

Recently, UAV assisted communication has attracted considerable attention as it provides wireless connectivity to devices in areas that lack infrastructure coverage (Zeng, Zhang & Lim, 2016b). Additionally, the high altitudes of UAVs allow for LoS communication which mitigates shadowing and signal blocking. UAVs can act as flying relays between transmitting and the receiving devices. Notably, two hop DF relays can provide significant improvements in the channel capacity, channel gain, as well as the QoS (Hu, Schmeink & Gross, 2016). IoT devices have typically limited battery and processing resources. These devices cannot transmit over large distances due to their energy constraints (Mozaffari, Saad, Bennis & Debbah, 2017). Thus, IoTs make use of intelligent interfaces such as UAVs to get connected. Nonetheless, several technical challenges must be addressed when UAVs are used as flying relays between IoT devices such as energy efficiency, node placement optimization, and mobility as outlined in (Mozaffari *et al.*, 2017; Yang *et al.*, 2018; Chen, Feng & Zheng, 2017; Zhang *et al.*, 2018).

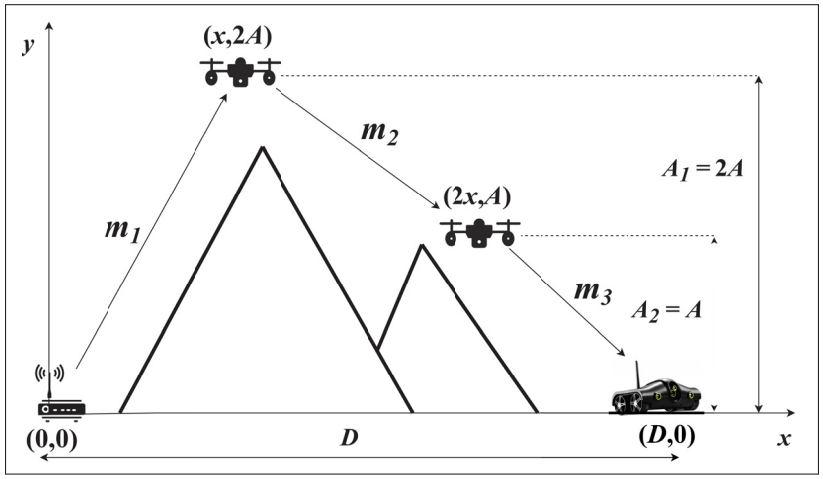

Figure 2.1 Multi-hop UAV DF relays for providing URLLC connectivity

The problem of joint trajectory and power optimization for multi-hop UAVs was studied in (Zhang *et al.*, 2018). The seminal work in (Yang *et al.*, 2018), presented the joint optimization of various system parameters like antenna beamwidth, allocated bandwidth, transmit power, UAV location, and altitude. In (Sharma *et al.*, 2016), a study of the optimal UAV placement and distribution in heterogeneous networks to optimize delays in the network was carried out. In (Jiang & Swindlehurst, 2012), the authors studied the optimization of UAV heading for the provision of enhanced uplink communication to the ground users. Recently, the problem of joint optimization of blocklength and location for single hop URLLC systems was studied in (Pan *et al.*, 2019). However, due to the high complexity of the multi-hop UAV problem, the authors left it as an open problem for the future. Despite the research efforts dedicated to UAV communications issues like latency and reliability have drawn little attention. Furthermore, the available work in the literature mostly focuses on numerical methods, i.e., perturbation based approaches, for URLLC constrained optimization while formal semi-numerical methods, i.e., the numerical analysis combined with empiricism, are missing in general. Such approaches are memory efficient and can lead to quasi-optimization problems. Since current research does not cover short packet communications with multi-hop UAV relay links, this letter considers UAV communications with ultra-high reliability constraints. The main contribution of this paper is the design of a low complexity algorithm for an IoT transmitter with limited processing memory. We aim to use quasi-optimization to find the globally optimal distance and blocklength for URLLC when finite blocklength regime is considered. By evaluating an exemplary scenario, we show that our algorithm executes in quasilinear time thus has lower time complexity than the considered exhaustive search algorithms.

2.3 System Model

We consider a two dimensional multi-hop downlink communication scenario between two IoT devices, namely a controller (T_{x} node) and a mobile robot (R_{x} node), in a remote hilly area as, shown in Fig. 2.1. UAVs serve as DF relays between the T_{x} and the R_{x} nodes. There is a strong LoS between the T_{x} and UAV node 1 as it is maneuvering right above. Hence, a free space

channel model is considered. Moreover, the T_{x} node is not able to communicate with the R_{x} node directly and must rely on the UAV chain to establish a communication link. At the other end, the robot waits for the instructions from the controller to perform tasks such as moving, navigating, and capturing pictures of the area. The T_{x} node produces short packets, each of size K bits, that must be communicated reliably over the UAV chain. Since the packets are short, they are in finite blocklength regime. Loss of a packet means failure of the robot to perform certain tasks in the operating area. Hence, the robot is only operational under the URR of the URLLC and cannot afford to lose many packets. The overall blocklength is M which is divided into three chunks. The first chunk, m_1 is allocated between the T_{x} and UAV node 1, the second chunk, m_2 is allocated between the two UAV nodes, and finally, chunk m_3 is allocated between UAV node 2 and the R_{x}. We can refer to this arrangement as the distribution of the blocklength m_i between the T_{x} and R_{x} nodes. The total blocklength is given by

$$M = B \cdot T_{\max}. \tag{2.1}$$

where B is the system bandwidth and $T_{\max}$ is the maximum time delay during the transmission phase. The positions of the T_{x} node, UAV node 1, UAV node 2, and the R_{x} node are $(0, 0)$, $(x, 2A)$, $(2x, A)$, and $(D, 0)$, respectively. Hence, the channel power gain h_i is given by

$$\begin{aligned} h_i &= \frac{\beta_0}{d_i}, \ \forall\, i \in \{1, 2, 3\}, \\ d_i &= (x_{i+1} - x_i)^2 + (y_{i+1} - y_i)^2, \\ d_1^2 &= x^2 + 4A^2, \\ d_2^2 &= x^2 + A^2, \ d_3^2 = (D - 2x)^2 + A^2. \end{aligned} \tag{2.2}$$

where β_0 is the channel power gain at a reference distance of 1 m and d_i represent the euclidean distance of the i^{th} path, respectively. According to (Polyanskiy *et al.*, 2010), we know that to transmit a short instructions packet of K bits using blocklength m_i over the i^{th} section of the

relaying link, the following equations are applicable

$$f\left(\gamma_i, m_i, K\right) = \ln\left(2\right)\sqrt{\frac{m_i}{v_i}}\left(\log_2\left(1+\gamma_i\right) - \frac{K}{m_i}\right), \\ v_i = 1 - \left(1+\gamma\right)^{-2},\ \gamma_i = P_i h_i. \tag{2.3}$$

where P_i, γ_i and v_i denote the power, SNR, and channel dispersion of the i^{th} path, respectively. The decoding error probability on the i^{th} section of the path and on the end-to-end (E2E) link are respectively given by

$$\varepsilon_i = Q\left(f\left(\gamma_i, m_i, K\right)\right). \tag{2.4}$$

$$\varepsilon_t = \varepsilon_1 + \left(1-\varepsilon_1\right)\varepsilon_2 + \left(1-\varepsilon_1\right)\left(1-\varepsilon_2\right)\varepsilon_3. \tag{2.5}$$

The simultaneous errors, $\varepsilon_1\varepsilon_2$, $\varepsilon_2\varepsilon_3$, $\varepsilon_1\varepsilon_3$, $\varepsilon_1\varepsilon_2\varepsilon_3 \rightarrow 0$; therefore, under the present URLLC scenario, (2.5) reduces to

$$\varepsilon_t \triangleq \varepsilon_1 + \varepsilon_2 + \varepsilon_3 = \sum_{i=1}^{n=3}\varepsilon_i. \tag{2.6}$$

2.4 Ultra-High Reliability Problem Formulation

Ultra-high reliability can be enabled by jointly optimizing the overall latency constraint M and the horizontal distance x. It is a constrained two dimensional optimization problem that can be formulated as

$$\min_{x, m_i} \quad \varepsilon_t \tag{2.7a}$$

$$\text{s.t.} \quad 0 \leq x \leq D/2, \tag{2.7b}$$

$$m_1 + m_2 + m_3 = M, \tag{2.7c}$$

$$m_1, m_2, m_3 \in \mathbb{Z}, \tag{2.7d}$$

(2.7a) is challenging because the objective function is non-convex and non-linear w.r.t. constraints (2.7b), (2.7c), and (2.7d).

2.4.1 Convex Analysis of Distance and Blocklength

In this subsection, we aim to reduce the complexity of our problem by performing convex analysis of the constraints. We check the convexity of the objective function w.r.t. to the distribution of the blocklength m_i. From (2.6) and (2.7c), we have

$$\varepsilon_t\left(m_1, m_2\right) = \varepsilon_1\left(m_1\right) + \varepsilon_2\left(m_2\right) + \varepsilon_3\left(m_3\right).$$

$$m_3 = M - m_1 - m_2.$$

The partial derivative of ε_t w.r.t. m_1 can be calculated as

$$\frac{\partial \varepsilon_t\left(m_1, m_2\right)}{\partial m_1} = \frac{\partial \varepsilon_1\left(m_1\right)}{\partial m_1} + \frac{\partial \varepsilon_3\left(m_3\right)}{\partial m_1},$$

$$\frac{\partial \varepsilon_t\left(m_1, m_2\right)}{\partial m_1} = \frac{\partial \varepsilon_1\left(m_1\right)}{\partial m_1} + \frac{\partial \varepsilon_3\left(m_3\right)}{\partial m_3}\frac{\partial m_3}{\partial m_1},$$

$$\frac{\partial \varepsilon_t\left(m_1, m_2\right)}{\partial m_1} = \frac{\partial \varepsilon_1\left(m_1\right)}{\partial m_1} - \frac{\partial \varepsilon_3\left(m_3\right)}{\partial m_3}. \tag{2.8}$$

The partial derivative of ε_t w.r.t. m_2 is given as

$$\frac{\partial \varepsilon_t\left(m_1, m_2\right)}{\partial m_2} = \frac{\partial \varepsilon_2\left(m_2\right)}{\partial m_2} - \frac{\partial \varepsilon_3\left(m_3\right)}{\partial m_3}. \tag{2.9}$$

The partial derivatives of (2.8) and (2.9) w.r.t. m_2 and m_1 are

$$\frac{\partial \varepsilon_t\left(m_1, m_2\right)}{\partial m_1 \partial m_2} = \frac{\partial \varepsilon_t\left(m_1, m_2\right)}{\partial m_2 \partial m_1} = -\frac{\partial \varepsilon_3\left(m_3\right)}{\partial m_3}. \tag{2.10}$$

Hence, the Hessian matrix of $\varepsilon_t\left(m_i\right)$ has the following form

$$\mathbf{H} = \begin{pmatrix} \dfrac{\partial^2 \varepsilon_t\left(m_1, m_2\right)}{\partial {m_1}^2} & \dfrac{\partial^2 \varepsilon_t\left(m_1, m_2\right)}{\partial m_1 \partial m_2} \\ \dfrac{\partial^2 \varepsilon_t\left(m_1, m_2\right)}{\partial m_2 \partial m_1} & \dfrac{\partial^2 \varepsilon_t\left(m_1, m_2\right)}{\partial {m_2}^2} \end{pmatrix},$$

$$= \begin{pmatrix} \dfrac{\partial^2 \varepsilon_1 (m_1)}{\partial m_1^2} + \dfrac{\partial^2 \varepsilon_3 (m_3)}{\partial m_3^2} & \dfrac{\partial^2 \varepsilon_3 (m_3)}{\partial m_3^2} \\ \dfrac{\partial^2 \varepsilon_3 (m_3)}{\partial m_3^2} & \dfrac{\partial^2 \varepsilon_2 (m_2)}{\partial m_2^2} + \dfrac{\partial^2 \varepsilon_3 (m_3)}{\partial m_3^2} \end{pmatrix}. \tag{2.11}$$

Let $a = \dfrac{\partial^2 \varepsilon_1 (m_1)}{\partial m_1^2}$, $b = \dfrac{\partial^2 \varepsilon_2 (m_2)}{\partial m_2^2}$, and $c = \dfrac{\partial^2 \varepsilon_3 (m_3)}{\partial m_3^2}$.

where $a;\ b;\ c > 0$; Matrix $\mathbf{H}$ is Hermitian in accordance to Sylvester's criterion. Moreover, it is positive-definite if its upper-left element and determinant are positive, and since we have

$$det(\mathbf{H}) = \begin{vmatrix} a + c & c \\ c & b + c \end{vmatrix} = ab + ac + bc > 0. \tag{2.12}$$

Therefore, Matrix $\mathbf{H}$ is positive-definite and this is a sufficient condition for the function $\varepsilon_t (m_i)$ to be strictly convex (Please refer to **Appendix I**). A Similar analysis reveals that $\varepsilon_t \left(x_j\right)$ is non-convex. Subsequently, the distribution problem of the blocklength m_i can be solved as convex while the problem of the distance x can be solved as non-convex.

2.5 Non-Linear Programming Algorithm

In this section, we develop a semi-empirical-based non-iterative approach to solve (2.7a) for fixed UAV positions. This algorithm, named Algorithm 1, is executed sequentially in three steps (i.e., Step 1, Step 2, Step 3) whereas, Step 0 is a sub-step used by each of the other three steps. At Step 1 the optimization problem is solved for the blocklength m_i with the fixed distance x. Optimal values are found by performing exhaustive search on the coarse grid. At this step, we calculate two objective functions, namely $\varepsilon_{t_0} \left(m_i, x_j\right)$ and $\varepsilon_{t_1} \left(m_i, x_j\right)$.

Step 1 and 2 consider the objective function $\varepsilon_{t0} \left(m_i, x_j\right)$ to reduce the complexity of the optimization problem (2.7a). These two steps generate a smooth unimodal function to optimize. However, it does not represent the entire solution to the optimization problem (2.7a) as the constraint (2.7d) is violated. Step 2 searches for the local minima by considering the optimal

Algorithm 2.1 – **(Step 0)** Calculation of the objective function $\varepsilon_{tk}\left(m_i, x_j\right)$

Initialize m_i, x_j from Step 1, 2, 3;
while $(m_{1\ high} - m_{1\ low}) > 1/2$ **do**
  Set $m_{1\ avg.} = (1/2(m_{1\ high} + m_{1\ low}) + 1/2) - 1/2$.
  Set $m_{2\ high} = M - 1 - m_{1\ avg.}$, $m_{2\ low} = 1$.
  while $(m_{2\ high} - m_{2\ low}) > 1/2$. **do**
    Set $m_{2\ avg.} = (1/2(m_{2\ high} + m_{2\ low}) + 1/2) - 1/2$.
    Set $m_{3\ avg.} = M - m_{1\ avg.} - m_{2\ avg.}$.
    Set $\bar{f}_{marg.} = \varepsilon_{t_k}(m_{avg.})$.
    if $(\bar{f}_{marg.}(3) > \bar{f}_{marg.}(2))$. **then**
      Set $m_{2\ high} = m_{2\ avg.}$.
    else
      Set $m_{2\ low} = m_{2\ avg.}$.
    end if
  end while
  if $(\bar{f}_{marg.}(2) + \bar{f}_{marg.}(3) > 2\bar{f}_{marg.}(1))$. **then**
    Set $m_{1\ high} = m_{1\ avg.}$.
  else
    Set $m_{1\ low} = m_{1\ avg.}$.
  end if
end while
Return: $\varepsilon_{t_0}\left(m_i, x_j\right)$ and $\varepsilon_{t_1}\left(m_i, x_j\right)$ at $m_i^* = m_{i\ avg.}$

Algorithm 2.1 – **(Step 1)** Calculation of the $x_{b_1}^*$ from the discretization of the distance

Initialize $x_j = \frac{j}{2N} D,\ j \leftarrow 1, 2, ..., N$;
for $j = 0, 1, 2, ..., N$ **do**
  Use Step 0 to find $\varepsilon_{t_0}(m_i, x_j)$, $m_i \notin \mathbb{Z}$ and $\varepsilon_{t_1}(m_i, x_j)$, $m_i \in \mathbb{Z}$
end for
Set $x_{b_1}^* = \text{argmin}\ \varepsilon_{t_0}(m_i, x_j)$.

solution from the previous step within the range $x \in \left[x_{b_1}^* - 1,\ x_{b_1}^* + 1\right]$. The golden section search is applicable here because the objective function is convex and the minima lies within this range. This step refines the solution from the previous step.

Algorithm 2.1 **– (Step 2)** Calculation of the $x^*_{b_2}$ using the golden section search method

Initialize $a = x^*_{b_1} - 1$, $b = x^*_{b_1} + 1$, $F1 = (1 + \sqrt{5})/2$;
while $(b - a) > 0.1$ **do**
  Set $x_1 = b - (b - a)/FI$, $x_2 = a + (b - a)/FI$.
  Set $y_1 = \varepsilon_{t_0}(x_1)$ and $y_2 = \varepsilon_{t_0}(x_2)$ using Step 0.
  if $(y_1 \geq y_2)$ **then**
    Set $a = x_1$.
  else
    Set $b = x_2$.
  end if
end while
Set $x^*_{b_2} = (a + b)/2$..

In Step 3, we use the polynomial approximation to deal with the non-convexity and non-linearity of the objective function $\varepsilon_{t1}\left(m_i, x_j\right)$ w.r.t. constraints (2.7b), (2.7c), and (2.7d). At this step we calculate the minima of $\varepsilon_{t1}\left(m_i, x_j\right)$.

Algorithm 2.1 **– (Step 3)** Calculation of the $x^*_{b_3}$ using quadratic polynomial regression

Initialize $x_c = x^*_{b_2}$, $x_{c\ new} = -1e6$;
while $|x_{c\ new} - x_c| < 0.01$ **do**
  Set $x_c = x_{c\ new}$, $\Delta x = 0.01$.
  Set $y\,(x - \Delta x) = \varepsilon_{t_1}\,(x - \Delta x)$.
  Set $y\,(x) = \varepsilon_{t_1}\,(x)$, $y\,(x + \Delta x) = \varepsilon_{t_1}\,(x + \Delta x)$.
  Fit the two vectors $[x - \Delta x, x, x + \Delta x]$ and $[y(x - \Delta x), y(x), y(x + \Delta x)]$ onto the quadratic equation $ax^2 + bx + c$ to compute quadratic polynomial coefficients a, b, c.
  Set $x_{c\ new} = -b/2a$.
end while
Set $x^*_{b_3} = x_{c\ new}$
Return: minima of $\varepsilon_{t_1}(m_i, x_j)$ using Step 0 and optimal value of distance $x^*_{b_3}$.

2.6 Simulation Results and Analysis

In this section we present the time complexity, convergence, and performance analysis of our algorithm, compared to two benchmarks, namely the full exhaustive and the smart exhaustive search. The full exhaustive search uses every possible combination of the distance x and the blocklength m_i, whereas the smart exhaustive search calculates the objective function for every value of x using the golden search method for m_i. Time complexity for these two benchmarks and the proposed algorithm are tabulated below.

Table 2.1 Time Complexity

Algorithms and Steps	**Complexity**
Full Exhaustive Search	$\mathcal{O}(\frac{D}{2\Delta x}M^2)$
Smart Exhaustive Search	$\mathcal{O}(\frac{D}{2\Delta x}\log_2(M)^2)$
Proposed Algorithm	$\mathcal{O}(N\log_2(M)^2)$
Step 0 and Step 3	$\mathcal{O}(\log_2(M)^2)$
Step 1	$\mathcal{O}(N\log_2(M)^2)$
Step 2	$\mathcal{O}(\log_2(\frac{D}{2N\Delta x})\log_2(M)^2)$

As depicted in Table 2.1, the time complexity of the proposed algorithm is lower than the comparison benchmark algorithms. In fact it executes in quasilinear time. Next we analyze the convergence of our proposed algorithm by setting:- $K = 60$ bits, $B = 10$ MHz, $T_{\max} = 6\ \mu s$, $M = 60$ symbols, $D = 400$ m, $\Delta x = 0.01$ m, $A = 150$ m, $P_1 = 3.1$ W, $P_2 = P_3 = 1.75$ W, $N = 200$, and $\beta_0 = 58.5$ dB. For this set of parameters, the sub-optimal solution for a distance x is obtained as shown in Fig. 2.2a. Afterwards, we increase the power at the T_{x} node to $P_1 = 3.3$ W it is observed in Fig. 2.2b that for this nominal increase of power the proposed algorithm converges to the optimal solution. The convergence of the algorithm is non-iterative and it is guaranteed as it can be seen from both Fig. 2.2a and Fig. 2.2b. The algorithm finds the optimal/sub-optimal solution by assuming that the local minima of the objective function $\varepsilon_{t_0}(m_i, x_j)$ is related to the global minima of the objective function $\varepsilon_{t_1}(m_i, x_j)$. For a given set of parameters, when the global minimas of both objective functions, namely $\varepsilon_{t0}(m_i, x_j)$ and

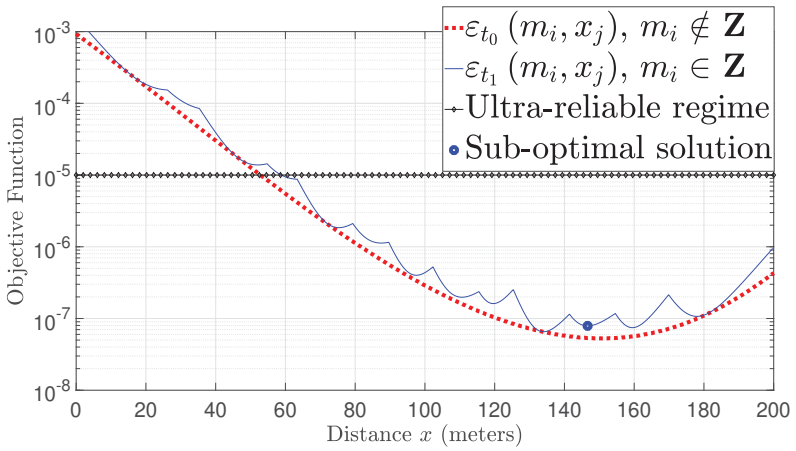

a) Objective function converging to sub-optimal solution

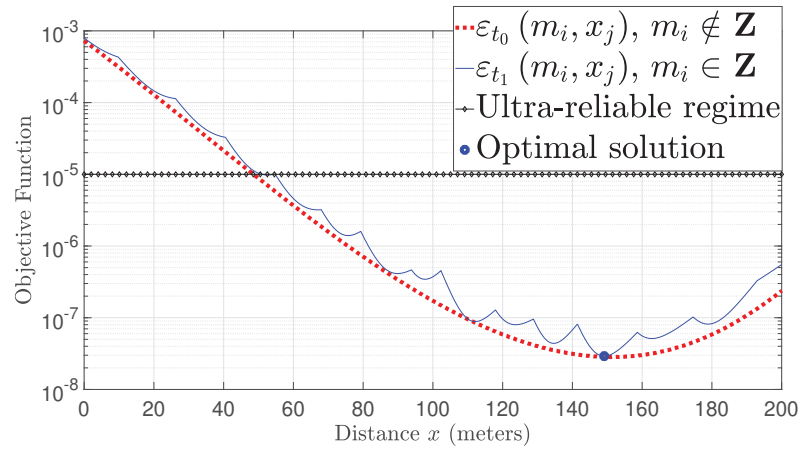

b) Objective function converging to globally optimal solution

Figure 2.2 Convergence behaviour of the proposed algorithm

$\varepsilon_{t1}(m_i, x_j)$ coincide the algorithm converges to the global minima as illustrated in Fig. 2.2b. Overall the convergence behavior of the proposed algorithm can be termed as quasi-optimal.

Finally, we make a performance comparison of the decoding error probability of the algorithms mentioned in Table 2.1. As evidenced in Fig. 2.3, the performance of the proposed algorithm is equal to that of the exhaustive search algorithms.

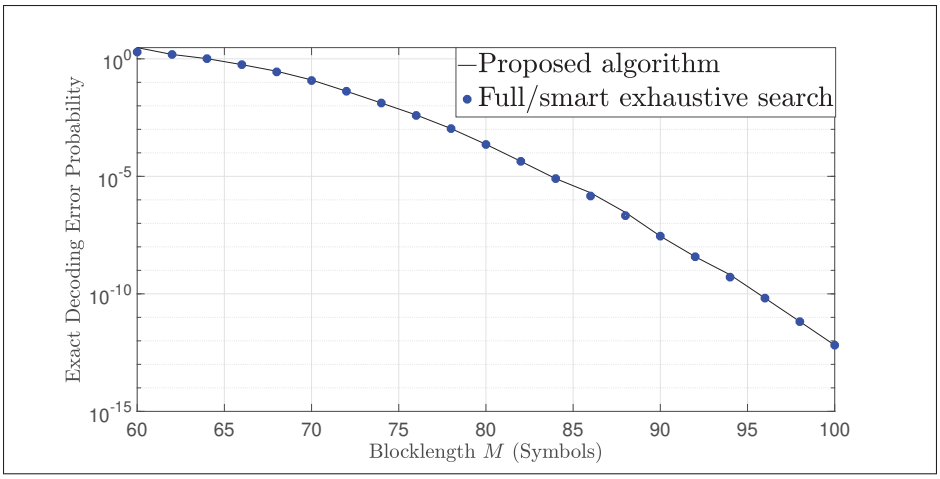

Figure 2.3 Comparison of the proposed algorithm with the benchmark algorithms

2.7 Conclusion

In this paper, we introduced the quasi-optimization of the distance and the blocklength for ground IoT devices communicating over multihop UAV relay links operating under URLLC and finite blocklength constraints. The goal was to mitigate the overall decoding error probability so that the short packets are received with ultra high reliability at the R_{x} node. To achieve this goal, we optimized the latency constraint to enter the URR based on our proposed algorithm. Simulation results show that our proposed algorithm is highly suitable for implementation at the T_{x} node because of its low time complexity, while it yields the same performance as more complicated exhaustive search algorithms. Lastly, in the next chapter, we shall study uplink power optimization in UAV-assisted IoT networks facilitating URLLC.

CHAPTER 3

QUASI-OPTIMIZATION OF UPLINK POWER FOR ENABLING GREEN URLLC IN MOBILE UAV-ASSISTED IOT NETWORKS: A PERTURBATION-BASED APPROACH

Ali Nawaz Ranjha[1] , Georges Kaddoum[1]

[1] Department of Electrical Engineering, École de Technologie Supérieure,
1100 Notre-Dame Ouest, Montréal, Québec, Canada H3C 1K3

Paper published in *IEEE Internet of Things Journal*, August 2020.

3.1 Abstract

Efficient resource allocation can maximize power efficiency, which is an important performance metric in future 5G communications. Minimization of sum uplink power in order to enable green communications while concurrently fulfilling the strict demands of ultra-reliability for short packets is an essential and central challenge that needs to be addressed in the design of 5G, and subsequent wireless communication systems. To address this challenge, this paper analyzes the joint optimization of various UAV systems parameters including the UAV's position, height, beamwidth, and the resource allocation for uplink communications between ground IoT devices and a UAV employing short URLLC data packets. Towards achieving the aforesaid task, we proposed a perturbation-based iterative optimization to minimize the sum uplink power in order to determine the optimal position for the UAV, its height, beamwidth of its antenna, and the blocklength allocated for each IoT device. It is shown that the proposed algorithm has lower time complexity, yields a better performance than other benchmark algorithms, and achieves similar performance to exhaustive search. Moreover, the results also demonstrate that Shannon's formula is not an optimum choice for modeling sum power for short packets as it can significantly underestimate the sum power, where our calculations show that there is an average difference of 47.51% for the given parameters between our proposed approach and Shannon's formula. Lastly, our results confirm that the proposed algorithm allows ultra-high reliability for all the users, and converges rapidly.

3.2 Introduction

URLLC has been envisioned as one of the pivotal and core services to be provided in the upcoming 5G networks alongside with eMBB and massive machine type communication (mMTC). URLLC provide support for mission critical IoT applications such as UAVs control information delivery, E-health, smart grids, autonomous driving, intelligent transport system (ITS), industrial automation, etc. (Bennis *et al.*, 2018). URLLC systems must utilize short packets in order to reduce latency; however, short packets adversely affect the coding gain of the channel. On the other hand, URC requires a packet error rate of 10^{-5} or even lower, depending on the considered mission critical application. In URC, short data packets are transmitted using a moderately low throughput (i.e., 1-50 Mbps) but ultra-high reliability (99.999%) with typically 1 ms latency is a must (Durisi, Koch & Popovski, 2015). In this regard, Shannon's capacity is based on the Strong law of large numbers, which is an idealistic assumption that coding is performed over an infinite blocklength. Thus, it is only valid for data packets of large size, and it can't facilitate in the study and analysis of short data packets. Channel capacity bounds, and coding rate were studied and reviewed in (Polyanskiy *et al.*, 2010) for short data packets having finite blocklenghs. Furthermore, a reduction of the power consumption while satisfying the end user demands is of paramount importance in order to realize future 5G communication networks and their services (Andrews *et al.*, 2014). This requires the design of advanced resource allocation techniques that maintain certain quality of service (QoS) i.e., packet error probabilities, while reducing the overall transmission power to achieve green communications.

Unmanned aerial vehicles (UAVs) are a cutting-edge technology that can be fully exploited for use in civil, public, and military applications, where the world has already been introduced to the next-generation of advanced military UAVs, such as Predator, and Global hawk (Khan *et al.*, 2017a; Gupta *et al.*, 2015). In this context, the past couple of years have seen a sharp surge in the demand for UAVs that are to be employed for personal or commerical purposes, such as the Phantom, Mavic, and Inspire from DJI, the Solo from 3D Robotics, the AR, and Bebop from Parrot (Gupta *et al.*, 2015). Moreover, technical advancements in various engineering fields such as electronics, artificial intelligence, computer, and sensor technology have expanded

the horizon of UAVs to include an array of diverse applications like wind estimation, traffic monitoring, and remote sensing (Bekmezci *et al.*, 2013). Besides, UAVs can be viewed as dynamical aircrafts with added degrees of freedom. Thus, there has recently been a boom in the production, supply, demand, and deployment of UAVs. In this context, it is worth mentioning that according to a report from the Federal Aviation Administration (FAA) that has been made public, the fleet of drones will be increased from 1.1 million vehicles in 2017 to 2.4 million units by 2022 (Fotouhi *et al.*, 2019). As control and communications are essential parts of UAV systems this rapid increase will fuel new use cases for UAVs, and it is forecasted that it will bring promising and favourable new business opportunities for cellular operators. More recently, as part of the Google Project Loon, in place of traditional terrestrial evolved node B (eNodeBs), new large-scale high-altitude UAV LTE eNodeBs were proposed as alternatives (Fotouhi *et al.*, 2019). The 3GPP, has latterly conducted a thorough investigation of the potential usecases, opportunities, and challenges that arise when UAVs are employed as a novel type of user equipment (UE) referred to as aerial UE (Meredith, 2017). A core finding of these studies is that UAVs allow for an enhanced line-of-sight (LoS) between the aerial UE and the ground base stations (BSs). Thus, UAV based communications have a significant and clear advantage over non line-of-sight communications where the signal only arrives at the receiver after multi-path propagation. Meanwhile, UAV LoS links are prone to signal blockage, and shadowing due to buildings, and obstacles. The studies also mention the disadvantage of employing a UAV as it can lead to an increase in interference in a system which accommodates both aerial and ground user equipments (Lin *et al.*, 2018). A variety of novel techniques, showing promising results, have already been proposed in this regard to address such interference issues (Liu, Zhang & Zhang, 2019) - and references therein. Currently, the primary concern of 3GPP is the successful integration of the UAVs into the cellular networks. Therefore, the research community from both academia and industry are concurrently playing their part to take up the gigantic challenge of research and development that promises to exploit the full potential of UAV-based communications. They are traversing through this unique unprecedented opportunity to develop UAV-mounted flying relays and BSs that have the tendency to dynamically reposition themselves in real time while simultaneously boosting spectral efficiency, coverage, and maintaining high

user quality of service (QoS) (Hu *et al.*, 2016; Arribas, Mancuso & Cholvi, 2019; Chiaraviglio, D'Andreagiovanni, Liu, Gutierrez, Blefari-Melazzi, Choo & Alouini, 2020). Such dynamicity can also play a crucial role in disaster struck areas where UAV communication infrastructure can be setup (Karlsson, Jiang, Wicker, Adams, Ma, van Renesse & Weatherspoon, 2018). This makes UAV communication infrastructures unique and quite different from the general communication infrastructure which is comprised of static BSs. It is worth mentioning here that IoT are integral part of vehicular technologies including UAVs. Additionally, IoT are limited in terms of battery and processing capacity. Thus, the finite battery energy of these devices restricts their transmission over a long distance. An infrastructure less communication system to that end can be the amalgamation of UAV-IoT technologies. In this vein, many vendors have already began to field-trial their designed prototypes in order to demonstrate the proof-of-concept of such UAV-mounted flying BSs (Russon, 2016b; Zach, 2018a).

3.2.1 Related Work

Significant progress has been made by the research community in the past few years proposing advanced and novel approaches to tackle the convoluted problems of positioning, trajectory planning, node placement, rate maximization, and mobility of UAVs serving as flying BSs or aerial relays, as outlined in (Mozaffari *et al.*, 2017; Zhan & Lai, 2019; Jiang & Swindlehurst, 2012; Chen *et al.*, 2017; Sharma *et al.*, 2016; Zhang *et al.*, 2018; He, Zhang, Zeng & Zhang, 2017; Jiang, Wu, Yin, Yang & Yang, 2019; Yang *et al.*, 2018). Particularly in (Mozaffari *et al.*, 2017), the authors consider a UAV-IoT communication scenario, where multiple UAVs serve as flying BSs and they are tasked to collect data from ground IoT devices. The authors aim to optimize UAV deployment, uplink power control, and device-UAV association. Similarly, the authors in (Zhan & Lai, 2019) study the energy minimization problem in IoT devices using the so-called *propulsion energy model*, which is based on a rotary wing UAV. In this regard, the authors seek to jointly optimize UAV trajectory, power allocation, and communication scheduling. The authors in (Jiang & Swindlehurst, 2012), consider ground-to-air communication links between ground nodes equipped with single antenna and UAV equipped with multiple antennas. The ergodic sum

rate of the uplink channel is optimized subject to UAV heading and the positions of the ground nodes. In (Chen *et al.*, 2017), Chen *et al.* study the optimal placement of UAVs as relays and derives the overall outage, overall bit error rate, and power loss as measures for communication reliability. The problem of multi-UAV distribution and optimal deployment in the framework of heterogeneous networks is studied in (Sharma *et al.*, 2016), with an aim to optimize the overall network delays. In (Zhang *et al.*, 2018), the authors consider multiple UAVs serving as relays and seek to maximize end-to-end throughput via joint UAV trajectory path planning, transmit power, and collision avoidance constraints. In (He *et al.*, 2017), He *et al.* study the problem of joint altitude and beamwidth optimization in multi-user scenarios using a UAV as a flying base station. The authors consider three distinct scenarios, namely UAV-enabled downlink multicasting and broadcasting, as well as uplink multiple access. The work in (Jiang *et al.*, 2019), studies the problem of joint trajectory and communication design for UAV assisted wireless networks using time division by dividing their problem into two sub-problems and solving them alternatively, i.e., first the sub-problem of time slot allocation with fixed system parameters including power and trajectory is solved and then the second sub-problem of optimization of trajectory and power with fixed time slot allocation is solved. The seminal work in (Yang *et al.*, 2018), presents the sum uplink power optimization while considering various optimization variables including antenna beamwidth, allocated bandwidth, UAV position, and altitude. The authors employ the so-called *divide-and-conquer* rule to solve this problem. Nonetheless, in the aforementioned studies (Mozaffari *et al.*, 2017; Zhan & Lai, 2019; Jiang & Swindlehurst, 2012; Chen *et al.*, 2017; Sharma *et al.*, 2016; Zhang *et al.*, 2018; He *et al.*, 2017; Jiang *et al.*, 2019; Yang *et al.*, 2018), the authors commonly make use of Shannon's capacity formula for the transmission power and rate analysis which possesses both monotonicity and convexity (Xu, Chang, Lin, Shen & Zhu, 2016). Unfortunately, URLLC systems utilize the finite blocklength capacity formula which does not guarantee such monotonic and convex properties. Furthermore, the finite blocklength capacity formula is neither convex nor concave with respect to the transmit power and the blocklength. Consequently, it significantly complicates the mathematical analysis of the optimization to reach the global optima (Ren, Pan, Deng, Elkashlan & Nallanathan, 2020a). Moreover, only a few works in the literature consider URLLC, by examining the aforementioned

finite blocklength formula as outlined in (She, Yang & Quek, 2017; Ren *et al.*, 2020b; Ren *et al.*, 2020b). In (She *et al.*, 2017), the authors study URLLC in radio access networks subject to both transmission delay and queuing delay. The authors propose a novel proactive packet dropping mechanism by jointly optimizing packet dropping policies, power allocation, and bandwidth allocation to minimize the transmit power under the required QoS constraint. Similarly, in (Ren *et al.*, 2020b), the authors study URLLC in the context of mission-critical industrial applications under the umbrella of the fourth industrial revolution (Industrial 4.0). In this context, the authors employ massive MIMO systems to provide wireless connectivity as similar to wired lines, and it has the advantage of providing deterministic communications thanks to its channel hardening effects. The authors aim to optimize both the pilot and data power allocation by proposing novel low complexity algorithms to maximize the sum-rate under MRC and ZF receivers. In (Ren *et al.*, 2020b), the authors consider the problem of resource allocation for secure URLLC in mission-critical IoT scenarios. The authors aim to optimize both the secrecy date rate and transmission power, where they employ security capacity formula under finite blocklength as the performance metric in their study. However, these works (She *et al.*, 2017; Ren *et al.*, 2020b; Ren *et al.*, 2020b), do not consider URLLC-enabled UAV communications. Thus, they provide limited insights. Furthermore, regarding the research efforts dedicated to UAV communications, issues like reliability and latency have drawn little attention. Presently, only a few works in literature discuss URLLC-enabled UAV communications, as outlined in (She *et al.*, 2019; Ren *et al.*; Pan *et al.*, 2019; Ranjha & Kaddoum, 2020a; Ren *et al.*, 2020c). In the seminal work in (She *et al.*, 2019), authors study a framework to facilitate URLLC in CNPC links of the UAVs. The authors aim to exploit the macro-diversity gain of multi-antenna systems by considering three distinct scenarios, namely DAS, CAS, as well as a modified DAS (M-DAS). Moreover, the authors jointly optimize the antenna configuration, altitude of UAVs, and the duration of uplink and downlink phases with a goal to maximize the available range which is the maximum horizontal communication distance within which the round-trip delay and the overall packet loss probability can be ensured with a required probability. The problem of AADR for URLLC-enabled UAV systems is studied in (Ren *et al.*). The authors use the so-called *Gaussian-Chebyshev quadrature* method to derive an expression of achievable data

rate in a system considering short packet delivery from a ground station to a UAV. Their approach supposedly provides insights about packet design in such communication systems. In (Pan *et al.*, 2019), the authors study the problem of joint blocklength allocation and UAV location to enable ultra-high reliability in single-hop UAV relay systems. Most recently, we study the problem of joint distance and blocklength optimization for URLLC-enabled multi-hop UAVs links for an IoT transmitter/receiver pair in (Ranjha & Kaddoum, 2020a). We employ the so-called *semi-empirical* approach to perform quasi-optimization, and show that the system supports URC for short packets. In (Ren *et al.*, 2020c), the authors study URLLC enabled by a UAV serving as an AF relay system. The authors propose low complexity algorithms to jointly optimize UAV placement and power in a three-dimensional (3-D) channel to guarantee a minimum decoding error probability. Moreover, the authors demonstrate that AF relays benefit from low signal processing delays compared to their decode-and-forward (DF) counterparts. Nevertheless, these works (She *et al.*, 2019; Ren *et al.*; Pan *et al.*, 2019; Ranjha & Kaddoum, 2020a; Ren *et al.*, 2020c), are not generalized for multi-user and the mobility of UAV is rather fixed, which tends to provide limited insights. Additionally, to design realistic, robust, and workable multi-user URLLC-enabled UAV systems it is imperative to jointly optimize resource allocation which includes blocklength and power, UAV location, and UAV antenna parameters such as beamwidth under the given requirements of reliability and latency.

3.2.2 Novelty and Contributions

Despite, all the research efforts studying URLLC, UAV-enabled communication, and their fusion UAV enabled URLLC, a study on the performance analysis of a UAV enabled green URLLC system with multi-user under finite blocklength regime is still missing. To fill this gap, we study the sum uplink power in the context of UAV-IoT communication systems. The main contributions of this paper can be summarized as follows:

- We study and formulate the problem of sum uplink power for enabling green URLLC assisted by a mobile UAV in a multi-user IoT communication scenario under short packet transmissions.

- We perform the convexity analysis in order to show the objective function is non-convex in nature, which makes it a cumbersome and tedious mathematical problem.
- We divide a significantly complicated mathematical problem into relatively easier sub-problems using the so-called *divide-and-conquer* rule, and proceed to effectively solve them by using perturbation-theory.
- We show that the proposed approach yields better performance than other benchmark algorithms, while giving similar performance as the exhaustive search. Simultaneously, the proposed approach maintains a lower time complexity than the exhaustive search. Furthermore, we demonstrate through simulations that Shannon's capacity formula is inapplicable for modelling the sum power of short packets.

3.3 System Model and Problem Formulation

We consider a two dimensional uplink communication scenario between IoT devices, namely users ($T_{\mathrm{x}_k}, \forall\ k \in \{1, \ldots, K\}$ nodes) and a UAV flying base station BS (R_{x} node), in a circular cell, as shown in Fig. 3.1. The position of the UAV is $\boldsymbol{y} = \boldsymbol{(y(1); y(2))}$, where $\boldsymbol{y(1)}$ and $\boldsymbol{y(2)}$ denote the horizontal and vertical coordinates, respectively. The UAV is flying at a height of H whereas, the horizontal and vertical position of each T_{x_k} node is denoted by $\boldsymbol{x_k} = \boldsymbol{(x_k(1); x_k(2))}$ with $\boldsymbol{x_k, y} \in \mathbb{R}^2$. For simplicity, we assume that the height of the UAV is sufficiently greater than the height of each T_{x_k} node deployed in the circular cell.

We conveniently consider a free space channel model as there is a strong LoS between ground T_{x_k} nodes and the UAV, hovering above them. The sensors in ground T_{x_k} nodes produce short data packets that must be supported by URC and are to be communicated to the UAV in the uplink channel. The packets, because of their short size, are in finite blocklength regime. Moreover, the UAV is equipped with a directional antenna with a gain G and adjustable beamwidth. Each T_{x_k} node is equipped with an omnidirectional antenna with unit gain. Without loss of generality we make the assumption that both the azimuth and elevation half-power beamwidths of the UAV antenna are equal, both of which are denoted by 2Θ, with $\Theta \in \left(0, \frac{\pi}{2}\right)$ (Yang *et al.*, 2018). According to (Balanis, 2016), the corresponding antenna gain in the direction (θ, ϕ) is

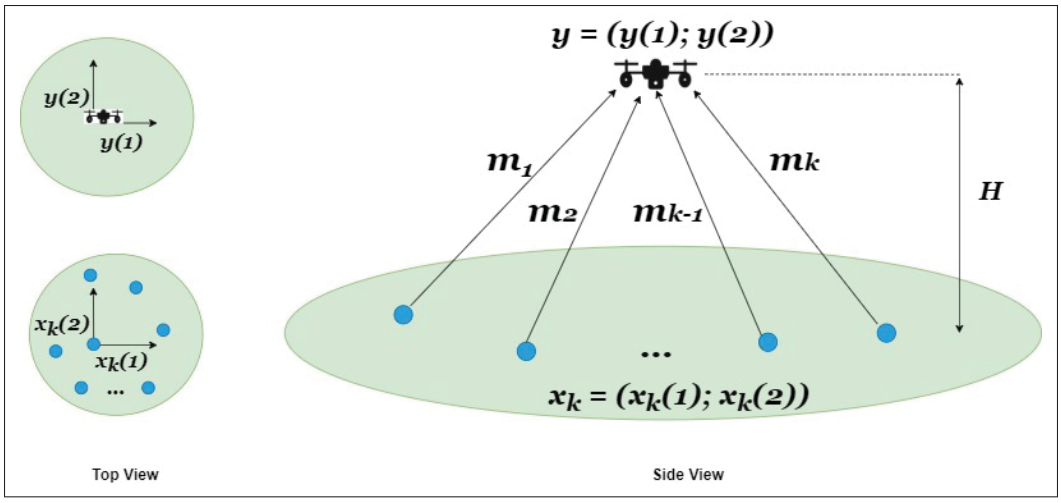

Figure 3.1 Illustration of UAV facilitated uplink communication scenario for supporting green URLLC connectivity

approximately given as

$$G(\theta,\phi) = G = \begin{cases} \frac{G_0}{\Theta^2}, \; if \; 0 \le \theta \le \Theta \; and \; 0 \le \phi \le \Theta, \\ g \approx 0, \; \text{otherwise}, \end{cases} \tag{3.1}$$

where $G_0 \approx 2.2846$, θ and ϕ represent the azimuth and elevation angles, and g denotes the antenna gain, where $g \approx 0$ for any region that lies outside the beamwidth of the antenna. Further, the uplink channel gain of each T_{x_k} node is respectively given as

$$h_k = \frac{\beta_0}{(\|\boldsymbol{y} - \boldsymbol{x}_k\|^2 + H^2)^{\frac{\rho}{2}}}, \tag{3.2}$$

where β_0 is the channel power gain at a reference distance of 1 m and $\rho \ge 2$ is the pathloss exponent. For the given UAV, the circular cell region on the ground is covered by the antenna main lobe, known as the coverage area, given by $\bar{r} = H \tan\Theta$. The overall blocklength is assumed to be M, which is to be divided into K parts. The first part, m_1 is to be allocated to the T_{x_1} node, while the second part, m_2 is to be allocated to the T_{x_2} node, and finally, the last part m_K is to

be allocated to the T_{x_K} node. The total blocklength is given by $M = W \times \tau_{\max}$, where W is the system bandwidth and $\tau_{\max}$ is the maximum transmit time interval for different blocklengths. According to (Polyanskiy *et al.*, 2010), the finite blocklength capacity or rate is given as

$$\begin{aligned} R_k &= \log_2(1+\gamma_k) - \sqrt{\frac{V_k}{m_k}}\frac{Q^{-1}(\varepsilon_k)}{\ln(2)} + \frac{\mathcal{O}(\log m_k)}{m_k}, \\ R_k &\approx \log_2(1+\gamma_k) - \sqrt{\frac{V_k}{m_k}}\frac{Q^{-1}(\varepsilon_k)}{\ln(2)}, \\ \gamma_k &= P_k\, h_k\, G, \\ V_k &= 1-(1+\gamma_k)^{-2} \approx 1, \end{aligned} \tag{3.3}$$

where P_k, γ_k V_k, and ε_k denote the power, SNR, channel dispersion, and decoding error probability of each T_{x_k} node, respectively. Here, the noise is normalized to unity. Additionally, $Q^{-1}(\varepsilon_k)$ is the complementary Gaussian Q-function [1] of variable ε_k. It is to be noted here that in the IoT devices, we assume that we have separate modules for communication and processing. Here, the processing module containing the system-on-chip (SoC) consumes the circuit power denoted by P_c. Nonetheless, the power consumed by the communication module indicated by P_k is significantly higher than the power required by the SoC to process short-data packets. Hence, we have $P_k >> P_c$, and consequently, hereafter, the circuit power is ignored. Based on the works outlined in (Darwazeh, Al-Qassas, AlDosari et al., 2015; Rathore, Paul, Hong, Seo, Awan & Saeed, 2018; Kulkarni, Kute & More, 2016; Chen, Chen, You, Ling, Liang & Zimmermann, 2016; Sheng, Mahapatra, Zhu & Leung, 2015), a reasonable assumption that can be made here is the consideration that the processing time is directly proportional to the data packet size. Furthermore, we assume that the UAV battery is fully replenished when it hovers over the IoT devices. Hence, to better facilitate uplink communications in UAV-IoT networks, we only consider the uplink communication power of the IoT devices when dealing with the UAV's mobility. Lastly, investigation into more sophisticated UAV-IoT systems, including downlink communication power and onboard circuit power for UAV hovering, is beyond this current work's scope. A joint co-design involving both uplink and downlink communication powers will

[1] As usual, $Q(x) = \frac{1}{\sqrt{2\pi}}\int_x^\infty e^{-t^2/2}dt$.

be considered for future work. Furthermore, the approximation of V_k equals to 1 is valid when the received SNR is higher than 5 dB, which can be easily achieved in communication networks supporting URLLC (Sun, She, Yang, Quek, Li & Vucetic, 2018a; Ren *et al.*, 2020a). For more details about the approximation, please refer to **Appendix II**. Separating P_k from (3.3), we have

$$P_k \triangleq \frac{1}{h_k G}\left[2^{R_k+\frac{Q^{-1}(\varepsilon_k)}{ln(2)\sqrt{m_k}}}-1\right]. \tag{3.4}$$

Furthermore, for URC, the primary target is ultra-high reliability with a moderately low throughput requirement (Durisi *et al.*, 2015). Therefore, for the sake of mathematical tractability we assume equal rate demand, i.e. $R_k = R$, and rewrite (3.4) as

$$P_k \triangleq \frac{1}{h_k G}\left[2^{R}\exp\left(\frac{Q^{-1}(\varepsilon_k)}{\sqrt{m_k}}\right)-1\right]. \tag{3.5}$$

Now, substituting (3.1) and (3.2) in (3.5) we get

$$P_k \triangleq \frac{(\|\boldsymbol{y}-\boldsymbol{x}_k\|^2+H^2)^{\frac{\rho}{2}}\Theta^2}{\beta_0 G_0}\left[2^{R}\exp\left(\frac{Q^{-1}(\varepsilon_k)}{\sqrt{m_k}}\right)-1\right]. \tag{3.6}$$

Finally, the optimization problem for the sum uplink power can be formulated as

$$\min_{\boldsymbol{y},H,\Theta,m_k} \quad \sum_{k=1}^{K} P_k \tag{3.7a}$$

$$\text{s.t.} \quad \|\boldsymbol{y}-\boldsymbol{x}_k\|^2 \leq H^2\tan^2\Theta, \forall\, k\in\{1,\ldots,K\}, \tag{3.7b}$$

$$H_{\min} \leq H \leq H_{\max}, \tag{3.7c}$$

$$\Theta_{\min} \leq \Theta \leq \Theta_{\max}, \tag{3.7d}$$

$$\sum_{k=1}^{K} m_k \leq M, \forall\, k\in\{1,\ldots,K\}, \tag{3.7e}$$

$$m_k \in \mathbb{N}, \forall\, k\in\{1,\ldots,K\}. \tag{3.7f}$$

It is noted that (3.7) is a cumbersome and tedious mathematical problem because the objective function is jointly non-convex and non-linear w.r.t. constraints (3.7b), (3.7c), (3.7d), (3.7e), and

(3.7f). It is to be noted that the problem (3.7) can be feasible or infeasible. If the radius denoted by $\bar{r} = H \tan\Theta$ is too large, then the problem becomes infeasible. Nonetheless, the height $H_{\max}$ and beamwidth $\Theta_{\max}$ of the UAV should also be adjusted accordingly. Hence, the constraint (3.7b) always holds. It should be noted here that we conducted thorough empirical studies to prevent this from happening. In conclusion, we can say that constraint (3.7b) is violated (problem (3.7) is infeasible) for any IoT device outside the coverage area, i.e. it is not served by the UAV, and constraint (3.7b) is satisfied (problem (3.7) is feasible) for all the IoT devices inside the coverage area of the UAV, i.e. served by the UAV. Furthermore, for detailed convexity analysis please refer to **Appendix II**. Subsequently, we detail our approach to solve (3.7) in the next section.

3.4 The Proposed Approach

Due to the non-convexity of problem (3.7), it is difficult to obtain a globally optimal solution. Therefore, we employ an iterative approach based on perturbation-theory to obtain a sub-optimal solution to the problem. Hence, we divide (3.7) into three sub-problems and iteratively perform global optimization for each constraint, including the UAV's position y, the UAV's height H, the beamwidth Θ, and the blocklength m_k.

3.4.1 Optimizing the UAV position

In the first sub-problem we only seek to optimize the UAV's position y while keeping the other constraints fixed, we formulate the following problem

$$\min_{\boldsymbol{y}} \qquad f_1(y) = \sum_{k=1}^{K} A_k \left(\|\boldsymbol{y} - \boldsymbol{x}_k\|^2 + H^{*2} \right)^{\frac{\rho}{2}} \tag{3.8a}$$

$$\text{s.t.} \qquad \|\boldsymbol{y} - \boldsymbol{x}_k\|^2 \leq H^{*2} \tan^2\Theta^*, \forall\, k \in \{1, \ldots, K\}\,, \tag{3.8b}$$

where $A_k = \frac{1}{\beta_0 G}\left[2^R \exp\left(\frac{Q^{-1}(\varepsilon_k)}{\sqrt{m_k^*}}\right) - 1\right]$. Here, the objective function $f_1(y)$ is non-linear, continuous, and convex. Consequently, proceeding with the Karush-Kuhn-Tucker (KKT)

conditions leads to a non-positive KKT multiplier, violating the dual feasibility condition (Boyd & Vandenberghe, 2004). Therefore, we must use an iterative optimization method to solve (3.8). This is shown below as

$$-2\lambda_k(\boldsymbol{y}-\boldsymbol{x}_k) = A_k\rho\left(\|\boldsymbol{y}-\boldsymbol{x}_k\|^2 + H^{*2}\right)^{\frac{\rho}{2}-1}(\boldsymbol{y}-\boldsymbol{x}_k), \tag{3.9}$$

$$\lambda_k = -\frac{A_k\rho}{2}\left(\|\boldsymbol{y}-\boldsymbol{x}_k\|^2 + H^{*2}\right)^{\frac{\rho}{2}-1}. \tag{3.10}$$

Hence, we propose the famous steepest descent method with penalty constraint, it searches for the solution as the limit of a sequence, that is updated iteratively with respect to the objective function, gradient, and the previous descent direction. To apply this technique we consider the objective function (3.8) where we set a penalty coefficient to handle the constraint as

$$\tilde{f_1}(y) = \sum_{k=1}^{K}\left[A_k\left(\|\boldsymbol{y}-\boldsymbol{x}_k\|^2 + H^{*2}\right)^{\frac{\rho}{2}} + \kappa_m \max\left\{0,\ \|\boldsymbol{y}-\boldsymbol{x}_k\|^2 - [H^*\tan\Theta^*]^2\right\}^2\right], \tag{3.11}$$

where $\kappa_m \in \mathbb{R}_+$ represents the penalty coefficients which are updated at each m iterations by a factor of 10. Minimizing $\tilde{f_1}(y)$ is equivalent to solving problem (3.8). To guarantee convergence to the global minimum, $\tilde{f_1}(y)$ must be convex. Since $f_1(y)$, which is the first part of (3.11) is convex, we need to verify that $f_2(\boldsymbol{y}) = \max\left\{0,\ \|\boldsymbol{y}-\boldsymbol{x}_k\|^2 - [H^*\tan\Theta^*]^2\right\}^2$, the second part of (3.11) is also convex. Now, let us define a function as $l(\boldsymbol{y}) = \|\boldsymbol{y}-\boldsymbol{x}_k\|^2 - [H^*\tan\Theta^*]^2$, which is a convex function. The $\max(\cdot)$ function preserves convexity and x^2 is a convex and non-decreasing function, hence $f_2(\boldsymbol{y})$ is also a convex function. The steepest descent method searches for $\boldsymbol{y}$ as the limit of the sequence given by

$$\boldsymbol{y}_{n+1} = \boldsymbol{y}_n - \eta_n\nabla\tilde{f_1}\left(\boldsymbol{y}_n\right), \tag{3.12}$$

$$\nabla\tilde{f_1}(\boldsymbol{y}_n) = \sum_{k=1}^{K}\left[\alpha_0(\boldsymbol{y}_n-\boldsymbol{x}_k) + \kappa_m g(\boldsymbol{y}_n)\right], \tag{3.13}$$

where $\alpha_0 = A_k \rho \left(\|\boldsymbol{y}_n - \boldsymbol{x}_k\|^2 + H^{*2} \right)^{\frac{\rho}{2}-1}$, and $\nabla \tilde{f}_1(\boldsymbol{y}_n)$ is the gradient of $\tilde{f}_1$ with respect to $\boldsymbol{y}_n$. It is to be noted that $\boldsymbol{y}_n$ is updated at each iteration n. Further, we define $g(\boldsymbol{y}_n)$ as

$$g(\boldsymbol{y_n}) = \begin{cases} 4\alpha_1(\boldsymbol{y_n} - \boldsymbol{x}_k), & \text{if} \quad \|\boldsymbol{y}_n - \boldsymbol{x}_k\|^2 > (H^* \tan\Theta^*)^2, \\ 0, & \text{otherwise}, \end{cases} \tag{3.14}$$

where $\alpha_1 = \|\boldsymbol{y}_n - \boldsymbol{x}_k\|^2 - (H^* \tan\Theta^*)^2]$, and the step size η_n is chosen based on the Barzilai–Borwein method as

$$\eta_n = \frac{\left|(\boldsymbol{y}_n - \boldsymbol{y}_{n-1})^T \left[\nabla \tilde{f}_1(\boldsymbol{y}_n) - \nabla \tilde{f}_1(\boldsymbol{y}_{n-1})\right]\right|}{\left\|\nabla \tilde{f}_1(\boldsymbol{y}_n) - \nabla \tilde{f}_1(\boldsymbol{y}_{n-1})\right\|^2}. \tag{3.15}$$

The method for solving problem (3.8) with the above mentioned approach is presented in **Algorithm 3.1**.

Algorithm 3.1 Steepest descent method for computing the optimal UAV position

Initialize: $\boldsymbol{y}$, η_n, $\texttt{tol}$, κ_t, and $\texttt{tol}_\kappa$.
Set $m = 0$ and $n = 0$.
while $|y_m - y_{m-1}| < \texttt{tol}_\kappa$ **do**
    Update penalty coefficient $\kappa_m = 10^{m-1}$.
    while $|\nabla \tilde{f}_1(\boldsymbol{y}_n)| \leq \texttt{tol}$ **do**
        Update $\nabla \tilde{f}_1(\boldsymbol{y}_n)$ and η_n.
        Compute $y_{n+1} = y_n - \eta_n \nabla \tilde{f}_1(\boldsymbol{y}_n)$.
        $n = n + 1$.
    end while
    Set $m = m + 1$.
    Until the termination conditions are met.
    Return an optimized solution.
end while

3.4.2 Optimizing the UAV Height and Beamwidth

The second optimization sub-problem deals with finding the optimal height of the UAV and beamwidth of its antenna, it can be formulated as follows

$$\min_{H,\Theta} \quad f_2(H,\Theta) = \sum_{k=1}^{K} C_k \Theta^2 (D_k + H^2)^{\frac{\rho}{2}} \tag{3.16a}$$

$$\text{s.t.} \quad D_{\max} \leq H^2 \tan^2 \Theta, \tag{3.16b}$$

$$\Theta_{\min} \leq \Theta \leq \Theta_{\max}, \tag{3.16c}$$

$$H_{\min} \leq H \leq H_{\max}, \tag{3.16d}$$

where $C_k = \frac{1}{\beta_0 G_0}\left[2^R \exp\left(\frac{Q^{-1}(\varepsilon_k)}{\sqrt{m_k^*}}\right) - 1\right]$, $D_k = \|\boldsymbol{y}^* - \boldsymbol{x}_k\|^2$, and $D_{\max} = \max_k\{D_k\}$. For fixed beamwidth Θ, the function $f_2(H)$ is strictly increasing, thus its minimum will be obtained for minimum feasible H, which, according to constraints (3.16b) and (3.16d), occurs for $H^* = \max\left\{H_{\min}, \frac{\sqrt{D_{\max}}}{\tan\Theta}\right\}$. Therefore, for the first case $H^* = H_{min}$, the problem is easy to solve for Θ, but for the second case $H^* = \max\left\{H_{\min}, \frac{\sqrt{D_{\max}}}{\tan\Theta}\right\}$ the problem becomes difficult to solve due to the complicated expression of the objective function (3.16a), which requires an exhaustive search over Θ. As such, the value of H^* is computed for each Θ in the range $[\Theta_{\min}, \Theta_{\max}]$ and the final solution is obtained for the lowest objective value. It is to be noted that the exhaustive search is performed only for the Θ variable, i.e. it is not performed for all the possible combinations of H and Θ. Moreover, as mentioned earlier, H is evaluated as $H^* = \max\left\{H_{\min}, \frac{\sqrt{D_{\max}}}{\tan\Theta}\right\}$ for each value of Θ and then the objective function is calculated based on these two values. At each Θ and H, the radius constraint $(16b)$ given as $D_{\max} \leq H^2 \tan^2\Theta$ is checked.. If it is violated, the solution is discarded as an infeasible solution. The search is quasi-optimal in the sense that it is impossible to test all the values for Θ; this is an infinite set. However, it can be considered a good approximation, depending on the number of values tested. For the given problem, based on our empirical studies and inspired from our work in (Ranjha & Kaddoum, 2020a), we used 100 values between 0 and $\pi/2$ for Θ. Hence, the exhaustive search performed here is smart or partial exhaustive.

3.4.3 Optimizing the Blocklength

In the third sub-problem, which deals with finding the optimal blocklength for each T_{x_k} node, we assume that the constraints y, H, Θ, and ε_k are fixed, and thus the optimization problem can be reduced to

$$\min_{m_k} \quad f_3(m_k) = \sum_{k=1}^{K} E_k \exp\left(\frac{Q^{-1}(\varepsilon_k)}{\sqrt{m_k}}\right) + B \tag{3.17a}$$

$$\text{s.t.} \quad \sum_{k=1}^{K} m_k \leq M, \forall\, k \in \{1, \ldots, K\}, \tag{3.17b}$$

$$m_k \in \mathbb{N}, \forall\, k \in \{1, \ldots, K\}, \tag{3.17c}$$

where $E_k = 2^R B$, and $B = \frac{\Theta^{*2}(||\boldsymbol{y}^* - \boldsymbol{x}_k||^2 + H^{*2})^{\frac{\rho}{2}}}{\beta_0 G_0}$. Now, we define a function $u(x) = E_k \exp\left(\frac{Q^{-1}(\varepsilon_k)}{\sqrt{m_k}}\right) + B$ and compute it's first derivative as

$$u'(m_k) = -\frac{Q^{-1}(\varepsilon_k) E_k}{2\sqrt{m_k^3}} \exp\left(\frac{Q^{-1}(\varepsilon_k)}{\sqrt{m_k}}\right), \tag{3.18}$$

while it's second derivative is given by

$$u''(m_k) = \frac{Q^{-1}(\varepsilon_k) E_k}{4m_k^3} \exp\left(\frac{Q^{-1}(\varepsilon_k)}{\sqrt{m_k}}\right) \left[Q^{-1}(\varepsilon_k) + B_0\right], \tag{3.19}$$

where $B_0 = 3\sqrt{m_k}$ and from (3.19), we note that $u''(m_k) > 0$, which renders $f_3(m_k)$ a convex function. However, since $m_k \in \mathbb{N}$, the problem is not convex due to the non-convexity of the feasible region. As such, the problem is relaxed, where the constraint $m_k \in \mathbb{N}$ is replaced by $m_k \geq 0$. The Lagrangian associated with problem (3.17), is given by

$$\mathcal{L}(m_k, \lambda) = f_2(m_k) + \lambda \left(\sum_{k=1}^{K} m_k - M\right), \forall\, k \in \{1, \ldots, K\}, \tag{3.20}$$

and the KKT conditions are

$$\lambda = \frac{Q^{-1}\left(\varepsilon_k\right) E_k}{2\sqrt{m_k^3}} \exp\left(\frac{Q^{-1}\left(\varepsilon_k\right)}{\sqrt{m_k}}\right), \tag{3.21a}$$

$$\lambda \left(\sum_{k=1}^{K} m_k \leq M\right) = 0, \tag{3.21b}$$

$$\sum_{k=1}^{K} m_k \leq M, \forall\, k \in \{1, \ldots, K\}, \tag{3.21c}$$

$$\lambda \geq 0, \quad m_k > 0, \forall\, k \in \{1, \ldots, K\}. \tag{3.21d}$$

From equation (3.21a) one concludes that $\lambda > 0$, which from (3.21b) implies that (3.21c) holds with equality. Let us assume another function given as

$$v(x) = \frac{1}{2} Q^{-1}(\varepsilon_k) x^3 \exp\left(Q^{-1}(\varepsilon_k) x\right). \tag{3.22}$$

From (3.21a), we have

$$m_k = \left(\frac{1}{v^{-1}(\frac{\lambda}{E_k})}\right)^2. \tag{3.23}$$

Substituting (3.23) into (3.21c) yields

$$M = \sum_{k=1}^{K} \left(\frac{1}{v^{-1}(\lambda)}\right)^2. \tag{3.24}$$

Since, $v(x)$ is strictly increasing for $x > 0$, $v^{-1}(x)$ is also an increasing function for this interval, thus (3.24) has a unique solution $\lambda > 0$. After computing λ, the solution of m_k can be calculated using (3.23). It is noted that for the blocklength sub-problem, the variables must be continuous for the sub-problem to be convex. Such continuity can be obtained using the floor function. The solution obtained after applying the floor function is quasi-optimal because one is underestimating the blocklength. For instance, if we consider a UAV and two IoT devices, to allocate a total blocklength of $M = 200$ among them, where the solution is 99.5 and 100.5, the final solution will be 99 and 100. However, it would be more optimal if both are 100. Moreover,

Table 3.1 Time-complexity

Algorithm	**Time-complexity**
Proposed algorithm	$O\left(L\log_2\left(\frac{1}{\epsilon}\right)+L\frac{\Theta_{\max}-\Theta_{\min}}{\delta}+LKmn\right)$
FP	$O\left(L\log_2\left(\frac{1}{\epsilon}\right)+L\frac{\Theta_{\max}-\Theta_{\min}}{\delta}\right)$
FHBW	$O\left(L\log_2\left(\frac{1}{\epsilon}\right)+LKmn\right)$
FBL	$O\left(L\frac{\Theta_{\max}-\Theta_{\min}}{\delta}+LKmn\right)$
Exhaustive search	$O\left(h\times t\times Y^2\times M^K\right)$

Table 3.2 Set of chosen parameters for UAV-IoT communication system

Parameters	**Descriptions**	**Values**
K	Total number of IoT devices/users inside the circular cell	20
β_0	Channel power gain of UAV	58.5 dB
ρ	Path loss exponent of the environment	2
W	Bandwidth of the system	2 MHz
$\tau_{\max}$	Maximum transmit time interval for different blocklengths	1 ms
M	Total Blocklength of the system	2000
$\Theta_{\min}$	Minimum value of beamwidth of UAV antenna	0
$\Theta_{\max}$	Maximum value of beamwidth of UAV antenna	$\frac{\pi}{2}$
$H_{\min}$	Minimum value of UAV height	50 m
$H_{\max}$	Maximum value of UAV height	500 m
ε_k	Decoding error probability of an IoT device/user	10^{-5}
$\sum_{k=1}^{K}\varepsilon_k$	Sum decoding error probability of all IoT devices/users	$K\varepsilon_k$

if we round the result, we get 100 and 101, which violates the total blocklength constraint (3.17b), given as $\sum_{k=1}^{K} m_k \leq M, \forall\, k \in \{1,\ldots,K\}$, hence we utilize the floor function.

3.4.4 Proposed Algorithm

Based on the above analysis, the main algorithm to solve the problem (3.7) is presented in **Algorithm 3.2**. The central idea can be summarized as follows. Using the so-called *divide-and-conquer* rule, we divide a significantly complicated mathematical problem (3.7) into three relatively simpler sub-problems (3.8), (3.16), and (3.17) and proceed to effectively solving them by using perturbation-theory. As mentioned earlier, the overall problem is non-convex, and thus a global solution to the problem (3.7) is not guaranteed. Nonetheless, as each sub-problem is convex, we perform global optimization for each variable by fixing the other variables. At first, we generate an initial solution $S^0 = (H^0, \Theta^0, \boldsymbol{m}^0, \boldsymbol{y}^0)$. Afterward, the proposed algorithm solves each subproblem individually through a series of iterations and stops when the difference between two numerical solutions $S^n - S^{n-1}$ is below a given tolerance `tol`. An initial solution S^0 is provided to solve the first iteration, and the solution to each subproblem at each step is then used to solve the next subproblem. Lastly, we present all the aforementioned steps involved in each of the previous three sub-problems in **Algorithm 3.2**.

Algorithm 3.2 Perturbation-based iterative approach for computing sum uplink power

Initialize: Generate an initial solution and set it equal to S^0=$(H^0, \Theta^0, \boldsymbol{m}^0, \boldsymbol{y}^0)$.
Set $n = 1$, and a tolerance `tol`.
while $|S^n - S^{n-1}| > tol$ **do**
    Compute y^{n+1} solution of (3.8), with m^n and (H^n, Θ^n) using **Algorithm 3.1**.
    Compute (H^{n+1}, Θ^{n+1}) solution of (3.16), with m^n and y^{n+1}.
    Compute m^{n+1} solution of (3.17), with (H^{n+1}, Θ^{n+1}) and y^{n+1}.
    Compute final solution S^{n+1} as in (3.7).
    Set $n = n + 1$.
    Until the termination conditions are met.
    Return an optimized solution.
end while

3.5 Complexity Analysis of the Proposed and Benchmark Algorithms

In this section, we perform a complexity analysis of the proposed and benchmark algorithms. For problem (3.8), in each iteration n of the steepest descent method, the gradient $\nabla \tilde{f}_1(\boldsymbol{y}_n)$ and the step η_n are updated, costing $O(Kn)$. Adding the penalty method with m iterations, the total complexity of solving problem (3.8) is $O(Knm)$. Similarly, for problem (3.16), the cost of the exhaustive search through the interval $[\Theta_{\min}, \Theta_{\max}]$ depends on the step size δ chosen, providing a complexity of $O(\frac{\Theta_{\max}-\Theta_{\min}}{\delta})$. Lastly, to solve problem (3.17), the significant complexity lies in solving (3.24), which has a complexity of $O(\log_2\left(\frac{1}{\epsilon}\right))$ for the golden section method with accuracy ϵ. In the literature, besides the golden section method, there are various other optimization methods also that can be used for solving (3.24), including the bisection method and Newton method. Nonetheless, the optimization variable m_k is an integer value and such algorithms are not well-suited and well-tailored for use. Therefore, in this paper, we use the golden section method to search for the solution. The main idea behind the golden section method is to calculate the golden ratio, and values of two distinct points. These points can be viewed as upper and lower bounds of the function we are trying to minimize in an iterative manner within a certain domain. Then the region is narrowed down after each iteration by comparing these values in a bid to reach the optima. During the first iteration, these two aforementioned points a_1 and b_1 are selected as follows

$$\begin{aligned} a_1 &= \lfloor a_0 + \sigma\,(b_0 - a_0) \rfloor\,, \\ b_1 &= \lfloor a_0 + (1-\sigma)\,(b_0 - a_0) \rfloor\,, \end{aligned} \tag{3.25}$$

where a_0 and b_0 are the initial points, $\lfloor . \rfloor$ denotes the floor function which guarantees the obtained results lie within the feasible region, and σ is the reduction factor or the golden ratio, which narrows down the feasible region in each iteration of the algorithm. If $f\,(a_1) \leq f\,(b_1)$, the optimal solution lies within the interval $[a_1, b_0]$. Else, if $f\,(a_1) > f\,(b_1)$, then it must lie within the interval $[a_0, b_1]$. This process is repeated until convergence. Therefore, after solving (3.24), the total complexity of the proposed approach is $O\left(L\log_2\left(\frac{1}{\epsilon}\right) + L\frac{\Theta_{\max}-\Theta_{\min}}{\delta} + LKmn\right)$, where L indicates the number of iterations of **Algorithm 3.2**. We compare our solution to four benchmark

methods, namely the fixed position method with optimized height, beamwidth and blocklength (FP), the fixed height and beamwidth method with optimized position and blocklength (FHBW), the fixed blocklength method with optimized position, height and beamwidth (FBL), and the exhaustive method searching for the optimal solution for several combinations of the problem's variables (Exhaustive). The time complexity is $O\left(L\log_2\left(\frac{1}{\epsilon}\right)+L\frac{\Theta_{\max}-\Theta_{\min}}{\delta}\right)$ for FP, $O\left(L\log_2\left(\frac{1}{\epsilon}\right)+LKmn\right)$ for FHBW and $O\left(L\frac{\Theta_{\max}-\Theta_{\min}}{\delta}+LKmn\right)$ for FBL. Finally, the time complexity of the exhaustive search method is $O\left(h\times t\times Y^2\times M^K\right)$, where h denotes the number of points tested for H, t denotes the number of points tested for Θ, Y denotes the number of points tested for each dimension of $\boldsymbol{y}$ and M denotes the number of points tested for each m_k. These complexities are summarized in Table 3.1. It is noted here that for a problem with a large number of variables, a full, exhaustive search that checks all possible combinations of such variables is impractical due to computational limitations. According to (Ranjha & Kaddoum, 2020a), a more realistic and practical implementation of exhaustive search is the smart or partial exhaustive search where some variables are fixed, and others are not. In terms of optimality, such an exhaustive search can be termed as quasi-optimal. In contrast, the exhaustive search that is implemented by checking all possible combinations of variables is termed as truly optimal. Furthermore, the blocklength (integer variable) of the partial exhaustive search we implemented is fixed. In contrast, the search is done on the three other variables, including location, height, and a beamwidth of the UAV, which are all continuous. Moreover, we check all the combinations between the three variables and discard the infeasible ones. In the end, we choose the lowest one. The number of combinations is given by $N_c = Y_1 \times Y_2 \times H_1 \times T_1$, where Y_1, Y_2 represents position variable, H_1 height variable and T_1 beamwidth variable for the partial exhaustive search and the total number of combinations for a full, exhaustive search is $N_t = N_c \times M_1^K$, where K is the number of users and M_1 represents the blocklength variable. Once more, it is noted here that all of these notations indicate the number of values tested for each variable. Moreover, the search is not optimal; it depends on the blocklength value fixed and the number of combinations tested. Hence, based on the discussion above, we say that the partial exhaustive search implemented here is quasi-optimal in nature.

3.6 Simulation Results and Discussions

In this section, we present numerical results to show the validity of the proposed algorithm in solving the optimization problem (3.7). Here, we assume K IoT devices are uniformly distributed in a circular area of radius 100 m and set the system parameters as shown in Table 3.2. Fig. 3.2 compares the proposed approach ($\varepsilon_k = 10^{-5}$) with the aforementioned benchmark algorithms, i.e. FP, FHBW, FBL, and the exhaustive search. To quantify the uplink power savings we use the percentage difference between benchmark algorithms and the proposed algorithm as follows

$$\begin{aligned} \Delta_{signal} &= \left|\zeta_b - \zeta_p\right|, \\ \Delta_{\%} &= \frac{\Delta_{signal}}{\zeta_p}, \\ \Delta_{mean} &= \mu\left(\Delta_{\%}\right). \end{aligned} \tag{3.26}$$

where Δ_{signal} is the difference between the two signals, ζ_b is benchmark signal, ζ_p is the proposed signal, $\Delta_{\%}$ is the percentage difference by each element between the two signals, and Δ_{mean} is the mean percentage by all the elements of the resultant signal. Using (3.26), the percentage difference between FHBW and the proposed algorithm is 23.55%, between FP and proposed algorithm is 11.51%, and between FBL and the proposed algorithm is 4.79%. It can be observed that the proposed approach has a superior performance than FP, FHBW, and FBL, where the difference becomes more visible as the minimal rate demand increases. This is because the proposed algorithm jointly optimizes the position for the UAV, its height, beamwidth of its antenna, and the blocklength allocation for each IoT device inside the circular cell. For comparison purposes, the number of points for the exhaustive search are set to $h = t = Y = M = 2000$, and the exhaustive search method is run via **Algorithm 3.2**. Thereafter, it is observed that the solution obtained with the proposed method produces slightly higher sum power than the one obtained with the exhaustive search method, meaning that the proposed method approaches the global optimum solution at infinity. The time complexity of the proposed algorithm is lower than the exhaustive search, while it is higher than the other benchmark

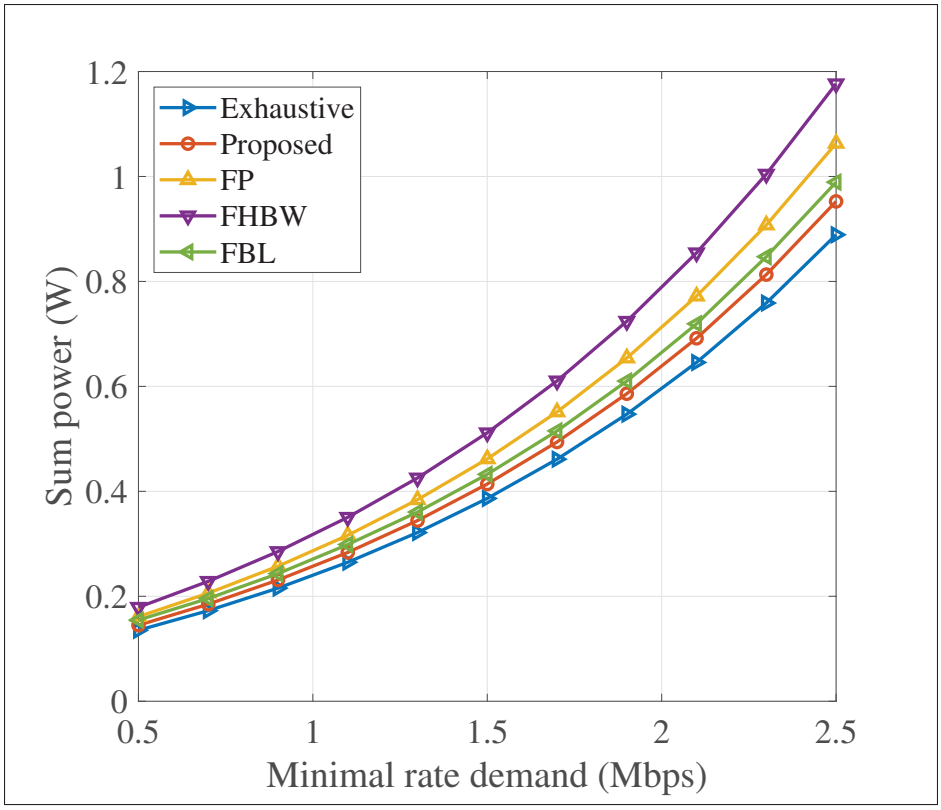

Figure 3.2 Sum power versus rate demand for the proposed algorithm compared to benchmark algorithms

algorithms as indicated in Table 3.1. Nevertheless, it provides higher uplink power saving than the other benchmark algorithms. Therefore, achieving green URLLC in the considered mobile UAV-assisted IoT network. The uplink power savings of the proposed algorithm are summarized in Table 3.3. For comparison purposes in Fig. 3.3, the sum power of Shannon's

Table 3.3 Uplink Power Savings and Underestimation

Benchmark Algorithm in Comparison	**Uplink Power Saving of the Proposed Algorithm**
FHBW	23.55%
FP	11.51%
FBL	4.79%
Shannon's formula	47.51% (underestimation)

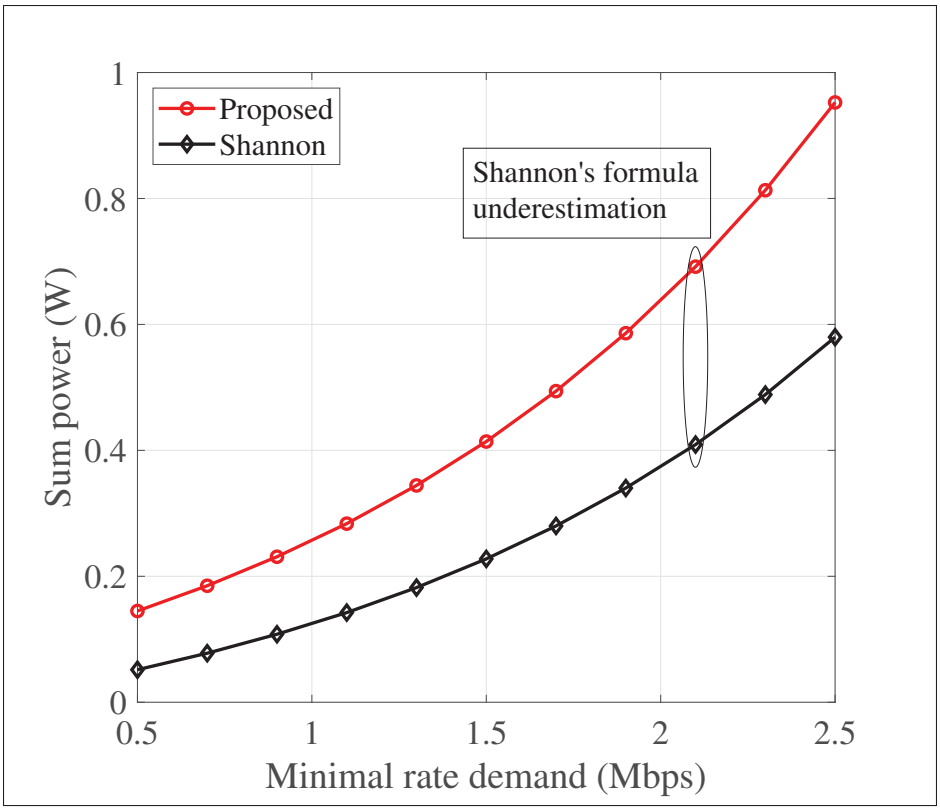

Figure 3.3 Sum power versus rate demand for the proposed algorithm compared to Shannon's formula

formula and the finite blocklength formula are presented. Using (3.26), the percentage difference between the aforesaid sum power of the finite blocklength formula and Shannon's formula is found to be 47.51%, which means it's sum power is notably lower than that of the proposed method. This highlights the fact that Shannon's formula significantly underestimates the sum power and therefore is not suitable for short-packets. The reason for this prominent gap is because Shannon's formula obeys the Strong law of large numbers, which is very accurate when the blocklength is infinite but it fails to account for short blocklengths. Moreover, it is worth mentioning that for a negligible decoding error, the difference between Shannon's formula and the finite blocklength formula will vanish if the blocklength tends to approach infinity. Additionally, the finite blocklength formula can be viewed as an extension of Shannon's formula with penalty coefficients in terms of channel dispersion, decoding error, and blocklength. Consequently, employing Shannon's formula can reveal inaccurate engineering insights into the

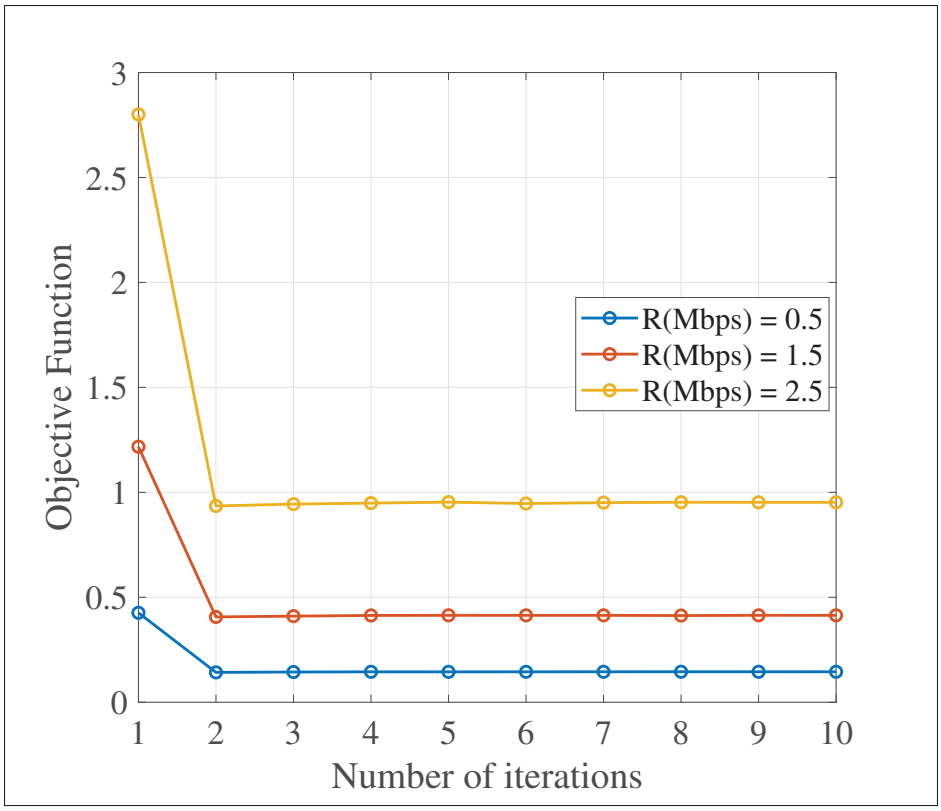

Figure 3.4 Convergence plot of the proposed approach for different rate demands

packet design and the system design for URLLC systems, especially when the blocklength is finite and URC is required. Fig. 3.3 also confirms the intuition that energy/power efficiency of a URLLC system is lower than a traditional communication system which is designed using Shannon's capacity formula. By observing Fig. 3.2 and Fig. 3.3, it is evident that the difference between benchmarks and the proposed algorithm increases as the minimal rate demand increases. For a higher value of minimal rate demand, the proposed algorithm's performance gain is bound to increase from Fig. 3.2 for different benchmarks; we have different sum uplink power savings ranging from 23.55% to 4.79%. It is to be noted that these sum power savings are obtained when the minimal rate demand ranges from 0.5 to 2.5 Mbps. For a higher range, higher sum uplink savings are obtained. Based on (Beyene, Jantti, Ruttik & Iraji, 2017; Mekki, Bajic, Chaxel & Meyer, 2019; Elarabi, Deep & Rai, 2015; Schulz, Matthe, Klessig, Simsek, Fettweis, Ansari, Ashraf, Almeroth, Voigt, Riedel, Puschmann, Mitschele-Thiel, Muller, Elste & Windisch,

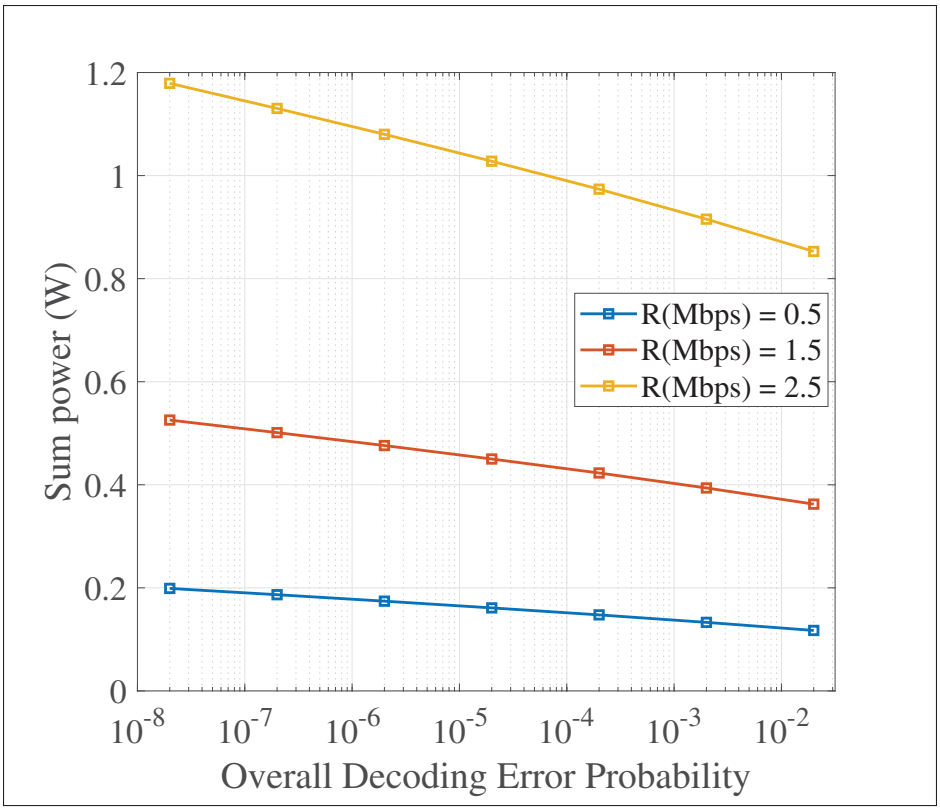

Figure 3.5 Sum power versus the overall decoding error for the different rate demands

2017), we consider such applications where IoT devices do not require a very high data rate. Hence, we defined the minimal rate demand by extensive empirical studies from 0.5 to 2.5 Mbps. In conclusion, we say that the proposed method's performance gain depends on the type of IoT application considered. Which, in turn, is dependent on the minimal rate demand. Here, the uplink power savings is greater than 10% for two benchmark algorithms and less than 10% for the last benchmark algorithm. Additionally, as mentioned earlier, Fig. 3.3 also demonstrates that Shannon's capacity formula underestimates the sum uplink power by 47.51% compared to the proposed algorithm making it an impractical choice for modelling URLLC systems with moderately low data rate requirements. The convergence plots of **Algorithm 3.2** are shown in Fig. 3.4, where the sum power is plotted for each iteration of the process for the three different rate demands. It is seen that a higher rate demand converges to a higher value of objective function, which intuitively makes sense. As evidenced, the algorithm guarantees a

quick convergences. This in-turn demonstrates the efficiency of the proposed algorithm. Finally, Fig. 3.5 shows the sum power of the proposed algorithm against the overall decoding error probability $K\varepsilon_k$. As the sum power tends to decrease, the total decoding error increases for the three above mentioned rate demands. In other words, to maintain a certain QoS for URLLC systems i.e, higher reliability, a higher amount of sum power is required.

3.7 Conclusion and Future Work

In this paper, we studied the quasi-optimization of the sum uplink power of IoT devices communicating to a UAV BS utilizing short data packets supported by URC. The study was performed under finite blocklength regime. The overall goal was to minimize the sum power to enable green URLLC communication for short packets with ultra-high reliability at the R_{x} node. To achieve this goal, we jointly optimized the UAV position, height, beamwidth, and resource allocation for each T_{x_k} node while also guaranteeing ultra-high reliability. Simulation results show that our proposed algorithm has a lower sum consumption than benchmark algorithms including FP, FHBW, and FBL and achieves a performance similar to the exhaustive search while maintaining lower time complexity. Moreover, we showed that Shannon's formula is not an optimum choice to model sum power consumption for short packets as it can significantly underestimate the sum power. Lastly, we also showed that the proposed algorithm allows ultra-high reliability for all the users, and converges rapidly. To conclude this paper, we studied the convoluted problem of quasi-optimization of the UAV position, the UAV height and beamwidth, and blocklength under the finite-blocklength regime for IoT applications with low data-rate requirements. We shall extend this work to consider the fairness problem for the devices that need to send more data in our future work. Lastly, in the next chapter, we shall study a joint design of passive beamforming, blocklength, and UAV positioning in hybrid UAV relay and RIS systems facilitating URLLC.

CHAPTER 4

URLLC FACILITATED BY MOBILE UAV RELAY AND RIS: A JOINT DESIGN OF PASSIVE BEAMFORMING, BLOCKLENGTH AND UAV POSITIONING

Ali Nawaz Ranjha[1] , Georges Kaddoum[1]

[1] Department of Electrical Engineering, École de Technologie Supérieure,
1100 Notre-Dame Ouest, Montréal, Québec, Canada H3C 1K3

Paper published in *IEEE Internet of Things Journal*, September 2020.

4.1 Abstract

Upcoming 5G networks need to support novel URLLC traffic that utilizes short packets. This requires a paradigm shift as traditional communication systems are designed to transmit only long data packets based on Shannon's capacity formula, which poses a challenge for system designers. To address this challenge, this paper relies on a UAV and a reconfigurable intelligent surface (RIS) to deliver short URLLC instruction packets between ground IoT devices. In this context, we perform passive beamforming of RIS antenna elements as well as non-linear and non-convex optimization to minimize the total decoding error rate and find the UAV's optimal position and blocklength. In this paper, a novel, polytope-based method from the class of DSM named NMS is used to solve the optimization problem based on its computational efficiency; in terms of lesser number of required iterations to evaluate objective function. The proposed approach yields better convergence performance than the traditional gradient descent optimization algorithm and a lower computation time and equivalent performance for the blocklength variable as the exhaustive search. Moreover, the proposed approach allows ultra-high reliability, which can be attained by increasing the number of antenna elements in RIS as well as increasing the allocated blocklengths. Simulations demonstrate the RIS's performance gain and conclusively show that the UAV's position is crucial for achieving ultra-high reliability in short packet transmission.

4.2 Introduction

URLLC is one of the three diverse features to be offered by upcoming 5G networks next to eMBB, and mMTC. URLLC is indispensable to support important use cases of mission-critical applications, including UAVs control information delivery, vehicle to vehicle (V2V) communications, self-driving cars, intelligent transportation, tactile internet, E-health, industrial automation, etc. (Bennis *et al.*, 2018). Such URLLC applications require deterministic communications with ultra-high reliability where the packet decoding error rates are of 10^{-9} or even lower, subject to the considered mission-critical application. Additionally, URLLC systems must resort to short packets in order to reduce latency; however, short packets have a negative impact on the coding gain of the channel. In this regard, Shannon's capacity bound is inapplicable for URLLC as it assumes that coding is performed over an infinite blocklength whereas URLLC operates under a finite blocklength regime. For finite blocklength, channel coding rate and capacity bounds were studied and reviewed in (Polyanskiy *et al.*, 2010).

UAVs are a futuristic technology that can be harnessed for military, public, and civil applications (Khan *et al.*, 2017a; Gupta *et al.*, 2015). Furthermore, recent technological advancements in the electronics, artificial intelligence, computer, and sensor technology fields have expanded the horizon of UAVs to include an array of diverse applications like wind estimation, traffic monitoring, and even remote sensing (Bekmezci *et al.*, 2013). In this regard, it is worth mentioning that natural disasters, e.g., hurricanes, can cause damages to communication infrastructures, including cell towers and LMRS repeaters. In such cases, there is an urgent need to deploy a temporary communication infrastructure in order to provide coverage as the existing cloud and communication infrastructure are not well designed to cope with such conditions (Karlsson *et al.*, 2018). Additionally, according to a public report from the Federal Aviation Administration (FAA), the drones fleet will be increased from 1.1 million vehicles in 2017 to 2.4 million units by 2022 (Fotouhi *et al.*, 2019). Since communication is an integral part of UAV systems, this will bring new business opportunities to cellular service providers. Recently, the 3GPP has investigated the potential use cases and has identified challenges and opportunities of utilizing UAVs as novel aerial user equipments (UE) (Meredith, 2017). An

essential finding of this report is LoS communication is made possible with the ground base station (BS) thanks to the high altitudes of aerial UE, which mitigates shadowing and signal blockage. Moreover, UAVs' maneuverability allows them to reposition themselves in real-time to support the communication needs dynamically. UAVs can become aerial relays between the transmitters and receivers. Notably, aerial DF relays can provide significant improvements to the communication throughput, channel gain, and the quality of service (QoS) compared to the conventional DF relay at a fixed position (Zeng, Zhang & Lim, 2016a). Therefore, both the research community and industry are very interested in the research and development of UAV-based communications.

RIS are comprised of an array containing RIS elements that are energy-efficient and cost-effective. Additionally, these elements can introduce some changes to the incident signal (Huang, Zappone, Alexandropoulos, Debbah & Yuen, 2019). As mentioned earlier, such changes can affect the phase, frequency, amplitude, or polarization. To this day, most of the available works in the literature (Guo, Liang, Chen & Larsson, 2019; Yu, Xu & Schober, 2019; Jung, Saad, Jang, Kong & Choi, 2020; Hu, Rusek & Edfors, 2017), consider a change in the phase shift only, which results in no transmit power consumption by the RIS. In general, RIS are beneficial in a radio environment where the direct communication link suffers from total blockage or has a bad signal quality. Therefore, buildings, ceilings, walls, and facades are the best places to mount RIS (Wu & Zhang, 2020). Moreover, RIS can provide phase alignment of signals arriving from different transmission paths by jointly adjusting phase shifts of all its antenna elements to focus on a target receiver. This process is called passive beamforming. Furthermore, RIS makes use of its antenna elements to reflect the arriving signals passively, which in turn provides low energy consumption, a clear advantage over traditional DF relaying (Li, Duo, Yuan, Liang & Di Renzo, 2020).

4.2.1 Related Work

Recently, a remarkable effort has been made by the research community to study the complicated problems of UAV path planning, positioning, node placement as flying relays or aerial BSs as

well as rate maximization for UAV networks (Zhan & Lai, 2019; Mozaffari *et al.*, 2017; Zhang *et al.*, 2018; Jiang & Swindlehurst, 2012; Yang *et al.*, 2018; He *et al.*, 2017; Sharma *et al.*, 2016; Chen *et al.*, 2017; Jiang *et al.*, 2019). Notably, the authors in (Zhan & Lai, 2019) studied the problem of energy minimization in IoT devices by considering a rotary-wing UAV and using the so-called *propulsion energy model*. To achieve this goal, the authors jointly optimized the power allocation, communication scheduling, and UAV trajectory design. Likewise, Mozaffari *et al.* in (Mozaffari *et al.*, 2017), considered a communication scenario between UAVs and IoT devices where UAVs serve as aerial base stations to collect data from the IoT devices. The authors sought to optimize uplink power control, UAV node placement, and UAV-IoT device association. The authors in (Zhang *et al.*, 2018) considered multi-hop UAVs to study the joint problem of power and trajectory optimization subject to UAV trajectory, collision avoidance, and transmit power constraints. In the recent work (Jiang & Swindlehurst, 2012), the authors considered the ground-to-air communication scenario between ground users and UAVs. They sought to optimize UAV heading to achieve enhanced uplink communication links with the ground users. The pioneering work in (Yang *et al.*, 2018) presented the joint optimization of UAV location, altitude, half-power beamwidth, allocated bandwidth, and transmit power. Similarly, in (He *et al.*, 2017), He *et al.* studied the convoluted problem of joint altitude and beamwidth optimization by tackling the so-called *travelling salesman problem*. In their approach, they considered three distinct scenarios between multi-users and a UAV flying base station. These scenarios were named UAV-enabled downlink broadcasting, downlink multicasting, and uplink multiple access. In (Sharma *et al.*, 2016), Sharma *et al.* studied the problem of optimal UAV node placement and distribution in heterogeneous networks to optimize the overall network delays. In (Chen *et al.*, 2017), Chen *et al.* studied UAV as flying relays and derived communication reliability measures in the form of total decoding error rate, total outage, and power loss. In (Jiang *et al.*, 2019), Jiang *et al.* considered a UAV-enabled wireless network and sought to optimize UAV trajectory and communication design. Nevertheless, in these studies (Zhan & Lai, 2019; Mozaffari *et al.*, 2017; Zhang *et al.*, 2018; Jiang & Swindlehurst, 2012; Yang *et al.*, 2018; He *et al.*, 2017; Sharma *et al.*, 2016; Chen *et al.*, 2017; Jiang *et al.*, 2019), the authors commonly employed Shannon's capacity formula for the design of communication systems and to perform rate analysis which possesses

both convexity and monotonicity (Xu *et al.*, 2016). Unfortunately, as mentioned earlier, URLLC systems use short packets, which does not obey the Shannon's capacity formula based on the Strong law of large numbers. Consequently, URLLC systems employ the finite blocklength formula, which does not possess the desired convexity and monotonicity properties as the aforementioned Shannon's capacity formula. Moreover, the finite blocklength capacity formula is neither convex nor concave for transmitting power and blocklength. Hence, it becomes a mathematically challenging task to perform convexity analysis in a bid to reach the optima (Ren *et al.*, 2020a). Moreover, only a few works in the literature considered URLLC, by examining the aforementioned finite blocklength formula as outlined in (Ren *et al.*, 2020b; Ren *et al.*, 2020b). In (Ren *et al.*, 2020b), the authors considered the problem of resource allocation for secure URLLC in mission-critical IoT scenarios. The authors aimed to optimize both the secrecy date rate and transmission power, where they employed security capacity formula under finite blocklength as the performance metric in their study. Similarly, in (Ren *et al.*, 2020b), the authors studied URLLC in the context of mission-critical industrial applications under the umbrella of the fourth industrial revolution (Industrial 4.0). In this context, the authors employed massive MIMO systems to provide a wireless connectivity similar to that of wired lines, and it has the advantage of providing deterministic communications thanks to its channel hardening effects. The authors aimed to optimize both the pilot and data power allocation by proposing novel low complexity algorithms to maximize the sum-rate in MRC and ZF receivers.

The idea of using intelligent surfaces for communications only recently came into limelight on the dissecting table of wireless communications researchers as outlined in (Liang *et al.*, 2019b; Wu & Zhang, 2019; He & Yuan, 2019; Basar *et al.*, 2019). The authors in (Liang *et al.*, 2019b) studied the fundamentals and implementation of LISA, a variant of intelligent surfaces. The authors aimed to provide necessary details of using LISA for backscatter communication as well as reflective relaying. In (Wu & Zhang, 2019), Wu *et al.* studied a communication scenario employing an intelligent surface assisting the communication between multiple users equipped with a single antenna and a multiantenna access point (AP). The authors sought to minimize the total transmit power at the AP subject to users' individual SINR constraints. In (He & Yuan,

2019), the authors studied and laid the general framework for estimating the channel between MIMO systems assisted by a LIM. Similarly, in (Basar *et al.*, 2019), the authors studied the theoretical performance limits of RIS and identified potential use cases for RIS in 5G and beyond wireless networks. In the seminal work (Pan *et al.*, 2020b), the authors considered an IRS at the cell boundary of multiple cells to mitigate inter-cell interference in downlink communication channels for cell-edge users. To accomplish the goal mentioned above, the authors jointly optimized the active precoding matrices at the BSs and the phase shifts of the IRS subject to the constrained BS's power and unit modulus to maximize the WSR of all users. Similarly, in (Pan *et al.*, 2020a), the authors invoked an IRS for improving the energy harvesting performance of a SWIFT system, where a multi-antenna assisted BS communicates with several multi-antenna aided information receivers (IRs). The authors aimed to jointly optimize the transmit precoding matrices of the BS as well as the passive precoding matrices of the IRS to maximize the WSR of IRs. Recently, in (Bai *et al.*, 2020), the authors considered an IRS to mitigate propagation induced impairments and fully exploit the benefit of MEC systems for offloading computational tasks. Moreover, this work considered single antenna devices for offloading part of their computational tasks to edge computing nodes employing a multi-antenna access point facilitated by an IRS. The authors formulated latency minimization problems in the framework of both single device and multi-device scenarios subject to the constraints of MEC capabilities and IRS phase shift design. In (Zhou *et al.*, 2020), the authors considered an IRS-aided MU-MISO system with an assumption of imperfect CSI. The authors aimed to minimize transmit power while guaranteeing each user's QoS requirements subject to unit modulus and rate constraints. Similarly, in (Zhou *et al.*, 2020), the authors studied the problem of robust beamforming based on the imperfect cascaded BS-IRS user channels at the transmitter end (CBIUT). Moreover, the transmit power minimization problems subject to worst-case rate constraints under the bounded CSI error model and the rate outage probability constraints under the statistical CSI error model were formulated. Regarding the research efforts dedicated to UAV and RIS assisted communications, issues like reliability and latency have drawn little to no attention. Presently, as outlined in (Ren *et al.*; Pan *et al.*, 2019; Ranjha & Kaddoum, 2020a; Ren *et al.*, 2020c; Wang, Wang, Pan, Xu & Aslam, 2020b), only a few works in the literature have

considered URLLC-enabled UAV communications, whereas a framework that considers URLLC facilitated by both UAV and RIS is not available in the open technical literature. The problem of the AADR for URLLC-enabled UAV systems is studied in (Ren *et al.*). The authors used the so-called *Gaussian-Chebyshev quadrature* method to derive an expression of achievable data rate in a system considering short packet delivery from a ground station to a UAV. In (Pan *et al.*, 2019), the authors studied the problem of joint blocklength allocation and UAV location to enable ultra-high reliability in single-hop UAV relay systems. Most recently, we studied the problem of joint distance and blocklength optimization for URLLC-enabled multi-hop UAVs links for an IoT transmitter/receiver pair in (Ranjha & Kaddoum, 2020a). We employed the so-called *semi-empirical* approach to perform quasi-optimization and showed that the system supported ultra-high reliability for short packets. In (Ren *et al.*, 2020c), the authors studied URLLC enabled by a UAV serving as a DF relay system. The authors proposed low complexity algorithms to jointly optimize UAV placement and power in a three-dimensional (3-D) channel to guarantee a minimum decoding error probability. Moreover, the authors demonstrated that AF relays benefit from low signal processing delays compared to their DF counterparts. In (Wang *et al.*, 2020b), the authors studied RIS assisted UAV communications by considering fairness and sum-rate maximization of all users via jointly optimizing the UAV's trajectory and the phase shifts of RIS reflecting elements. Nevertheless, in (Ren *et al.*; Pan *et al.*, 2019; Ranjha & Kaddoum, 2020a; Ren *et al.*, 2020c; Wang *et al.*, 2020b), the mobility of the UAV is rather fixed and the severe degradation of the LoS links caused by the UAV's immobility in operational areas is not considered, which limits the insights provided by these works. Additionally, to design realizable, workable, and robust URLLC-systems assisted by both UAV and RIS systems, it is essential to jointly perform passive beamforming and optimize the resource allocation, which includes blocklength and UAV positioning under the given requirements of reliability and latency.

4.2.2 Novelty and Contributions

Regardless of the research efforts studying URLLC, UAV-enabled communication, RIS, and the fusion of UAV enabled URLLC, a study on the performance analysis of a URLLC network

assisted by both UAVs and RIS under finite blocklength regime is still missing. It is worth mentioning here that this analysis is imperative as it will lay the foundation of supporting URLLC assisted by UAVs and RIS in 5G and beyond networks. To fill this gap, we study the ultra-high reliability in mobile UAV relaying and RIS communication systems. The main contributions of this paper can be summarized as follows:

- We study and formulate the problem of ultra-high reliability in URLLC assisted by a mobile UAV and RIS in a short packet transmissions communication scenario. Furthermore, our objective function is non-convex, which makes it a cumbersome and tedious mathematical problem. Afterward, we employ a polytope-based method from the class of direct search methods (DSM) named Nelder-Mead Simplex (NMS) to solve our non-convex and non-linear problem. It is to be noted that NMS is chosen because of its inherent ability to evaluate the objective function in $n + 1$ iterations, which is relatively lower than other DSM requiring anywhere from $2n$ to 2^n evaluations of the objective function to complete the search.
- We show that the proposed approach yields better convergence performance than traditional optimization approaches, like the gradient descent. It also has a superior computation time and better performance for the blocklength variable compared to the exhaustive search. Additionally, the proposed approach allows ultra-high reliability, where we show the variation of the decoding error rate with respect to (w.r.t.) the number of antenna elements in RIS as well as the allocated blocklength.
- Lastly, simulation results show the performance gain of RIS and demonstrate that the UAV's position is crucial for achieving ultra-high reliability for short packets.

4.3 System Model and Problem Formulation

4.3.1 System Model

We consider a downlink communication scenario between the ground transmitter, UAV, RIS, and ground user, all of which are placed in a three-dimensional cartesian coordinate system, as shown in Fig. 4.1.

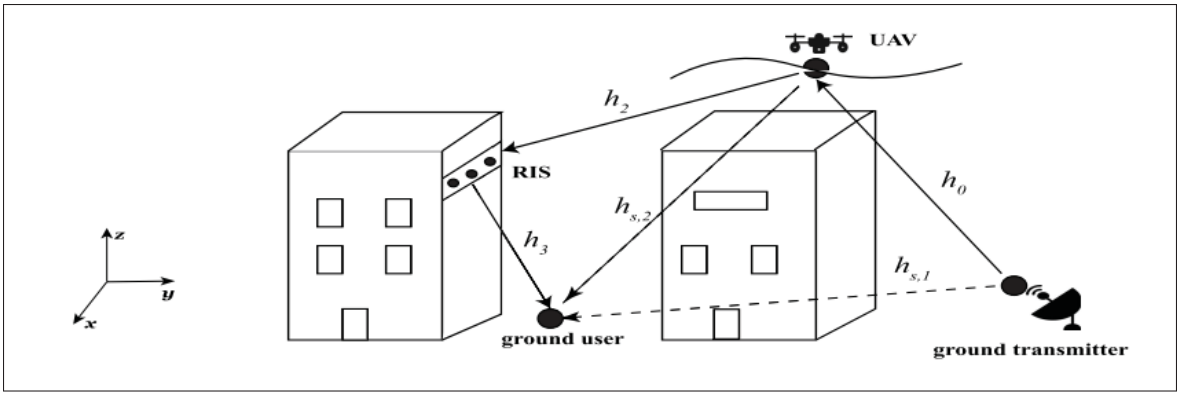

Figure 4.1 Illustration of a URLLC system facilitated by a mobile UAV relay and a RIS

The coordinates of the ground transmitter are given by $\vec{g} = (x_g, y_g, z_g)^T$, whereas the ground user coordinates are $\vec{u} = (x_u, y_u, 0)^T$. The UAV, which serves as a DF relay, flies at a fixed altitude denoted by z and has coordinates $\vec{a} = (x, y, z)^T$. Additionally, the ground transmitter and receiver are a pair of IoT devices. Thus, the transmitter produces short packets, each of size N bits, that must be communicated reliably over the UAV and the RIS to the ground user. Since the packets are short, they are processed in a finite blocklength regime. Packet loss signifies a violation of QoS for the ground user in the operating area, located between two buildings. Hence, the present UAV-RIS communication system requires ultra-high reliability. Moreover, we assume that the UAV's position is fixed during the transmission of a packet from UAV to RIS and ground user. This is a reasonable assumption since a considerable UAV position change would require several seconds, which is considerably longer than a typical transmission event. Inherent UAV mobility characteristics impose a mobility constraint on its position $\vec{a}$ and on its linear velocity $\dot{\vec{a}}$. Practically, the UAV cannot go too far from its initial position since it would cause connectivity interruptions to the ground transmitter. We can express the limited spherical range of motion as $\|\dot{\vec{a}}\|_2 < D$, where D is the region radius. As mentioned before, the first derivative of the UAV's position known as linear velocity is limited due to the rotational speed of its rotors and the maximal angle of attack. This can be expressed as $\|\vec{a} - \vec{a}_0\|_2 < V_{\max}$, where $V_{\max}$ is the maximal velocity and $\vec{a}_0$ is the mean location of the UAV. Further, we assume that the UAV and the user are equipped with a single omnidirectional antenna, while the RIS is

equipped with a uniform linear array (ULA) of M reflecting elements with a controller for the phase shift of each element. The phase shift matrix of the RIS is given as

$$M_\theta(t) = \text{diag}(e^{j\theta_1(t)}, \ldots, e^{j\theta_m(t)}), \tag{4.1}$$

where θ_m is the phase shift of the m^{th} RIS element. The RIS position is denoted with coordinates $\vec{r} = (x_r, y_r, z_r)^T$, which is constant over time. Moreover, the urban environment introduces scattering to the radio signal before it arrives at the receiver, which implies that multipath propagation models have to be used. Thus, here, we consider the Rayleigh fading model. Therefore, the channel gain between the ground transmitter and the UAV at position $\vec{a}$ is modeled as a line-of-sight (LoS) channel given as

$$h_0(t) = \sqrt{\rho d_0^{-2}(t)}, \tag{4.2}$$

where ρ is the ground transmitter-to-UAV path loss at a reference distance of 1 m, and $d_0(t) = \|\vec{g} - \vec{a}\|_2$ is the Euclidean distance between these nodes. It is assumed that the ground transmitter is located at a high position at z_g. In the present investigation, we assume that direct links between the user and UAV or ground transmitter are blocked, yet we still have to account for the scatters between them. Therefore, the distance from the ground user to the UAV is denoted by $s_1 = \|\vec{u} - \vec{a}\|_2$ and the distance from the ground user to the ground transmitter is denoted by $s_2 = \|\vec{u} - \vec{g}\|_2$, which is assumed to be fixed for the blocklength transmission period. The channel gains between the UAV and the ground user and the ground transmitter and the ground user are respectively given as

$$h_{s,2} = \sqrt{\rho s_2^{-k_2}}\tilde{h}_2, \; h_{s,1}(t) = \sqrt{\rho s_1^{-k_1}(t)}\tilde{h}_1, \tag{4.3}$$

where $\tilde{h}_1$ and $\tilde{h}_2$ represent the random scattering components modeled as circularly symmetric complex random variables with zero-mean and unit-variance, k_1 and k_2 are the respective path loss exponents. Assuming no correlation between random scatters from the UAV and ground transmitter $E[\tilde{h}_1\tilde{h}_2] = 0$, the channel gain between the UAV at position $\vec{a}$ and the one

dimensional RIS with M elements at position $\vec{r}$ is also modeled as a LoS channel accounting for the current phase shift of a selected RIS reflective element with an index $m = 0, \ldots, M-1$. The channel gain is given as

$$h_2(t,m) = \sqrt{\rho d_2^{-2}(t)} e^{-j\frac{2\pi}{\lambda} m d \phi_2(t)}, \tag{4.4}$$

where $d_2 = \|\vec{r} - \vec{a}\|_2$ is the distance between the UAV and the RIS array, λ is the carrier wavelength, $\phi_2 = \frac{\text{Proj}_{xy}(\vec{r}-\vec{a})}{d_2}$ is the cosine of the angle of arrival of the signal from the UAV to the RIS, $\text{Proj}_{xy}(\cdot)$ is the projection operator eliminating the vertical coordinate, and d is the antenna separation distance. The channel gain between the RIS at position $\vec{r}$ and the ground user at position $\vec{u}$ is appropriately modeled as a Rician fading channel, which accounts for the direct LoS and indirect non-LoS components due to scatters. Here, the channel gain also depends on the total number of selected RIS elements. The channel gain is given as

$$h_3(t,m) = \underbrace{\sqrt{\rho d_3^{-k_3}(t)}}_{\text{path loss}} \underbrace{\left(\sqrt{\frac{\beta}{1+\beta}} h_3^{\text{LoS}}(m) + \sqrt{\frac{1}{1+\beta}} \tilde{h}_3^{\text{nLoS}} \right)}_{\text{array response and small-scale fading}}, \tag{4.5}$$

where $d_3 = \|\vec{u} - \vec{r}\|_2$ is the distance between the ground user and the RIS array, which is fixed for the blocklength transmission period, $h_3^{\text{LoS}}(m) = e^{-j\frac{2\pi}{\lambda} m d \phi_3}$ is the deterministic LoS component and $\tilde{h}_3^{\text{nLoS}}$ is the non-deterministic LoS component modeled as circularly symmetric complex random variables with zero mean and unit variance, β is the Rician fading factor, and k_3 is the path loss exponent. Moreover, the complex vector $h_3(t,m)$ can also be expressed as follows

$$h_3(t,m) = |h_3(t)| e^{j\omega_m(t)}, \tag{4.6}$$

where $|h_3(t)|$ and $[0; 2\pi)$ represent the magnitude and phase angle of the m^{th} element of the complex vector $h_3(t,m)$, respectively. In this work, we assume that the CSI is obtained based on existing channel estimation techniques for RIS assisted channels, as outlined in (He & Yuan, 2019; Li *et al.*, 2020). Furthermore, we assume that the signal processing capability at the RIS is enough to obtain accurate CSI. According to the transmission power summation principle, the

total downlink channel gain from the ground transmitter to the ground user becomes

$$\begin{aligned} h(t) &= h_{s,1}(t) + h_{s,2} + \sum_{m=0}^{M-1} h_3^*(t,m) h_2(t,m) h_0(t) e^{j\theta_m}, \\ &= h_{s,1}(t) + h_{s,2} + \Phi(t,\theta_m), \end{aligned} \tag{4.7}$$

where the $\Phi(t,\theta_m)$ term contains the LoS channel gains between the ground transmitter, UAV, RIS, and ground user. As mentioned earlier, the phase shifts of each of the RIS elements denoted by θ_m can be adjusted to achieve phase alignment of the signals from different transmission paths at a desired receiver to perform passive beamforming.

4.3.1.1 Coherence and Maximal Channel Gain Conditions

Here, we investigate how to maximize the coherence and channel gain. We start by examining expression (4.7) of the total channel gain. Note that the position of the ground transmitter and the ground user are assumed to be fixed. Then, let us fix the UAV position $\vec{a}$ and observe the contribution of the RIS array

$$\begin{aligned} \Phi(\theta_m) &= \sum_{m=0}^{M-1} h_3^*(m) h_2(m) h_0 e^{j\theta_m}, \\ &= \frac{\rho \sum_{m=0}^{M-1} |h_3| e^{j(\theta_m - \omega_m - \frac{2\pi}{\lambda} m d \phi_2)}}{d_2 d_0}. \end{aligned} \tag{4.8}$$

If the signals from different antenna elements of the RIS array arrive coherently at the ground user, then it is clear that the signal power will be maximized. Thus, the coherence condition is given as

$$\theta_m - \omega_m - \frac{2\pi}{\lambda} m d \phi_2 = \theta, \tag{4.9}$$

where θ is a fixed constant. To further improve the coherence, we would require the scatter gains $h_{s,1}$ and $h_{s,2}$ to have the same phase, i.e. $\text{Arg}(\tilde{h}_1) = \text{Arg}(\tilde{h}_2) = \theta$. However, since $\tilde{h}_1$ and $\tilde{h}_2$ are

both random variables, such a requirement is infeasible. Instead, we require

$$\theta = \begin{cases} \text{Arg}(\tilde{h}_1), \ s_1 < s_2^{k_1-k_2} \\ \text{Arg}(\tilde{h}_2), \ s_1 > s_2^{k_1-k_2} \end{cases} \tag{4.10}$$

Since the distance from the ground user to the ground transmitter is fixed, the value of θ depends on the distance from the ground user to the UAV. If the UAV is considerably closer to the ground user than the ground transmitter, we have $\theta = \text{Arg}(\tilde{h}_1)$. In this case the contribution of the RIS to the gain becomes

$$\Phi = \frac{\rho e^{j\theta} \sum_{m=0}^{M-1} |h_3|}{d_2 d_0}. \tag{4.11}$$

Hence, the expression for the total channel gain with coherence condition becomes

$$h = h_{s,1} + h_{s,2} + \Phi = \frac{\sqrt{\rho}\tilde{h}_1}{s_1^{0.5k_1}} + \frac{\sqrt{\rho}\tilde{h}_2}{s_2^{0.5k_2}} + \frac{\rho e^{j\theta} \sum_{m=0}^{M-1} |h_3|}{d_2 d_0}. \tag{4.12}$$

4.3.2 Problem Formulation

In this subsection, we formulate our problem according to the coherence and maximal channel gain conditions mentioned above. Then, we define the two SNR values given as

$$\gamma_1(\vec{a}) = \frac{P_1 h_0(x, y, z)}{\sigma^2}, \gamma_2(\vec{a}, \theta_m) = \frac{P_2 h(x, y, z, \theta_m)}{\sigma^2}, \tag{4.13}$$

where the SNR value $\gamma_1(\vec{a})$ contains the channel gain h_0 between the ground transmitter and the UAV. In contrast, the second SNR value $\gamma_2(\vec{a}, \theta_m)$ includes the total channel gain with coherence condition denoted by h and indicated in (4.12). It is noted here that $\gamma_1(\vec{a})$ is dependent on the UAV position $\vec{a}$, whereas $\gamma_2(\vec{a}, \theta_m)$ is dependent on the UAV position $\vec{a}$ as well as the phase shifts of the RIS elements controlled by θ_m. Moreover, P_1 and P_2 represent the transmission power of the aforementioned nodes, and σ^2 is the environmental noise variance. It is worth mentioning here that due to spatial diversity corresponding to an increase in the number of antenna elements in the RIS array also corresponds to the maximization of the SNR $\gamma_2(\vec{a}, \theta_m)$

and total channel gain at the ground user, as evidenced by (12). In addition, the phase shifts introduced by the RIS elements have to be calculated according to the coherence condition (4.9). Moreover, according to (Polyanskiy *et al.*, 2010), we know that to transmit a short command packet of N bits using blocklength $L_k, \forall\ k \in \{1, 2\}$, the following equations for individual channel decoding error rates are applicable

$$\begin{aligned} \varepsilon_1(x, y, z, L_1, N) &= Q(f_1(\gamma_1, L_1, N)), \\ \varepsilon_2(x, y, z, L_2, \theta_m, N) &= Q(f_2(\gamma_2, L_2, N)), \end{aligned} \tag{4.14}$$

where Q represents the Gaussian Q-function [1], L_1 and L_2 are the respective blocklengths on each path, and N is the information content of the encoded message. It is to be noted that according to (Andrews, 1998), the Q-function is monotonically decreasing. Moreover, the decoding error rate of the two paths is dependent on the function $f_k, \forall\ k \in \{1, 2\}$ defined as

$$\begin{aligned} f_1(\gamma_1, L_1, N) &= \ln(2)\sqrt{\frac{L_1}{v_1}}\left(\log_2(1+\gamma_1) - \frac{N}{L_1}\right), \\ f_2(\gamma_2, L_2, N) &= \ln(2)\sqrt{\frac{L_2}{v_2}}\left(\log_2(1+\gamma_2) - \frac{N}{L_2}\right), \end{aligned} \tag{4.15}$$

where $v_1 = 1 - (1+\gamma_1)^{-2}$, and $v_2 = 1 - (1+\gamma_2)^{-2}$ denote the channel dispersions. The total decoding error rate over the link between the ground transmitter and the ground user becomes

$$\varepsilon_t = \varepsilon_1 + (1 - \varepsilon_1)\,\varepsilon_2 = \varepsilon_1 + \varepsilon_2 - \varepsilon_1\varepsilon_2. \tag{4.16}$$

The simultaneous error $\varepsilon_1\varepsilon_2$ takes small values and can therefore be ignored. Therefore, under the present URLLC scenario, (4.16) reduces to

$$\varepsilon_t \triangleq \varepsilon_1 + \varepsilon_2. \tag{4.17}$$

[1] As usual, $Q(p) = \frac{1}{\sqrt{2\pi}}\int_p^\infty e^{-\frac{s^2}{2}}ds$.

Ultra-high reliability can be enabled by performing passive beamforming for each of the phase shifts introduced by the m^{th} RIS element represented by θ_m, and by jointly optimizing the overall latency constraint L_{tot} and UAV position $\vec{a}$. Moreover, L_{tot} is divided into two parts L_1 and L_2. L_1 is allocated between the ground transmitter and the UAV, L_2 is allocated between the UAV and the RIS. Since the RIS is a passive element, L_2 is also allocated between the RIS and the ground user. Hence, the total blocklength L_{tot} is given by

$$L_{\text{tot}} = W \times T_{\max}, \tag{4.18}$$

where W is the system bandwidth and $T_{\max}$ is the maximum transmit time interval for the two different blocklengths. Finally, the optimization problem is formulated as

$$\min_{L_1, L_2, x, y, z, \theta_m} \quad \varepsilon_t \tag{4.19a}$$

$$\text{s.t.} \quad 0 \leq \theta_m(t) \leq 2\pi, \ \forall\, t, m, \tag{4.19b}$$

$$L_1 + L_2 = L_{\text{tot}}, \ L_1, L_2 \in \mathbb{Z}, \tag{4.19c}$$

$$\varepsilon_k \leq \epsilon_1, \forall\, k \in \{1, 2\}, \tag{4.19d}$$

$$\|\vec{a} - \vec{a}_0\|_2 \leq D, \tag{4.19e}$$

where constraint (4.19d) guarantees ultra-high reliability for each of the two individual decoding error rates. Moreover, D in (4.19e) is the operation region of the UAV around its initial position $\vec{a}_0$. The flight envelope of the UAV is represented as a spherical region with a center $\vec{a}_0$ and a radius D. Furthermore, it is noted that (4.19) is a cumbersome and tedious mathematical problem because the objective function is jointly non-convex and non-linear w.r.t. constraints (4.19c), (4.19c), (4.19d), and (4.19e). Finally, here, objective function (4.17) is the summation of the composition of two functions, i.e. $f(g_1(a_1, b_1, c)), f(g_2(a_2, b_2, c))$. Thus, the DSM are the methods of choice for the given problem (4.19) because the application of derivative-based techniques, i.e. gradient descent, is difficult and would lead to an inefficient solution.

4.4 Proposed Algorithm

There are numerous DSM available in the open technical literature; however, they require anywhere from $2n$ to 2^n evaluations of the objective function to complete the search. A typical example is the Pattern Search (PS) algorithm requiring $2n + 1$ evaluations, including the central point and 2 points in each search dimension. Meanwhile according to (Lewis, Torczon & Trosset, 2000; Spendley, Hext & Himsworth, 1962), a simplex method would require $n + 1$ evaluations of the objective function to complete the search. Hence, it is computationally more efficient than the algorithms described above. Consequently, the NMS method is applied to find the minimum of the scalar objective function $\varepsilon_t(\vec{X})$ of several variables. This method is often applied to nonlinear optimization problems, where it uses a special polytope of $n + 1$ vertices denoted as $\vec{X}_i$ in n dimensions and approximates a local optimum of a problem with n variables. Moreover, if we optimize w.r.t. the UAV position in a three dimensional space and the blocklength L_{tot}, i.e. $\vec{X}_i = (\vec{a}_i, L_{tot,i})$, the number of polytope vertices is four, which gives us a pyramidal simplex. We assume that the vertices are sorted in an ascending order, i.e. $\varepsilon_t(\vec{X}_1) < \varepsilon_t(\vec{X}_2) < \ldots < \varepsilon_t(\vec{X}_{n+1})$, and that the last vertex $\varepsilon_t(\vec{X}_{n+1}) = \max\left(\varepsilon_t(\vec{X}_i)\right)$. The pseudocode of the algorithm is shown in **Algorithm 4.1**. In the NMS method, $\vec{X}_c$ denotes the center point, $\vec{X}_i$ denotes simplex vertices, $\vec{V}$ refers to the vector between the center point and the worst solution (which is $\vec{X}_5$ after reordering), $\vec{T}$ denotes reflected worst point w.r.t. the center, b denotes the minimal objective function value, and $\vec{U}$ denotes exponential expansion in the direction of the reflection vector. The algorithm begins with the computation of the reflected point with the **reflect(·)** method defined as

$$\vec{T} = \vec{X}_c + \alpha(\vec{X}_c - \vec{X}_5), \quad \alpha > 0. \tag{4.20}$$

If the reflected point is better than the second worst point, but not better than the best point, we obtain a new simplex by replacing the worst point $\vec{X}_5$ by the reflected point $\vec{T}$. Otherwise, if the reflected point is the best point so far, i.e. $\varepsilon_t(\vec{T}) < \varepsilon_t(\vec{X}_1)$, then we compute the expanded point with the **expand(·)** method defined as

$$\vec{U} = \vec{X}_c + \zeta(\vec{T} - \vec{X}_c), \quad \zeta > 1. \tag{4.21}$$

Algorithm 4.1 NMS polytope-based DSM for minimizing ε_t by performing passive beamforming by θ_m and optimizing for blocklength L_{tot}, and UAV position $\vec{a}$

Initialize $\vec{X}_1 = (\vec{a}, L_{\text{tot}})$ $\vec{X}_2 = (\vec{a}, L_{\text{tot}}) + (\delta_{a,x}, 0)$ $\vec{X}_3 = (\vec{a}, L_{\text{tot}}) + (\delta_{a,y}, 0)$, $\vec{X}_4 = (\vec{a}, L_{\text{tot}}) + (\delta_{a,z}, 0)$ $\vec{X}_5 = (\vec{a}, L_{\text{tot}}) + (0, \delta_L)$
Calculate θ_m according to (4.9), and $\gamma_1(\vec{a})$ and $\gamma_2(\vec{a}, \theta_m)$ according to (14)
Reorder $\vec{X}_i$ such that $\varepsilon_t(\vec{X}_i) < \varepsilon_t(\vec{X}_{i+1})$
Set $\vec{X}_c$ = **center**$(\vec{X}_1, \ldots, \vec{X}_5)$, `tol`
Set $\varepsilon_{t,\max} = \varepsilon_t(\vec{X}_5))$
Set $\vec{V} = \vec{X}_c - \vec{X}_5$
Set $\vec{T}$ = **reflect**$(\vec{X}_5, \vec{V})$
while $|\varepsilon(\vec{X}_n) - \varepsilon(\vec{X}_{n-1})| <$ `tol` **do**
    if $\varepsilon_t(\vec{T}) < \varepsilon_t(\vec{X}_5)$ **then**
        if $\varepsilon_t(\vec{T}) < b$ **then**
            $b = \varepsilon_t(\vec{T})$
        end if
        $\vec{U}$ = **expand**$(\vec{T}, \vec{V})$.
        if $\varepsilon_t(\vec{U}) < b - \eta \times l$ ***and*** $l > 0$ **then**
            $\vec{X}_5 = \vec{U}$.
            $b = \varepsilon_t(\vec{U})$.
            $l = l - 1$.
        else
            $\vec{X}_5 = \vec{T}$.
        end if
    else
        $\vec{X}_5$ = **contract**$(\vec{X}_5, \vec{V})$.
        if $\varepsilon_t(\vec{X}_{next}) < b$ **then**
            $b = \varepsilon_t(\vec{X}_{next})$.
        end if
        $l = l + 1$.
    end if
end while

If the expanded point is better than the reflected point ($\varepsilon_t(\vec{U}) < \varepsilon_t(\vec{T})$), then we obtain a new simplex by replacing the worst point $\vec{X}_5$ with the expanded point $\vec{U}$. Otherwise, we obtain a new simplex by replacing the worst point $\vec{X}_5$ with the reflected point $\vec{T}$. Here it is certain that

$\varepsilon_t(\vec{T}) \geq \varepsilon_t(\vec{X}_5)$. We compute the contracted point with the **contract(·)** method defined as

$$\vec{C} = \vec{X}_c + \xi(\vec{X}_5 - \vec{X}_c), \quad 0 < \xi \leq 0.5. \tag{4.22}$$

If the contracted point is better than the worst point, i.e. $\varepsilon_t(\vec{C}) < \varepsilon_t(\vec{X}_5)$, then we obtain a new simplex by replacing the worst point $\vec{X}_5$ with the contracted point $\vec{C}$. As outlined in the pseudo-code, at the start, an initial simplex is provided, and the NMS method solves the problem (20) through a series of iterations and stops when the difference between two numerical solutions $\varepsilon(\vec{X}_n)) - \varepsilon(\vec{X}_{n-1})$ is below a given tolerance `tol`. It is to be noted here that NMS is a derivative-free optimization technique where gradient descent commonly employs derivatives. Therefore, we make a comparison of the most popular derivative-free and derivative-based optimization techniques in this work, where Fig. 4.2 demonstrates the convergence of the iterative procedure to the optimal solution for a blocklength of 100 symbols and 100 RIS elements in the antenna array for both Nelder-Mead and gradient-descent methods. It can be seen that for Nelder-Mead, the solution is achieved in four main slopes, taking approximately 135 iterations. Moreover, the number of iterations for the Nelder–Mead is higher than in alternative optimization methods like gradient descent, as shown in Fig. 4.2. However, the presented method performs better when the initial conditions are unknown, as evidenced in Fig. 4.2, the gradient-descent method converges to a higher value of the total decoding error rate. Hence, based on NMS's superior performance, it is chosen over the gradient descent method for solving the optimization problem (20).

A particular implementation of the NMS algorithm depends on the selection of convergence or termination criteria and the values of the parameters α, η, ξ, ζ, δ_x, δ_y and δ_z. According to (Singer, 1999), the complexity analysis of the NMS algorithm is still in development, and there is no general convergence theory to calculate the number of iterations required to satisfy an accuracy constraint given in a termination test. Nonetheless, for the problem (4.19) the

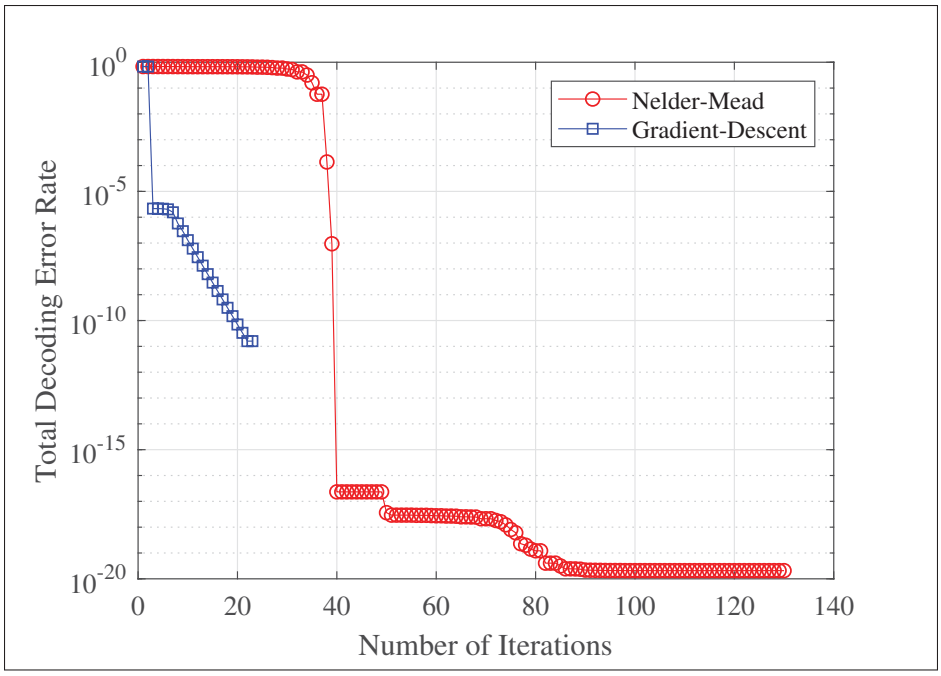

Figure 4.2 Objective function minimization for blocklength of 180 symbols and 80 RIS elements

superiority of NMS over the exhaustive search in terms of computation time[2] is demonstrated in Table 4.1.

Table 4.1 Computation Time

Algorithms	**Computation Time**
NMS	6.3949 seconds
Exhaustive Search	2131.7790 seconds

Moreover, to further solidify the choice of NMS, we plot the performance of NMS against exhaustive search. As shown in Fig. 4.3, the performance of NMS is almost equivalent to the said exhaustive search for different values of the blocklength.

[2] Simulations are performed on a PC with 2.6 GHz Intel Core i7 processor and 16 GB of RAM (DDR4) running MATLAB R2018a.

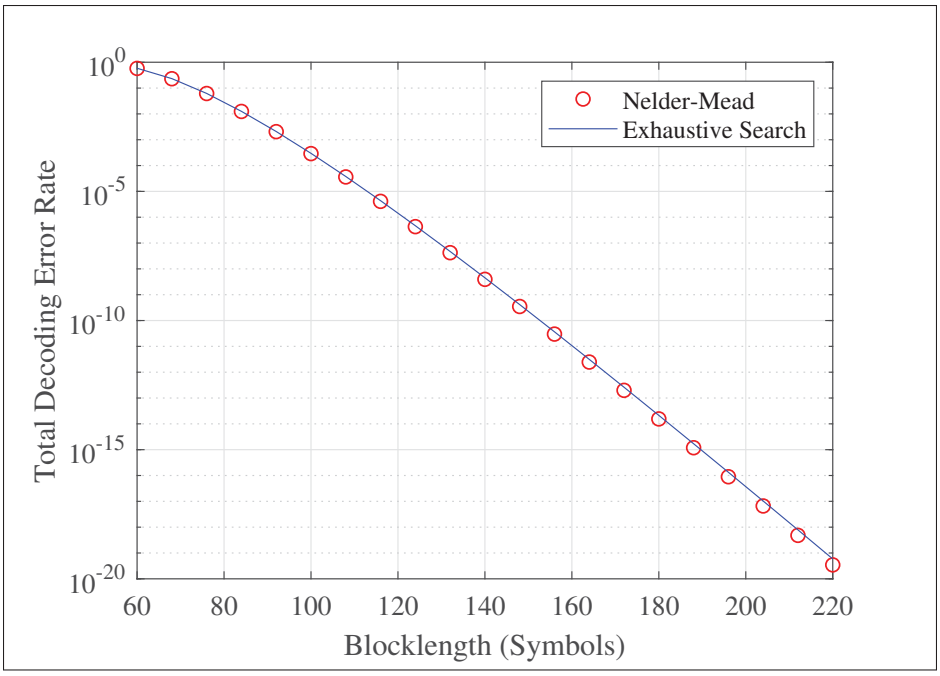

Figure 4.3 Comparison of the NMS with the exhaustive search for 80 RIS elements

4.5 Simulation Results and Discussion

In this section, we provide simulation results to demonstrate the validity of the proposed optimization approach. The initial position of the ground transmitter is at a location $x_g = 2$ km, $y_g = 2$ km, and $z_g = 1$ m. The geometric position of the RIS is at coordinates $x_r = -500$ m, $y_r = -500$ m, and $z_r = 10$ m. We set the other parameters to $N = 60$ bits, $\epsilon_1 = 10^{-9}$, $W = 10$ MHz, $T_{\max} = 10\ \mu s$, $\rho = 2$, $d = \lambda/2$, $\lambda = 0.1667$, $k_1 = 2k_2$, $k_2 = 2.3$, $k_3 = 2$, $\beta = 10$ dB, $\sigma^2 = -80$ dBm, $P_1 = 40.4$ dBm, and $P_2 = 0.37$ dBm. Additionally, the parameters of the NMS algorithm are set to $\alpha = 1$, $\eta = 1$, $\xi = 0.5$, $\zeta = 2$, $\delta_x = 0.05\ a_{x,0}$, $\delta_y = 0.05\ a_{y,0}$ and $\delta_z = 0.05\ a_{z,0}$, where $a_{x,0} = 0.00125$ km, $a_{y,0} = 0.00125$ km, and $a_{z,0} = 2$ km.

First, in Fig. 4.4, we examine the relationship between the decoding error rate and the number of antenna elements in a RIS. This figure presents a comparison between the achievable decoding error rate as a function of the number of elements in the linear RIS array for different message blocklengths. As can be seen from the figure, when the number of passive antenna elements is

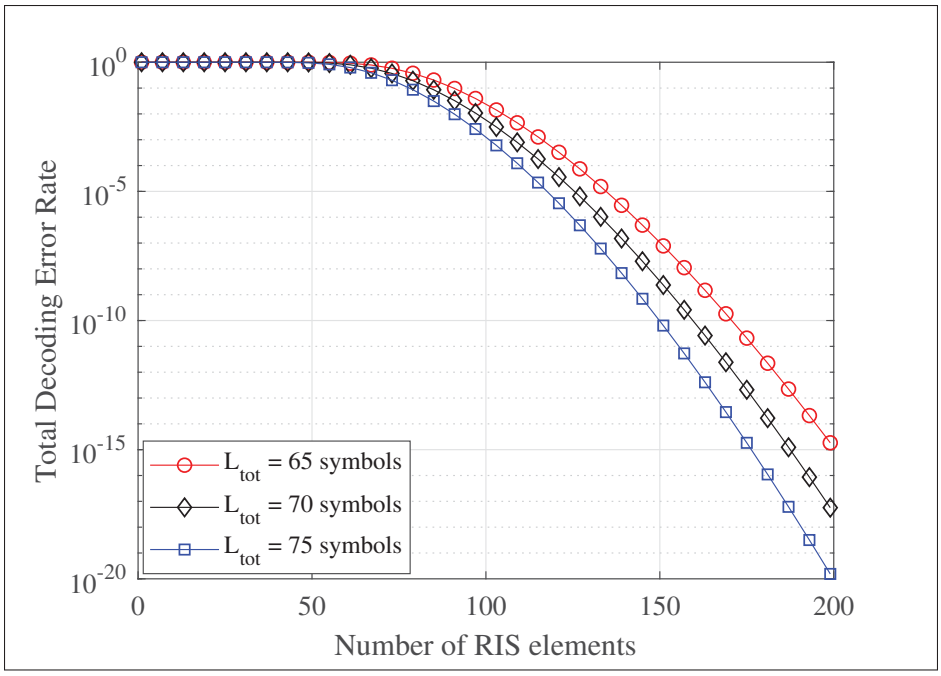

Figure 4.4 Dependence of the decoding error rate on the number of RIS elements

increased, the decoding error rate decreases dramatically. This effect is observed because of spatial diversity, which corresponds to an increase in the number of elements in the RIS array correlating to the maximization of the SNR $\gamma_2(\vec{a}, \theta_m)$ and total channel gain at the ground user. A similar effect is also observed with the increase of blocklength, which is a software measure controlled by the system designer; however, in this case, the impact on the decoding error rate is less evident.

Next, in Fig. 4.5, we examine the relationship between the decoding error rate and the blocklength. As expected, the decoding error rate decreases with the blocklength, reaching 10^{-20} for a blocklength of 220 symbols with 80 RIS elements. Thus, when increasing the blocklength, we minimize the probability of decoding error rate; however, this comes at the cost of decreasing the message transmission rate. In addition, in Fig. 4.6, the dependence of the decoding error rate on the instantaneous UAV position is established. Different error probabilities are achieved at different locations of the UAV due to the change of distances between the ground transmitter, passive RIS antenna array, and the ground user. This figure aims to illustrate the sensitivity of

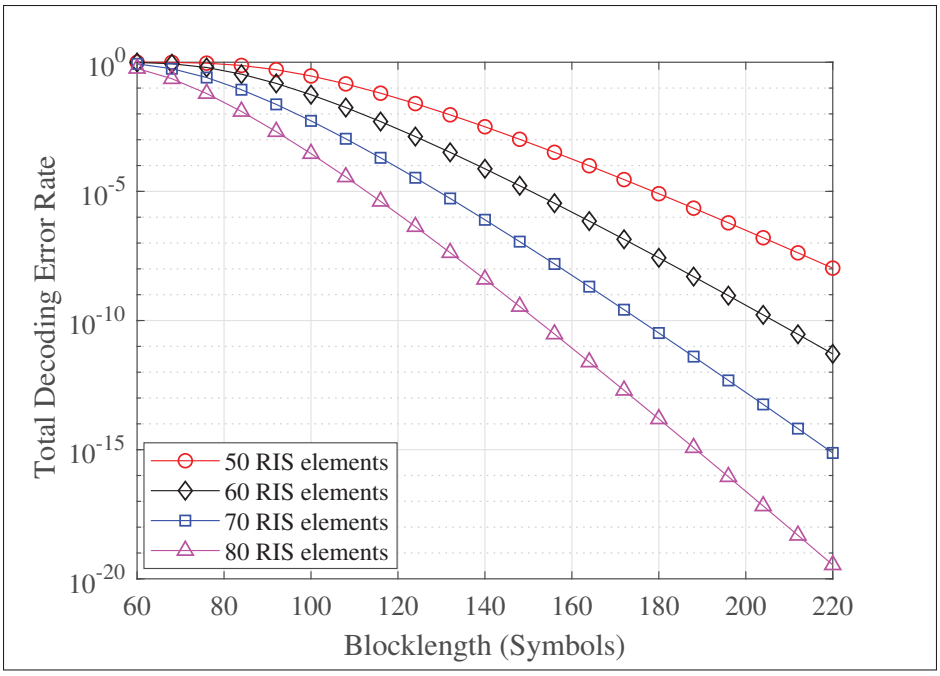

Figure 4.5 Dependence of the decoding error rate on the blocklength

the decoding error rate to the UAV position. It is observed that when the UAV is between the ground user location and the ground transmitter, the decoding error rate drops. However, as the number of users increases, the UAV position becomes more constrained, and multiple UAVs will be required to serve the multiple users. In summary, the figures depicted in this section lead to the following important observations. First, it is evident that the decoding error rate decreases logarithmically with the increase in the number of RIS elements. Second, the decoding error rate decreases with the increase of blocklength, which intuitively makes sense. Third, passive beamforming is energy-efficient as it changes the phase shifts only without amplifying the signal and has a superior error rate performance to AF relaying. Finally, UAV positioning is critical to achieve ultra-high reliability.

4.6 Conclusion

In this paper, we studied the joint design of passive beamforming, resource allocation, and UAV positioning for IoT devices communicating by both UAV and RIS utilizing short data

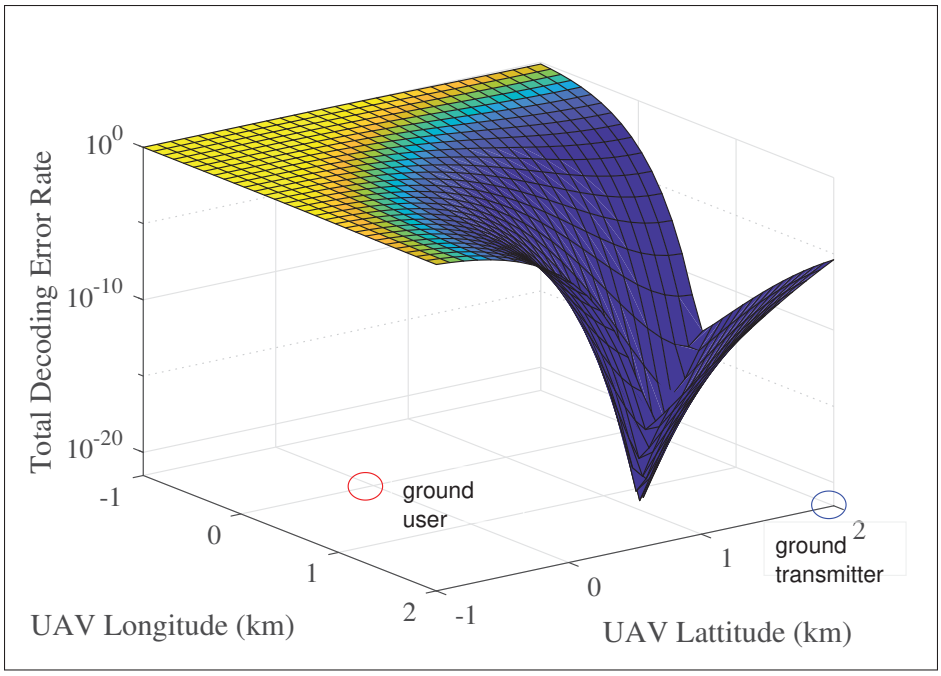

Figure 4.6 Dependence of decoding error rate on the UAV position for a blocklength of 180 symbols with 80 RIS elements

packets operating under finite blocklength constraints. The overall goal was to mitigate the total decoding error rate so that the short packets are received with ultra-high reliability at the ground user node. To achieve this goal, we performed passive beamforming and jointly optimized the blocklength and UAV position. Simulation results show that the proposed approach yields favourable convergence performance compared to traditional optimization algorithms, i.e., gradient descent. Simultaneously, it also has a better computation time and better performance for the blocklength variable than the exhaustive search. Moreover, the proposed approach allows ultra-high reliability, which could be attained by increasing the number of antenna elements in RIS as well as increasing the allocated blocklength. Simulation results demonstrated the RIS's performance gain, and conclusively shown that the UAV's position is crucial for achieving ultra-high reliability for short packets. Lastly, in the next chapter, we shall study UAV-assisted relay systems with multiple mobile robots facilitating URLLC under the umbrella of Agriculture 4.0.

CHAPTER 5

FACILITATING URLLC IN UAV-ASSISTED RELAY SYSTEMS WITH MULTIPLE-MOBILE ROBOTS FOR 6G NETWORKS: A PROSPECTIVE OF AGRICULTURE 4.0

Ali Nawaz Ranjha[1] , Georges Kaddoum[1] , Kapal Dev[2]

[1] Department of Electrical Engineering, École de Technologie Supérieure,
1100 Notre-Dame Ouest, Montréal, Québec, Canada H3C 1K3
[2] Department of Institute of Intelligent Systems,
University of Johannesburg, South Africa

Paper published in *IEEE Transactions on Industrial Informatics*, December 2021, early access

5.1 Abstract

In the upcoming sixth-generation (6G) networks, ultra-reliable and low-latency communication (URLLC) is considered as an essential service that will empower real-time wireless systems, smart grids, and industrial applications. In this context, URLLC traffic relies on short blocklength packets to reduce the latency, which poses a daunting challenge for network operators and system designers since classical communication systems are designed based on the classical Shannon's capacity formula. Therefore, to tackle this challenge, this paper considers an unmanned aerial vehicle (UAV) acting as a decode-and-forward (DF) relay to communicate short URLLC control packets between a controller and multiple-mobile robots in a cell to enable a use-case of Agriculture 4.0. Moreover, this paper employs perturbation theory and studies the quasi-optimization of the UAV's location, height, beamwidth, and resource allocation, including time-varying power and blocklength for the two phases of transmission from the controller to UAV and from UAV to robots. In this regard, we propose an iterative optimization method to find the optimal UAV's height and location, the antenna beamwidth, and the variable power and blocklength allocated to each robot inside the circular cell to minimize the average overall decoding error. It is demonstrated that the proposed algorithm outperforms other benchmark algorithms based on fixed parameters and performs nearly as well as the smart exhaustive search.

Lastly, our results emphasize the need to jointly optimize all of the above-mentioned UAV's system parameters and resource allocation for the two phases of transmission to achieve URLLC for multiple-mobile robots.

5.2 Introduction

The upcoming sixth-generation (6G) networks will succeed the fifth generation (5G) networks as the unprecedented demand for ultra-reliability, ultra-low latency, and extremely high data rates will push 5G systems to their limit within the next ten years (Bariah, Mohjazi, Muhaidat, Sofotasios, Kurt, Yanikomeroglu & Dobre, 2020). Moreover, 6G networks will also consider latency and reliability-centric designs rather than solely considering throughput-centric designs, which were dominant in the previous generations of mobile cellular technology. In addition, the emergence of new services indicates the integration of control, communication and computing technologies into a single network design. In this regard, ultra-reliable and low-latency communications (URLLC) is one of the three pillar services for the present 5G networks as well as upcoming 6G networks besides massive machine-type communication (mMTC) and enhanced mobile broadband (eMBB). The research community has made an extensive effort to study mMTC and eMBB; however, less effort has been made to undertake studies on URLLC. Furthermore, URLLC is vital to enable essential use cases of mission-critical applications, including vehicle to vehicle (V2V) communications, unmanned aerial vehicles (UAVs) control information delivery, industrial automation, intelligent transportation systems, autonomous vehicles, robots, etc., (Bennis *et al.*, 2018). Furthermore, 5G networks support ultra-reliable communication (URC), where the packet decoding error rates reach the reliability target of 10^{-7} within 1 ms end-to-end (E2E) latency/delay. Nonetheless, as subjected to the considered mission-critical application, the reliability target can change to a lower value, i.e., 10^{-25}, which 5G networks have not achieved. In this regard, as compared to 5G networks, the upcoming 6G networks aim to enhance the reliability and latency requirements of URLLC by at least two orders of magnitude; presently, 5G networks can reach the target of 1 ms transmission delay in radio access networks (RAN) (She, Sun, Gu, Li, Yang, Poor & Vucetic, 2021b). However,

transmission delay contributes to a small fraction of the E2E latency/delay, whereas queuing, processing, packet decoding and round trip hybrid automatic repeat request (HARQ) delays contribute significantly and become bottlenecks for achieving URLLC. Moreover, latency and reliability are closely coupled, i.e., they are inversely proportional. Thus, these specific issues about latency and reliability have not been adequately addressed by 5G networks.

Additionally, URLLC is a key enabler of the fourth industrial revolution (Industry 4.0), which signals a paradigm shift in industrial manufacturing by fully automating the cyber-physical systems surrounding us today. Moreover, Industry 4.0 is characterized by the amalgamation of state-of-the-art technologies, including robotics, the internet of things (IoT), artificial intelligence, and blockchain technology. Traditionally, industrial control systems for both indoor and outdoor applications relied on wired connections, including cables and optical fiber (Ren *et al.*, 2020a; Ren, Pan, Deng, Elkashlan & Nallanathan, 2020a). These wired connections are not sustainable and are, in fact, susceptible to wear and tear. Moreover, wired connections cannot be deployed in harsh environments, particularly in areas with moving or rotating parts. Therefore, wireless connections are more suitable for the use-cases of URLLC, which is pivotal to fulfill the vision of realizing Industry 4.0. In this context, URLLC will facilitate the critical use cases of Agriculture 4.0, in which the farm ecosystem is fully automated. Consequently, the high degree of automation will facilitate real-time farm management and provide food safety, food supply chain efficiency, and better utilization of natural resources (Liu, Ma, Shu, Hancke & Abu-Mahfouz, 2020). Furthermore, to reduce latency, URLLC systems utilize short blocklength packets; nevertheless, the channel's coding gain is adversely affected by the short blocklength packets. As such, for the industrial URLLC applications, the transmitted information is in the form of short blocklength control packets, i.e., for robots or autonomous vehicles, this information includes commands such as moving forward or backward, turning around left or right, turn on/off etc., typically the control packet size is in the magnitude of 100 bits or less. On this subject, Shannon's capacity bound becomes obsolete for URLLC systems as it relies on the idealistic assumption, that the coding is performed over an infinite blocklength. In contrast, URLLC operates under a finite blocklength regime. For finite blocklength, the capacity bounds and the channel coding rate

were studied and reviewed in (Polyanskiy *et al.*, 2010). Unmanned aerial vehicles (UAVs) are an innovative technology that can be used for various applications, including those in public, military, and civil sectors (Khan *et al.*, 2017a; Gupta *et al.*, 2015; Lin *et al.*, 2018; Zeng *et al.*, 2016b). Moreover, recent advancements in artificial intelligence, electronics, sensor technology, and computer fields have expanded UAVs' horizons to include more diverse and sophisticated applications such as traffic monitoring, remote sensing, and wind estimation (Bekmezci *et al.*, 2013). In this context, it is to be noted that according to a public report from the Federal Aviation Administration (FAA), the fleet of drones will almost double from 1.1 million vehicular units in 2017 to almost 2.4 million units by the year 2022 (Fotouhi *et al.*, 2019). Evidently, as both communications and control are core parts of UAV systems, thus, this immediate increase in their number will rapidly fuel the demand for UAVs' new use cases. Moreover, it is also forecasted that it will enhance the business prospects for telecommunication operators and technology companies. Furthermore, the 3rd Generation Partnership Project (3GPP) has recently studied the opportunities and challenges of employing UAVs as a novel type of user equipment (UE), which are referred to as aerial UE (Meredith, 2017). These studies concluded that UAVs, because of their dynamic nature, facilitate an enhanced line-of-sight (LoS) between the ground base stations (BSs) and aerial UE, thus mitigating shadowing and signal blockage. Therefore, as UAV-assisted communications can establish direct LoS links, they have a significant advantage over non-line-of-sight communications (nLoS), i.e., signal undergoes multipath propagation. Additionally, UAVs' dynamicity can help in their deployment in disaster-struck areas (Karlsson *et al.*, 2018). This makes UAV-assisted communication infrastructures unique and different from the general communication infrastructure, which consists of static base stations (BSs). Consequently, UAV-assisted communication has added advantages of fast deployment and favourable channel gain over the generally fixed communication infrastructure.

5.2.1 Related Work

Over the last few years, the research community has invested tremendous efforts into studying the complex and novel problems of UAV positioning as aerial base stations (ABSs) or flying relays,

trajectory design as well as rate maximization and delay minimization for UAV networks (Lyu, Zeng & Zhang, 2016; Mei & Zhang, 2020; Xu, Chen, Chen, Yang, Chaccour, Saad & Hong, 2021; Guo, Yin, Hao & Du, 2020). Notably, the authors in (Lyu *et al.*, 2016), studied UAV as an ABS communicating with ground terminals (GTs). The authors proposed a novel cyclical multiple access (CMA) to exploit the channel variations in a periodic manner existing between ABS and GTs. On this subject, the authors aimed to maximize the throughput in delay-tolerant UAV applications. Similarly, the authors in (Mei & Zhang, 2020) studied UAV-based communications subject to air-to-ground and ground-to-air interference. Moreover, the authors intent to mitigate the interference by employing a cognitive approach that divides terrestrial users into two sets of primary and secondary users. Recently, the authors in (Xu *et al.*, 2021), considered the convoluted problem of resource allocation and UAV placement for terahertz (THz) frequency bands for delay-sensitive UAV applications. The authors proposed an optimization framework to minimize the delays in uplink and downlink communications between UAV and the ground users by optimizing transmit power, bandwidth allocation of users, and UAV placement. Comparably, Guo *et al.* in (Guo *et al.*, 2020), considered a trajectory design for max-min rate in a UAV-GT communication scenario where the UAV serves as an ABS for the GT devices. Moreover, the authors studied the trajectory design using the so-called finite Fourier series (FFS) with harmonics. The authors show the proposed approach yields superior performance in terms of reduction of variables and computation time when compared to trajectory design based on discrete waypoints. Nevertheless, in these studies (Lyu *et al.*, 2016; Mei & Zhang, 2020; Xu *et al.*, 2021; Guo *et al.*, 2020), the authors make the use of Shannon's capacity formula, which inherently possesses the desirable properties of monotonicity and convexity to perform rate analysis as well as communication system's design (Xu *et al.*, 2016). However, the URLLC systems employ the finite blocklength capacity formula, which is a penalized version of Shannon's capacity formula. Resultantly, this formula is complex to analyze as it is neither convex nor concave for the variables of blocklength and transmitting power. Hence, it's a mathematically challenging task to reach an optimal solution, when analyzing the finite blocklength capacity formula (Ren *et al.*, 2020a). Presently, in the open technical literature, only a few works are available that discuss URLLC-assisted UAV communications, as outlined in

(Yu, Guan & Cai, 2020; Pan *et al.*, 2019; Ranjha & Kaddoum, 2020a; Ranjha & Kaddoum, 2020; A. Ranjha and G. Kaddoum, 2020). In (Yu *et al.*, 2020), the authors aimed to jointly optimize the transmit power and the blocklength to maximize transmitted information with short packets for half-duplex UAV relay systems to facilitate URLLC. Additionally, in (Pan *et al.*, 2019), the authors considered URLLC in the context of a single-hop UAV-assisted relay system. Moreover, the authors sought to jointly optimize the distribution of the blocklength as well as UAV location subject to a latency constraint. However, the authors did not consider the multi-hop UAV relay system due to the associated increase in complexity. Consequently, the problem of URC between an IoT transmitter/receiver pair employing a multi-hop UAV relay mechanism is studied in (Ranjha & Kaddoum, 2020a). Furthermore, the authors jointly optimized distance and blocklength constraints using the so-called *semi-empirical approach*. In this regard, the authors proposed low-complexity algorithms for implementation on memory-constrained IoT devices. Comparably, in (Ranjha & Kaddoum, 2020), the authors considered a UAV-IoT uplink communication scenario and aim to minimize the overall sum of uplink power. To achieve this task, we employed a *divide-and-conquer* rule and iteratively solved optimization problems for optimal UAV altitude, beamwidth, location, and distribution of the blocklength between transmitter and receiver pairs. Similarly, the authors in (Ren *et al.*) considered a 3-D channel model to derive an average achievable data rate (AADR) between a ground control station (GCS) and a UAV. The authors utilized the so-called *Gaussian-Chebyshev quadrature* method to derive an exact expression of AADR from the GCS to the UAV. Moreover, the authors also presented the lower bound of AADR under such systems. However, time-varying resource allocation with multiple-mobile ground users is not considered in these works, limiting the insights provided by these works. Additionally, to design real-time robust URLLC-systems assisted by a DF UAV relay, it is imperative to jointly optimize the UAV's positioning, antenna beamwidth, and the variable transmit power and the blocklength allocation under the given requirements of reliability and latency.

5.2.2 Novelty and Contributions

Despite all the research efforts dedicated to the study of URLLC, UAV-assisted communication, and their combination, i.e., UAV-assisted URLLC, a framework considering URLLC-facilitated by UAV relay systems with multiple-mobile robots is missing. Therefore, to cover this gap, we study the ultra-high reliability problem in UAV-assisted agricultural systems. The main contributions of this paper can be summarized as follows:

- We consider the problem of average overall decoding error for UAV relay-assisted URLLC in a multiple-mobile robot communication scenario under short blocklength packet transmissions.
- We solve our primary problem as well as its constraints. Since our problem is challenging to solve optimally, we use the so-called *divide-and-conquer* rule, and divide our main problem into smaller sub-problems. We consequently present an effective technique to solve each sub-problem by employing perturbation theory.
- We demonstrate that our proposed technique yields a superior performance compared to other benchmark algorithms based on fixed parameters. Moreover, its performance is almost equivalent to that of a smart exhaustive search. Concurrently, we show through simulations that it is imperative to jointly optimize the UAV's location, height, beamwidth of its antenna, and the time-varying power and blocklength allocation for the two transmission phases to enable URLLC under the given scenario.

5.3 System Model and Problem formulation

We consider downlink communication in a UAV-assisted agricultural system[1], consisting of a controller located at the origin $(0, 0, 0)$ of a three-dimensional cartesian coordinate system, and a rotary-wing UAV at position $\boldsymbol{q} = (q_1, q_2)$, where q_1 and q_2 denote the horizontal and vertical coordinates, respectively, as shown in Fig.5.1. Here, the UAV, which is acting as a DF relay, is

[1] A UAV-assisted agricultural system is a UAV-IoT system supporting the critical use-case of Agriculture 4.0, where URLLC is required. In this regard, communication links are essential such that the transmitter IoT device (controller) can send control instructions to receiver IoT devices (robots) via short blocklength control packets. Additionally, the UAV is relaying these packets between the controller and the robots. Furthermore, robots are equipped with sophisticated cutters that are pruning weeds to increase agricultural production.

flying at the height of H, and the time period T can be discretized into N evenly divided slots, where each duration is $\delta = \frac{T}{N}$.

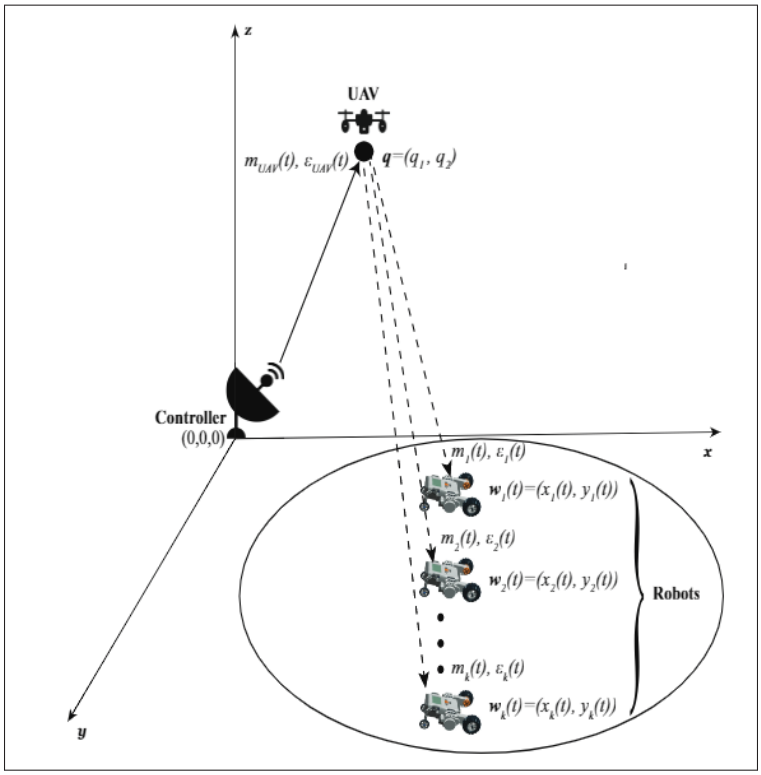

Figure 5.1 A 3D schematic representation of the system model with multiple-mobile robots

We also consider K similar robots with a time-varying position $\boldsymbol{w_k}(t) = (x_k(t), y_k(t)), \forall k = 1, \ldots, K, \forall t = 1, \ldots, N$, where $x_k(t)$ and $y_k(t)$ denote the horizontal and vertical coordinates of each robot inside the circular cell. Moreover, the robots perform agricultural tasks in the agriculture field. Without loss of generality, we assume that the direct links between the controller and the robots face blockage and that the height of the UAV is greater than the height of the controller and the robots deployed in the circular cell. Therefore, we assume that a free space channel model exists between the robots and the UAV, hovering above them. Furthermore, the controller generates a command signal of L bits, whose transmission needs to be completed within $T_{\max}$ seconds. Therefore, the overall blocklength is $M = B \times T_{\max}$, where B is the system bandwidth. As such, the controller produces short blocklength control packets that must be

supported by URLLC and are to be communicated to the UAV in the downlink channel. The packets are in a finite blocklength regime, because of their short size. Each transmission period consists of two phases, the first phase corresponds to the transmission from the controller to the UAV, while the second is from the UAV to the robots. The blocklengths allocated for each of the two phases are given as, $m_{UAV}(t)$, and $m_1(t), m_2(t), \ldots, m_k(t)$, respectively. Additionally, according to (Sun *et al.*, 2018a), the E2E latency/delay in the URLLC system is comprised of the queuing delay, transmission delay, packet decoding delay, processing delay, and the round-trip HARQ retransmission delay. Consequently, we define E2E latency/delay as $D_{E2E} = \tau + T_{\max} + T_{pp} + T_{re}$, where τ is the queuing delay, T_{pp} is the packet decoding and processing delay, and T_{re} is the round-trip HARQ retransmission delay. Furthermore, the time-varying transmission powers from the controller to the UAV and from the UAV to the robots are denoted by $P_C(t)$ and $P_D(t)$, respectively. The UAV has a directional antenna with adjustable beamwidth. According to (Balanis, 2016), the antenna gain of the UAV is given by

$$G(\theta, \phi) = \begin{cases} \dfrac{G_0}{\Theta^2}, \; if \; 0 \leq \theta \leq \Theta \; and \; 0 \leq \phi \leq \Theta, \\ g \approx 0, \; \text{otherwise.} \end{cases} \tag{5.1}$$

where $G_0 \approx 2.2846$, θ and ϕ represent the azimuth and elevation angles, respectively. Moreover, g denotes the antenna gain, where $g \approx 0$ for any region that lies outside the beamwidth of the antenna. On the other hand, we assume that each robot is equipped with an omnidirectional antenna with unit gain. Thus, for any given UAV location, the disk region on the ground that is covered by the antenna's main lobe with radius $\bar{r} = H \tan \Theta$, corresponds to the ground coverage area of the UAV. Therefore, the channel power gains from the controller to the UAV, and from the UAV to the robots are denoted by h_{UAV} and $h_k, \forall k = 1, \ldots, K$ are represented by

$$h_{UAV} = \frac{\beta_0}{\|\boldsymbol{q}\|^2 + H^2}, \qquad h_k(t) = \frac{\beta_0}{\|\boldsymbol{q} - \boldsymbol{w_k}(t)\|^2 + H^2}, \tag{5.2}$$

for (5.2), β_0 is the channel power gain at a reference distance of $d_0 = 1$ m. According to (Polyanskiy *et al.*, 2010), to transmit a short blocklength packet of size L bits in a codeword block of M symbols with a non-zero transmit power, such that each symbol in the codeword is

dependent on all L bits and correlate with some other symbols within the same block and subject to channel dispersion[2] which estimates the variability of a channel, for the two transmission phases. The following equations are applicable:

$$\begin{aligned}
\textbf{Phase 1}: f(\gamma_{UAV}(t), m_{UAV}(t), L) &= \ln(2)\sqrt{\frac{m_{UAV}(t)}{V_{UAV}(t)}}\left(\log_2\left(1+\gamma_{UAV}(t)\right) - \frac{L}{m_{UAV}(t)}\right), \quad \forall t, \\
\gamma_{UAV}(t) &= P_C(t)h_{UAV}, \quad \forall t, \\
V_{UAV}(t) &= 1 - \frac{1}{\left(1+\gamma_{UAV}(t)\right)^2} \approx 1, \quad \forall t,
\end{aligned} \tag{5.3}$$

$$\begin{aligned}
\textbf{Phase 2}: f(\gamma_k(t), m_k(t), L) &= \ln(2)\sqrt{\frac{m_k(t)}{V_k(t)}}\left(\log_2\left(1+\gamma_k(t)\right) - \frac{L}{m_k(t)}\right), \quad \forall t, k, \\
\gamma_k(t) &= P_D(t)h_k, \quad \forall t, k, \\
V_k(t) &= 1 - \frac{1}{\left(1+\gamma_k(t)\right)^2} \approx 1, \quad \forall t, k,
\end{aligned} \tag{5.4}$$

where, during the first transmission phase, γ_{UAV}, m_{UAV}, V_{UAV}, and ε_{UAV} respectively denote the SNR, the blocklength, the channel dispersion, and the decoding error of the UAV whereas, γ_k, m_k, V_k, and ε_k denote the k^{th} robot's SNR, the blocklength, the channel dispersion, and the decoding error, respectively during the second transmission phase. Here, the noise is normalized to unity. Moreover, the approximation of channel dispersion $V_{UAV}(t) \approx 1$, and $V_k(t) \approx 1$ holds for the received SNR of 5 dB or higher, which holds true for communication networks facilitating

[2] It is to be noted that Shannon's capacity for the k^{th} user is given by $\frac{L}{m_k} = log_2(1+\gamma_k)$, whereas the short blocklength capacity is given by $\frac{L}{m_k} = log_2\left(1+\gamma_k\right) - \sqrt{\frac{V_k}{m_k}}\frac{Q^{-1}(\varepsilon_k)}{\ln(2)}$. Moreover, the second term in the short blocklength capacity is a penalty term. If the blocklength approaches infinity, then the penalty term disappears, and the short blocklength capacity simplifies to Shannon's capacity. Thus, channel dispersion gauging the channel variability is the part of the penalty term introduced to Shannon's capacity incurred due to finite blocklengths.

URLLC (Sun *et al.*, 2018a) and (Ren *et al.*). The decoding error ε_{UAV} at the UAV is given as

$$\varepsilon_{UAV}(t) = Q\left(f\left(\gamma_{UAV}(t), m_{UAV}(t), L\right)\right), \tag{5.5}$$

where $Q(\cdot)$ is the Gaussian Q-function[3]. Similarly, the decoding error probability at robots is given by

$$\varepsilon_k(t) = Q\left(f\left(\gamma_k(t), m_k(t), L\right)\right), \quad \forall t, k, \tag{5.6}$$

where $\gamma_k(t) = P_D(t)h_k(t)G$. Since the UAV acts as a DF relay, at arbitrary time t, the overall decoding error probability from the controller to the robots is given by

$$\varepsilon(t) = \varepsilon_{UAV}(t) + (1 - \varepsilon_{UAV}(t)) \sum_{k=1}^{K} \varepsilon_k(t). \tag{5.7}$$

Since the simultaneous errors $\varepsilon_{UAV}\varepsilon_k \rightarrow 0$, for $\forall k = 1, \ldots, K$, the overall decoding error probability is given as

$$\varepsilon(t) = \varepsilon_{UAV}(t) + \sum_{k=1}^{K} \varepsilon_k(t). \tag{5.8}$$

To enable URLLC, we seek to simultaneously optimize the height H, location $\boldsymbol{q}$, and beamwidth Θ of the UAV, and the blocklength $\boldsymbol{m} = \{m_{UAV}(t), m_k(t), \forall k = 1, \ldots, K\}$ and power $\boldsymbol{P} = \{P_C(t), P_D(t), \forall t\}$ for two phases, with the goal of minimizing the overall decoding error probability under the latency/blocklength constraint. Thus, the optimization problem can be

[3] A composite function is mathematically represented as $f\left(g\left(x\right)\right)$, where function $f(\cdot)$ is dependent on another function $g\left(x\right)$. Thus, $\varepsilon_{UAV}(t)$ is the composite Gaussian Q-function of the finite blocklength function given by $f\left(\gamma_{UAV}(t), m_{UAV}(t), L\right)$.

formulated as the following constrained minimization problem:

$$\min_{\boldsymbol{q},H,\Theta,\boldsymbol{m},\boldsymbol{P}} \quad \frac{1}{N}\sum_{t=1}^{N}\varepsilon(t), \tag{5.9a}$$

$$\text{s.t.} \quad \|\boldsymbol{q}-\boldsymbol{w}_k(t)\|^2 \leq H^2\tan^2\Theta, \tag{5.9b}$$

$$m_{UAV}(t)+\sum_{k=1}^{K} m_k(t) \leq M, \tag{5.9c}$$

$$m_{UAV}(t), m_k(t) \in \mathbb{N}, \tag{5.9d}$$

$$P_C(t)m_{UAV}(t)+P_D(t)\sum_{k=1}^{K} m_k(t) \leq E_{\text{tot}}, \forall t, \tag{5.9e}$$

$$H_{\min} \leq H \leq H_{\max}, \tag{5.9f}$$

$$\Theta_{\min} \leq \Theta \leq \Theta_{\max}, \tag{5.9g}$$

$$d_1 \leq q_1 \leq d_2, \quad l_1 \leq q_2 \leq l_2, \tag{5.9h}$$

$$\varepsilon_{UAV}(t) \leq \epsilon_1, \quad \varepsilon_k(t) \leq \epsilon_2, \forall k, t, \tag{5.9i}$$

$$P_C(t) \geq 0, \quad P_D(t) \geq 0, \forall t, \tag{5.9j}$$

$$D_{E2E} \leq T_{th}, \forall t, \tag{5.9k}$$

where E_{tot} ensures the system total energy consumption is within a budget $\tilde{E}_{tot} = E_{\text{tot}}T_s$, with T_s representing the symbol duration, that is equal to $1/B$. At time t, the maximum errors for the UAV and for each robot are given by ϵ_1 and ϵ_2, as represented in constraint (5.9i). It is important to note that the $Q(x)$ function is convex and $Q(x) < 0.5$ for $x \geq 0$. Here, $\varepsilon_{UAV}(t) \leq \epsilon_1$ and $\varepsilon_k(t) \leq \epsilon_2$, where ϵ_1 and ϵ_2 take small values, i.e., below 0.1. This implies that function f needs to be positive, hence $\log_2(1+\gamma(t)) - \frac{L}{m(t)} \geq 0$. This result will be used throughout this work. Moreover, T_{th} denotes the threshold of E2E latency/delay in our URLLC scenario and the optimal solution to the minimization problem of average overall decoding error is found when equality holds in constraint (5.9k). Additionally, it is a cumbersome task to prove that the objective function (5.9a) is convex/non-convex. Nonetheless, the problem is clearly non-convex due to constraints (5.9b), (5.9d), and (5.9e). The proofs can be seen in **Appendix III**

5.4 The Proposed Approach

Generally, the problem (5.9) is non-convex. Consequently, it is a tedious task to solve the given problem. Hence, we use *divide-and-conquer* rule to divide (5.9) into four sub-problems. Thereafter, we iteratively perform optimization for the sub-problems of time-varying blocklengths $m_{UAV}(t)$ and $m_k(t)$, the time-varying powers $P_C(t)$ and $P_D(t)$, for the two phases of transmission, and the UAV's height H, the beamwidth Θ, and the UAV's location $\boldsymbol{q}$. Our proposed approach is based on our detailed convexity analysis outlined in **Appendix III**.

5.4.1 Optimizing the Time-Varying Blocklength

The first sub-problem optimizes the time-varying optimal blocklengths $m_{UAV}(t)$ and $m_k(t)$ for each of the two transmission phases. Moreover, we assume that the constraints P, H, Θ, and q are fixed, and thus the sub-problem can be formulated as

$$\min_{\boldsymbol{m}} \quad \frac{1}{N}\sum_{t=1}^{N}\varepsilon(t), \tag{5.10a}$$

$$\text{s.t.} \quad m_{UAV}(t) + \sum_{k=1}^{K} m_k(t) \leq M, \forall t, \tag{5.10b}$$

$$P_C^*(t)m_{UAV}(t) + P_D^*(t)\sum_{k=1}^{K} m_k(t) \leq E_{\text{tot}}, \forall t, \tag{5.10c}$$

$$\varepsilon_{UAV}(t) \leq \epsilon_1, \quad \varepsilon_k(t) \leq \epsilon_2, \forall k, t, \tag{5.10d}$$

$$m_{UAV}(t) \geq 0, \quad m_k(t) \geq 0, \quad \forall k, t, \tag{5.10e}$$

The focus will be on ε_{UAV} and we can obtain ε_k by analogy since G is constant. Let $f(m_{UAV}) = f(\gamma^*_{UAV}(t), m_{UAV}(t), L)$, at an arbitrary time t. The first term of the objective function can be written as

$$Q(f(m_{UAV})) = Q\left(A_1\sqrt{m_{UAV}}\left(B_1 - \frac{L}{m_{UAV}}\right)\right), \tag{5.11}$$

where $A_1 = \ln(2)$ and $B_1 = \log_2\left(1 + \gamma^*_{UAV}(t)\right)$ are constants that do not depend on m_{UAV}. Moreover, the second derivative of $f(m_{UAV})$ is

$$\frac{\partial^2 f(\gamma_{UAV})}{\partial m^2_{UAV}} = -\frac{A_1(3L + B_1 m_{UAV})}{4\sqrt{m^5_{UAV}}}. \tag{5.12}$$

Since m_{UAV}, A_1, B_1, and L are positive values, $\frac{\partial^2 f(\gamma_{UAV})}{\partial m^2_{UAV}} < 0$, and hence f is a concave function. Since $Q(x)$ is convex and non-increasing for $x \geq 0$ and $f(m_{UAV})$ is a concave function, hence the composition $Q(f(m_{UAV}))$ is a convex function. Similarly, ε_k is a convex function $\forall k = 1, \ldots, K$, thus their summation is a convex function. The constraints are convex functions, which makes problem (5.10) convex. Therefore, the golden section method is used to solve this problem.

5.4.2 Optimizing the Time-Varying Power

In the second sub-problem we aim to optimize the time-varying power $P_C(t)$ and $P_D(t)$ for the two transmission phases of the communication system while keeping the other constraints fixed, we formulate the following problem:

$$\min_{\boldsymbol{P}} \quad \frac{1}{N}\sum_{t=1}^{N} \varepsilon(t), \tag{5.13a}$$

$$\text{s.t.} \quad P_C(t) m^*_{UAV}(t) + P_D(t) \sum_{k=1}^{K} m^*_k(t) \leq E_{\text{tot}}, \forall t, \tag{5.13b}$$

$$\varepsilon_{UAV}(t) \leq \epsilon_1, \quad \varepsilon_k(t) \leq \epsilon_2, \forall k, t, \tag{5.13c}$$

$$P_C(t) \geq 0, \quad P_D(t) \geq 0, \forall t. \tag{5.13d}$$

As in the previous case, ε_{UAV} depends on P_C the same way as ε_k depends on P_D. Presently, $\gamma_{UAV}(t) = P_C(t) h^*_{UAV}$ is not constant since it is a function of $P_C(t)$. For an arbitrary time t, let

$f(\gamma_{UAV}) = f(\gamma_{UAV}(t), m^*_{UAV}(t), L)$, which is given by

$$f(\gamma_{UAV}) = A_2 \left(\log_2 (1 + \gamma_{UAV}) - B_2\right), \tag{5.14}$$

where $A_2 = \ln(2)\sqrt{m^*_{UAV}}$ and $B_2 = \frac{L}{m^*_{UAV}}$. The second derivative of $f(\gamma_{UAV})$ is

$$\frac{\partial^2 f(\gamma_{UAV})}{\partial P_C^2} = -\frac{A_2 (h^*_{UAV})^2}{\ln(2)(P_C h^*_{UAV} + 1)^2}, \tag{5.15}$$

which is non-positive, thus this function is concave. Since $Q(x)$ is convex and non-increasing, hence $\varepsilon_{UAV} = Q(f(\gamma_{UAV}))$ is convex, the same hold for ε_k. Thus the objective function of the problem (5.13) is convex and the constraints are also convex, which makes the problem convex. Consequently, the interior-point method is chosen to solve this sub-problem.

5.4.3 Optimizing the UAV Height and Beamwidth

The third optimization sub-problem deals with finding the optimal height of the UAV and beamwidth of its antenna, it can be formulated as follows

$$\min_{H,\Theta} \quad \frac{1}{N}\sum_{t=1}^{N} \varepsilon(t), \tag{5.16a}$$

$$\text{s.t.} \quad D_{\max} \leq H \tan\Theta, \tag{5.16b}$$

$$H_{\min} \leq H \leq H_{\max}, \tag{5.16c}$$

$$\Theta_{\min} \leq \Theta \leq \Theta_{\max}, \tag{5.16d}$$

$$\varepsilon_{UAV}(t) \leq \epsilon_1, \quad \varepsilon_k(t) \leq \epsilon_2, \forall k, t, \tag{5.16e}$$

where $D_{\max} = \max_{k,t} (\|\boldsymbol{q}^* - \boldsymbol{w}_k(t)\|)$. For a given time t, $D_{\max}$ parameter computes the maximum value of the Euclidean distance between the UAV and the robot k deployed in the cell. Additionally, (5.16b) ensures that $D_{\max}$ value is less than equal to the cell radius denoted by $H \tan\Theta$ as outlined in (Ranjha & Kaddoum, 2020) and (Yang *et al.*, 2018). Moreover, (5.16b) guarantees that the optimization problem (5.16) does not become infeasible by adjusting both the UAV

height H and its beamwidth Θ. Once again, ε_{UAV} depends on H^4 in the same way as ε_k, but the case is different for Θ, that it is not present in the terms related to the UAV. The first term of the objective function for an arbitrary time t is given by

$$Q(f(\gamma_{UAV})) = Q(C_3\left(\log_2\left(1+\gamma_{UAV}\right) - D_3\right)), \tag{5.17}$$

where $\gamma_{UAV} = \frac{A_3}{B_3+H^2}$, with $A_3 = P_C^*\beta_0$, $B_3 = \|\boldsymbol{q}^*\|^2$, $C_3 = \ln(2)\sqrt{m_{UAV}^*(t)}$, and $D_3 = \frac{L}{m_{UAV}^*(t)}$. B_3 can be replaced by $\|\boldsymbol{q^*} - \boldsymbol{w_k}(t)\|^2$ to check convexity of ε_k. Thereafter, we compute the first derivative of $Q(f(\gamma_{UAV}))$, which is always positive, meaning that the function increases with H,

$$\frac{\partial Q(f(\gamma_{UAV}))}{\partial H} = \frac{\sqrt{2}A_3C_3H\exp\left(-\frac{f(\gamma_{UAV})^2}{2}\right)}{\sqrt{\pi}\ln(2)\left(H^2+B_3\right)^2\left(\gamma_{UAV}+1\right)}. \tag{5.18}$$

Since $Q(f(\gamma_{UAV}))$ is increasing, the minimum is obtained for the minimum feasible H. The same is valid for ε_k. As such, the optimal solution for H is $H^* = \max\left(H_{\min}, \frac{D_{\max}}{\tan\Theta}\right)$. If $H^* = H_{\min}$, the objective function is an increasing function of Θ, and again the optimal value of Θ is the minimum feasible value, given by $\Theta^* = \max\left(\Theta_{\min}, \arctan\left(\frac{D_{\max}}{H_{\min}}\right)\right)$. On the contrary, if $H^* = \frac{D_{\max}}{\tan\Theta}$, the problem becomes complicated to solve. In this case, an exhaustive search through $[\Theta_{\min}, \Theta_{\max}]$ needs to be performed. It should be noted that the values of H and Θ also have upper bounds due to constraint (5.16e). For H, this upper bound is given by

$$H \leq \min\left(H_{\max}, \sqrt{\frac{A_3}{2^{D_3+\frac{Q^{-1}(\epsilon_1)}{C_3}}-1} - B_3}, \sqrt{\frac{A_k}{2^{D_k+\frac{Q^{-1}(\epsilon_2)}{C_k}}-1} - B_k}\right), \tag{5.19}$$

where $A_3 = P_C^*(t)\beta_0$, $B_3 = \|\boldsymbol{q}^*\|^2$, $C_3 = \ln(2)\sqrt{m_{UAV}^*(t)}$, $D_3 = \frac{L}{m_{UAV}^*(t)}$, $A_k = \frac{G_0P_D^*(t)\beta_0}{\Theta^2}$, $B_k = \|\boldsymbol{q}^* - \boldsymbol{w}_k\|^2$, $C_k = \ln(2)\sqrt{m_k^*(t)}$, and $D_k = \frac{L}{m_k^*(t)}$. Similarly, for Θ, the upper bound is given by

$$\Theta \leq \min\left(\Theta_{\max}, \sqrt{\frac{A_5}{2^{C_5+\frac{Q^{-1}(\epsilon_2)}{B_5}}-1}}\right), \tag{5.20}$$

[4] In our work, the UAV is assumed to fly at a minimum height of 80 meters, where, according to 3GPP Release 15, there is a 100% probability of achieving LoS communication.

where $A_5 = P_D^*(t)h_k^*(t)G_0$, $B_5 = \ln(2)\sqrt{m_k^*(t)}$, and $C_5 = \frac{L}{m_k^*(t)}$.

5.4.4 Optimizing the UAV location

For the final sub-problem, we optimize the UAV's location q while all the other constraints are kept fixed. Thus, we formulate the final-subproblem as

$$\min_{\boldsymbol{q}} \quad \frac{1}{N}\sum_{t=1}^{N}\varepsilon(t), \tag{5.21a}$$

$$\text{s.t.} \quad \|\boldsymbol{q} - \boldsymbol{w}_k(t)\|^2 \leq H^{*2}\tan^2\Theta^*, \forall k, t, \tag{5.21b}$$

$$d_1 \leq q_1 \leq d_2, \quad l_1 \leq q_2 \leq l_2, \tag{5.21c}$$

$$\varepsilon_{UAV}(t) \leq \epsilon_1, \quad \varepsilon_k(t) \leq \epsilon_2, \forall k, t, \tag{5.21d}$$

All constraints of problem (5.21) are convex, except for constraint (5.21d), which needs to be convex in order for the feasible region of problem (5.21) to be convex. As with the previous problem, the constraints can be solved for $\|\boldsymbol{q}\|^2$ and $\|\boldsymbol{q} - \boldsymbol{w}(t)\|^2$, hence the constraints become

$$\|\boldsymbol{q}\|^2 \leq \min_t \left(\frac{A_4}{2^{D_4 + \frac{Q^{-1}(\epsilon_1)}{C_4}} - 1} - B_4 \right), \tag{5.22}$$

$$\|\boldsymbol{q} - \boldsymbol{w}_k(t)\|^2 \leq \frac{A_k}{2^{D_k + \frac{Q^{-1}(\epsilon_2)}{C_k}} - 1} - B_k, \tag{5.23}$$

where $A_4 = P_C^*(t)\beta_0$, $B_4 = H^{*2}$, $C_4 = \ln(2)\sqrt{m_{UAV}^*(t)}$, $D_4 = \frac{L}{m_{UAV}^*(t)}$, $A_k = P_D^*(t)\beta_0$, $B_k = H^{*2}$, $C_k = \ln(2)\sqrt{m_k^*(t)}$, and $D_k = \frac{L}{m_k^*(t)}$. Consequently, the equivalent problem is formulated as

$$\min_{\boldsymbol{q}} \quad \log\left(\frac{1}{N}\sum_{t=1}^{N}\varepsilon(t)\right), \tag{5.24a}$$

$$\text{s.t.} \quad \|\boldsymbol{q} - \boldsymbol{w}_k(t)\|^2 \leq U_1, \forall k, t, \tag{5.24b}$$

$$\|\boldsymbol{q}\|^2 \leq U_2, \tag{5.24c}$$

$$d_1 \leq q_1 \leq d_2, \quad l_1 \leq q_2 \leq l_2, \tag{5.24d}$$

where U_1 and U_2 are defined as

$$U_1 = \min\left(H^{*2}\tan^2\Theta^*, \min_{t,k}\left(\frac{A_k}{2^{D_k+\frac{Q^{-1}(\epsilon_2)}{C_k}}-1} - B_k\right)\right), \tag{5.25}$$

$$U_2 = \min_{t}\left(\frac{A_4}{2^{D_4+\frac{Q^{-1}(\epsilon_1)}{C_4}}-1} - B_4\right). \tag{5.26}$$

Thus, the feasible region is convex. Although the objective function is non-convex, convergence to the global minimum is guaranteed and the interior-point method can be used. Furthermore, details about convergence and convexity analysis are provided in **Appendix III**.

5.4.5 Proposed Algorithm

As a result of the analysis shown above, we present an effective algorithm, namely **Algorithm 1**, where we employ the so-called divide-and-conquer rule to divide our main problem into four smaller sub-problems, in order to solve the main problem (5.9). Thereafter, we efficiently solve two of them, including (5.13) and (5.21) by using the interior-point method, whereas problem (5.16) is solved using the method described in **Subsection C**. Moreover, (5.10) is solved by using golden section search. As it is clear from the above discussion, the main problem (5.9) is non-convex, pointing to the fact that a global solution is not guaranteed. However, we can perform global optimization for each of the sub-problems as they have unique minima. In the first step, we produce an initial solution and initialize the parameters $(H^0, \Theta^0, \boldsymbol{m}^0, \boldsymbol{q}^0, \boldsymbol{P}^0)$. After that, the proposed algorithm considers each sub-problem separately and runs a series of iterations and halts only when the difference between two numerical solutions $Sol^n - Sol^{n-1}$ is below a certain predefined threshold called tolerance. In the beginning, an initial solution Sol^0 is provided, and afterwards, at each step, the solution to each sub-problem is used iteratively to solve the next sub-problem. Lastly, we summarize these steps in **Algorithm 5.1** as follows:

Algorithm 5.1 Perturbation-based iterative approach for solving optimization problem (5.9).

Initialize $(H^0, \Theta^0, \boldsymbol{m}^0, \boldsymbol{q}^0, \boldsymbol{P}^0)$ with objective value Sol^0.
Set $n = 1$ and a tolerance `tol`.
while $|Sol^n - Sol^{n-1}| > tol$ **do**
    Compute $\boldsymbol{m}^{n+1}$ solution of (5.10), with (H^n, Θ^n), $\boldsymbol{q}^n$ and $\boldsymbol{P}^n$.
    Compute $\boldsymbol{P}^{n+1}$ solution of (5.13), with (H^n, Θ^n), $\boldsymbol{q}^n$ and $\boldsymbol{m}^{n+1}$.
    Compute (H^{n+1}, Θ^{n+1}) solution of (5.16), with $\boldsymbol{q}^n$, $\boldsymbol{m}^{n+1}$ and $\boldsymbol{P}^{n+1}$.
    Compute $\boldsymbol{q}^{n+1}$ solution of (5.21), with (H^n, Θ^n), $\boldsymbol{m}^n$ and $\boldsymbol{P}^{n+1}$.
    Compute final objective value Sol^{n+1} as in (5.9a).
    Set $n = n + 1$.
end while
Until the termination conditions are reached.
Return an optimized solution.

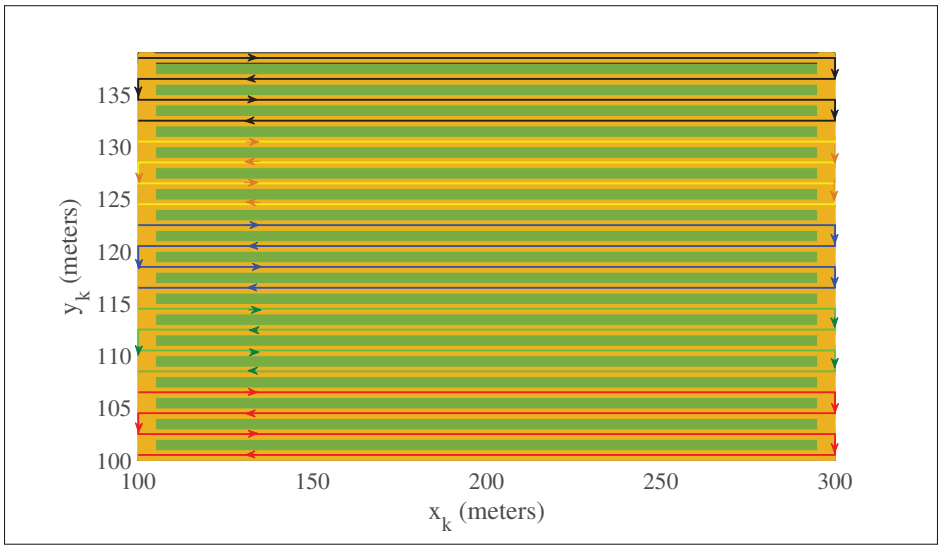

Figure 5.2 Robots trajectories

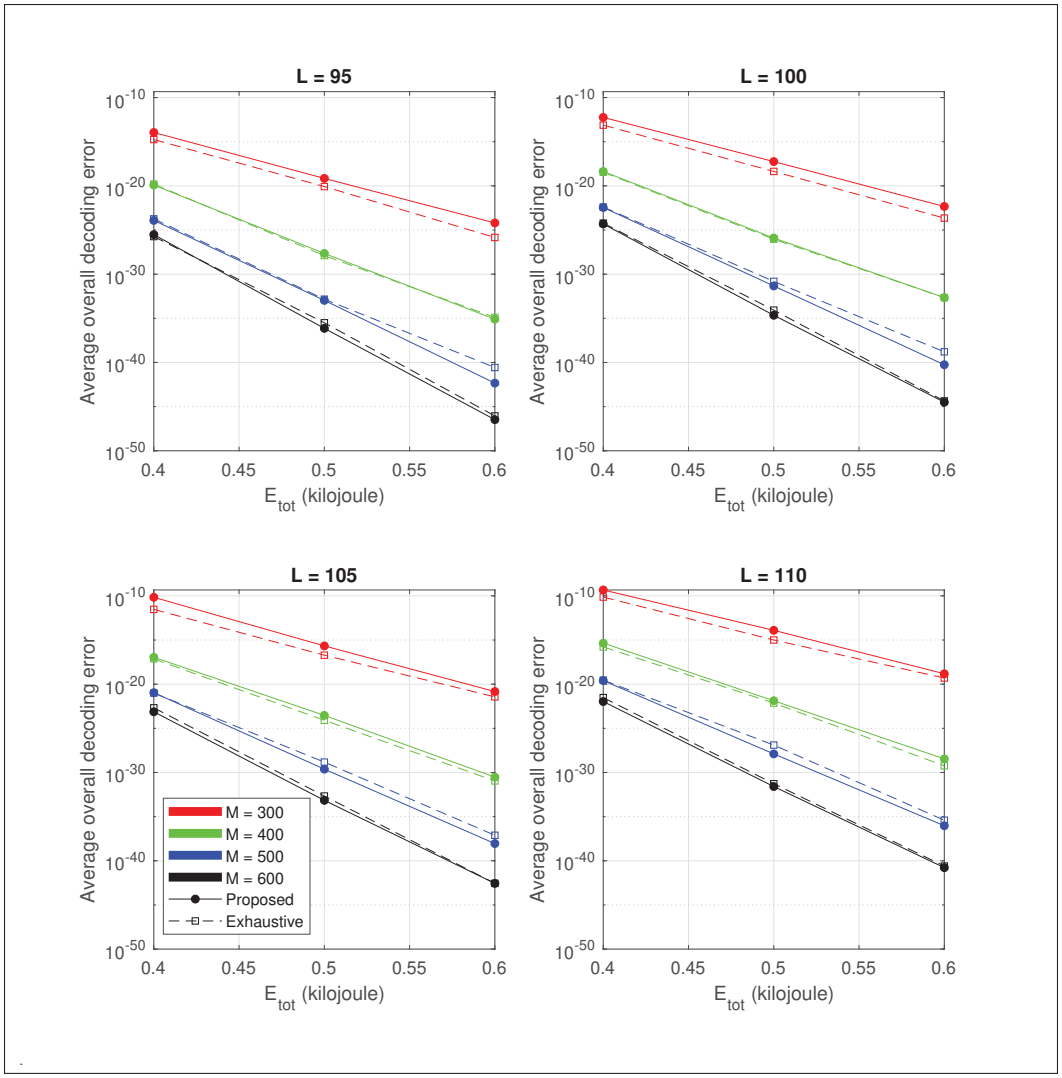

Figure 5.3 Average overall decoding error versus E_{tot}

5.5 Simulation results and Discussion

In this section we provide some numerical results to show the validity of the proposed algorithm to solve problem (5.9). For that, we consider $K = 5$ robots that travel through an agriculture field. The trajectories can be seen in Fig. 5.2. The robots are moving at a speed of 2 m/s inside a field with 200×40 m^2 through the paths represented by different colours and in between the rows represented in green. Each robot travels through 4 rows in its path and the robots depart and arrive at the same time. The total time the robots need to transverse through this path is

400 seconds. To solve the problem efficiently, these paths were sampled every 10 seconds, such that the total number of time slots is 40. The channel power gain is $\beta_0 = 50$ dB, for the UAV's antenna the maximum and minimum beamwidth are $\Theta_{\min} = 0$ and $\Theta_{\max} = \frac{\pi}{2}$, the minimum and maximum height are $H_{\min} = 80$ m and $H_{\max} = 250$ m, the UAV's coordinates take values between $d_1 = l_1 = 50$ m, and $d_2 = 150$ m, $l_2 = 300$ m. Moreover, the delays are set as $\tau = 0.01$ ms, $T_{\max} = 0.04$ ms, $T_{re} = 0.02$ ms, $T_{pp} = 0.03$ ms, whereas the threshold of E2E latency/delay is set as $T_{th} = 1$ ms. Finally, the maximum decoding errors for the UAV and the robot are given by $\epsilon_1 = 10^{-5}$ and $\epsilon_2 = 10^{-6}$, respectively.

5.5.1 Exhaustive search

To compare the results of the proposed method with a baseline, we simulate a partial or smart exhaustive search. This search needs to be partial due to the enormous number of possible combinations of the time-varying variables blocklength $\boldsymbol{m}$ and power $\boldsymbol{P}$ variables. To illustrate this point, we assume $N = 40$ time slots, which translates to 240 variables for the blocklength and 80 for the power. Furthermore, there are also two variables for the UAV location, one for the UAV height, and one for the beamwidth, making a total of 304 variables. For simplicity, let x be the number of values tested for each variable. Then, the total number of possible combinations is x^{304}; this number is too large to make a full-exhaustive search computationally affordable. Therefore, we implement a smart exhaustive search performed only on the location $\boldsymbol{q}$, height H, and beamwidth Θ variables, while the time-varying blocklengths $m_{UAV}(t)$ and $m_k(t)$, and time-varying powers $P_C(t)$ and $P_D(t)$ for the two transmission phases are fixed.

Moreover, Fig. 5.3 shows the average overall decoding error versus E_{tot} for the proposed method and the partial exhaustive search for different blocklengths, i.e., $M = 300, 400, 500,$ and 600 symbols and for different data packet sizes i.e., $L = 95, 100, 105,$ and 110 bits. Here, it is observed that the performance of the proposed method is very close to that of the smart exhaustive search method, meaning that the proposed method approaches the global optimum solution at infinity, which can be observed as the blocklength increases. Furthermore, we also modified the problem (5.9) to fix each variable(s) one at a time, to compare the proposed method

with these sub-problems. As such, the considered sub-problems are fixed blocklength (FB) which includes **Algorithm 1** without solving problem (5.10) and considering $\boldsymbol{m}^n = \boldsymbol{m}^0$, $\forall n$. Afterwards, we have fixed power (FP) that includes **Algorithm 1** without solving problem (5.13) and considering $\boldsymbol{P}^n = \boldsymbol{P}^0$, $\forall n$. Then, we have fixed altitude and beamwidth (FAB) which includes **Algorithm 1** without solving problem (5.16) and considering $(H, \Theta)^n = (H, \Theta)^0$, $\forall n$. Lastly, we have fixed location (FL) including **Algorithm 1** without solving problem (5.21) and considering $\boldsymbol{q}^n = \boldsymbol{q}^0$, $\forall n$. The results in Fig. 5.4d present the average overall decoding error versus E_{tot} for different values of M and for $L = 100$ bits. Through the figures, we can see that the average overall decoding error decreases as E_{tot} and M increases. FP returned higher decoding error than the other problems for all the values tested. In general, we observe that FB and FAB return similar values and are the ones with lower average overall decoding error.

5.5.2 Time-complexity and Optimality Analysis

Firstly, in **Algorithm 1**, to solve the problem of blocklength distribution (5.10a), the complexity is $\mathcal{O}(\log_2\left(\frac{1}{\epsilon}\right))$ for the golden section method with accuracy ϵ. Thereafter, for the power allocation problem (5.13a), the complexity is $\mathcal{O}(P^{3.5})$. Similarly, for the UAV height and beamwidth allocation problem (5.16a), the complexity is represented as $\mathcal{O}(\frac{\Theta_{\max}-\Theta_{\min}}{\delta})$, where δ is the chosen step size. Moreover, the complexity of the UAV location optimization problem (5.21a) is given by $\mathcal{O}((q_1 q_2)^{3.5})$. Lastly, the overall complexity of **Algorithm 1** is $\mathcal{O}\left(I_t \log_2\left(\frac{1}{\epsilon}\right) + I_t \frac{\Theta_{\max} - \Theta_{\min}}{\delta} + I_t P^{3.5} + I_t (q_1 q_2)^{3.5}\right)$, where I_t represents the total numbers of iterations required. Furthermore, for the smart exhaustive search, the time-complexity is given by $\mathcal{O}\left(h \times t \times q^2\right)$, where the number of points tested for H is h, for θ is t and for each of q_1 and q_2 is q. It is to be noted that we choose $h = t = q = 1000$ points, which makes the exhaustive search complexity much greater than that of the proposed **Algorithm 5.1**. Additionally, due to limited memory resources, a full exhaustive search with many variables is impractical. Alternatively, the smart exhaustive search with a limited number of variables becomes a viable option (Ranjha & Kaddoum, 2020a). In such an exhaustive search, a few variables are fixed

while others are not. Consequently, only a full exhaustive search is truly optimal while the smart exhaustive search is quasi-optimal.

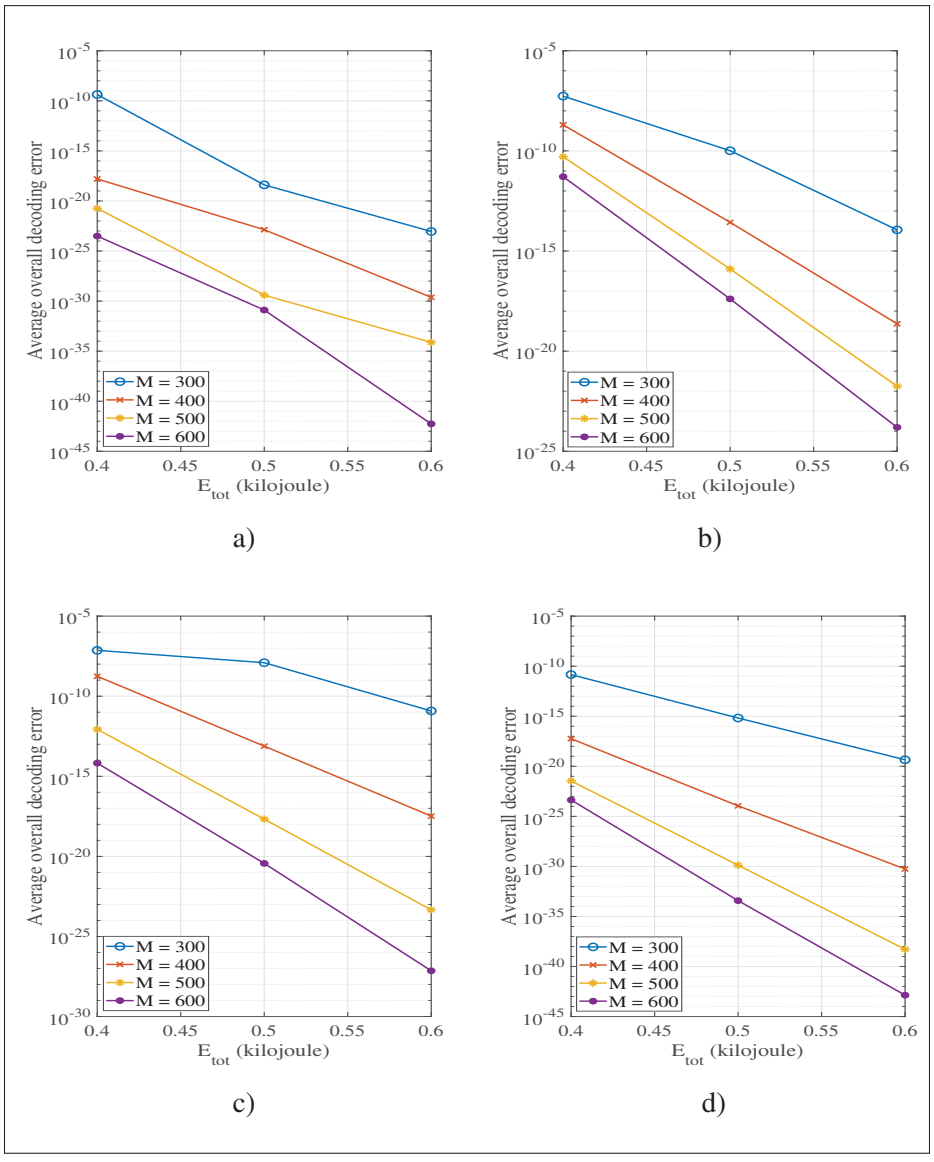

Figure 5.4 (a) Fixed blocklength (FB) (b) Fixed power (FP)
(c) Fixed altitude and beamwidth (FAB) (d) Fixed location (FL)

5.5.3 Comparisons

Finally, Fig. 5.5 summarizes the previous results, showing the proposed method, the exhaustive search, and the sub-problems. In Fig. 5.5(a), we set $E_{\text{tot}} = 0.5$ kJ and $L = 100$ bits. It can be

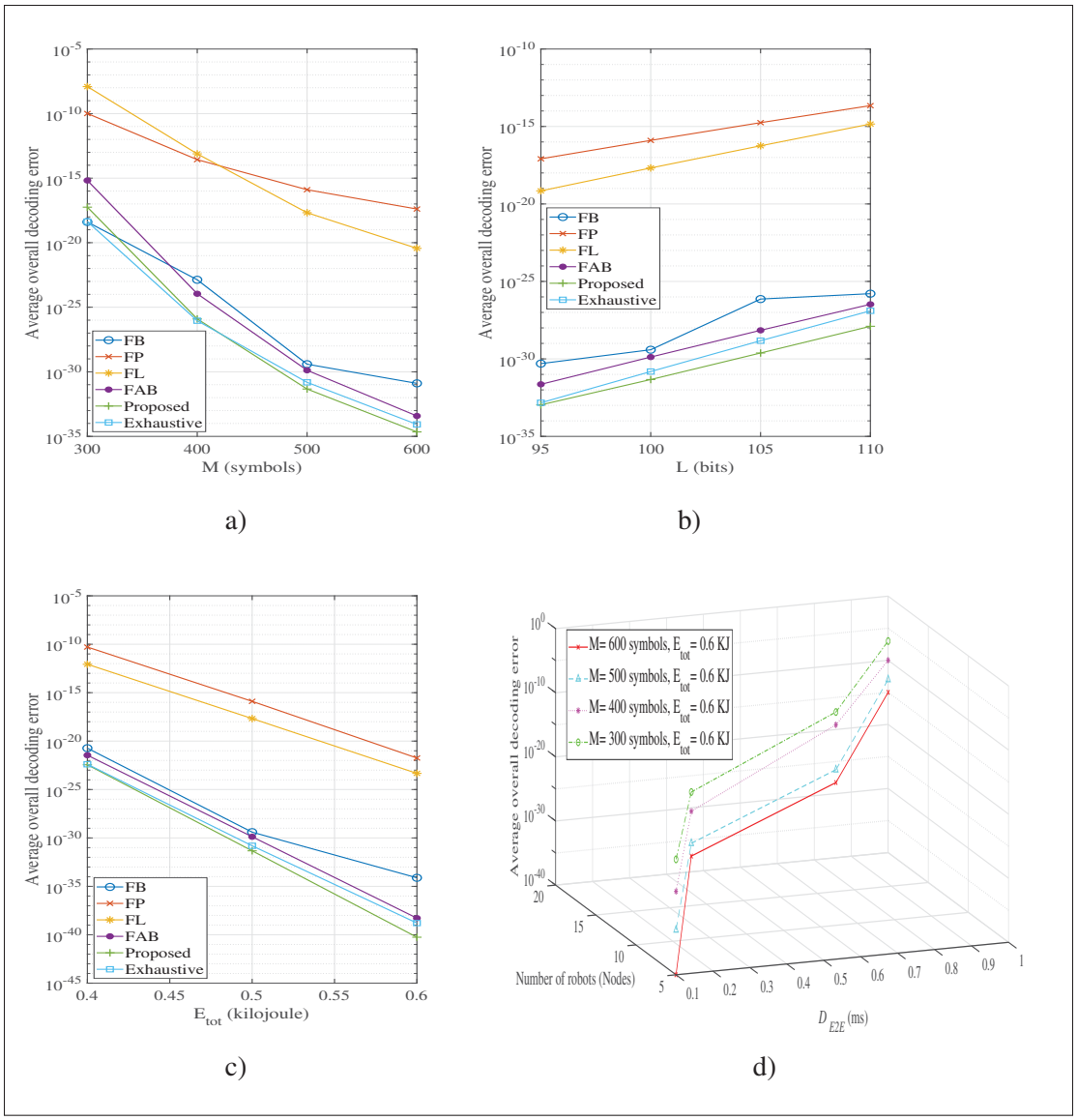

Figure 5.5 (a) Overall Decoding Error versus M (b) Overall Decoding Error versus L (c) Overall Decoding Error versus E_{tot} (d) Decoding Error versus number of robots versus latency

seen that FP returns a lower decoding error than FL for $M = 300$ symbols and $M = 400$ symbols. However, for $M = 500, 600$ symbols, FP is higher than FL. The same behavior is observed for the proposed method where compared to the exhaustive search, the exhaustive search decoding error is lower than the one for the proposed method for $M = 300, 400$ symbols and higher for higher values of M. Moreover, FB returns an unexpected value for $M = 300$ symbols, which

is lower than the proposed method and the exhaustive search, although very close to the latter. The reason for this is because the blocklength variables were constrained to be continuous. Since the floor function is applied to the problem solution to obtain an integer solution, the final solution can have a lower blocklength than the optimal one, leading to higher decoding error. In Fig. 5.5(b), we present the average overall decoding error versus L for $M = 500$ symbols and $E_{\text{tot}} = 0.5$ kJ. It can be seen that, as expected, the average overall decoding error increases as L. This plot shows the highest decoding error for FP; comparable decoding errors for the proposed method and the exhaustive search and similar performance for FB and FAB. In general, it can be observed that the proposed method has a superior performance than FB, FP, FL, FAB, and smart exhaustive search, where the difference becomes more visible as the total energy E_{tot} increases. This is because the proposed algorithm jointly optimizes the location of the UAV, its height, the beamwidth of its antenna, and the power and blocklength allocation for the two transmission phases. In Fig. 5.5(c), we present the average overall decoding error versus E_{tot} for $M = 500$ symbols and $L = 100$ bits. Here, once more, FB and FAB return similar values; however, FAB returns a lower decoding error. Moreover, FP returns the highest decoding error. The proposed method returns lower decoding error than the partial exhaustive search, where the gap between the two increases as E_{tot} increases. In Fig. 5.5(d), we present the average overall decoding error versus the number of robots (Nodes) versus E2E latency/delay D_{E2E} for the blocklengths of $M = 300, 400, 500$, and 600 symbols and $E_{\text{tot}} = 0.6$ KJ. It is evident from the plot that as the number of robots (Nodes) increases, latency and average overall decoding error increases as well, which is an undesirable effect. Hence, to achieve the set targets of reliability and latency, the maximum number of deployed robots in the agricultural field must be balanced. Lastly, it is clearly shown in Fig. 5.3, Fig. 5.4, and Fig. 5.5 that URLLC is established using the proposed **Algorithm 5.1**, guaranteeing overall decoding errors reaching up to 10^{-45} for two phases of transmission. It is thus fulfilling the stringent communication demands for URLLC-assisted UAV relay systems with multiple-mobile robots.

5.6 Conclusion and Future Work

In this paper, we considered a UAV-assisted agricultural system, including a controller and multiple-mobile robots communicating under finite blocklength constraints via UAV serving as a DF relay. The goal was to minimize the average overall decoding error to enable UAV-assisted URLLC for two phases of transmission; the first phase of transmission was between controller and UAV, while the second phase of transmission was between UAV and the robots. To accomplish this goal, we jointly optimized the UAV's height, beamwidth, and location and resource allocation, including variable blocklength and power for each of the k^{th} robot present in the agricultural area corresponding to a circular cell. Furthermore, simulation results show that our proposed algorithm achieves nearly equivalent performance to the smart exhaustive search and has a lower average overall decoding error than benchmark algorithms with fixed parameters, namely FB, FP, FL, and FAB. Finally, we showed that it is necessary to jointly optimize the UAV location, height, beamwidth of its antenna, and the power and blocklength allocation for the two transmission phases to guarantee URLLC for multiple-mobile robots. To conclude this article, we considered that the UAV battery is fully charged when it hovers over the robots. Therefore, to better facilitate downlink communications in UAV-IoT networks, we only considered the downlink communication power of the controller and the UAV. Lastly, an investigation into more sophisticated UAV-IoT systems, including uplink communication and onboard circuit power for UAV hovering, is beyond this current work's scope. Therefore, a joint co-design involving both uplink and downlink communication will be considered for future work. Lastly, in the next chapter, we shall study laser-powered UAV relay systems facilitating URLLC by a joint design of resource allocation, trajectory planning, and energy harvesting.

CHAPTER 6

URLLC-ENABLED BY LASER POWERED UAV RELAY: A QUASI-OPTIMAL DESIGN OF RESOURCE ALLOCATION, TRAJECTORY PLANNING AND ENERGY HARVESTING

Ali Nawaz Ranjha[1] , Georges Kaddoum[1]

[1] Department of Electrical Engineering, École de Technologie Supérieure,
1100 Notre-Dame Ouest, Montréal, Québec, Canada H3C 1K3

Paper published in *IEEE Transactions on Vehicular Technology*, November 2021, early access

6.1 Abstract

Ultra-reliable and low-latency (URLLC) traffic in the upcoming sixth-generation (6G) systems utilize short packets, signalling a distancing from traditional communication systems devised only to support long data packets based on Shannon's capacity formula. This poses a formidable challenge for system designers and network operators. Many URLLC scenarios involve infrastructure-less unmanned aerial vehicle (UAV)-assisted communications. One of the biggest challenges with UAVs is their limited battery capacity, which can cause abrupt disruption of UAV-assisted communications. To overcome these limitations, we consider URLLC-enabled *over-the-air* charging of UAV relay system using a laser transmitter. Furthermore, we formulate a non-convex optimization problem to minimize the total decoding error rate subject to optimal resource allocation, including blocklength allocation, power control, trajectory planning, and energy harvesting to facilitate URLLC in such systems. In this regard, given its lower complexity, a novel perturbation-based iterative method is proposed to solve the optimization problem. The proposed method yields optimal blocklength allocation and power control for the two transmission phases, i.e., from the source node to the UAV and from the UAV to the robot acting as a ground station. It also maps the UAV trajectory from the initial position to the final position, and the UAV completes the flight using the laser's harvested energy. It is shown that the proposed algorithm and fixed baseline scheme, named fixed blocklength (FB), yield a similar performance as the exhaustive search in terms of UAV energy consumption. In contrast, fixed

trajectory (FT) delivers the worst performance. Simultaneously, the proposed method yields the best performance in terms of the lowest average overall decoding error compared to fixed baseline schemes, including FB and FT, showing the efficacy of the proposed technique.

6.2 Introduction

URLLC is among the three distinct service types supported by the upcoming sixth-generation (6G) networks along with enhanced mobile broadband (eMBB) and massive machine-type communication (mMTC). URLLC is essential for mission-critical applications, including unmanned aerial vehicles (UAVs) control information delivery, vehicle to vehicle (V2V) communications, intelligent transportation, self-driving cars, tactile internet, industrial automation, etc. (Bennis *et al.*, 2018). In this regard, these URLLC applications need to establish deterministic communications demanding ultra-high reliability such that the packet decoding error rates are of 10^{-9} or lower, depending on the considered mission-critical application. Additionally, URLLC systems require low latency, and therefore utilize short packets. However, short packets have a drawback of adversely affecting the channel's coding gain. In this respect, Shannon's capacity bound based on the so-called *Law of large numbers* is inapplicable for URLLC as it considers infinite blocklength. Therefore, for finite blocklength transmission, the channel coding rate and capacity bounds were studied and reviewed in (Polyanskiy *et al.*, 2010).

Unmanned aerial vehicles (UAVs) are an innovative and ground-breaking technology that can be utilized for the public, military, and civil sectors (Khan *et al.*, 2017a; Gupta *et al.*, 2015). Additionally, during recent years, technological advancements in the various fields of artificial intelligence, electronics, computer, and sensor technology have expanded UAV applications' scope including wind estimation, remote sensing, and traffic monitoring (Bekmezci *et al.*, 2013). Hereof, it should be noted that natural disasters, e.g., tornadoes, hurricanes, etc., can cause serious damage to communication infrastructures, including cell towers and Land Mobile Radio System (LMRS) repeaters. Under such conditions, there is a need to immediately deploy a temporary communication infrastructure to provide coverage for the existing cloud systems and users while the traditional infrastructure is down (Karlsson *et al.*, 2018). Recently,

UAV-assisted communications has emerged as a favourable candidate for wireless connectivity in such situations (Zeng *et al.*, 2016b). Additionally, UAVs add a degree of freedom, and can enhance performance by dynamically adjusting their positions to meet the required quality of service (QoS). Moreover, the UAVs' high altitudes allows for line of sight (LoS) communication, thus mitigating shadowing and signal blockage. UAVs can act as both flying relays and flying base stations (BSs) between the transmitting and receiving devices (Jiang & Swindlehurst, 2012; Sharma *et al.*, 2016; Ren *et al.*; Pan *et al.*, 2019; Zhang *et al.*, 2018; Shiri, Park & Bennis, 2020; Yang *et al.*, 2018). Notably, under the decode-and-forward (DF) mode, UAV relays can significantly improve channel capacity, channel gain, as well as the quality of service (QoS) (Hu *et al.*, 2016). However, UAVs require a lot of onboard energy to support their propulsion through the air and establish communication links with ground devices. It is crucial to enhance the UAVs' operational time with a sustainable energy supply as they can be deployed in hazardous zones and no-go areas where deploying on-ground personnel is potentially dangerous.

6.2.1 Related Work

In recent years, researchers made tremendous progress to study the complex problems of UAV trajectory planning, UAV beamforming, rate maximization in UAV networks, UAV secrecy rate analysis, UAV node placement as flying BSs or relays, and UAV energy efficiency, as outlined in (Zhang, Zeng & Zhang, 2019; Mozaffari *et al.*, 2017; Guo *et al.*, 2020; Lin, Mei & Zhang, 2019; Chen *et al.*, 2017; Ye, Zhang, Lei, Pan & Ding, 2018; Yuan, Liu, Liu, Li & Ng, 2020; Cai, Wei, Li, Ng & Yuan, 2020). In (Zhang *et al.*, 2019), the authors considered a fixed-wing UAV tasked to collect information from ground nodes (GNs) and proposed a novel receding horizon optimization method to minimize the UAV's energy efficiency defined as the achievable data rate per unit energy consumption. Similarly, the authors in (Mozaffari *et al.*, 2017) considered a multi UAV-IoT communication scenario, where UAVs serve as aerial BSs tasked to collect data from the IoT devices, and sought to jointly optimize the UAV node placement, uplink power control, and UAV-IoT device association. In (Guo *et al.*, 2020), the authors studied a UAV-assisted communication scenario where a single UAV serves multiple ground users (GUs), and aimed

to optimize the so-called *max-min* rate of all users by proposing an optimal trajectory design based on finite Fourier series. The authors in (Lin *et al.*, 2019), considered UAV-assisted mobile relaying with two users lacking a direct link and proposed a novel store-then-amplify-and-forward (SAF) relaying protocol where they jointly optimize the UAV trajectory, transmit power, and time-slot pairing. Similarly, in (Chen *et al.*, 2017), Chen *et al.* considered the UAVs as flying relays and studied the problem of maximum reliability. Moreover, the authors sought to derive analytical expressions for the total outage, power loss, and error rate as reliability measures.

In (Ye *et al.*, 2018), the authors studied the physical layer security of UAV transmitting information to a legitimate UAV, while a group of similar UAVs behave as eavesdroppers. Specifically, the authors aimed to derive analytical expressions for the secrecy outage probability and the average secrecy capacity under such systems. The authors in (Yuan *et al.*, 2020) studied beam alignment between a flying UAV BS and a user equipment (UE). In this regard, they introduced a novel learning-based predictive beamforming technique to mitigate beam misalignment caused by wind gusts. Likewise, in (Cai *et al.*, 2020), the authors studied the joint trajectory and resource allocation design for ensuring security in downlink UAV communication systems. Furthermore, the authors aimed to maximize the system energy efficiency by jointly optimizing the trajectory of the legitimate information UAV and the jamming policy of the jammer UAV. Additionally, only a few works (Petrov, Gapeyenko, Moltchanov, Andreev & Heath, 2020; Guo, Yin & Hao, 2019; Sun, Xu, Ng, Dai & Schober, 2019) in the literature take into account the limited on board battery capacity in the system's design. The authors presented an alternative deployment scheme for millimetre-wave (mmWave) UAV access points (APs) in areas with fluctuating user traffic for prospective 6G networks in (Petrov *et al.*, 2020). Here, the authors suggested to land the UAV on nearby buildings equipped with charging stations, instead of hovering over the areas to conserve and replenish its battery. The authors also developed a mathematical framework for UAV deployment as an interplay of separation distance between service area, charging station, battery duration, and the total number of UAVs required. In (Guo *et al.*, 2019), the authors studied UAV-assisted downlink communication for multiple GUs, where the UAV replenishes its battery periodically at a fixed depot or charging station before resuming the service. In

this regard, the authors aimed to jointly optimize the UAV's time slot allocation for service duration, its trajectory, as well as transmit power. In (Sun *et al.*, 2019), the authors designed a multi-carrier solar-powered UAV system aiming to provide communication services to ground users. The authors sought to maximize the sum throughput of the system by jointly optimizing UAV trajectory and resource allocation over a given time interval. However, for such a system, the harvested energy depends on the intensity of the sunlight reaching the solar panels, which is largely affected by environmental factors such as clouds present in the upper atmosphere (Duffie & Beckman, 2013). Consequently, the harvested energy intended to be utilized for communication purposes is not constant and broadly fluctuates based on environmental changes.

Nevertheless, in these studies (Zhang *et al.*, 2019; Mozaffari *et al.*, 2017; Guo *et al.*, 2020; Cai *et al.*, 2020; Lin *et al.*, 2019; Chen *et al.*, 2017; Ye *et al.*, 2018; Yuan *et al.*, 2020; Petrov *et al.*, 2020; Guo *et al.*, 2019; Sun *et al.*, 2019), the authors employ Shannon's capacity formula for UAV-assisted communication system design, which inherently possesses the desirable properties of monotonicity and convexity (Xu *et al.*, 2016). However, as stated earlier, URLLC systems use short packets for which the Shannon's capacity formula is inapplicable (Ren *et al.*, 2020a; Ranjha & Kaddoum, 2020; A. Ranjha and G. Kaddoum, 2020). Additionally, in UAV-assisted communications, the various UAV operations, such as its propulsion through the air, its communication in uplink/downlink channels with the GNs etc., are energy-consuming tasks where a battery with limited capacity supports UAV. Resultantly, the UAV operations in a service area must be disrupted periodically for the UAV to replenish its battery, triggering periodic disruptions in communication systems, which becomes a bottleneck to deploy large-scale UAV-assisted communications. To resolve this issue, some approaches have been proposed by the researchers in open technical literature, such as designing an energy-efficient UAV trajectory, reducing the overall weight of UAV to prolong its operation time in a service area etc., as outlined in (Cui, Wang & Fang, 2005) and (Zeng & Zhang, 2017). Nonetheless, the energy supply for the UAV is still finite and unsustainable because of the limited battery capacity. To this end, laser-powered UAV systems have been proposed in the literature to provide a sustainable and suitable energy supply (Ouyang, Che, Xu & Wu, 2018) and (Zhao, Shi & Zhao, 2020).

Laser-powered UAV systems use a laser array based on a complex optical system containing a set of mirrors shined on the target UAV. This technique was proven to extend the UAV's mission duration in service areas without causing any significant disruptions as it is an *over-the-air* operation (Lahmeri, Kishk & Alouini, 2019). In (Ouyang *et al.*, 2018), Jie *et al.* presented a laser-powered UAV-assisted communication system. The authors considered that a laser transmitter charges a fixed-wing UAV, establishing communication links with the ground station. Here, the authors sought to optimize power allocation and UAV's trajectory jointly. Similarly, in (Zhao *et al.*, 2020), the authors considered a UAV-enabled relaying system powered by a laser transmitter, where they sought to optimize trajectory and power allocation for rotary-wing UAV. Nonetheless, (Ouyang *et al.*, 2018; Lahmeri *et al.*, 2019; **?**) do not study to provide support for URLLC services. Therefore, to realize the vision of 6G networks, it is essential to consider URLLC enabled over laser-powered mobile UAV relaying systems.

6.2.2 Novelty and Contributions

It is clear from our previous discussions that most of the research efforts studying URLLC, UAV-enabled communications, and their combination, i.e., UAV-enabled URLLC, do not consider *over-the-air* charging of UAV systems using laser transmitters. A well-designed laser charging and energy harvesting system to study URLLC-enabled UAV communications is still missing in the open technical literature. This study is crucial as UAVs are power-hungry devices, and for that a sustainable and steady energy source must be provided to keep UAVs aloft. Besides, the limited battery capacity also hampers UAV deployment in the upcoming 6G communication systems. To this end, the main contributions of this paper can be summarized as follows:

- We propose and formulate a joint resource allocation, trajectory design, and energy harvesting problem to enable URLLC in laser-powered UAV relay systems operating in DF mode. Afterwards, we perform a convexity analysis of our formulated optimization problem to show that it is non-convex, making it difficult to solve optimally. Consequently, we employ the so-called *divide-and-conquer* rule to divide our optimization problem into two sub-problems.

We then solve each sub-problem using perturbation theory based on our low complexity proposed algorithm.

- We demonstrate that our proposed algorithm performs optimal resource allocation, including both blocklength allocation and power control for the two transmission phases. Additionally, we show through simulations that the allocated blocklength is directly proportional to the total available blocklength M_{tot}, while the power is inversely proportional to M_{tot}.
- We show that, in terms of energy consumption in the available time slots, our proposed algorithm and the baseline scheme, called fixed blocklength (FB), yielded comparable performance to the exhaustive search, while fixed trajectory (FT) delivers the worst performance. We further demonstrate that the proposed algorithm can successfully map the UAV trajectory from an initial to a final position. Additionally, we show the efficacy of the proposed algorithm by showing that it yields better performance for the average overall decoding error compared to baseline schemes, including FB and FT.

6.3 System Model and Problem Formulation

In this work, we consider a UAV-enabled mobile relaying system that contains a source node serving as a controller, a robot acting as a ground station, a UAV serving as a decode-and-forward (DF) relay, and a laser transmitter or power beacon (PB). We assume that the direct link between the source and the destination is sufficiently weak to be ignored due to severe blockage, etc., and thus the UAV serves as a mobile relay node to assist their communications. Furthermore, we assume that the UAV is powered wirelessly by the PB using a properly designed laser charging and energy harvesting system, as illustrated in Fig. 6.1. We focus on a particular time period with finite duration $T > 0$, which is discretized into N time slots each with equal duration $\delta_t = \frac{T}{N}$. We assume that the source node is located at the origin $(0, 0, 0)$ in a three-dimensional (3D) cartesian coordinate system, the laser transmitter is located at $(x_p, y_p, 0)$, and the ground station is located at $(x_w, y_w, 0)$. Additionally, at time slot $n \in \{1, \ldots, N\}$, we suppose that the UAV flies at a constant altitude [1] $H > 0$, with a time-varying location $(x_u[n], y_u[n], H)$,

[1] Generally, if the UAV is flying at the height of 80 to 100 meters, there is a 100% probability of achieving LoS communication, according to 3GPP Release 15.

and we let (x_I, y_I, H) and (x_F, y_F, H) denote as the initial and final locations of the UAV. For notational convenience, we denote $\boldsymbol{q}[n] = (x_u[n], y_u[n])$ as the UAV's location projected on the horizontal plane at time slot n, $\boldsymbol{q}_I = (x_I, y_I)$ and $\boldsymbol{q}_F = (x_F, y_F)$ as the initial and final locations of the UAV, respectively, $\boldsymbol{p} = (x_p, y_p, 0)$ as the laser transmitter's position, and $\boldsymbol{w} = (x_w, y_w, 0)$ as that of the ground station. At time slot n, the distance between the UAV and the laser transmitter is $d_b[n] = \sqrt{\|\boldsymbol{q}[n] - \boldsymbol{p}\|^2 + H^2}$, and that between the UAV and the ground station is $d_s[n] = \sqrt{\|\boldsymbol{q}[n] - \boldsymbol{w}\|^2 + H^2}$. Furthermore, the UAV's velocity is given by,

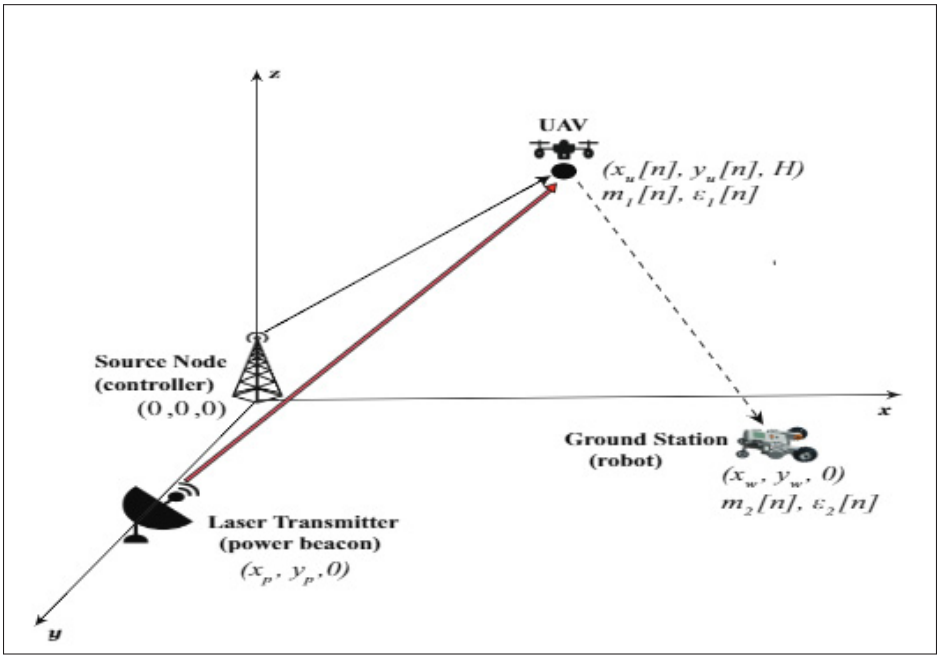

Figure 6.1 Laser powered UAV relay system for enabling URLLC connectivity

$$\|\boldsymbol{v}[n]\| = \frac{\|\boldsymbol{q}[n+1] - \boldsymbol{q}[n]\|}{\delta_t}, \tag{6.1}$$

where $\|\boldsymbol{v}[n]\|$ is limited by the UAV's maximum velocity $V_{\max}$, $\forall n \in \{2, ..., N\}$ and the velocity at time slot $n = 1$ is the same as at time slot $n = 2$. Moreover, each transmission period has two phases, i.e., the first phase corresponds to the transmission from the controller to the UAV, while the second is from the UAV to the robot. The blocklength allocated for each phase is given by $m_1[n]$ and $m_2[n]$, respectively. Additionally, according to (Ranjha & Kaddoum, 2020a;

Zhao *et al.*, 2020), the channel power gains and the signal to noise ratios from the controller to the UAV and from the UAV to the robot are denoted as $h_1[n]$ and $h_2[n]$, $\gamma_1[n]$ and $\gamma_2[n]$, respectively, and are represented as,

$$h_1[n] = \frac{\beta_0}{\|\boldsymbol{q}[n]\|^2 + H^2}, \qquad h_2[n] = \frac{\beta_0}{\|\boldsymbol{q}[n] - \boldsymbol{w}\|^2 + H^2}, \tag{6.2}$$

where β_0 is the channel power gain at a reference distance of $d_0 = 1$ meter and the time-varying transmission powers from the controller to the UAV and from the UAV to the robot are denoted as $P_1[n]$ and $P_2[n]$, respectively. Moreover, the decoding error at the UAV and at the robot at time slot n are given by,

$$\varepsilon_1[n] = Q\left(f\left(\gamma_1[n], m_1[n], L\right)\right), \tag{6.3}$$

$$\varepsilon_2[n] = Q\left(f\left(\gamma_2[n], m_2[n], L\right)\right), \tag{6.4}$$

where $Q(\cdot)$ denotes the Gaussian Q-function[2]. Moreover, the packet size of the command signal generated at the controller is L bits, and its transmission needs to be completed within $\mathcal{T}_{\max}$ seconds. Then, the overall blocklength would be $M_{\text{tot}} = B \times \mathcal{T}_{\max}$, where B is the system bandwidth. Furthermore, according to (Polyanskiy *et al.*, 2010), the following equations are applicable for short packet transmissions,

$$\begin{aligned} f(\gamma_i, m_i, L) &= \ln(2)\sqrt{\frac{m_i}{V(\gamma_i)}}\left(\log_2\left(1+\gamma_i\right) - \frac{L}{m_i}\right), \\ V(\gamma_i) &= 1 - \frac{1}{\left(1+\gamma_i\right)^2} \approx 1, \forall\, i \in \{1,2\} \\ \gamma_1[n] &= P_1[n]h_1[n], \quad \gamma_2[n] = P_2[n]h_2[n]. \end{aligned} \tag{6.5}$$

Since the UAV acts as a DF relay, then the overall decoding error probability from the controller to robot at time slot n is given by

$$\varepsilon[n] = \varepsilon_1[n] + \left(1 - \varepsilon_1[n]\right)\varepsilon_2[n], \tag{6.6}$$

[2] $Q(p) = \frac{1}{\sqrt{2\pi}} \int_p^\infty e^{-\frac{s^2}{2}} ds.$

Since the simultaneous errors $\varepsilon_1[n]\varepsilon_2[n] \rightarrow 0$, the expression is simplified and the overall decoding error probability is

$$\varepsilon[n] = \varepsilon_1[n] + \varepsilon_2[n]. \tag{6.7}$$

We model the downlink communication energy of the UAV as its dominant energy consumption. Here, the negligible energy dissipation values contributed by thermal noise in electronics, baseband signal processing, and the RF chain are ignored (Ouyang *et al.*, 2018). Therefore, the downlink communication energy of the UAV at time slot n is given as

$$P_m[n] = \frac{\delta_t}{\eta} P_2[n], \ \forall n \in \{1, \ldots, N\}, \tag{6.8}$$

where $0 < \eta \leq 1$ denotes the radio frequency (RF) chain efficiency. According to (Ouyang *et al.*, 2018), we consider a model to characterize the energy consumption of the UAV due to flying, which postulates that the energy consumed while flying at each time slot n depends only on the velocity vector $\boldsymbol{v}[n]$. Hence, the energy consumption due to flying is

$$P_f[n] = \psi \|\boldsymbol{v}[n]\|^2, \ \forall n \in \{1, \ldots, N\}, \tag{6.9}$$

where $\psi = 0.5\mu\delta_t$ and μ is the UAV's mass, including its payload. The total amount of energy consumption at the UAV at time slot n is a summation of the energy consumption for communication and energy consumption for propulsion, respectively denoted as $P_m[n]$ and $P_f[n]$. Hence, according to (Ouyang *et al.*, 2018), the total amount of energy consumption at the UAV can be expressed as

$$P_c[n] = P_m[n] + P_f[n], \ \forall n \in \{1, \ldots, N\}, \tag{6.10}$$

We assume that the laser transmitter has a fixed transmit power expressed by $\varphi > 0$. Moreover, we consider energy harvesting at the UAV over the laser transmitter's link. Consequently, at the UAV, the received signal strength at time slot n is expressed as

$$P_s[n] = \delta_t \varphi \frac{A}{(D + d_b[n]\Delta\theta)^2} \chi e^{-\alpha d_b[n]}, \ \forall n \in \{1, \ldots, N\}, \tag{6.11}$$

where D is the initial laser beam's size, χ is the combined transmission receiver's optical efficiency, $\Delta\theta$ is the angular spread, A is the area of collection lens, and α is the medium's attenuation coefficient expressed in m^{-1}. Additionally, we assume an energy harvesting model with a constant laser energy harvesting efficiency $\omega \in (0, 1)$. Hence, the amount of harvested laser energy at the UAV at time slot n is given as

$$P_h[n] = \omega P_s[n] = \frac{\delta_t C \varphi e^{-\alpha d_b[n]}}{(D + d_b[n]\Delta\theta)^2}, \ \forall n \in \{1, \ldots, N\}, \tag{6.12}$$

where $C = \omega A \chi$ and α is a very small value. Therefore, the variations of $P_s[n]$ and $P_h[n]$ over the distance $d_b[n]$ are dominated by the term $(D + d_b[n]\Delta\theta)^{-2}$. Additionally, we notice that $\Delta\theta$ is normally very small, and the laser transmit power φ is quite large. Hence, $P_h[n]$ decreases much slower over the distance $d_b[n]$ as compared to the RF energy harvesting case. It also provides a reasonable justification that a laser transmitter can have a greater charging range to meet the demands of power-hungry applications such as UAVs. To guarantee that the UAV can safely reach the final location with enough battery level in case of emergence and to avoid overcharging, the following laser energy harvesting constraints must be satisfied:

$$\zeta \leq Z + \sum_{n=1}^{m} P_h[n] - \sum_{n=1}^{m} P_c[n] \leq Z, \ \forall m \in \{1, \ldots N\}, \tag{6.13}$$

where Z represents the UAV's energy budget i.e., the maximum energy storage capacity of the UAV's battery, if we assume that the UAV is fully charged before taking off and ζ is a predefined threshold which characterizes the minimum energy storage during the flight. The objective is to minimize the mean overall decoding error probability by jointly optimizing the UAV's trajectory $\boldsymbol{Q_u} = \{\boldsymbol{q}[n], \forall n\}$, and blocklength $\boldsymbol{M} = \{m_1[n], m_2[n], \forall n\}$ over the N time slots. To simplify constraint (6.13), an auxiliary variable $\boldsymbol{d} = \{d[n], \forall n\}$ is introduced, such that

$$\begin{aligned} d[n] &\geq \|\boldsymbol{q}[n] - \boldsymbol{p}\|^2 + H^2, \\ F_m(\boldsymbol{d}) &= \sum_{n=1}^{m} \frac{\delta_t C \varphi e^{-\alpha\sqrt{d[n]}}}{(D + \sqrt{d[n]}\Delta\theta)^2}, \end{aligned} \tag{6.14}$$

where $F_m(d)$ is used to shorten the mathematical notation of constraint (6.13), similarly we also introduce another variable $G_m(d)$ as follows:

$$G_m(\boldsymbol{q}) = \sum_{n=1}^{m} \psi \frac{\|\boldsymbol{v}[n]\|^2}{\delta_t^2} + \frac{1}{\eta} \sum_{n=1}^{m} P_2[n]\delta_t, \ \forall m \in \{1, \dots N\}, \tag{6.15}$$

Therefore, the optimization problem is mathematically formulated as

$$\min_{\boldsymbol{Q_u}, \boldsymbol{d}, \boldsymbol{M}} \quad \frac{1}{N} \sum_{n=1}^{N} \varepsilon[n] \tag{6.16a}$$

$$\text{s.t.} \quad \zeta \leq Z + F_m(\boldsymbol{d}) - G_m(\boldsymbol{q}) \leq Z, \ \forall m \in \{1, \dots N\}, \tag{6.16b}$$

$$\|\boldsymbol{q}[n] - \boldsymbol{p}\|^2 + H^2 \leq d[n], \quad \forall n \in \{1, \dots N\}, \tag{6.16c}$$

$$\|\boldsymbol{q}[n+1] - \boldsymbol{q}[n]\| \leq V_{\max}\delta_t, \quad \forall n \in \{1, \dots, N\}, \tag{6.16d}$$

$$\boldsymbol{q}[1] = \boldsymbol{q}_I, \quad \boldsymbol{q}[N] = \boldsymbol{q}_F, \tag{6.16e}$$

$$m_1[n] + m_2[n] \leq M_{\text{tot}}, \quad \forall n \in \{1, \dots, N\}, \tag{6.16f}$$

$$\varepsilon_1[n] \leq \epsilon_1, \quad \varepsilon_2[n] \leq \epsilon_2, \quad \forall n \in \{1, \dots, N\}, \tag{6.16g}$$

$$P_1[n] \geq 0, \quad P_2[n] \geq 0, \quad \forall n \in \{1, \dots, N\}, \tag{6.16h}$$

$$m_1[n], m_2[n] \in \mathbb{N}, \quad \forall n \in \{1, \dots, N\}, \tag{6.16i}$$

The problem is being non-convex because the objective function and constraints (6.16b), (6.16g) and (6.16i) are not convex (more details are provided in the **Appendix IV**). Hence, it is a complicated problem to solve.

6.4 The Proposed Approach

As discussed before the problem (5.9) is non-convex, due to which it is difficult to obtain a globally optimal solution. Consequently, we employ an iterative approach and we divide (6.16) into two sub-problems and iteratively perform global optimization for each constraint, including the time-varying blocklength $m_i[n], \forall n \in \{1, \dots, N\}$, the UAV's trajectory $q[n], \forall n \in \{1, \dots, N\}$, whereas the power $P_i[n], \forall n \in \{1, \dots, N\}$, for the two transmission phases is fixed.

6.4.1 Blocklength

In the first sub-problem, which deals with finding the time-varying optimal blocklength $m_i[n], \forall i \in \{1,2\},\ \forall n \in \{1,\dots,N\}$, for each of the two transmission phases, we assume that the constraints $P_i[n], q[n], \forall i \in \{1,2\},\ \forall n \in \{1,\dots,N\}$, are fixed. It is noted that the blocklength variable is an integer, which makes the problem non-convex. To solve the problem, this constraint is relaxed, where $m_1[n]$ and $m_2[n]$ are assumed to be continuous variables. Hence, the problem reduces to

$$\min_{\boldsymbol{M}} \quad \frac{1}{N}\sum_{n=1}^{N} \varepsilon[n] \tag{6.17a}$$

$$\text{s.t.} \quad m_1[n] + m_2[n] \le M_{\text{tot}}, \quad \forall n \in \{1,\dots,N\}, \tag{6.17b}$$

$$\varepsilon_1[n] \le \epsilon_1, \quad \varepsilon_2[n] \le \epsilon_2, \quad \forall n \in \{1,\dots,N\}, \tag{6.17c}$$

$$m_1[n] \ge 0, \quad m_2[n] \ge 0, \quad \forall n \in \{1,\dots,N\}, \tag{6.17d}$$

To prove the convexity of the objective function of problem (6.17), one first notices that $\varepsilon_1[n]$ and $\varepsilon_2[n]$ have similar expressions, hence it is sufficient to prove convexity for just one of these terms. We assume that $f(m_1[n]) = f(\gamma_1^*[n], m_1[n], L)$, at an arbitrary time slot n. The first term of the objective function can be written as

$$\varepsilon_1[n] = Q(f(m_1[n])) = Q\left(A_1\sqrt{m_1[n]}\left(B_1 - \frac{L}{m_1[n]}\right)\right), \tag{6.18}$$

where $A_1 = \ln(2)$ and $B_1 = \log_2\left(1+\gamma_1^*[n]\right)$ are constants that do not depend on $m_1[n]$. The second derivative of $f(m_1[n])$ is

$$\frac{\partial^2 f(m_1[n])}{\partial m_1^2[n]} = -\frac{A_1(3L + B_1 m_1[n])}{4\sqrt{m_1^5[n]}}. \tag{6.19}$$

Since $m_1[n]$, A_1, B_1, and L are positive values, $\frac{\partial^2 f(m_1[n])}{\partial m_1^2} < 0$ and hence f is a concave function. Since $Q(x)$ is convex and non-increasing for $x \ge 0$ and $f(m_1[n])$ is a concave function, the composition $Q(f(m_1[n]))$ is a convex function. Similarly, $\varepsilon_2[n]$ is a convex function, thus their

summation is a convex function. The constraints are convex functions, which makes problem (6.17) convex.Constraints (6.17c) can be transformed into lower bounds by taking $m_i[n]$ as

$$m_i[n] \geq L_b^i[n] = \frac{\epsilon_i \sqrt{4\ln(2)^2 A_i L + \epsilon_i^2} 2 + \ln(2)^2 A_i L}{2\ln(2)^2 A_i^2} + \frac{\epsilon_i^2}{2\ln(2)^2 A_i^2}, \ \forall i \in \{1,2\}, \ \forall n \in \{1,\ldots,N\}, \tag{6.20}$$

Since $L_b^i \geq 0$, constraint $m_i[n] \geq 0$ is redundant and can be eliminated. Therefore, to solve problem (6.17) one first notices that the constraints of this problem are dependent on the time slot n, thus minimize $\frac{1}{N}\sum_{n=1}^{N} \varepsilon[n]$ is equivalent to minimize $\varepsilon_1[n] + \varepsilon_2[n], \forall\, n \in \{1,\ldots,N\}$. As such, problem (6.17) can be equivalently represented as

$$\min_{\{m_1[n], m_2[n]\}} \quad \varepsilon_1[n] + \varepsilon_2[n] \tag{6.21a}$$

$$\text{s.t.} \quad m_1[n] + m_2[n] \leq M_{\text{tot}}, \tag{6.21b}$$

$$m_1[n] \geq L_b^1[n], \quad m_2[n] \geq L_b^2[n], \tag{6.21c}$$

The first derivative of the objective function is negative, thus the error decreases as the blocklength increases, which indicates that the optimal solution will be found on the boundary of constraint (6.21b), allowing $m_2[n]$ to be represented in terms of $m_1[n]$ as $m_2[n] = M - m_1[n]$. The lower bound of $m_2[n]$ is used to compute the upper bound of $m_1[n]$ as $U_b^1[n] = M - L_b^2[n]$ and the objective function is given by $f_{\text{obj}}(m_1[n]) = Q(f(m_1[n])) + Q(f(M - m_1[n]))$. Each problem is a one variable problem only, $m_1[n]$. In this regard, to solve (6.21), different optimization algorithms in the literature can be utilized, including the bisection method and Newton method. Nonetheless, the optimization variable $m_i[n]$ is an integer value, and such algorithms are not well-suited and well-tailored for use (Wang, Wang, Ding, Wang, Tsiftsis & Sharma, 2017). Therefore, to solve each problem, we choose a derivative-free method known as the golden section method. It is known to be computationally efficient (Braun & Murdoch, 2016), and as outlined in **Algorithm 6.1**, it searches for a minimum of a given function in a certain domain.

Algorithm 6.1 Golden section for the blocklength problem:

Compute $L_b^1[n]$ and U_b^1, $n = 1, \ldots, N$. Set $\texttt{tol} = 0.5$, $\phi = \frac{1+\sqrt{5}}{2}$.
Set $n = 1$ and a tolerance $\texttt{tol}$.
for $n = 1, \ldots, N$ **do**
    Set $a = L_b^1[n]$, $b = U_b^1[n]$.
    Set $c = b - \frac{b-a}{\phi}$, $d = a + \frac{b-a}{\phi}$.
    while $|c - d| > \texttt{tol}$ **do**
        Set $sol_c = f_{\text{obj}}(c)$, $sol_d = f_{\text{obj}}(d)$.
        if $(sol_c < sol_d)$ **then**
            Set $b = d$.
        else
            Set $a = c$.
        end if
        Recalculate c and d.
    end while
    Set Set $sol = \frac{b+a}{2}$.
    Set Return the optimal $m_1[n]$ as $m_1^*[n] =_{\{sol,sol\}} f_{\text{obj}}$ and the optimal $m_2[n]$ as $m_2^*[n] = M - m_1^*[n]$.
end for

6.4.2 UAV Trajectory

In the second sub-problem, which deals with finding the optimal UAV trajectory $q[n], \forall n$, we assume that the constraints $m_i[n], P_i[n], \forall\, i \in \{1, 2\}$ are fixed. Therefore, the problem reduces

to

$$\min_{\boldsymbol{Q_u},\boldsymbol{d}} \quad \frac{1}{N}\sum_{n=1}^{N}\varepsilon[n] \tag{6.22a}$$

$$\text{s.t.} \quad \zeta \leq Z + \sum_{n=1}^{m} P_h[n] - \sum_{n=1}^{m} P_c[n] \leq Z, \forall m \in \{1,\dots N\}, \tag{6.22b}$$

$$\|\boldsymbol{q}[n+1] - \boldsymbol{q}[n]\| \leq V_{\max}\delta_t, \quad \forall n \in \{1,\dots,N\} \tag{6.22c}$$

$$\boldsymbol{q}[1] = \boldsymbol{q}_I, \quad \boldsymbol{q}[N] = \boldsymbol{q}_F \tag{6.22d}$$

$$\varepsilon_1[n] \leq \epsilon_1, \quad \varepsilon_2[n] \leq \epsilon_2, \quad \forall n \in \{1,\dots,N\} \tag{6.22e}$$

This problem is non-convex due to the fact that the objective function and constraint (6.22b), are a non-convex function and a non-convex set, respectively. Starting with the objective function, introduce auxiliary variables $d_1[n]$ and $d_2[n]$ such that $d_1[n] \geq \|\boldsymbol{q}[n]\|^2 + H^2$ and $d_2[n] \geq \|\boldsymbol{q}[n] - \boldsymbol{w}\|^2 + H^2$, which are added to the problem as constraints. These two conditions represent convex sets, where it can be shown that both will hold equally at the optimum solution, otherwise one could keep decreasing $d_i[n]$, $\forall\ i \in \{1,2\}$ to decrease the objective function value. The objective function is jointly concave w.r.t. $d_1[n]$ and $d_2[n]$, which means that the first order Taylor series expansion provides an upper-bound of this function. Let $f(d_i[n]) = f(\gamma_i[n], m_i^*[n], L)$, $\forall\ i \in \{1,2\}$, and consider a term $\varepsilon[n]$ of the objective function, at an arbitrary time slot n

$$\varepsilon[n] = E_1(d_1[n]) + E_2(d_2[n]), \tag{6.23}$$

$$\begin{aligned} E_i(d_i[n]) &= Q(f(d_i[n])), \\ &= Q\left(B_i[n]\left(\log_2\left(1 + \frac{A_i[n]}{d_i[n]}\right) - C_i[n]\right)\right). \end{aligned} \tag{6.24}$$

where $A_i[n] = P_i[n]\beta_0$, $B_i[n] = \ln(2)\sqrt{m_i^*[n]}$ and $C_i[n] = \frac{L}{m_i^*[n]}$, $\forall\ i \in \{1,2\}$. The first derivative of $E_i(d_i[n])$ is

$$\frac{\partial E_i(d_i[n])}{\partial d_i} = \frac{\sqrt{2}A_iC_i\exp\left(-\frac{f(d_i[n])}{2}\right)}{2d_i^2\sqrt{\pi}\log(2)\left(\frac{A_i}{d_i[n]}+1\right)}, \tag{6.25}$$

and the first order Taylor expansion of $\varepsilon[n]$ at point $(\hat{d}_1[n], \hat{d}_2[n])$, which is given by

$$\begin{aligned}\hat{\varepsilon}[n] = E_1(\hat{d}_1[n]) + (d_1[n] - \hat{d}_1[n])\frac{\partial E_1(d_1[n])}{\partial d_1}\bigg|_{d_1[n]=\hat{d}_1[n]} \\ + E_2(\hat{d}_2[n]) + (d_2[n] - \hat{d}_2[n])\frac{\partial E_2(d_2[n])}{\partial d_2}\bigg|_{d_2[n]=\hat{d}_2[n]},\end{aligned} \tag{6.26}$$

which is an upper-bound of $\varepsilon[n]$. Since $\varepsilon[n] \leq \hat{\varepsilon}[n]$, the sum of $\varepsilon[n], \forall n \in \{1, \ldots, N\}$ is also upper-bounded by the sum of $\hat{\varepsilon}[n]$. Constraint (6.22b) is non-convex (please refer to Appendix IV 2), however it is possible to use the first order Taylor series expansion to transform the constraint into a convex one. As mentioned before, the constraint (6.16b) can be represented as

$$\zeta - Z + G_m(\boldsymbol{q}) \leq F_m(\boldsymbol{d}), \forall m \in \{1, \ldots, N\}, \tag{6.27}$$

Since $F_m(\boldsymbol{d})$ is convex, its first order Taylor series expansion provides a lower bound at point $\hat{\boldsymbol{d}}$. Thus, for the first case, this constraint can be expressed as

$$\zeta - Z + G_m(\boldsymbol{q}) \leq F_m(\hat{\boldsymbol{d}}) + \nabla F_m(\hat{\boldsymbol{d}})(\boldsymbol{d} - \hat{\boldsymbol{d}}), \forall m \in \{1, \ldots, N\}. \tag{6.28}$$

Moreover, for the second case, (6.16b) is represented by the following equation

$$F_m(\boldsymbol{d}) \leq G_m(\boldsymbol{q}), \forall m \in \{1, \ldots, N\}. \tag{6.29}$$

In this case, the first order Taylor series expansion of function G_m provides a lower bound at point $\hat{\boldsymbol{q}}$ given as

$$F_m(\boldsymbol{d}) \leq G_m(\hat{\boldsymbol{q}}) + \nabla G_m(\hat{\boldsymbol{q}})(\boldsymbol{q} - \hat{\boldsymbol{q}}), \forall m \in \{1, \ldots, N\}. \tag{6.30}$$

Finally, constraints (6.22e) become

$$d_i[n] \leq U_i[n] = \frac{A_i[n]}{2^{C_i[n] + \frac{Q^{-1}(\epsilon_1)}{B_i[n]}} - 1}, \ \forall i \in \{1, 2\}, \tag{6.31}$$

Hence, an approximated convex problem of problem (6.22) is given by

$$\min_{\boldsymbol{Q_u},\boldsymbol{d},\boldsymbol{d_1},\boldsymbol{d_2}} \quad \frac{1}{N}\sum_{n=1}^{N}\hat{\varepsilon}[n] \tag{6.32a}$$

$$\text{s.t.} \quad \mathbf{C1}: (28), \tag{6.32b}$$

$$\mathbf{C2}: (30), \tag{6.32c}$$

$$\|\boldsymbol{q}[n]\|^2 + H^2 \leq d_1[n], \forall n \in \{1,\dots,N\}, \tag{6.32d}$$

$$\|\boldsymbol{q}[n] - \boldsymbol{w}\|^2 + H^2 \leq d_2[n], \forall n \in \{1,\dots,N\}, \tag{6.32e}$$

$$\|\boldsymbol{q}[n] - \boldsymbol{p}\|^2 + H^2 \leq d[n], \forall n \in \{1,\dots,N\}, \tag{6.32f}$$

$$\|\boldsymbol{q}[n+1] - \boldsymbol{q}[n]\| \leq V_{\max}\delta_t, \forall n \in \{1,\dots,N\}, \tag{6.32g}$$

$$\boldsymbol{q}[1] = \boldsymbol{q}_I, \quad \boldsymbol{q}[N] = \boldsymbol{q}_F \tag{6.32h}$$

$$d_1[n] \leq U_1, \quad d_2[n] \leq U_2, \quad \forall n \in \{1,\dots,N\}, \tag{6.32i}$$

Additionally, the transmission powers $P_1[n]$ and $P_2[n]$, $\forall n \in \{1,\dots,N\}$, are not variables in this problem but rather fixed parameters. To guarantee that the initial solution is within the feasible region, i.e., that ε_1 and ε_2 are both below ϵ_1 and ϵ_2 respectively, the value chosen for these parameters will be based on their lower bounds at the initial solution. The lower bound of the transmission powers is given by

$$\begin{aligned} &\varepsilon_i[n] \leq \epsilon_i, \\ &P_i[n] \geq \frac{2^{\frac{\varepsilon_i}{A_i[n]}+B_i[n]}-1}{h_i}, \forall n \in \{1,\dots,N\}, \end{aligned} \tag{6.33}$$

where $A_i[n] = \log(2)\sqrt{m_i[n]}$ and $B_i[n] = \frac{L}{m_i[n]}$, $\forall i \in \{1,2\}$, $\forall n \in \{1,\dots,N\}$. To make sure the problem is feasible through iterations, the final value for these variables will be twice their lower bound.

Table 6.1 Set of chosen parameters for laser powered UAV relay system.

Parameters	Descriptions	Values
$\boldsymbol{q}_I[1]$	Initial UAV's location	[0, 500] m
$\boldsymbol{q}_F[N]$	Final UAV's location	[1000, 500] m
$\boldsymbol{w}$	Location of robot	[1000, 0] m
$\boldsymbol{p}$	Location of laser	[500, 800] m
β_0	Channel power gain of UAV	50 dB
L	Packet size	100 bits
T	Time period duration	120 sec
N	Number of time slots	30
δ_t	Discretization coefficient of time slots	4 sec
C	$C = \omega A \chi$	0.004 m^2
α	Attenuation coefficient of the medium	10^{-6} m
D	Size of the initial laser beam	0.1 m
$\Delta\theta$	Angular spread of the laser beam	3.4×10^{-5}
φ	Laser transmit power	600 W
$V_{\max}$	Maximum velocity of the UAV	20 m/s
μ	UAV's mass	20 kg
ζ	Minimum energy storage of the UAV	10^3 J
Z	Maximum energy storage of the UAV	10^5 J
η	RF chain efficiency	1
H	UAV's height	100 m
ϵ_1	Minimum error at the UAV	10^{-6}
ϵ_2	Minimum error at the robot	10^{-5}

6.4.3 Proposed Algorithm

As mentioned before, we divide the significantly complicated mathematical problem (6.16) into two relatively simpler sub-problems, namely (6.17) and (6.22) that we proceed to solve. From Appendix, we know that the overall problem is non-convex, and thus a global solution to the problem (6.16) is not guaranteed. However, each sub-problem is convex; therefore, we perform global optimization for each variable by fixing the other variables. At the first step, we generate an initial solution S^0, initialize $(\boldsymbol{m}^0, \boldsymbol{q}^0)$ and compute $\boldsymbol{P} = \{P_1[n], P_2[n], \forall n\}$ which is based on (6.33). It is to be noted that the initial solution S^0 is generated through a rigorous process of trial and error. After that, the proposed algorithm solves each sub-problem individually through

a series of iterations and stops when the difference between two numerical solutions $S^n - S^{n-1}$ is below a given tolerance `tol` as shown in **Algorithm 6.2**. Subsequently, an initial solution S^0 is provided to solve the first iteration, and the solution to each sub-problem at each step is then used to solve the next sub-problem. We present the aforementioned steps involved in each of the previous two sub-problems in **Algorithm 6.2**.

Algorithm 6.2 Perturbation-based iterative method for computing the optimal blocklength allocation, power control and UAV's trajectory

Initialize $(\boldsymbol{m}^0, \boldsymbol{q}^0)$ and compute $\boldsymbol{P}$, obtaining an objective value S^0.
Set $k = 1$ and a tolerance `tol`.
while $|S^k - S^{k-1}| >$ `tol` **do**
    Compute $\boldsymbol{m}^{k+1}$ solution of (6.21), with $\boldsymbol{q}^k$ using **Algorithm 6.1**.
    Compute $\boldsymbol{q}^{k+1}$ solution of (6.32), with $\boldsymbol{m}^{k+1}$.
    Compute final objective value S^{k+1} as in (6.16a).
    Set $k = k + 1$.
    Until the termination conditions are met.
    Return an optimized solution.
end while

6.5 Simulation Results and Discussion

In this section, we present the results obtained with the proposed method for two different total blocklengths $M_{\text{tot}} \in \{300, 450\}$ symbols. The parameters chosen for the laser-powered UAV communication system are shown in Table 7.1. Moreover, for comparison purposes, an exhaustive search was performed. Furthermore, it is noted that the parameters $P_1[n]$ and $P_2[n]$ used are based on the initial solution used for the proposed method. Fig. 6.2, shows the distribution of the blocklength versus the total available time slots for the two transmission phases obtained for different total blocklengths M_{tot}.

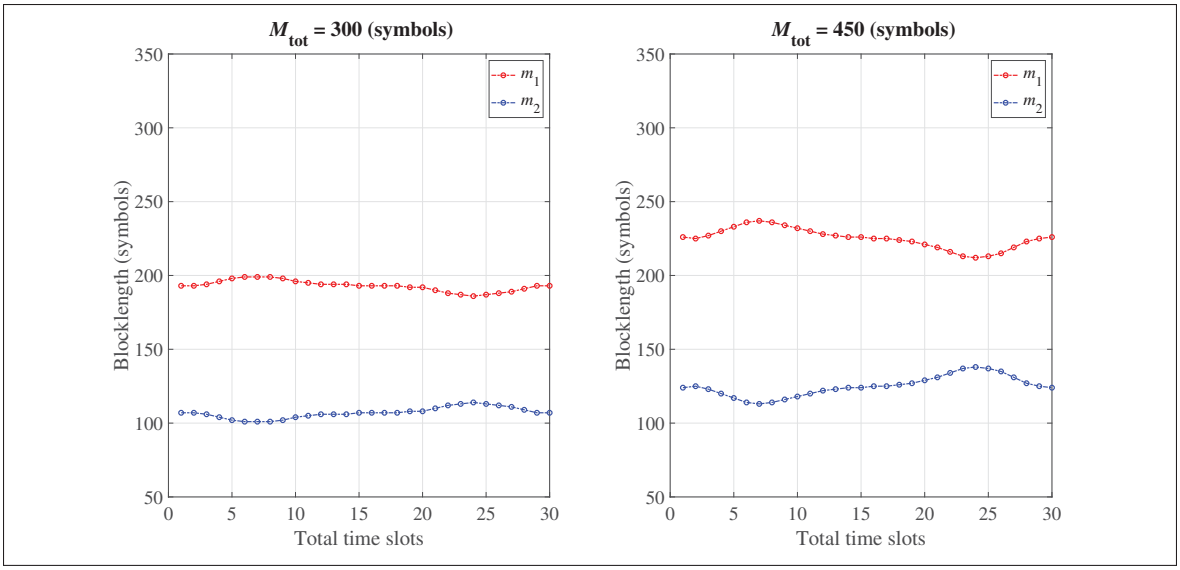

Figure 6.2 Blocklength versus the available time slots

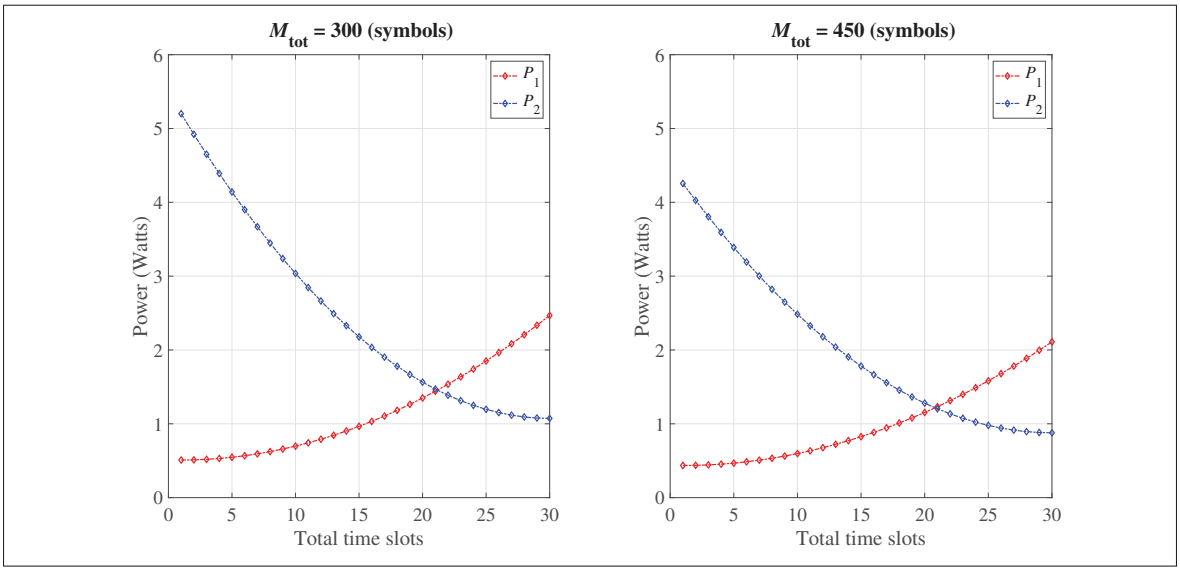

Figure 6.3 Power versus the available time slots

In these two subplots, it is also noticeable that $m_1[n]$ increases slightly at the beginning of the UAV's flight and then decreases towards the end, while the situation is reversed for $m_2[n]$. It can be observed that both $m_1[n]$ and $m_2[n]$ are directly proportional to the increase in M_{tot}. Thus, it can be concluded that as M_{tot} increases, the blocklength distribution for the two transmission

phases, i.e., from the ground station to the UAV and from the UAV to the robot, also increases. Similarly, Fig. 6.3, shows the values of $P_1[n]$ and $P_2[n]$ for different M_{tot}. It can be seen that the powers obtained for $M_{\text{tot}} \in \{300, 450\}$ symbols are similar, indicating that the overall blocklength has more influence on the power's lower bound when it is smaller. Additionally, it is also observed that the two powers $P_1[n]$ and $P_2[n]$ are inversely proportional to M_{tot}. Therefore, as the total blocklength increases, the two powers for the two transmission phases decrease. It is to be noted that Fig. 6.2 and Fig. 6.3 represent the resource allocation, including blocklength and power allocation of our laser-powered UAV-assisted URLLC system for the two transmission phases.

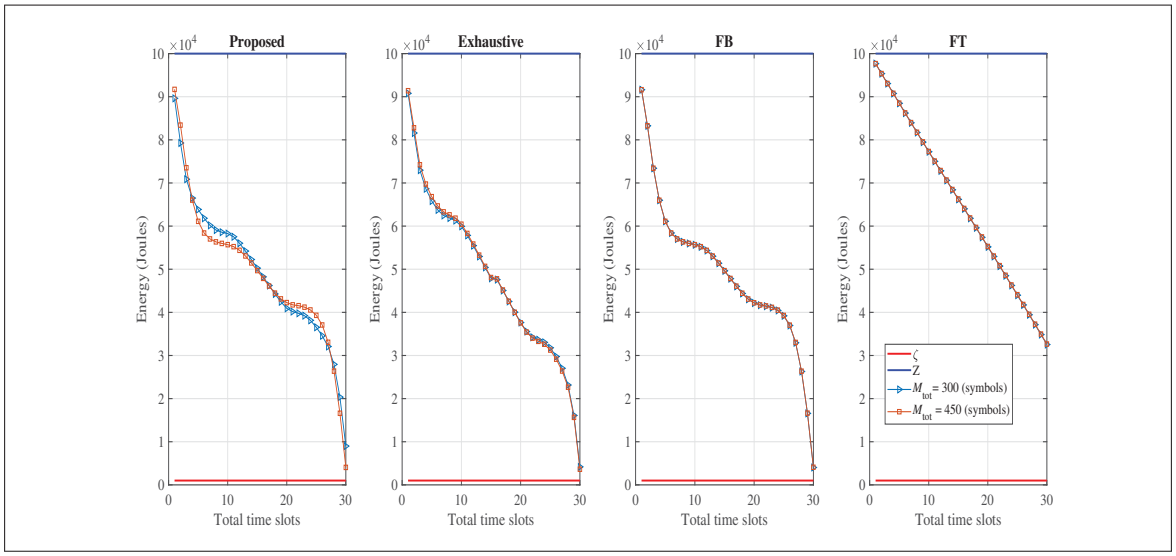

Figure 6.4 Energy usage versus the available time slots

Fig. 6.4 shows the energy available at the UAV during the flight, as well as the minimum and maximum energy storage capacities of the UAV. Moreover, Fig. 6.4 demonstrates the UAV's efficient energy usage of the harvested laser's energy in the available time slots. Again, the proposed method returns different values for the available energy for $M_{\text{tot}} \in \{300, 450\}$ symbols, while the exhaustive search returns almost similar results for the two chosen blocklengths i.e., $M_{\text{tot}} \in \{300, 450\}$ symbols. It should be noted that the proposed algorithm finds a quasi-optimal solution that uses all the available energy through the time slots in an efficient way, finishing the flight with almost no energy available. Additionally, we propose two fixed methods named

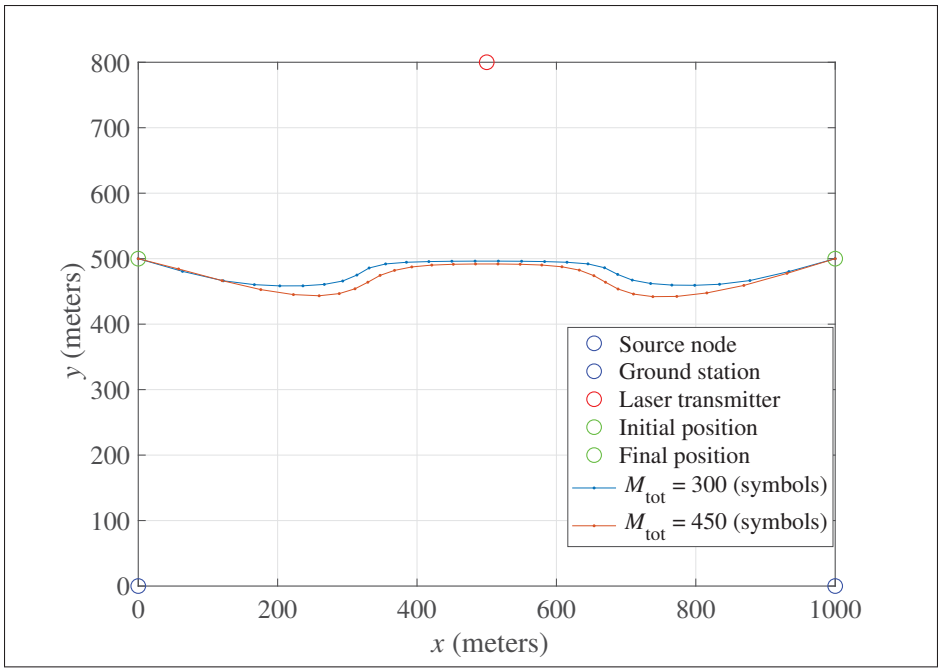

Figure 6.5 UAV's trajectory

fixed blocklength (FB) and fixed trajectory (FT). Here, FB only solves the UAV trajectory Q_u optimization problem, whereas FT only considers the blocklength problem M. Afterwards, we compare the so-called fixed methods with our proposed method for the aforementioned blocklengths i.e, $M_{\text{tot}} \in \{300, 450\}$ symbols. For FB, the results are similar since the blocklength is fixed and only optimized UAV trajectory Q_u does not immensely affect the two solutions through the available time slots; hence there is no variation between the two blocklength plots. Similarly, for FT, the results are again similar for the two blocklengths. Here, we notice that the available energy decreases almost in a linear manner with the available time slots. Furthermore, the FT plot is different in shape compared to proposed, exhaustive, and FB plots as UAV's trajectory that significantly affects the shape of the energy consumption plot. Additionally, for FT, since the trajectory is fixed, the solution for the two blocklengths mentioned above is the same. The proposed method and FB yield comparable performance to the exhaustive search, whereas FT yields the worst performance in terms of energy usage in the available time slots. It is to be taken into consideration that FB and FT partially solve the optimization problem (16), and only the proposed method fully solves it; this will be shown in the last graph. Fig. 6.5 shows

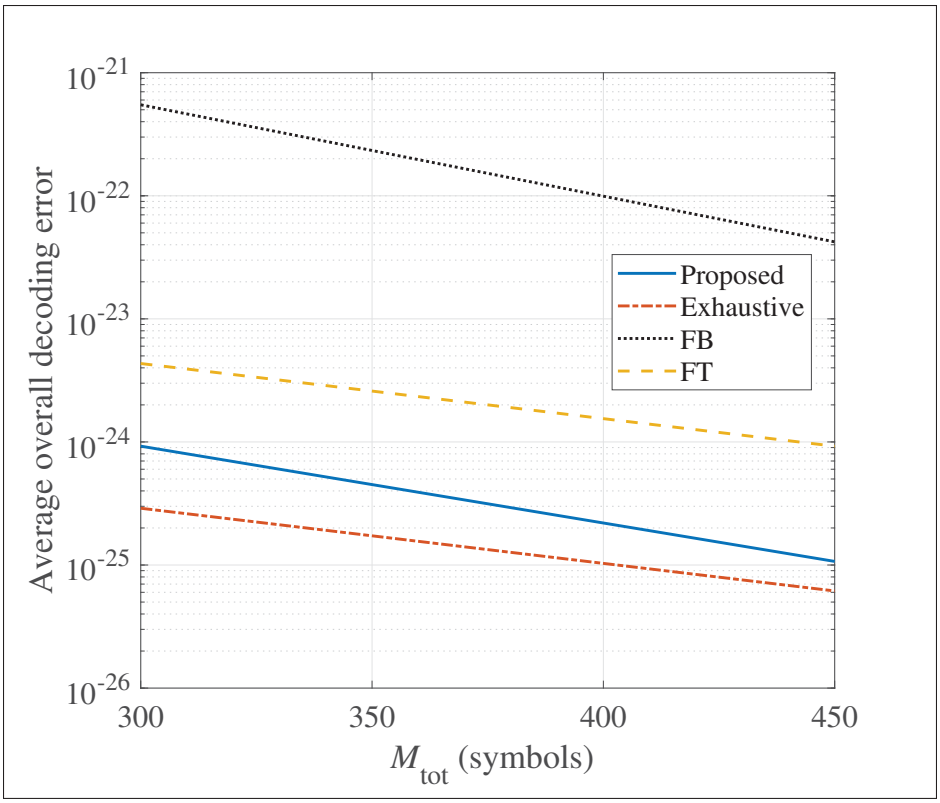

Figure 6.6 Average overall decoding error versus blocklength

the location obtained with the proposed method for different M_{tot}. For convenience, the positions of the source node, ground station, laser transmitter, and initial as well as final points are represented in Fig. 6.5. The trajectories of the UAV for two blocklengths, i.e., $M_{\text{tot}} \in \{300, 450\}$ symbols are identical when the UAV starts the flight, and then the trajectories deviate around the coordinates $(120, 466)$, where the first term represents the abscissa and the second corresponds to the ordinate. Similarly, the two trajectories are superimposed again around the coordinates $(930, 466)$. Furthermore, the difference between the trajectories generated for different allocated blocklengths becomes indistinguishable as the total blocklength M_{tot} increases. Fig. 6.6 shows the average overall decoding error, i.e., the objective function value, for the proposed method and for the exhaustive search, for different M_{tot}. As expected, the average overall decoding error decreases when M_{tot} increases for all of the approaches. The error obtained with the proposed method is higher than that of the exhaustive search which is also expected. However, they do not differ much, indicating that the proposed method can efficiently find an approximate solution

that is close to the global solution. Additionally, we also plot the aforementioned fixed methods, i.e., FB and FT. Here, the worst performance for our objective function is yielded by FB, while the best performance is provided by our proposed method, hence demonstrating the efficacy of the proposed method to solve problem (6.16).

6.5.1 Time-Complexity Analysis

The computational complexity of **Algorithm 6.1** is $O\left(\log_2\left(\frac{1}{\epsilon}\right)\right)$, where ϵ denotes the accuracy of the golden section method. Similarly, the time complexity of **Algorithm 6.2**, which is composed of **Algorithm 6.1** utilizing the golden section method for solving the blocklength allocation problem and the interior-point method for solving the UAV trajectory design problem is $O\left(L\log_2\left(\frac{1}{\epsilon}\right) + L(\boldsymbol{Q_u d})^{3.5}\right)$, where L denotes the number of iterations for **Algorithm 6.2**, $\boldsymbol{Q_u}$ denotes the UAV trajectory, and $\boldsymbol{d}$ represents an auxiliary variable for distance. In this context, the time complexities of FB and FT are given by $O\left(L(\boldsymbol{Q_u d})^{3.5}\right)$ and $O\left(L\log_2\left(\frac{1}{\epsilon}\right)\right)$, respectively. Moreover, the time complexity of the exhaustive search is given by $O\left(n \times d^2 \times M_p^2\right)$, where n is the number of points tested for trajectory, d is the number of points tested for the auxiliary variable for distance, and M_p is the number of points tested for blocklength. It is clearly evident that the lower time-complexity and efficient resource allocation provided by **Algorithm 6.2** makes it an ideal candidate for memory-limited UAV networks. It is to be noted that both of the algorithms are implemented at the source node or the controller. The rationale behind this is that the controller has a reasonable amount of computational resources available at its disposal compared to the UAV, laser transmitter, ground station, or robot. Additionally, all the simulations are performed at the physical layer using a PC with a 2.6 GHz Intel Core i7 processor and 16 GB of RAM (DDR4) running MATLAB R2018a.

6.6 Conclusion

In this paper, we considered a laser-powered UAV relaying system, including a source node, a laser transmitter, a UAV acting as a DF relay, and a robot acting as a ground station. The goal is to minimize the average overall decoding error over the two transmission phases to enable

UAV-assisted URLLC; the first phase of transmission is between the ground station and the UAV, while the second phase is between the UAV and the robot. We jointly optimized the resource allocation to accomplish this goal, including the variable blocklength and power control and the UAV's trajectory for each of the two transmission phases. Simulation results demonstrated that our proposed algorithm yields an optimal blocklength allocation and power control for the two phases of transmission. Additionally, the proposed method demonstrated an efficient usage of the harvested laser's energy in the available time slots to complete the UAV's flight. Our proposed algorithm has low complexity. Additionally, the proposed method and baseline scheme FB showed comparable performance to the exhaustive search in terms of energy usage in the available time-slots, whereas FT yielded the worst performance. Furthermore, the proposed method also mapped an optimal UAV trajectory from the initial position to a final position. On the other hand, for our objective of minimizing average overall decoding error again, the best performance is yielded by the proposed method, whereas the fixed baseline schemes, including FT and FB, yielded average and worst performance, which shows the efficacy of the proposed technique. Subsequently, we shall extend this work to consider the energy storage challenges in laser-powered UAV systems in our future work. In this regard, we shall use a non-linear energy harvesting model to establish a clear relationship between UAV trajectory, battery dynamics, and energy consumption/ harvesting. After that, we shall study the impact of various design parameters, e.g., air turbulence, size, angular spread of the laser beam, and distance to charging laser beacon, on UAV battery charging. Lastly, in the next chapter, we shall study a dual time and energy minimization problem for UAV-enabled multicasting systems facilitating URLLC.

CHAPTER 7

URLLC IN UAV-ENABLED MULTICASTING SYSTEMS: A DUAL TIME AND ENERGY MINIMIZATION PROBLEM USING UAV SPEED, ALTITUDE AND BEAMWIDTH

Ali Nawaz Ranjha[1] , Georges Kaddoum[1] , Muddasir Rahim[1], Kapal Dev[2]

[1] Department of Electrical Engineering, École de Technologie Supérieure,
1100 Notre-Dame Ouest, Montréal, Québec, Canada H3C 1K3
[2] Department of Institute of Intelligent Systems,
University of Johannesburg, South Africa

Paper submitted in *Elsevier Computer Communications*, December 2021

7.1 Abstract

Realizing ultra-high reliability for short packets in sixth-generation (6G) networks is a crucial task for network designers as classical Shannonian capacity bounds become obsolete. Moreover, for multiuser communications, due to distinct aerodynamics, the trajectory design for a fixed-wing unmanned aerial vehicle (UAV) fundamentally differs from rotary-wing UAVs, which poses a challenge for systems designers. This paper addresses these challenges and relies on a fixed-wing UAV-enabled multicasting system to deliver common short blocklength ultra-reliable and low-latency (URLLC) packets to the ground nodes (GNs) using a *Snake Traversal* trajectory path. To accomplish this task, we consider the fly-and-communicate protocol for the UAV, where the UAV sweeps a large rectangular area to disperse a common file to GNs with obscure positions. In this vein, we investigate the dual time and energy minimization problems by presenting a quasi-optimal design of the UAV's flying speed, altitude, and antenna beamwidth. Simulation results of numerical search reveal the optimal altitude and half-power beamwidth, which minimize the completion time and energy consumption, respectively. Moreover, for optimized beamwidth, the UAV speed monotonically increases with the altitude, whereas both the completion time and energy consumption monotonically decrease with the altitude. We also analyze the effects of the blocklength and decoding error probability on optimal UAV speed,

completion time, and energy consumption. Additionally, simulation results show that for the completion time, the percentage difference between minimum UAV altitude $h_{\min}$ and maximum UAV altitude $h_{\max}$ is 195.252 %, whereas for the energy consumption, the percentage difference at $h_{\min}$ and $h_{\max}$ is 196.912 %. Similarly, for the completion time, the percentage difference at minimum UAV antenna beamwidth $\theta_{\min}$ and maximum UAV antenna beamwidth $\theta_{\max}$ is 181.586 %, whereas for the energy consumption the percentage difference at $\theta_{\min}$ and $\theta_{\max}$ is 189.269 %. This demonstrates the efficacy of the proposed technique is almost two times in reducing the completion time and the energy consumption effectively between the minimum and the maximum values of the UAV altitude and the UAV antenna beamwidth. Lastly, the results show that for both the blocklength and decoding error probability, the UAV speed monotonically increases, while completion time and energy consumption monotonically decrease.

7.2 Introduction

URLLC in the upcoming sixth-generation (6G) networks are going to empower mission-critical applications such as remote control of unmanned aerial vehicles (UAVs) control information delivery, internet of things (IoT) communication, tactile internet, smart grids, self-driving cars, etc. (Bennis *et al.*, 2018; She, Sun, Gu, Li, Yang, Poor & Vucetic, 2021a; Adeogun, Berardinelli, Mogensen, Rodriguez & Razzaghpour, 2020; Dogra, Jha & Jain, 2021). In addition to ultra-fast 6G systems, depending on the considered scenario, such mission-critical applications could also require fog computation capabilities to function appropriately in the communication network. In (Hazra, Adhikari, Amgoth & Srirama, 2020), the authors studied a fog federation model for 6G networks for better utilization of fog resources and to provide enhanced services over the network. Likewise, the authors aimed to minimize service delays and prices for IoT users while concurrently maximizing the revenue of the fog service providers. In this regard, the authors proposed a non-cooperative Stackelberg game to schedule cloud and fog resources in a distributed manner. Similarly, in (Adhikari, Munusamy, Hazra, Menon, Anavangot & Puthal, 2021), the authors discussed various attack models for the edge-centric intelligent internet of vehicles (IoV) frameworks to minimize end-to-end latency by efficiently managing energy.

Moreover, the authors also shed some light on the future research directions concerning security in edge-centric IoV systems. Comparably, in (Hazra, Adhikari, Amgoth & Srirama, 2021), the authors proposed deep reinforcement learning (DRL)-assisted partial service provisioning for industrial fog networks to minimize energy consumption and latency. Furthermore, the proposed strategy used maximum fog resources in the network by utilizing multiple fog nodes to execute the overwhelming workload of industrial internet of things (IIoT) applications. Additionally, finite blocklength URLLC packets have dual requirements of stringent latency and ultra-high reliability. As such, the decoding error probability must be at least 10^{-5} or lower. Traditional communication systems utilize the Shannon capacity bound and make idealistic assumptions that channel coding is performed over an infinite blocklength. On the other hand, for finite blocklength, the channel coding rate and capacity bounds were studied and reviewed in (Polyanskiy *et al.*, 2010).

UAVs are a rising technology that is now used for civil, public, and military sectors; currently, advanced UAVs are used by the military to perform search and surveillance operations; the examples include Predator, and Global hawk (Khan *et al.*, 2017a). Similarly, the past few years have also seen a surge in the usage of UAVs for the public domain, including the Mavic, Phantom, Inspire from DJI, and the Bebop and the AR from Parrot (Gupta *et al.*, 2015). The advantages provided by the UAVs are countless; as such, they can provide advanced warning for any imminent natural disasters and can establish communication in infrastructure-less areas. Additionally, they can provide *over-the-air* delivery of medical supplies to save precious human lives in volatile situations such as wildfires, warzones, and poisonous gas infiltration. Moreover, the use cases of UAVs vary from aerial photography to aerial package delivery; the demand for UAVs is booming in many sectors. Furthermore, UAVs are made available in all sizes and shapes. In this regard, large UAVs find their utility in individual missions, whereas small UAVs can be used to form swarms for light shows and entertainment purposes. As such, the latter ones are proving to be quite valuable for civil applications. Generally, the high-altitude platforms (HAPs) comprise large UAVs, airships, and ballons, whereas the low-altitude platforms (LAPs) consist of small cooperative drones (Yan *et al.*, 2019). The rapid advancements in the domain of

electronics, sensors, artificial intelligence, and computing technologies have diversified the UAV applications to include the use cases of traffic monitoring, remote sensing, wind estimation, and night-time detection (Bekmezci *et al.*, 2013). In this regard, it is worth mentioning that according to a recent report published by Federal Aviation Administration (FAA), the fleet of drones will be increased from 1.1 million vehicles in 2017 to 2.4 million units by 2022 (Fotouhi *et al.*, 2019). Furthermore, as both control and communications are the backbones of UAV systems, it is forecasted to bring promising new and intriguing business opportunities for cellular operators. In this context, recently, the third-generation partnership project (3GPP) has undertaken an interesting study to explore the potential opportunities and challenges for employing UAVs as a piece of new user equipment (UE), referred to as aerial UE (Meredith, 2017). This study's essential crux is that the enhanced line-of-sight (LoS) communication links are established between the aerial UE and ground base stations (BSs), subject to the considered environment. Simultaneously, a disadvantage is increased system interference, requiring interference mitigation strategies to accommodate both aerial and ground UEs in the same system (Lin *et al.*, 2018). To address such interference issues, a variety of novel techniques have already been proposed showing promising results as outlined in (Liu *et al.*, 2019), and reference therein. Although 3GPP is mainly dealing with connecting UAVs to cellular networks, both industry and academia are moving towards the next level of research and development that promises to harness the full potential of UAVs communications.

7.2.1 Related work

UAV-enabled communication has recently emerged as a strong candidate to provide wireless connectivity in infrastructure-less areas. As discussed before, such an approach has many advantages; line of sight (LoS) communication is facilitated by the high altitudes of the UAV, thus alleviating the undesirable effects of shadowing and signal blockage. Moreover, to facilitate connectivity, UAVs can act as flying base stations (BSs) as well as flying relays (Dai, Zhang, Hua, Li, Huang & Wang, 2019; Shiri *et al.*, 2020; Guo *et al.*, 2019; Zhu, Zheng, Wong & Dagiuklas, 2020; Ren, Wang & Pan, 2021; Xi, Cao, Yang, Chen, Quek & Wu, 2020; Chen *et al.*, 2017;

Ranjha & Kaddoum, 2020a,b,c; **?**). Notably, the authors in (Dai *et al.*, 2019), consider the framework of game theory to study the joint problem of placement and power allocation of UAVs communicating with ground terminals (GTs). The authors aim to optimize the sum fairness for all GTs by proposing a distributed learning algorithm. In their recent work (Shiri *et al.*, 2020), the authors study the problem of UAV path planning. The authors employ a neural network-based opportunistic control approach to plan an optimal path and minimize the UAV's travel time and energy using a trade-off between uploading delays and control subject to bad channel conditions. The seminal work in (Guo *et al.*, 2019) presents the downlink communication for rechargeable UAV communicating with GTs. Moreover, the authors aim to jointly optimize the time allocation of the UAV between recharging and providing service, trajectory design, and power allocation. In this regard, the authors use the so-called successive convex optimization (SCO) to maximize the average rate among the GTs. In (Zhu *et al.*, 2020), the authors consider the joint framework for simultaneous downlink energy and uplink information transfer in UAV to ground millimeter-wave IoT networks. In this regard, the authors study the dynamic spectrum utilization and energy efficiency in such UAV-IoT networks. In (Ren *et al.*, 2021), the authors studied URLLC in a factory automation scenario. In this regard, the authors utilized an intelligent reflective surface (IRS) to facilitate URLLC and derived the average decoding error probability (ADEP) as well as the average data rate (ADR) subject to the availability of perfect/imperfect channel states information (CSI). Similarly, in (Xi *et al.*, 2020), the authors proposed a multiplexing framework for URLLC and enhanced mobile broadband (eMBB) in a multi-UAV relaying network. Accordingly, to improve the data rate and reduce the transmit power, the authors formulated the multiplexing problem as a joint transmit power and bandwidth allocation, and user association problem. Comparably, in (Chen, Wang, Zhao, Wang & Fei, 2021), the authors proposed a UAV-assisted framework to deliver URLLC services. Moreover, the authors aimed to optimize the average uplink transmit power of all the ground IoT devices subject to UAV positioning, resource allocation, user device scheduling, and association. Similarly, in (Li, Wang, Liu, Tsiftsis, Ding & Nallanathan, 2020), the authors studied UAV-assisted multi-way relaying in non-orthogonal multiple access (NOMA) systems by accounting for residual hardware impairments (RHIs) at the transceiver end. To

achieve this goal, the authors derived an achievable sum rate (ASR) in high signal-to-noise ratio (SNR) regime. However, these works (Dai *et al.*, 2019; Shiri *et al.*, 2020; Guo *et al.*, 2019; Zhu *et al.*, 2020; Ren *et al.*, 2021; Xi *et al.*, 2020; Chen *et al.*, 2017; Ranjha & Kaddoum, 2020a,b,c), do not take into account the limited on-board energy and endurance of UAVs, which could cause disruptions in the wireless connectivity. In the open technical literature, some works have considered the minimization of the completion time to enhance energy efficiency (Zeng & Zhang, 2017; Zeng, Xu & Zhang, 2018; He *et al.*, 2017). However, the proposed schemes assume the availability of prior knowledge on the users' location and are optimized for rotary-wing UAVs whose aerodynamic attributes differ from fixed-wing UAVs. For practical implementations, a fixed-wing UAV, which can sweep a large rectangular area doing *zigzag* motion using a *Snake Traversal* trajectory path utilizing the fly-and-communicate protocol is required (Song, Jin & Zheng, 2019; Liang, Gao, Nguyen, Orpilla & Yu, 2019a). To deliver data packets to all the ground nodes (GNs), the UAV must hover over each of them. In this regard, the *Snake Traversal* trajectory path is desirable since it guarantees coverage for all the GNs spread across a large geographic area (Liang *et al.*, 2019a). In contrast, no such guarantee is provided by the so-called *Hilbert Curve*. Furthermore, a rotary-wing UAV offers a limited flight time capability and a smaller coverage area. Thus, to facilitate control and non-payload communications (CNPC) links, terrestrial and maritime critical data collection for URLLC systems, a fixed-wing UAV with longer flight endurance and larger coverage area is preferred. Additionally, for UAV-enabled multicasting systems with a tunable beamwidth tasked to disperse common information, there is a tradeoff between several parameters, including the UAV speed, altitude, beamwidth, completion time, and energy consumption. Generally, at a fixed altitude the number of sweeps required to cover an area is inversely proportional to the beamwidth. However, there is a dilemma as a higher beamwidth leads to a lower signal-to-noise ratio (SNR) for the GNs at the sweep border, which must be compensated by increasing the UAV's speed. Only one work in the available technical literature considers the completion time and energy minimization for UAV-enabled multicasting systems (Song *et al.*, 2019). Nonetheless, the authors employ Shannon's capacity formula whereas, as discussed earlier, URLLC systems employ a short blocklength equation.

7.2.2 Novelty and Contributions

Despite the dedicated research efforts towards studying URLLC, UAV-enabled communication, and the UAV-enabled URLLC, a study on URLLC in UAV-enabled multicasting systems under the finite blocklength regime is missing. However, it is worth mentioning here that such a study is necessary as it will lay the foundation of supporting URLLC assisted by UAVs in futuristic 6G networks. Therefore, the main contributions of this paper can be summarized as follows:

- We propose a novel URLLC multicasting system facilitated by a fixed wing UAV following a *Snake Traversal* trajectory path and employing the fly-and-communicate protocol.
- We jointly study the quasi-optimal design of the UAV speed, altitude, and beamwidth with dual objectives of minimizing the completion time and energy consumption without prior knowledge of the GNs positions at the UAV.
- We design the UAV to fly in a *zigzag* pattern to disseminate a common small data file to GNs. For completion time minimization, the simulation results show that the optimal UAV altitude is the maximum value of the altitude. Similarly, simulation results also demonstrate that the optimal half-power beamwidth is the maximum value of the beamwidth found by performing a low-complexity two-dimensional (2D) iterative search. Alternatively, for energy minimization, the simulation results show that the optimal UAV speed, altitude, and beamwidth can be obtained by similar 2D iterative processes.

7.3 System Model and Problem Formulation

We assume a flying UAV BS at an altitude h, where h satisfies $0 < h_{\min} \leq h \leq h_{\max}$. The UAV BS is tasked to multicast some common small data file containing K bits to all GNs in a large rectangular area $\mathcal{A}$ of the dimension of $X_1 \times X_2$ m^2. In this context, the positions of the GNs are fixed; however, they are unavailable at the UAV BS. Additionally, by utilizing the so-called *Snake Traversal* path, the UAV BS can efficiently and effectively sweep the considered rectangular area with a constant speed v m/s by the *zigzag* motion along rows that are perpendicular to the UAV's coverage direction, as illustrated in Fig. 7.1.

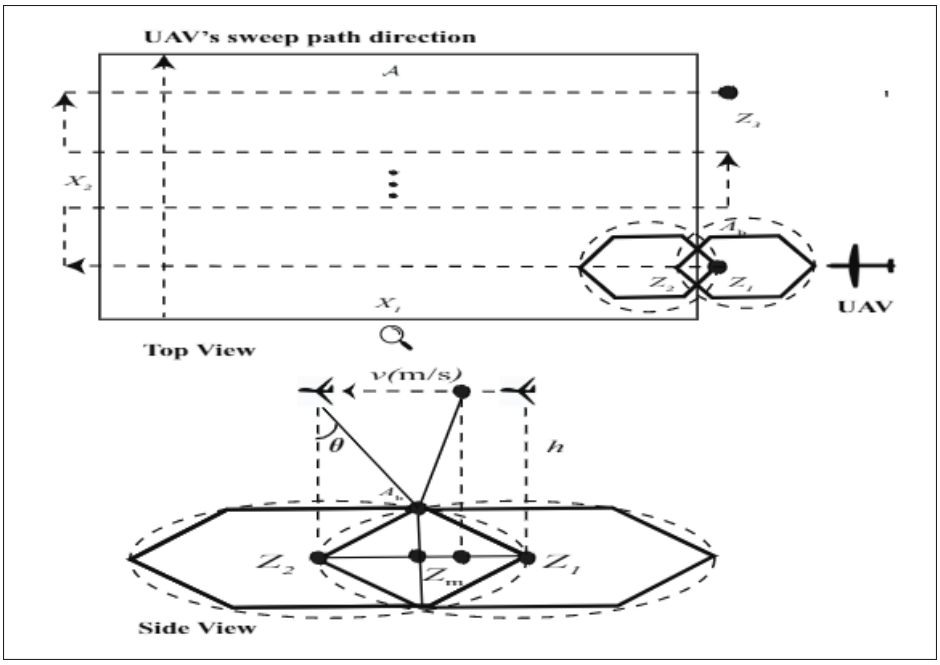

Figure 7.1 UAV's sweep direction on a *Snake Traversal* trajectory path and enlarged coverage area of border user

Now, we consider that time is divided into slots, where a time slot being infinitesimal, the location of the UAV is fixed throughout its duration. Meanwhile, the location of the UAV varies across different time-slots. Besides, we assume that the shape of the coverage area of the UAV is hexagonal. Generally, the UAV's ground projection is denoted by Z, where initial and final projections are denoted by Z_1 and Z_3, respectively. Here, the UAV's speed is assumed to be sufficiently large such that the constraint on the UAV's flying speed is relaxed. Moreover, the UAV is equipped with a directional antenna with tunable beamwidth, while each GN is equipped with an omnidirectional antenna. Without loss of generality, we assume that the UAV antenna beamwidth is denoted by θ and both the azimuth and elevation half-power beamwidths of the UAV antenna are equal, both of which are denoted by 2θ, with $\theta \in \left(0, \frac{\pi}{2}\right)$. According to (Balanis, 2016), the corresponding antenna gain is approximately given by $\frac{G_0}{\theta^2}$, where $G_0 \approx 2.2846$ within the main lobe and the antenna gain is zero for any region that lies outside the main lobe. Additionally, the UAV's coverage area is belt-shaped with a total width of $\Delta_w = \sqrt{3}h \tan\theta$. It is a well-known fact that the UAV multicasting system's performance is only restricted by the

users that are physically located furthest away from the UAV BS; hence the common small data file K must be dispersed to such users (Song *et al.*, 2019). In this regard, we assume that the user conveniently denoted by A_{b} is located at the sweep border of the UAV, as shown in Fig. 7.1. If A_{b} can receive the common small data file K, then all the remaining users located inside the belt-shaped areas are also guaranteed to receive it. Now, we assume that at time slot $t = 0$, at the initial UAV's projection Z_1, the total distance covered by A_{b} is denoted as $d_{Z_1Z_2} = h\tan\theta$. Moreover, the time period in which A_{b} is covered is given as $T_1 = d_{Z_1Z_2}/v = h\tan\theta/v$. Likewise, the distance between the UAV BS and A_{b} varies as UAV flies from Z_1 to Z_2. At an arbitrary moment t, where $0 \leq t \leq T_1$, the distance between the UAV BS and the user at the sweep border A_{b} can be expressed as

$$d(t) = \sqrt{\left(\frac{\sqrt{3}}{2}h\tan\theta\right)^2 + \left(\frac{h\tan\theta}{2} - vt\right)^2 + h^2}. \tag{7.1}$$

Furthermore, at an arbitrary moment t, the received SNR at A_{b} can be expressed as

$$\gamma(\theta, d(t)) = \frac{\tilde{C}}{d^2(t)} e^{\frac{\tilde{A}}{1+a/e^{b(\theta-a)}}}, \tag{7.2}$$

where $\tilde{A} = (\eta_{\mathrm{NLoS}} - \eta_{\mathrm{LoS}})\frac{\ln 10}{10}$ and $\tilde{C} = \frac{P}{\sigma^2}10^{-\frac{C}{10}}$, with P being the fixed transmission power of the UAV, σ^2 the noise power at the UAV, and $C = 20\log_{10}(4\pi f_c/c) + \eta_{\mathrm{NLoS}}$. Moreover, η_{LoS} and η_{NLoS} (in dB) are respectively the losses corresponding to the LoS and non-LoS links, f_c is the carrier frequency (Hz), c is the speed of light (m/s), and a and b are positive constants that depend on the environment (Ren *et al.*). In general, η_{NLoS} is much larger than η_{LoS} due to the severe path loss in NLoS transmission. Finally, at an arbitrary moment t, the achievable rate of User A_{b}, when transmitting a short blocklength M packet is given as

$$R(\gamma(\theta, d(t))) = B\log_2(1 + \gamma(\theta, d(t))) - B\frac{Q^{-1}(\varepsilon)}{\ln 2}\sqrt{\frac{V(\gamma(\theta, d(t)))}{M}}, \tag{7.3}$$

where $Q^{-1}(\varepsilon) = \sqrt{2}\text{erfc}^{-1}(2\varepsilon)$ is the inverse Q-function[1], $V(\gamma(\theta, d(t)))$ is the channel dispersion, which is a function of $\gamma(\theta, d(t))$ and is given by $V(\gamma) = 1 - (1+\gamma)^{-2}$, and B is the bandwidth used. The second term in (7.3) can be regarded as the penalty on the data rate due to the short blocklength. When the UAV flies from location Z_1 to Z_2 within the coverage interval T_1, the total amount of the received data at A_b is given as

$$K \leq \int_0^{T_1} R(\gamma(\theta, d(t)))dt. \tag{7.4}$$

Additionally, we consider that the rectangular area $\mathcal{A}$ width is large enough to be split into $N = X_2/\Delta_w$ belt-shaped areas for any given values of h and θ. Hence, the UAV's flying time is only considered for the rectangular area $\mathcal{A}$ and is ignored for any outside area. Finally, the completion time can be simply approximated as

$$T \approx N \times \frac{X_1}{v} = \frac{X_1 X_2}{\sqrt{3} v h \tan\theta}. \tag{7.5}$$

Moreover, from (Zeng & Zhang, 2017), we know that the power consumption model of the UAV in straight-and-level flight with speed v[2] can be represented as $P_m = c_1 v^3 + \frac{c_2}{v}$, where c_1 and c_2 are constants related to the aerodynamics and aircraft design. Additionally, we only consider the UAV's propulsion energy. This is because the UAV communicates with GNs using short packets at moderately lower data rates to facilitate URLLC, which require minimal energy for communications (Ranjha & Kaddoum, 2020b). Thus, the UAV's communication energy attributed to the signal processing, radiation, and other circuitry can be ignored (Zeng & Zhang, 2017; Eom, Lee, Park & Lee, 2019; Di Franco & Buttazzo, 2015). Therefore, the total energy consumption can be approximated as

$$E_t = P_m T. \tag{7.6}$$

[1] erfc is the complementary error function.

[2] It is to be noted that if the UAV has speed limits and the optimal speed ends up outside those limits for some given inputs, it is necessary to clip the speed at those respective bounds. Of course, if we clip v, then we obtain a suboptimal value. However, to generalize our results, there is no need to put minimum and maximum bounds on v, mainly because this wouldn't change the theoretical aspect of our work.

7.4 Minimization of Completion Time and Energy Consumption

The dual objectives of this paper are to jointly minimize the overall completion time T and the total energy consumption E_t by the joint design of three variables, namely the UAV's flying speed v, altitude h, and half-power beamwidth θ.

7.4.1 Completion Time Minimization

We denote Z_m as the middle point of Z_1Z_2. Now, (7.4) can be rewritten as

$$K \leq 2B \int_0^{\frac{T_1}{2}} \left(\log_2 \left(1 + \frac{\alpha}{d^2(t)}\right) - \frac{Q^{-1}(\varepsilon)}{\sqrt{M}\ln 2} \sqrt{1 - \frac{1}{\left(1 + \frac{\alpha}{d^2(t)}\right)^2}} \right) dt, \tag{7.7}$$

where $\alpha = \alpha(\theta) = \tilde{C}e^{\tilde{A}/(1+a/e^{b(\theta-a)})}$. Moreover, we perform a change of variable $x = vt$, and substitute $u = (\frac{3}{4}\tan^2\theta + 1)h^2$ and $w = \frac{h\tan\theta}{2}$. Then, after some simplifications, we have

$$v \leq \frac{2B}{K\ln 2} \left(\int_0^w \ln\left(1 + \frac{\alpha}{u + (w-x)^2}\right) dx - \frac{Q^{-1}(\varepsilon)}{\sqrt{M}} \int_0^w \sqrt{1 - \frac{1}{\left(1 + \frac{\alpha}{u+(w-x)^2}\right)^2}} dx \right). \tag{7.8}$$

To minimize the completion time, the optimal speed v^* should satisfy the above inequality with equality. By integrating and simplifying, we get

$$\begin{aligned} v^* = \frac{2B}{K\ln 2} \Bigg(& w \ln\left(1 + \frac{\alpha}{u + w^2}\right) + 2\sqrt{\alpha + u}\tan^{-1}\frac{w}{\sqrt{\alpha + u}} \\ & - 2\sqrt{u}\tan^{-1}\frac{w}{\sqrt{u}} + \frac{Q^{-1}(\varepsilon)}{\sqrt{M}}\sqrt{\alpha}\Bigg(\sqrt{2}\ln\frac{\sqrt{\alpha + 2u}}{\sqrt{2}w + \sqrt{\alpha + 2(u + w^2)}} \\ & + \frac{\tanh^{-1}\frac{\sqrt{\alpha}w}{\sqrt{\alpha+u}\sqrt{\alpha+2(u+w^2)}}}{\sqrt{\alpha + u}\sqrt{\alpha + 2(u + w^2)}} \Bigg)\Bigg). \end{aligned} \tag{7.9}$$

Based on the obtained v^*, we minimize T by optimizing h with a given θ and vice-versa. The expression of v^* is quite complex; hence, it is hard to say anything about the shape of

v^*. Consequently, we find it appropriate to state some theorems based on the assumption of monotonic growth of v^* in h and θ.

Theorem 1. *Fix $\theta \in [\theta_{\min}, \theta_{\max}]$ and assume a monotonically increasing $v^*(h)$. Then the optimal altitude that minimizes the completion time T is $h_{\max}$.*

Proof. This is straightforwardly deduced from (7.5) as we see that T will decrease monotonically to 0 in h due to both h and $v^*(h)$ being in the denominator. □

The reason for $h_{\max}$ being optimal is because the reduction of the *zigzag* motion of the UAV is more dominant than the decrease of received SNR as h increases.

Theorem 2. *Fix $h \in [h_{\min}, h_{\max}]$ and assume a monotonically increasing $v^*(\theta)$. Then the optimal half-power beamwidth that minimizes the completion time T is $\theta_{\max}$.*

Proof. This is straightforwardly deduced from (7.5) due to the monotonically increasing $\tan\theta$ and $v^*(\theta)$ being in the denominator. □

Whether or not we make any assumptions about v^*, the problem can always be solved numerically through a 2-dimensional search. With the currently available computing technologies, it would take mere seconds to do so. One can search for the smallest value of T evaluated on a 2D mesh of h and θ values with a small step, e.g. 10 m for h and 0.01 rad for θ, or even smaller. Alternatively, an iterative search for finding h_{opt} and θ_{opt} repetitively one after the other can also work, but may not always converge fast enough, or converge at all, as seen in the Fig. 7.3 of the numerical results where $h_{opt}(\theta)$ and $\theta_{opt}(h)$ are constant. Since all the functions in question are most likely unchaotic, as evidenced by Fig. 7.4, it makes sense to do a repetitive 2D search, zooming in and refining the mesh at each repetition. It is noteworthy that the equation for v^* is easily vectorizable in both h and θ simultaneously; hence no loops are needed to calculate its values over a mesh of (h, θ) values. Therefore a 2D search over the plane (h, θ) is performed in constant time, i.e. in $O(1)$.

7.4.2 Energy Consumption Minimization

Combining (7.5) and (7.6) we get:

$$E_t = \frac{X_1 X_2}{\sqrt{3} h \tan\theta} \left(c_1 v^2 + \frac{c_2}{v^2} \right), \tag{7.10}$$

Since $c_1 v^2 + c_2/v^2$ is concave up with a parabolic-like shape, it has one minimum in the positive domain, which can be found by finding the roots of the partial derivative in v:

$$0 = \frac{\partial E_t}{\partial v} = \frac{X_1 X_2}{\sqrt{3} h \tan\theta} (2c_1 v - \frac{2c_2}{v^3}) \quad \Rightarrow \quad v = \sqrt[4]{\frac{c_2}{c_1}}. \tag{7.11}$$

We call this value v_E, which is the optimal speed that minimizes (7.10). To guarantee that the common information can be successfully disseminated and received by User A_b, v must be no higher than v^*. Hence, with this in mind, the optimal speed should be $v_E^* = \min(v^*, v_E)$. Since v_E is a constant, from (7.5), we deduce that h_max and θ_max are optimal for simultaneous time and energy minimization under $v_E^* = v_E$. Therefore, we shift our focus to the more general case of $v_E^* = v^*$. Due to tight coupling of h and θ with each other and v^* being very complex, it is hard to efficiently find the closed form of the globally optimal solution. Nonetheless, we can make a few conclusions with certain assumptions. We know that E_t is parabolic-like in v. Thus, if v^* itself is monotonically increasing everywhere on $[h_\mathrm{min}, h_\mathrm{max}]$, then, assuming fixed θ, we see that $E_t(h, v_E^*(h))$ will have a parabolic-like shape in h (upto the point where v^* exceeds v_E if that point exists in $[h_\mathrm{min}, h_\mathrm{max}]$). This shape will always have exactly one minimum, which can be found by taking the derivative of the energy with respect to the altitude. After finding this altitude, we must cap it off from the top and bottom, since we are restricted by $[h_\mathrm{min}, h_\mathrm{max}]$. Combining all this, we get:

Theorem 3. *Fix $\theta \in [\theta_\mathrm{min}, \theta_\mathrm{max}]$. Then the optimal altitude that minimizes E_t is:*

$$h_{\text{opt}} = \begin{cases} h_{\min} & \text{if } h^* < h_{\min}, \\ h_{\max} & \text{if } h^* > h_{\max}, \\ h^* & \text{otherwise,} \end{cases} \tag{7.12}$$

where h_{opt} is the solution to,

$$c_1 v^* \left(2h\frac{\partial v^*}{\partial h} - v^*\right) - \frac{c_2}{(v^*)^3}\left(2h\frac{\partial v^*}{\partial h} + v^*\right) = 0, \tag{7.13}$$

Cf. Appendix 7-A for the closed-form expression of $\frac{\partial v^*}{\partial h}$.

However, this only gives us the optimal h for a fixed θ, while we need to optimize both variables. Thus, for real-life modelling, the best option is a 2D search. Interestingly, in the numerical analysis section, we will show that our parameters are such that the optimal θ is always $\theta_{\max}$, i.e. constant for all h. Thus, we can apply the above result directly. However, one would have to numerically find the equation's roots making it a programmatically complex procedure that would be unnecessary when a 2D search could work with ease.

7.4.3 Effect of blocklength M and decoding error probability ε

Theorem 4. *The speed monotonically increases with both M and ε, while T monotonically decreases with them.*

Proof. We look at (7.9) by referring to (7.8) and remembering that they are the same, with a change of the inequality to equality. Thus, we see that the 2nd integral in (7.8) is positive since the integrand and its upper limit w are positive. The coefficient $Q^{-1}(\varepsilon)/\sqrt{M}$ multiplying this integral has M and ε in it, where no other terms in the equation do. If M increases, then the fraction $Q^{-1}(\varepsilon)/\sqrt{M}$ decreases, we are subtracting a lower positive value from the 1st integral, and therefore v^* increases. If ε increases, then Q^{-1}, which is a form of the monotonically decreasing inverse complementary error function erfc^{-1}, decreases. Therefore the coefficient

$Q^{-1}(\varepsilon)/\sqrt{M}$ decreases, and again v^* increases. The total time T is inversely proportional to the speed, and will therefore decrease. □

It is worth mentioning here that we presented an elaborate flowchart of the proposed scheme in Appendix 7-B.

7.5 Numerical Results and Discussion

Unless specified otherwise, the parameters chosen for our proposed system model are shown in Table 7.1.

Table 7.1 Set of chosen parameters for facilitating URLLC in UAV-enabled multicasting systems.

Parameters	**Descriptions**	**Values**
$X_1 \times X_2$	Size of the rectangular area	6 km × 5 km
K	Amount of common information	10 Mbits
a, b	Urban environmental constants	$8, 0.14$
η_{LoS}	LoS loss	1 dB
η_{NLoS}	Non-LoS loss	20 dB
B	Bandwidth	10 KHz
P	UAV transmit power	5 W
c_1, c_2	Power consumption model coefficients	$9.26 \times 10^{-4}, 2250$
$\theta_{\min}$	Minimum UAV antenna beamwidth	0.5 rad
$\theta_{\max}$	Maximum UAV antenna beamwidth	1.2 rad
$h_{\min}$	Minimum UAV height	100 m
$h_{\max}$	Maximum UAV height	1000 m

As implied earlier in **Theorem 1**, we see in Fig. 7.2 that v^* is indeed monotonically increasing with h and θ, while T is monotonically decreasing with the same. E_t is also decreasing on the whole domain of h and θ. Additionally, Fig. 7.2 demonstrate for the T the percentage difference[3] at $h_{\min}$ and $h_{\max}$ is 195.252%, whereas for E_t the percentage difference at $h_{\min}$ and $h_{\max}$ is

[3] Percentage difference= $\frac{|\Delta V|}{\left[\frac{\Sigma V}{2}\right]} \times 100$ %, where ΔV is the absolute difference between two given values and ΣV is the summation of these values (see Appendix 7-C for more details).

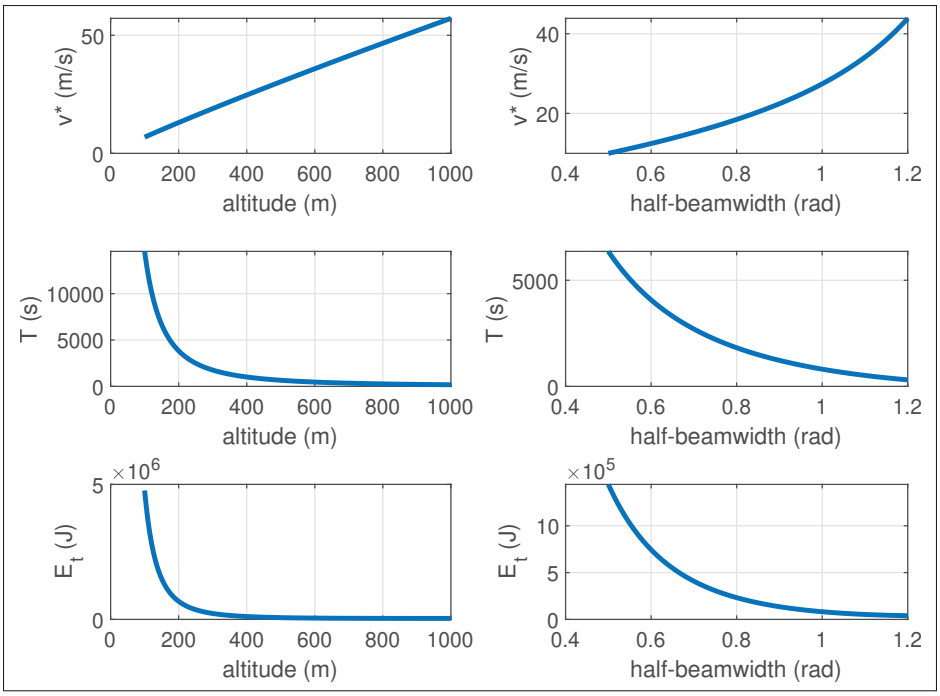

Figure 7.2 v^*, T, E_t as functions of h (with fixed $\theta = 1.0472$ rad) and as a function of θ (with fixed $h = 500$ m)

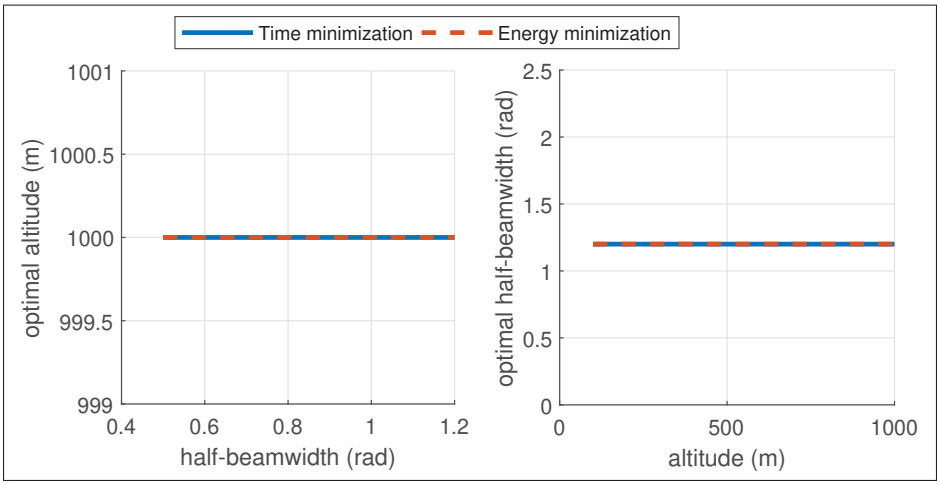

Figure 7.3 Optimal h and θ based on numerical search

196.912%. Similarly, for T the percentage difference at $\theta_{\min}$ and $\theta_{\max}$ is 181.586%, whereas for E_t the percentage difference at $\theta_{\min}$ and $\theta_{\max}$ is 189.269%. Consequently, percentage difference shows the effectiveness of the proposed technique to minimize the completion time and the

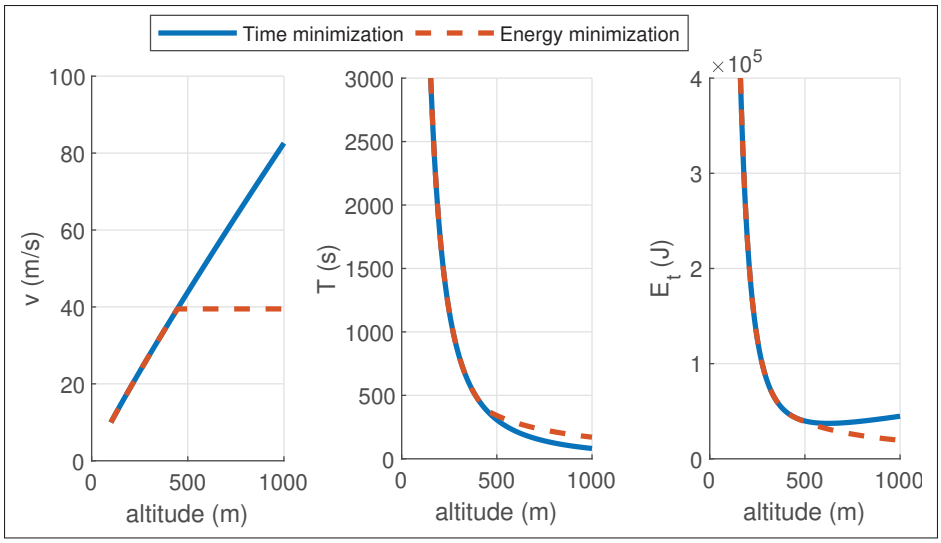

Figure 7.4 v, T, E_t as a function of h (with optimized θ) for time and energy minimization based on numerical search

energy consumption. Similarly, in Fig. 7.3 we plot the optimal h and θ obtained using numerical searches as outlined in **Theorem 2**. As predicted by our theorem, for time minimization, it is optimal to maximize both h and θ. Additionally, our chosen model parameters dictate the same optimal h and θ for energy and time minimization. In Fig. 7.4, for each h on the x-axis we use the optimal θ from Fig. 7.3 to calculate v, T, and E_t, which is always $\theta_{\max}$. The speeds split off because, for energy minimization, we have an additional constraint as described above, i.e., $v = v^*$, whereas for time minimization we have $v = v_E^*$. Hence, v_E^* value can be computed using (12) which is 39.5 m/s. These v-curves are optimal and are used as input for the T and E_t graphs, which also split at just under 500 m for the same reason. As one would expect, the completion time T for time minimization is no greater than for energy minimization, while the energy consumption E_t for energy minimization is no greater than for time minimization. Ultimately, these graphs tell us that, for our model, the optimal altitude for both time and energy minimization is $h_{\max}$. Also, as expected, one of the energy curves is parabolic in shape, with a minimum around 600 m. The exact value could be found with **Theorem 3**.

In Fig. 7.5 we present the effects of the blocklength M and decoding error probability ε on v^*, T, and E_t. The presented behaviour is summarized in **Theorem 4**, which states that the UAV

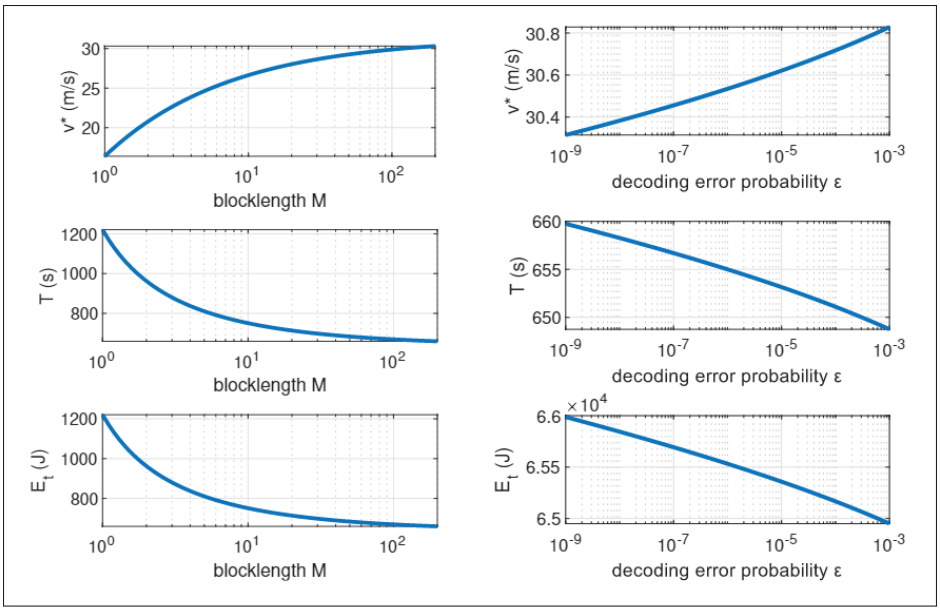

Figure 7.5 v^*, T, E_t as functions of the blocklength M (with fixed $\varepsilon = 10^{-9}$) and decoding error probability ε (with fixed $M = 200$) with fixed $h = 500$ m and $\theta = 1.0472$ rad

speed monotonically increases with both blocklength and decoding error probability while the completion time and energy consumption monotonically decrease with the same.

7.6 Conclusion

In this paper, we studied a URLLC-enabled multicasting system facilitated by a fixed-wing UAV following a *Snake Traversal* trajectory path and utilizing the fly-and-communicate protocol. Moreover, we presented a quasi-optimal design of the UAV speed, altitude, and beamwidth with the dual objective of minimizing the completion time and energy consumption. Our results demonstrate that the optimal altitude and half-power beamwidth that minimize the completion time and energy consumption in our model are $h_{\max}$ and $\theta_{\max}$. Furthermore, for optimized beamwidth, the UAV speed monotonically increases with altitude, whereas both the completion time and energy consumption monotonically decrease with the altitude. Lastly, we also analyzed the effects of the blocklength and decoding error probability on the optimal UAV speed, completion time, and energy consumption. The results showed that for both the

blocklength and decoding error probability, the UAV speed monotonically increases while completion time and energy consumption monotonically decrease with them. Lastly, in the next chapter, we shall present conclusions and recommend future research directions for resource allocation in URLLC-enabled UAV communication systems.

CONCLUSION AND RECOMMENDATIONS

8.1 Conclusions

In this thesis, we proposed and analyzed various optimization frameworks for URLLC over UAV-assisted communication systems. In this regard, we studied minimization problems for decoding error probability and sum uplink power subject to various constraints, including blocklength distribution, transmit power allocation, and UAV positioning.

In chapter 2, we introduced a quasi-optimization of the UAV relay distance and the blocklength for ground IoT devices communicating over multihop UAV relay links operating under URLLC and finite blocklength constraints. The goal was to mitigate the overall decoding error probability such that the short packets are received with ultra-high reliability at the R_{x} node. We optimized the latency constraint to enter the URR. Simulation results showed that our proposed algorithm is highly suitable for implementation at the T_{x} node because of its low time complexity. At the same time, it yields the same performance as more complicated exhaustive search algorithms.

In chapter 3, we studied the quasi-optimization of the sum uplink power of IoT devices communicating with a UAV BS utilizing short data packets supported by URC. The study was performed under a finite blocklength regime. The overall goal was to minimize the sum power to enable green URLLC communication for short packets with ultra-high reliability at the R_{x} node. To achieve this goal, we jointly optimized the UAV position, height, beamwidth, and resource allocation for each T_{x_k} node while also guaranteeing ultra-high reliability. Simulation results showed that our proposed algorithm has a lower sum power consumption than benchmark algorithms, including FP, FHBW, and FBL, and achieves a performance similar to the exhaustive search while maintaining lower time complexity. Moreover, we showed that Shannon's formula is not an optimum choice to model the sum power consumption for short packet communication as it can significantly underestimate the sum power. Lastly, we also showed that the proposed

algorithm allows ultra-high reliability for all the users and converges rapidly. To conclude this chapter, in the context of IoT applications with low data-rate requirements, we studied the convoluted problem of quasi-optimization of the UAV position, the UAV height and beamwidth, and blocklength under the finite-blocklength regime.

In chapter 4, we studied the joint design of passive beamforming, resource allocation, and UAV positioning for IoT devices communicating via both a UAV relay and RIS. Here, the IoT devices were assumed to utilize short data packets operating under finite blocklength constraints. The overall goal was to mitigate the total decoding error rate such that the short packets are received with ultra-high reliability at the ground user node. To achieve this goal, we performed passive beamforming and jointly optimized the blocklength and UAV position using NMS method. Simulation results showed that the proposed approach yields favourable convergence performance compared to traditional optimization algorithms, i.e., gradient descent. It was also shown to have a better computation time and better performance than the exhaustive search. Moreover, the proposed approach allows ultra-high reliability, which could be attained by increasing the number of antenna elements in the RIS as well as increasing the allocated blocklength. Simulation results demonstrated the RIS's performance gain and conclusively showed that the UAV's position is crucial for achieving ultra-high reliability for short packets.

In chapter 5, we considered a UAV-assisted military surveillance system, including a controller and multiple-mobile robots communicating under finite blocklength constraints via a UAV serving as a DF relay. The goal was to minimize the average overall decoding error to enable UAV-assisted URLLC for two phases of transmission; the first phase being between the controller and the UAV, while the second phase is between the UAV and the robots. To accomplish this goal, we jointly optimized the UAV's height, beamwidth, and location and resource allocation, including the variable blocklength and power for each of the k robots present in the military area corresponding to a circular cell. Simulation results demonstrated that our proposed algorithm has

a lower average overall decoding error than benchmark algorithms with fixed parameters, namely FB, FP, FL, and FAB; it achieved an almost equivalent performance to the smart exhaustive search. Finally, we showed that it is necessary to jointly optimize the UAV location, height, beamwidth of the antenna, and the power and blocklength allocation for the two transmission phases to guarantee URC for multiple-mobile robots.

In chapter 6, we considered a laser-powered UAV relaying system, including a source node, a laser transmitter, a UAV acting as a DF relay, and a robot acting as a ground station. The goal is to minimize the average overall decoding error over the two transmission phases to enable UAV-assisted URLLC; the first phase of transmission is between the ground station and the UAV, while the second phase is between the UAV and the robot. We jointly optimized the resource allocation to accomplish this goal, including the variable blocklength and power control and the UAV's trajectory for each of the two transmission phases. Simulation results demonstrated that our proposed algorithm yields an optimal blocklength allocation and power control for the two phases of transmission. Additionally, the proposed method demonstrated an efficient usage of the harvested laser's energy in the available time slots to complete the UAV's flight. Our proposed algorithm has low complexity. Additionally, the proposed method and baseline scheme FB showed comparable performance to the exhaustive search in terms of energy usage in the available time-slots, whereas FT yielded the worst performance. Furthermore, the proposed method also mapped an optimal UAV trajectory from the initial position to a final position. Lastly, for our objective of minimizing average overall decoding error again, the best performance is yielded by the proposed method, whereas the fixed baseline schemes, including FT and FB, yielded average and worst performance, which shows the efficacy of the proposed technique.

Lastly, in chapter 7, we studied a URLLC-enabled multicasting system facilitated by a fixed-wing UAV following a *Snake Traversal* trajectory path and utilizing the fly-and-communicate protocol.

Moreover, we presented a quasi-optimal design of the UAV speed, altitude, and beamwidth with the dual objective of minimizing the completion time and energy consumption. Our results demonstrated that the optimal altitude and half-power beamwidth that minimize the completion time and energy consumption in our model are $h_{\max}$ and $\theta_{\max}$. Furthermore, for optimized beamwidth, the UAV speed monotonically increases with altitude, whereas both the completion time and energy consumption monotonically decrease with the altitude. Lastly, we also analyzed the effects of the blocklength and decoding error probability on the optimal UAV speed, completion time, and energy consumption. The results showed that for both the blocklength and decoding error probability, the UAV speed monotonically increases while completion time and energy consumption monotonically decrease with them.

8.2 Future work

Based on the literature review and the research outcomes of this Ph.D. thesis, following future research directions could be worth investigating.

8.2.1 Data rate in URLLC assisted UAV communications

Most of the available works in the literature focus on data links, i.e. UAV-to-ground stations GS and GS-to-UAV. In (Al-Hourani, Kandeepan & Jamalipour, 2014a), the authors propose a model to study air to ground path loss in UAV communications. The work in (Al-Hourani, Kandeepan & Lardner, 2014b) extends (Al-Hourani *et al.*, 2014a) by considering the optimal UAV altitude to ensure maximum coverage for the ground users. In (Lin *et al.*, 2018), authors studied UAV communications in the framework of the LTE standard. The authors in (Bor-Yaliniz, El-Keyi & Yanikomeroglu, 2016) studied the three-dimensional placement of UAVs that maximizes the number of GS. The seminal work in (Azari, Rosas, Chen & Pollin, 2017) optimized the UAV altitude and analyzed the corresponding outage probability. These studies only focused on traditional services with data links, without considering strict delay and reliability

constraints in the control and non-payload communications (CNPC) links between the UAVs and the GCS. Moreover, in control links, very low data rates are required in order to transmit control payload between the GS and the UAV. This differs from conventional communications, which are based on long data packet transmission and can normally tolerate long transmission delays. Generally, small data packets are used to support low latency transmission for delivering the control payload. In (Ren *et al.*), the data rate for URLLC-enabled UAV systems with a three-dimensional channel model was derived. However, realistic assumptions, like pathloss, Doppler effect, and fading, were not considered. This motivates us to carry our research in this domain where we would like to derive a tighter lower bound for the achievable data rate over small data packets in UAV system with realistic assumptions.

8.2.2 Multi-user URLLC assisted UAV-RIS communications powered by laser transmitter

Only few works (Petrov *et al.*, 2020; Guo *et al.*, 2019) in the literature have considered limited on board battery capacity for the design of UAV communication system. In (Petrov *et al.*, 2020), the authors presented an alternative deployment scheme for mmWave UAV APs in areas with fluctuating user traffic for prospective 5G+ networks. Moreover, the authors suggested to land UAV on nearby buildings equipped with charging stations instead of hovering over the areas to conserve and replenish the UAV's battery. The authors also developed a mathematical framework for hover or perch options in UAVs, as an interplay of separation distance between service area, charging station, battery duration, and number of UAVs deployed in the said service area. In (Guo *et al.*, 2019), the authors studied UAV-assisted downlink communication for multiple GUs. Here, the UAV replenishes its battery periodically at a fixed depot or charging station before resuming the service. In this regard, the authors aimed to jointly optimize the UAV's time slot allocation for service duration, its trajectory, as well as its transmit power.

Nevertheless, in these studies, there are two fundamental drawbacks. The first one is that the authors employ Shannon's capacity formula for UAV system design, which inherently possesses the desirable properties of monotonicity and convexity (Xu *et al.*, 2016). Still, as stated earlier, URLLC systems use short packets for which the Shannon's capacity formula is inapplicable (Ren *et al.*, 2020a). The second drawback is that fixed depots do not provide an unlimited endurance for UAV aloft. In addition, the UAV operation in a service area must be disrupted periodically for the UAV to replenish its battery at the aforesaid fixed depots. For the first problem, UAV-enabled URLLC has recently came to the limelight, as outlined in (Ranjha & Kaddoum, 2020a; Ranjha & Kaddoum, 2020; A. Ranjha and G. Kaddoum, 2020). We studied the problem of ultra-reliability between an IoT transmitter/receiver pair employing a multi-hop UAV relay mechanism in (Ranjha & Kaddoum, 2020a). Moreover, we jointly optimized distance and blocklength constraints to accomplish this task. Comparably in (Ranjha & Kaddoum, 2020), we considered a UAV-IoT uplink communication scenario that aims to minimize the overall sum uplink power. To achieve this task, we employed a so-called *divide-and-conquer* rule and iteratively solved optimization problems for optimal UAV altitude, beamwidth, location and distribution of the blocklength between transmitter and receiver pairs. Most recently, in (A. Ranjha and G. Kaddoum, 2020) the URLLC scenario facilitated by a DF UAV relay and a RIS was studied. We propose a design based on a low complexity algorithm, namely NMS, to jointly optimize passive beamforming, blocklength and UAV positioning for such systems. For the second problem, laser powered UAV systems have been proposed in the literature to provide a sustainable and suitable energy supply (Ouyang *et al.*, 2018; Zhao *et al.*, 2020). Laser powered UAV systems use laser array based on a complex optical system containing a set of mirrors, which is then shined on the target UAV. It is proven to elongate UAV mission duration in service areas without causing any significant disruptions as it is an *over-the-air* operation (Lahmeri *et al.*, 2019). (Ouyang *et al.*, 2018), Jie *et al.* presented a laser-powered UAV-assisted communication system. The authors considered a laser transmitter that charges a fixed-wing UAV, and then

establishes communication links with the ground station. Moreover, the authors sought to optimize power allocation and UAV's trajectory jointly. Similarly, in (Zhao *et al.*, 2020), the authors considered a UAV-enabled relaying system powered by a laser transmitter. Moreover, the author attempted to optimize trajectory and power allocation jointly for rotary-wing UAV. Nonetheless, these two aforementioned problems for multi-user scenario facilitated by an RIS have not been studied in the context of URLLC- assisted UAV systems in the open technical literature.

8.2.3 Facilitating URLLC in UAV-assisted networks under jittering and imperfect CSI

In practical UAV-communication, a pertinent problem is jittering when UAV is flying in the air. According to a study, UAV's jittering angles can assume a value up to 10 degrees which is non-negligible. Consequently, the angle of departure between UAV and ground users becomes inaccurate. Moreover, the atmospheric conditions and interference may also lead to erroneous information about the ground users' location leading to imperfect CSI. It is worth mentioning that the CSI refers to channel properties in wireless communication, and it describes how a signal propagates from a transmitter to a receiver. Unfortunately, in practical implementations, perfect CSI is unavailable, and thus the system designer uses imperfect CSI to estimate the channel properties. Furthermore, only a few works in literature have tackled the UAV jittering problem in the context of wireless communications. In (Xu, Sun, Ng & Schober, 2018), the authors presented a novel resource allocation scheme for flying UAV BS to mitigate the effects of jittering and uncertainty of user locations. Similarly, in (Xu, Sun, Ng & Schober, 2020), the authors jointly studied trajectory and resource allocation design for UAVs providing wireless connectivity in uncertain environments under jittering. Nonetheless, the two works mentioned above did not consider a quasi-optimal resource allocation scheme to enable URLLC in UAV networks with jittering and imperfect CSI. From our previous discussions, it is evident that

to realize the vision of 5G+ networks; it is necessary to study such robust resource allocation schemes for URLLC systems in UAV transceivers under jittering.

APPENDIX I

APPENDIX OF CHAPTER 2

1. Proof of Convexity for $\varepsilon_t\,(m_i)$

From (2.3), we have

$$f\,(\gamma_i, m_i, K) = \ln(2)\sqrt{\frac{m_i}{v_i}}\left(\log_2(1+\gamma_i) - \frac{K}{m_i}\right),$$
$$v_i = 1-(1+\gamma_i)^{-2},\ \gamma_i = P_i h_i.$$

The function f is a monotonous function of m_i; however, it is not convex. The decoding error probability or Q-function is given as

$$\varepsilon_i = Q\,(f\,(\gamma_i, m_i, K)) = \int_f^{\infty} \frac{1}{\sqrt{2\pi}} e^{-\frac{f^2}{2}}\, df,\ \forall\, i \in \{1,2,3\}\,. \tag{A I-1}$$

Taking the partial derivative of (A I-1) w.r.t. m_i and substituting $f\,(\gamma_i, m_i, K)$ by its lower bound $C\sqrt{m_i}$ into (A I-1), we get

$$\begin{aligned}\frac{\partial\, Q\,(f\,(\gamma_i, m_i, K))}{\partial\, m_i} &= \frac{-1}{\sqrt{2\pi}} e^{-\frac{f^2}{2}} \frac{\partial\, f\,(\gamma_i, m_i, K)}{\partial\, m_i},\\ &\approx \frac{-1}{\sqrt{2\pi}} e^{-\frac{C^2 m_i}{2}} \frac{\partial\, C\sqrt{m_i}}{\partial\, m_i},\\ &\approx -\frac{C}{2\sqrt{2\pi m_i}} e^{-\frac{C^2 m_i}{2}}.\end{aligned} \tag{A I-2}$$

For $m_i > 0$, both $\frac{C}{2\sqrt{2m_i\pi}}$ and $e^{-\frac{C^2 m_i}{2}}$ are decreasing functions of m_i, thus the function $\frac{\partial\, Q(f(\gamma_i, m_i, K))}{\partial\, m_i}$ is increasing (due to the negative sign). Again, taking the derivative of (A I-2) w.r.t. m_i we have

$$\frac{\partial^2 Q\,(f\,(\gamma_i, m_i, K))}{\partial\, m_i^2} \approx \frac{e^{-\frac{C^2 m_i}{2}} C\left(C^2 m_i + 1\right)}{4 m_i \sqrt{2\pi m_i}} \tag{A I-3}$$

Therefore, $\frac{\partial^2 Q(f(\gamma_i, m_i, K))}{\partial\, m_i^2} > 0$ which means that, by the second derivative test, the function $Q(f\,(\gamma_i, m_i, K))$ or ε_i is convex, so $\varepsilon_t\,(m_i)$ which is the summation of these convex functions is also convex. This completes the proof.

APPENDIX II

APPENDIX OF CHAPTER 3

We first introduce the formulas of error denoted by δ_e and percentage error denoted by % δ_e as follows

$$\delta_e = \text{Measured value of } V_k - \text{Approximation value of } V_k, \tag{A II-1}$$

$$\% \ \delta_e = \frac{|\delta_e|}{\text{Approximation value of } V_k} \times 100\%, \tag{A II-2}$$

where $|.|$ represents the absolute value of a variable and Approximation of V_k equals to one. To validate this assumption, we create a table and calculate the error δ_e and percentage error % δ_e for the channel dispersion V_k against different values of the SNR γ_k as shown in table II-1. Moreover, according to table II-1, the percentage error % δ_e for an SNR γ_k of 5 dB is less than 6%, where this percentage error % δ_e further decreases reaching a value of 0.001% for an SNR γ_k of 25 dB. It is clear from the table II-1 that the approximation of the channel dispersion $V_k \approx 1$ is considered highly accurate for high SNR γ_k. Moreover, the UAV and IoT devices have LoS communication links; hence the assumption of high SNR γ_k is commonly made in the literature as outlined in (Sun *et al.*, 2018a; Ren *et al.*, 2020a,c; Ranjha & Kaddoum, 2020a). Therefore, there is a negligible to no loss in performance for the considered system model, taking the aforementioned approximation on the channel dispersion.

Table-A II-1 Calculations of error and percentage error for channel dispersion against different values of SNR

SNR γ_k(dB)	**SNR γ_k(linear)**	**Channel dispersion V_k(linear)**	**δ_e(linear)**	% δ_e
5 dB	3.1623	0.94227	−0.05773	5.773%
10 dB	10	0.99173	−0.00827	0.827%
15 dB	31.6228	0.99906	−0.00094	0.094%
20 dB	100	0.99990	−0.0001	0.01%
25 dB	316.2278	0.99999	−0.00001	0.001%

1. Convexity Analysis of $P_k(y_1, y_2, H, \Theta, m_k)$

To prove that the objective function (3.7a) is non-convex, one needs to check the definiteness of the Hessian matrix of the objective function. In this regard, the matrix is positive semi-definite *if and only if* all the principal minors are positive, which is known as *Sylvester's criterion*. Mathematically, we can compute the total number of principal minors for an $n \times k$ matrix, and express the criterion as follows

$$\begin{gathered} \sum_{k=1}^{k-1} \binom{n}{k} = 30, where\ n = k = 5. \\ \Delta_n \geq 0, \forall\ n \in \{1, \ldots, 30\}\,. \end{gathered} \tag{A II-3}$$

where Δ_n is the n^{th} principal minor. It should be noted that we did not consider the 0×0 and 5×5 principal minors, in our calculation. The Hessian matrix of the function $P_K(y_1, y_2, H, \Theta, m_k)$ from (3.6) is a 5×5 symmetric matrix shown in (A II-4)

$$\mathbf{H}(P_k) = \begin{bmatrix} \frac{\partial^2 P_k}{\partial H^2} & \frac{\partial^2 P_k}{\partial H\,\partial \Theta} & \frac{\partial^2 P_k}{\partial H\,\partial m_k} & \frac{\partial^2 P_k}{\partial H\,\partial y_1} & \frac{\partial^2 P_k}{\partial H\,\partial y_2} \\ \frac{\partial^2 P_k}{\partial \Theta\,\partial H} & \frac{\partial^2 P_k}{\partial \Theta^2} & \frac{\partial^2 P_k}{\partial \Theta\,\partial m_k} & \frac{\partial^2 P_k}{\partial \Theta\,\partial y_1} & \frac{\partial^2 P_k}{\partial \Theta\,\partial y_2} \\ \frac{\partial^2 P_k}{\partial m_k\,\partial H} & \frac{\partial^2 P_k}{\partial m_k\,\partial \Theta} & \frac{\partial^2 P_k}{\partial m_k^2} & \frac{\partial^2 P_k}{\partial m_k\,\partial y_1} & \frac{\partial^2 P_k}{\partial m_k\,\partial y_2} \\ \frac{\partial^2 P_k}{\partial y_1\,\partial H} & \frac{\partial^2 P_k}{\partial y_1 \partial \Theta} & \frac{\partial^2 P_k}{\partial y_1\,\partial m_k} & \frac{\partial^2 P_k}{\partial^2 y_1} & \frac{\partial^2 P_k}{\partial y_1\,\partial y_2} \\ \frac{\partial^2 P_k}{\partial y_2\,\partial H} & \frac{\partial^2 P_k}{\partial y_2\,\partial \Theta} & \frac{\partial^2 P_k}{\partial y_2 \partial m_k} & \frac{\partial^2 P_k}{\partial y_2\,\partial y_1} & \frac{\partial^2 P_k}{\partial^2 y_2} \end{bmatrix}, \tag{A II-4}$$

where its compact general form is given as

$$\mathbf{H}(P_k) = \begin{bmatrix} \mathbf{H_{11}} & \mathbf{H_{12}} & \mathbf{H_{13}} & \mathbf{H_{14}} & \mathbf{H_{15}} \\ \mathbf{H_{21}} & \mathbf{H_{22}} & \mathbf{H_{23}} & \mathbf{H_{24}} & \mathbf{H_{25}} \\ \mathbf{H_{31}} & \mathbf{H_{32}} & \mathbf{H_{33}} & \mathbf{H_{34}} & \mathbf{H_{35}} \\ \mathbf{H_{41}} & \mathbf{H_{42}} & \mathbf{H_{43}} & \mathbf{H_{44}} & \mathbf{H_{45}} \\ \mathbf{H_{51}} & \mathbf{H_{52}} & \mathbf{H_{53}} & \mathbf{H_{54}} & \mathbf{H_{55}} \end{bmatrix}. \tag{A II-5}$$

Since (A II-4), is symmetric across the main diagonal, it satisfies the following property

$$\mathbf{H} \Leftrightarrow \mathbf{H_{ij}} = \mathbf{H_{ji}}, \forall\, i, j \in \{1, \ldots, 5\}\,. \tag{A II-6}$$

where i, j are the indices of the matrix. Thus, we only include the top triangular part of the matrix.The elements of the first row are given as

$$\mathbf{H_{11}} = \frac{\partial^2 P_k}{\partial H^2} = \frac{\Theta^2 \rho \alpha_2 \alpha_3 F}{G_0 \beta_0}\,^{1}, \tag{A II-7}$$

$$\mathbf{H_{12}} = \frac{\partial^2 P_k}{\partial H \partial \Theta} = \frac{2H\Theta\rho G_0 \beta_0 F \alpha_4}{G_0 \beta_0}, \tag{A II-8}$$

$$\mathbf{H_{13}} = \frac{\partial^2 P_k}{\partial H \partial m_k} = -\frac{2^R H Q^{-1}(\varepsilon_k)\Theta^2 \rho \exp\left(\frac{Q^{-1}(\varepsilon_k)}{\sqrt{m_k}}\right)\alpha_4}{2G_0\beta_0\sqrt{m_k^3}}, \tag{A II-9}$$

The next entries are given as

$$\mathbf{H_{14}} = \frac{\partial^2 P_k}{\partial H \partial y_1} = -\frac{2H\Theta^2\rho(x_1 - y_1)(\frac{\rho}{2} - 1)F\alpha_2}{G_0\beta_0}, \tag{A II-10}$$

$$\mathbf{H_{15}} = \frac{\partial^2 P_k}{\partial H \partial y_2} = -\frac{2H\Theta^2\rho(x_2 - y_2)(\frac{\rho}{2} - 1)F\alpha_2}{G_0\beta_0}. \tag{A II-11}$$

[1] Please consult Table II-2 for the definition of matrix variables α_2, α_3, α_4, α_5, and F.

The elements of the second row are given as

$$\mathbf{H_{22}} = \frac{\partial^2 P_k}{\partial^2 \Theta} = \frac{2F\alpha_5}{G_0\beta_0}, \tag{A II-12}$$

$$\mathbf{H_{23}} = \frac{\partial^2 P_k}{\partial \Theta \partial m_k} = -\frac{2^R Q^{-1}(\varepsilon_k)\Theta \exp\left(\frac{Q^{-1}(\varepsilon_k)}{\sqrt{m_k}}\right)\alpha_5}{G_0\beta_0\sqrt{m_k^3}}, \tag{A II-13}$$

The next elements are

$$\mathbf{H_{24}} = \frac{\partial^2 P_k}{\partial \Theta \partial y_1} = -\frac{2\Theta\rho(x_1 - y_1)F\alpha_4}{G_0\beta_0}, \tag{A II-14}$$

$$\mathbf{H_{25}} = \frac{\partial^2 P_k}{\partial \Theta \partial y_2} = -\frac{2\Theta\rho(x_2 - y_2)F\alpha_4}{G_0\beta_0}. \tag{A II-15}$$

Similarly, the elements of the third row are given as

$$\mathbf{H_{33}} = \frac{\partial^2 P_k}{\partial m_k^2} = 3\frac{2^R Q^{-1}(\varepsilon_k)\Theta^2 \exp\left(\frac{Q^{-1}(\varepsilon_k)}{\sqrt{m_k}}\right)\alpha_5}{4G_0\beta_0\sqrt{m_k^5}} + \frac{2^R Q^{-1}(\varepsilon_k)^2\Theta^2 \exp\left(\frac{Q^{-1}(\varepsilon_k)}{\sqrt{m_k}}\right)\alpha_5}{4G_0\beta_0 m_k^3}, \tag{A II-16}$$

The next two entries of the following row are given by

$$\mathbf{H_{34}} = \frac{\partial^2 P_k}{\partial m_k \partial y_1} = \frac{2^{R+1} Q^{-1}(\varepsilon_k)\Theta^2\rho \exp\left(\frac{Q^{-1}(\varepsilon_k)}{\sqrt{m_k}}\right)}{4G_0\beta_0\sqrt{m_k^3}\alpha_4^{-1}(x_1 - y_1)^{-1}}, \tag{A II-17}$$

$$\mathbf{H_{35}} = \frac{\partial^2 P_k}{\partial m_k \partial y_2} = \frac{2^{R+1} Q^{-1}(\varepsilon_k)\Theta^2\rho \exp\left(\frac{Q^{-1}(\varepsilon_k)}{\sqrt{m_k}}\right)}{4G_0\beta_0\sqrt{m_k^3}\alpha_4^{-1}(x_2 - y_2)^{-1}}. \tag{A II-18}$$

The elements of the fourth row are given as

$$\mathbf{H_{44}} = \frac{\partial^2 P_k}{\partial y_1^2} = \frac{2\Theta^2\rho(\frac{\rho}{2} - 1)F(x_1 - y_1)^2\alpha_2}{G_0\beta_0} + \frac{\Theta^2\rho F\alpha_4}{G_0\beta_0}, \tag{A II-19}$$

$$\mathbf{H_{45}} = \frac{\partial^2 P_k}{\partial y_1 \partial y_2} = \frac{2\Theta^2\rho(x_1 - y_1)(x_2 - y_2)(\frac{\rho}{2} - 1)F\alpha_2}{G_0\beta_0}. \tag{A II-20}$$

Table-A II-2 Definitions of variables used in Hessian matrix

Variables	Definitions
α_2	$\left(\|\boldsymbol{y}-\boldsymbol{x}_k\|^2+H^2\right)^{\frac{\rho}{2}-2}$
α_3	$\left(\|\boldsymbol{y}-\boldsymbol{x}_k\|^2+H^2\rho-H^2\right)$
α_4	$\left(\|\boldsymbol{y}-\boldsymbol{x}_k\|^2+H^2\right)^{\frac{\rho}{2}-1}$
α_5	$\left(\|\boldsymbol{y}-\boldsymbol{x}_k\|^2+H^2\right)^{\frac{\rho}{2}}$
F	$2^R \exp\left(\frac{Q^{-1}(\varepsilon_k)}{\sqrt{m_k}}\right)-1$

Likewise, the elements of the fifth row are given as

$$\mathbf{H_{55}}=\frac{\partial^2 P_k}{\partial y_2^2}=\frac{\Theta^2\rho F\alpha_4}{G_0\beta_0}+\frac{2\Theta^2\rho(\frac{\rho}{2}-1)F(x_2-y_2)^2\alpha_2}{G_0\beta_0}. \tag{A II-21}$$

The leading first-order principal minor is given by

$$\Delta_1=det\left[\mathbf{H_{11}}\right], \tag{A II-22}$$

$$\Delta_1=\frac{\Theta^2\rho\left[2^R\exp\left(\frac{Q^{-1}(\varepsilon_k)}{\sqrt{m_k}}\right)-1\right]\left(H^2+\|\boldsymbol{y}-\boldsymbol{x}_k\|^2\right)^{\frac{\rho}{2}-2}\left(\|\boldsymbol{y}-\boldsymbol{x}_k\|^2+H^2\rho-H^2\right)}{G_0\beta_0}\geq 0. \tag{A II-23}$$

Since, all the variables and constants in (A II-23) are positive, we have

$$H^2\rho-H^2\geq 0, \tag{A II-24}$$

Therefore, (A II-24) holds for the chosen parameter values. Now, using the matrix property (A II-6), we compute the leading second-order principal minor as

$$\Delta_2 = det \begin{bmatrix} \mathbf{H_{11}} & \mathbf{H_{12}} \\ \mathbf{H_{21}} & \mathbf{H_{22}} \end{bmatrix}, where\ \mathbf{H_{12}} = \mathbf{H_{21}}. \tag{A II-25}$$

$$\Delta_2 = \frac{2\Theta^2\rho\left[2^R \exp\left(\frac{Q^{-1}(\varepsilon_k)}{\sqrt{m}_k}\right) - 1\right]^2 \left(H^2 + \|\boldsymbol{y} - \boldsymbol{x}_k\|^2\right)^{\rho-2} \left(\|\boldsymbol{y} - \boldsymbol{x}_k\|^2 - H^2\rho - H^2\right)}{G_0^2\beta_0^2} \geq 0. \tag{A II-26}$$

From (A II-26), we have

$$\begin{aligned} \|\boldsymbol{y} - \boldsymbol{x}_k\|^2 &\geq H^2\rho + H^2, \\ \|\boldsymbol{y} - \boldsymbol{x}_k\|^2 &\geq H^2(\rho + 1). \end{aligned} \tag{A II-27}$$

Therefore, the feasible region for constraint (3.7b) of the optimization problem (3.7a), is given by

$$\rho + 1 \leq \frac{\|\boldsymbol{y} - \boldsymbol{x}_k\|^2}{H^2} \leq \tan^2(\Theta), \tag{A II-28}$$

The inequality in (A II-28) cannot be guaranteed for all possible combinations of ρ and Θ. For example, if we consider $\Theta = \frac{\pi}{4}$, we have

$$\rho + 1 \leq \frac{\|\boldsymbol{y} - \boldsymbol{x}_k\|^2}{H^2} \leq 1. \tag{A II-29}$$

Similarly, the inequality in (A II-29) does not hold for $\rho \geq 2$. Since, one of the principal minors is negative, violating (A II-3), the objective-function (3.7a) is non-convex. This completes the proof.

APPENDIX III

APPENDIX OF CHAPTER 5

1. Convexity analysis of problem (5.9)

1.1 Convexity analysis of constraint (5.9b)

To analyze the convexity of the constraint (5.9b), we define a function as $C_1(\boldsymbol{q}, H, \Theta) = \|\boldsymbol{q} - \boldsymbol{w}_k\|^2 - H^2 \tan^2(\Theta)$. The **Hessian** matrix of C_1 is given by (A III-1). Here, the function is convex if the **Hessian** matrix is positive-semidefinite. According to Sylvester's criteria, a Hermitian matrix is positive-semidefinite if all principal minors of the matrix are positive (Hiriart-Urruty & Lemaréchal, 2012). This implies that the diagonal elements of the matrix have to be positive, which is not the case for matrix $\mathbf{H}_{\mathbf{C_1}}$. The second derivative w.r.t $\boldsymbol{q}_1$ is 2, which is positive, but the second derivative with respect to H is negative. Thus, $\mathbf{H}_{\mathbf{C_1}}$ is not positive semidefinite. Hence, the constraint (5.9b) is non-convex.

1.2 Convexity analysis of constraint (5.9d)

Constraint (5.9d) is non-convex due to the condition $m_{UAV}(t), m_k(t) \in \mathbb{N}$. To solve this issue, the constraint is substituted by $m_{UAV}(t), m_k(t) \geq 0$, making variables $m_{UAV}(t)$ and $m_k(t)$ continuous. The floor function is applied to the obtained solution.

1.3 Convexity analysis of constraint (5.9e)

Constraint (5.9e) is the sum of the product of two variables. Since function $a(x, y) = xy$ is non-convex, the constraint is also non-convex.

2. Convexity analysis of problem (5.16)

For problem (5.16), we compute the second derivative of $f(\gamma_{UAV})$ given by equation (A III-2). Here, $f(\gamma_{UAV})$ is concave if the conditions given in (A III-3) and (A III-4) are satisfied.

$$\mathbf{H_{C_1}} = \begin{bmatrix} \frac{\partial^2 C_1}{\partial \boldsymbol{q}_1^2} & \frac{\partial^2 C_1}{\partial \boldsymbol{q}_1 \partial \boldsymbol{q}_2} & \frac{\partial^2 C_1}{\partial \boldsymbol{q}_1 \partial H} & \frac{\partial^2 C_1}{\partial \boldsymbol{q}_1 \partial \Theta} \\ \frac{\partial^2 C_1}{\partial \boldsymbol{q}_2 \partial \boldsymbol{q}_1} & \frac{\partial^2 C_1}{\partial \boldsymbol{q}_2^2} & \frac{\partial^2 C_1}{\partial \boldsymbol{q}_2 \partial H} & \frac{\partial^2 C_1}{\partial \boldsymbol{q}_2 \partial \Theta} \\ \frac{\partial^2 C_1}{\partial H \partial \boldsymbol{q}_1} & \frac{\partial^2 C_1}{\partial H \boldsymbol{q}_2} & \frac{\partial^2 C_1}{\partial H^2} & \frac{\partial^2 C_1}{\partial H \partial \Theta} \\ \frac{\partial^2 C_1}{\partial \Theta \partial \boldsymbol{q}_1} & \frac{\partial^2 C_1}{\partial \Theta \boldsymbol{q}_2} & \frac{\partial^2 C_1}{\partial \Theta \partial H} & \frac{\partial^2 C_1}{\partial \Theta^2} \end{bmatrix}, \tag{A III-1}$$

$$= \begin{bmatrix} 2 & 0 & 0 & 0 \\ 0 & 2 & 0 & 0 \\ 0 & 0 & -2\tan(\Theta)^2 & -4H\tan(\Theta)(\tan(\Theta)^2+1) \\ 0 & 0 & -4H\tan(\Theta)(\tan(\Theta)^2+1) & -2H^2(4\tan(\Theta)^2+3\tan(\Theta)^4+1) \end{bmatrix}.$$

$$\frac{\partial^2 f(\gamma_{UAV})}{\partial H^2} = \frac{2A_3C_3\left(3H^4 + A_3H^2 + 2B_3H^2 - B_3^2 - A_3B_3\right)}{\ln(2)(H^2+B_3)^2(H^2+A_3+B_3)^2}, \tag{A III-2}$$

Condition C.1 : $3H^4 + A_3H^2 + 2B_3H^2 - B_3^2 - A_3B_3 \leq 0, \quad A_3, B_3 \neq 0,$ (A III-3)

$$\textbf{Condition C.2}: \qquad H_{\min} \leq H \leq \sqrt{\frac{\sqrt{A_3^2 + 16A_3B_3 + 16B_3^2} - A_3 - 2B_3}{6}}, \quad A_3, B_3 \neq 0, \tag{A III-4}$$

$$\frac{\partial^2 Q(f(\gamma_{UAV}))}{\partial H^2} = -\frac{\sqrt{2}A_3C_3 \exp\left(-\frac{f(\gamma_{UAV})^2}{2}\right)\left[\ln(2)\Psi_1 + 2A_3C_3^2H^2(D_3 - \sigma_1)\right]}{\sqrt{\pi}\ln(2)^2\left(H^2 + B_3\right)^2\left(H^2 + A_3 + B_3\right)^2}, \tag{A III-5}$$

$$\Psi_1 = 3H^4 + A_3H^2 + 2B_3H^2 - B_3^2 - A_3B_3,$$

$$\textbf{Condition C.3}: \qquad \ln(2)(3H^4 + A_3H^2 + 2B_3H^2 - B_3^2 - A_3B_3) + 2A_3C_3^2H^2(D_3 - \sigma_1) \leq 0, \tag{A III-6}$$

$$\textbf{Condition C.3.1}: \qquad 3H^4 + A_3H^2 + 2B_3H^2 - B_3^2 - A_3B_3 \leq 0 \wedge D_3 - \log_2(\gamma_{UAV} + 1) \leq 0, \tag{A III-7}$$

This is not always verified. For example, suppose $P_C^* = 3$ watts, $\beta_0 = 58.5$ dB and $\boldsymbol{q}^* = (50, 50)$ m, then $H \leq 70.38$ m, which is impractical since the height is lower than specifications provided in 3GPP release 15, which are followed for this work, as the UAV is supposed to fly at a minimum height of 80 m to maintain a high probability of line of sight (LoS) communications. Hence, the function f is neither concave nor convex and the convexity needs to be checked on $Q(f(\gamma_{UAV}))$. The second derivative of $Q(f(\gamma_{UAV}))$ with respect to H is given by (A III-5), where $\sigma_1 = \log_2(\gamma_{UAV} + 1)$. Moreover, $Q(f(\gamma_{UAV}))$ is convex if (A III-6) is verified. Consequently, due to the term σ_1 in (A III-6), it is not possible to find an explicit solution for H. One way to make sure the condition (A III-6) is true is to see if both terms are negative. In this case, the second condition (A III-7) is always verified ($Q(x) \leq 0.5$ implies that f needs to be positive). The first condition (A III-6) can be false. Thus, we conclude that problem (5.16) is only conditionally convex.

3. Convexity analysis of problem (5.21)

For problem (5.21), we analyze the first term of the objective function $\varepsilon_{UAV}(t)$, at an arbitrary time t, which depends on UAV position $\boldsymbol{q}$.

$$f(\gamma_{UAV}) = C_4 \left(\log_2 (1 + \gamma_{UAV}) - D_4\right), \tag{A III-8}$$

$$\boldsymbol{H}_{\boldsymbol{Q}(f_{UAV})} = \frac{\sqrt{2}A_4C_4 \exp\left(-\frac{f(\gamma_{UAV})^2}{2}\right)}{\sqrt{\pi}\ln(2)^2\left(\|\boldsymbol{q}\|^2 + B_4\right)^2\left(\|\boldsymbol{q}\|^2 + A_4 + B_4\right)^2} \begin{bmatrix} E_{12} & F \\ F & E_{21} \end{bmatrix}, \tag{A III-9}$$

$$\begin{aligned} E_{ij} &= \ln(2)\Psi_2 + 2A_4C_4^2q_i^2(\sigma_1 - D_4), \\ \Psi_2 &= B_4^2 - 3q_i^4 + q_j^4 - A_4q_i^2 + A_4q_j^2 - 2B_4q_i^2 + 2B_4q_j^2 + A_4B_4 - 2q_i^2q_j^2, \\ F &= -2q_1q_2\left(\ln(2)(A_4 + 2B_4 + 2q_1^2 + 2q_2^2) - A_4C_4^2(\sigma_1 + D_4)\right). \end{aligned}$$

$$\textbf{Condition C.4} : \ln(2)\Psi_3 + 2A_3C_3^2q_i^2(\sigma_1 - D_3) \geq 0,$$

$$\Psi_3 = B_4^2 - 3q_i^4 + q_j^4 - A_3q_i^2 + A_3q_j^2 - 2B_4q_i^2 + 2B_4q_j^2 + A_3B_4 - 2q_i^2q_j^2, \tag{A III-10}$$

$$\textbf{Condition C.5} : A_4(B_4 - q_i^2 + q_j^2) + (B_4 - 3q_i^2 + q_j^2)(B_4 + q_i^2 + q_j^2) \geq 0 \wedge \sigma_1 - D_4 \geq 0, \tag{A III-11}$$

$$\textbf{Condition C.6} : d_1 \leq c \leq d_2 \leq \sqrt[4]{\frac{H^2(A_4 + H^2)}{4}} \wedge l_1 \leq c \leq l_2 \leq \sqrt[4]{\frac{H^2(A_4 + H^2)}{4}}. \tag{A III-12}$$

$$\frac{\partial Q(f(\gamma_{UAV}))}{\partial \boldsymbol{q}} = \frac{\sqrt{2}A_4C_4\boldsymbol{q} \exp\left(-\frac{f(\gamma_{UAV})^2}{2}\right)}{\sqrt{\pi}\ln(2)(\gamma_{UAV} + 1)\left(\|\boldsymbol{q}\|^2 + B_4\right)^2}, \tag{A III-13}$$

$$\frac{\partial Q(f(\gamma_k))}{\partial \boldsymbol{q}} = \frac{\sqrt{2}A_4C_4(\boldsymbol{q} - \boldsymbol{w}_k) \exp\left(-\frac{f(\gamma_k)^2}{2}\right)}{\sqrt{\pi}\ln(2)(\gamma_k + 1)\left(\|\boldsymbol{q} - \boldsymbol{w}_k\|^2 + B_4\right)^2}. \tag{A III-14}$$

For the sake of simplicity, we denote $f(\gamma_{UAV}(t), m^*_{UAV}(t), L)$ by $f(\gamma_{UAV})$ which is defined in (A III-8), where $\gamma_{UAV} = \dfrac{A_4}{\|\boldsymbol{q}\|^2 + B_4}$, with $A_4 = P^*_C(t)\beta_0$, $B_4 = H^{*2}$, $C_4 = \ln(2)\sqrt{m^*_{UAV}(t)}$ and $D_4 = \frac{L}{m^*_{UAV}(t)}$. Since $\boldsymbol{q} = (q_1, q_2)$, the **Hessian** of $Q(f(\gamma_{UAV}))$ given by (A III-9), where for E_{ij}, $i, j = \{1, 2\} \wedge i \neq j$ and $\sigma_1 = \log_2(\gamma_{UAV} + 1)$. As mentioned before for the objective function to be convex, all the principal minors of the **Hessian** must be non-negative, according to *Sylvester's*

Criteria. The principal minors of order 1 are non-negative if the following conditions given by (A III-10), and (A III-11) hold.

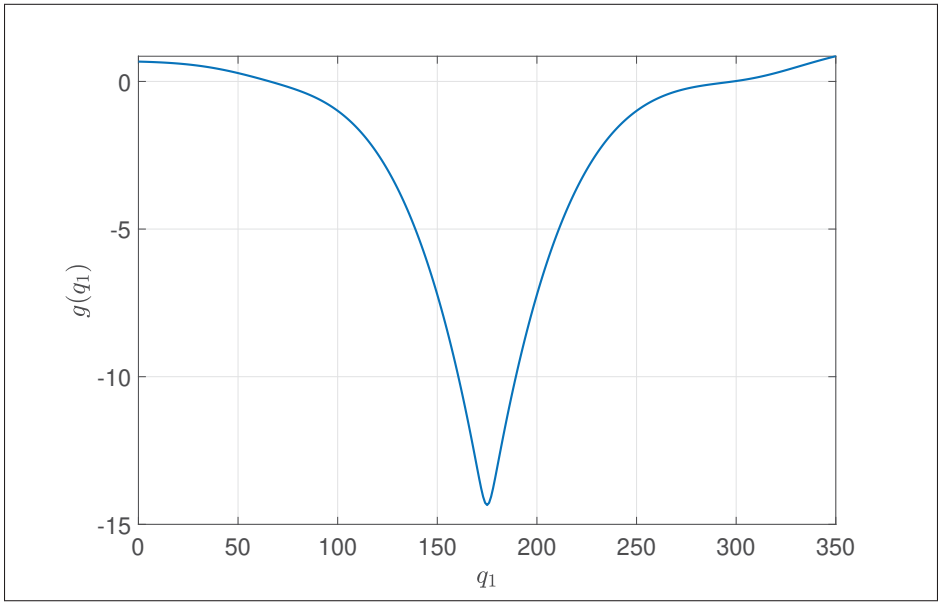

Figure-A III-1 Function $g(q_1)$

Again, the second condition (A III-11) is always true while the first condition (A III-10) is hard to prove. We suppose $c = q_1 = q_2$ and replacing B_4 by H^2, $A_4H^2 + H^4 - 4c^4 \geq 0$, thus the condition (A III-10) is true if the condition (A III-12) holds. Depending on the values chosen for the feasible region of the UAV $[d_1, d_2] \times [l_1, l_2]$, the power P_C^*, β_0, and the height H^*, this condition can be false. Once again, we suppose the same values as in the previous section and for $H^* = 80$ m, the condition is $d_2 \leq 241.6223$ m and $l_2 \leq 241.6223$ m. Choosing higher values may lead to a non-convex problem. The first derivative, given by equation (A III-13) of $Q(f(\gamma_{UAV}))$ is always positive. Meanwhile, the first derivative, given in (A III-14), of $Q(f(\gamma_k))$ is positive if $\boldsymbol{q} - \boldsymbol{w}_k > 0$ and negative if $\boldsymbol{q} - \boldsymbol{w}_k < 0$. Hence, the first derivative does not bring useful information in terms of convexity. As a final resort, we provide the guarantee of a global minimum graphically. Here, since the objective function can take on small values, we apply the logarithmic function, which is possible since the logarithmic function preserve the local extrema (Boyd & Vandenberghe, 2004). As such, we consider $g(q_1, q_2) = \ln(\varepsilon(t))$ for arbitrary time t. Without loss of generality, we can consider that both the UAV and the robots

are located on the straight line $q_1 = q_2$. Fig. III-1 shows $g(q_1)$, which is the same as $g(q_2)$. We chose the same parameters considered in the simulation results. Moreover, we tested several values for the problem variables, where the function behaved similarly for all the considered cases. Hence, we conclude that (5.21) has one local minimum, which is the global minimum of the convex function.

APPENDIX IV

APPENDIX OF CHAPTER 6

1. Convexity analysis of the problem

To prove that problem (6.16) is not a convex problem we need to prove that the objective function is not convex. In order to do so, it is sufficient to prove that the problem is not convex w.r.t. one of the variables, in this case $\boldsymbol{q}[n]$. For simplicity, we consider $f_i(\gamma_i) = f(\gamma_i, m, L), \forall i \in \{1, 2\}$, and $\varepsilon(\boldsymbol{q}[n]) = \varepsilon[n]$. Then we calculate the first derivative of $\varepsilon[n]$ w.r.t. $\boldsymbol{q}[n]$ as

$$\varepsilon'(\boldsymbol{q}[n]) = \varepsilon_1'(\boldsymbol{q}[n]) + \varepsilon_2'(\boldsymbol{q}[n]), \tag{A IV-1}$$

where $\varepsilon_i'(\boldsymbol{q}[n])$ is given by

$$\varepsilon_i'(\boldsymbol{q}[n]) = \frac{\partial \varepsilon_i\left(\gamma_i[n]\right)}{\partial \gamma_i[n]} \gamma_i'(\boldsymbol{q}[n]), \forall i \in \{1, 2\}, \tag{A IV-2}$$

with $\gamma_i'(\boldsymbol{q}[n])$ given by

$$\begin{aligned} \gamma_1'(\boldsymbol{q}[n]) &= -\frac{2P_1\beta_0 \boldsymbol{q}[n]}{(\|\boldsymbol{q}[n]\|^2 + H^2)^2}, \\ \gamma_2'(\boldsymbol{q}[n]) &= \frac{2P_2\beta_0(\boldsymbol{q}[n] - \boldsymbol{w})}{\left(\|\boldsymbol{q}[n] - \boldsymbol{w}\|^2 + H^2\right)^2}, \end{aligned} \tag{A IV-3}$$

and $\frac{\partial \varepsilon_i(\gamma_i)}{\partial \gamma_i}$ given by

$$\frac{\partial \varepsilon_i\left(\gamma_i\right)}{\partial \gamma_i} = -\frac{1}{\sqrt{2\pi}} e^{-\frac{f^2(\gamma_i)}{2}} \frac{\partial f_i\left(\gamma_i\right)}{\partial \gamma_i}. \tag{A IV-4}$$

In A IV-4, $\frac{\partial f_i(\gamma_i)}{\partial \gamma_i}$ is given as

$$\frac{\partial f_i\left(\gamma_i\right)}{\partial \gamma_i} = \frac{A}{\log(2)(\gamma_i + 1)}. \tag{A IV-5}$$

Similarly, the second derivative of $\varepsilon[n]$ w.r.t. $\boldsymbol{q}[n]$ can be calculated as

$$\varepsilon''(\boldsymbol{q}[n]) = \varepsilon_1''(\boldsymbol{q}[n]) + \varepsilon_2''(\boldsymbol{q}[n]), \tag{A IV-6}$$

where $\varepsilon_i''(\boldsymbol{q}[n]), \forall\, i \in \{1,2\}$ are given by

$$\varepsilon_i''(\boldsymbol{q}[n]) = \frac{\partial^2 \varepsilon_i(\gamma_i)}{\partial \gamma_i^2}\left(\gamma_i'\right)^2 + \frac{\partial \varepsilon_i(\gamma_i)}{\partial \gamma_i}\gamma_i'', \tag{A IV-7}$$

with $\gamma_i''(\boldsymbol{q}[n])$ given by

$$\gamma_1''(\boldsymbol{q}[n]) = -\frac{2P_1\beta_0\left(\|\boldsymbol{q}[n]\|^2 + H^2 - 4\boldsymbol{q}[\boldsymbol{n}]\right)}{(\|\boldsymbol{q}[n]\|^2 + H^2)^3}, \tag{A IV-8}$$

$$\gamma_2''(\boldsymbol{q}[n]) = -\frac{2P_2\beta_0\left(\|\boldsymbol{q}[n] - \boldsymbol{w}\|^2 + H^2 - 4(\boldsymbol{q}[\boldsymbol{n}] - \boldsymbol{w})\right)}{(\|\boldsymbol{q}[n] - \boldsymbol{w}\|^2 + H^2)^3}, \tag{A IV-9}$$

and $\frac{\partial^2 \varepsilon_i(\gamma_i)}{\partial \gamma_i^2}$ given by

$$\frac{\partial^2 \varepsilon_i(\gamma_i)}{\partial \gamma_i^2} = \frac{1}{\sqrt{2\pi}} e^{-\frac{f_i^2(\gamma_i)}{2}}\left(f_i(\gamma_i)\left(\frac{\partial f_i(\gamma_i)}{\partial \gamma_i}\right)^2 - \frac{\partial^2 f_i(\gamma_i)}{\partial \gamma_i^2}\right). \tag{A IV-10}$$

In A IV-9, $\frac{\partial^2 f_i(\gamma_i)}{\partial \gamma_i^2}$ is given by

$$\frac{\partial^2 f_i(\gamma_i)}{\partial \gamma_i^2} = -\frac{A}{\log(2)(\gamma_i + 1)^2}. \tag{A IV-11}$$

Thus, the objective function is a convex function if $\varepsilon_i''(\boldsymbol{q}[n]) \geq 0, \forall i \in \{1,2\}$. The first term $\frac{\partial^2 \varepsilon_i(\gamma_i)}{\partial \gamma_i^2}\left(\gamma_i'\right)^2$ is always non-negative, but the same does not happen for the second term $\frac{\partial \varepsilon_i(\gamma_i)}{\partial \gamma_i}\gamma_i''$ because the sign of $\gamma_i''(\boldsymbol{q}[n])$ may be positive or negative, depending on the position of the UAV. As such, the function is neither convex nor concave w.r.t. $\boldsymbol{q}[n]$, which means the function is not convex w.r.t. to the entire set of variables, including the blocklength.

2. Convexity analysis of the constraint (6.16b)

Function $F_m(\boldsymbol{d})$ is convex w.r.t. $\boldsymbol{d}$ and $G_m(\boldsymbol{q})$ is convex w.r.t. $\boldsymbol{q}$. Thus, the constraint $\zeta \leq Z + F_m(\boldsymbol{d}) - G_m(\boldsymbol{q}) \leq Z$ is not convex due to being the difference between two convex functions.

3. Convexity analysis of the constraint (6.16g)

To prove that constraints $\varepsilon_i[n] \leq \epsilon_i, \forall i \in \{1, 2\}$, do not represent a convex set we need to check the second derivative of function $\varepsilon_i[n] - \epsilon_i$. As seen in the Appendix 1, function $\varepsilon_i[n]$ is not convex w.r.t. $\boldsymbol{q}[n]$, thus we conclude that the constraint is also not convex.

4. Convexity analysis of the constraint (6.16i)

The problem is that the function is non-convex due to constraints $m_1[n], m_2[n] \in \mathbb{N}$ because the set of natural numbers is not a convex set (Hiriart-Urruty & Lemaréchal, 2012; Boyd & Vandenberghe, 2004). To overcome this, the constraints are substituted by $m_1[n], m_2[n] \geq 0$, making variables $m_1[n]$ and $m_2[n]$ continuous. Lastly, the floor function is applied to the obtained solution.

APPENDIX V

APPENDIX OF CHAPTER 7

1. Appendix A

Here, we show $\frac{\partial v^*}{\partial h}$ after a few algebraic manipulations and simplifications. For the sake of notational convenience, we define $S = \sec^2\theta$ and $\tilde{S} = 3S + 1$. Then we have

$$\begin{aligned}\frac{\partial v^*}{\partial h} = \frac{2B}{K\ln 2}\Bigg(&\frac{\tan\theta}{2}\ln\left(1+\frac{\alpha}{Sh^2}\right)\\ &+\frac{\tilde{S}h}{\sqrt{4\alpha+\tilde{S}h^2}}\tan^{-1}\left(\frac{h\tan\theta}{\sqrt{4\alpha+\tilde{S}h^2}}\right)-\sqrt{\tilde{S}}\tan^{-1}\left(\frac{\tan\theta}{\sqrt{\tilde{S}}}\right)\\ &+\frac{Q^{-1}(\varepsilon)}{\sqrt{M}}\frac{\alpha\tan\theta}{\sqrt{\alpha+2Sh^2}\left(2\alpha+\tilde{S}h^2\right)}\\ &\times\left(-2\sqrt{\alpha}+\frac{\tan\theta\left(2\alpha^2-S\tilde{S}h^4\right)}{\left(\alpha+Sh^2\right)\sqrt{4\alpha+\tilde{S}h^2}}\right)\Bigg).\end{aligned} \tag{A V-1}$$

2. Appendix B

The flowchart outlining the main steps of the proposed scheme is presented below.

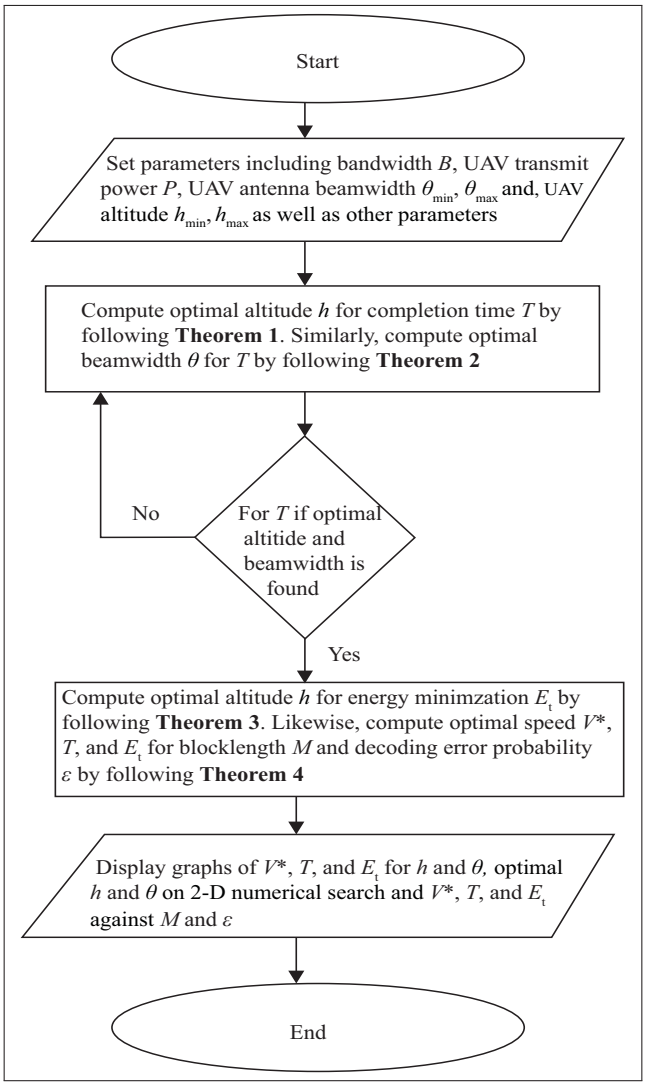

Figure-A V-1 Flowchart of the proposed scheme

3. Appendix C

From Fig. V-2, the percentage differences (pd) of $T(s)$ and $E_t(J)$ for V_1 and V_2 is calculated and presented in Table 5.1 below.

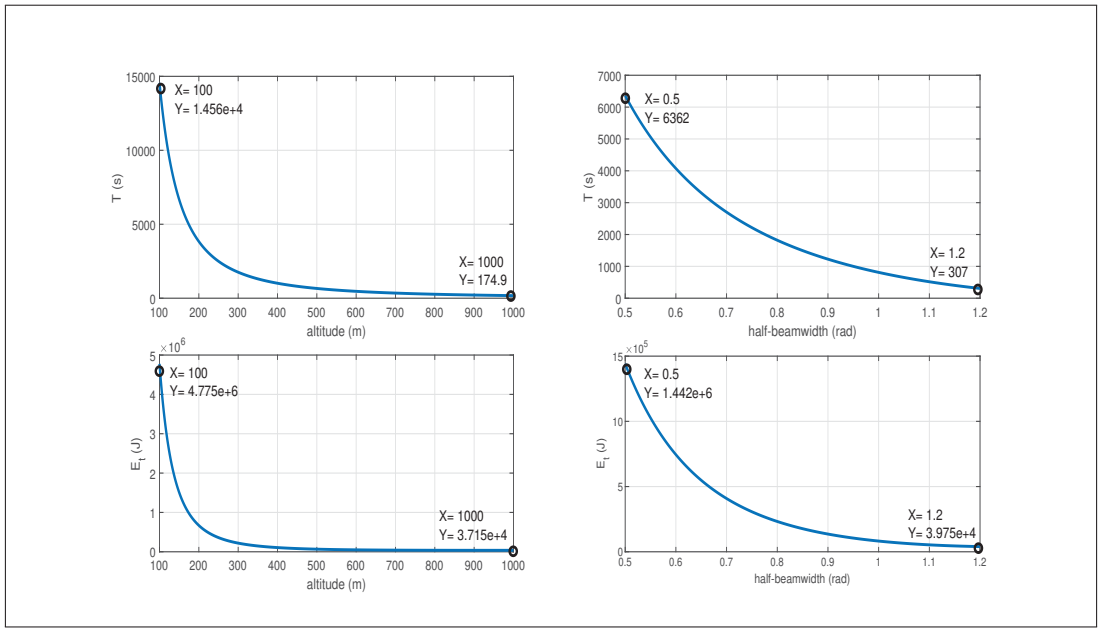

Figure-A V-2 $T(s)$ and $E_t(J)$ for V_1 and V_2, $\forall\ h_{\min} = 10$ m, $h_{\max} = 100$ m, and $\theta_{\min} = 0.5$ rad, $\theta_{\max} = 1.2$ rad

Table 5.1 Calculations of percentage differences for the completion time and the energy minimization.

V_1 / $T(s)$ and $E_t(J)$	V_2 / $T(s)$ and $E_t(J)$	$\Delta V = \lvert V_1 - V_2 \rvert$	$\Sigma V = \frac{V_1+V_2}{2}$	**pd**= $\frac{\lvert\Delta V\rvert}{\left[\frac{\Sigma V}{2}\right]} \times 100\%$
1.456×10^4 s	174.9 s	14385.1 s	7367.45 s	195.252 %
4.775×10^6 J	3.715×10^4 J	4737850 J	2406075 J	196.912 %
6362 s	307 s	6055 s	3334.5 s	181.586 %
1.442×10^6 J	3.975×10^4 J	1402250 J	740875 J	189.269 %

AUTHOR'S PUBLICATIONS

During the course of his Ph.D. research, the author contributed to the following published and submitted research articles.

Ranjha, A. & Kaddoum, G. (2020). Quasi-Optimization of Distance and Blocklength in URLLC Aided Multi-Hop UAV Relay Links. *IEEE Wireless Communications Letters*, 9(3), 306-310. doi: 10.1109/LWC.2019.2953165.

Ranjha, A. & Kaddoum, G. (2021a). Quasi-Optimization of Uplink Power for Enabling Green URLLC in Mobile UAV-Assisted IoT Networks: A Perturbation-Based Approach. *IEEE Internet of Things Journal*, 8(3), 1674-1686. doi: 10.1109/JIOT.2020.3014039.

Ranjha, A. & Kaddoum, G. (2021b). URLLC Facilitated by Mobile UAV Relay and RIS: A Joint Design of Passive Beamforming, Blocklength, and UAV Positioning. *IEEE Internet of Things Journal*, 8(6), 4618-4627. doi: 10.1109/JIOT.2020.3027149.

Ranjha, A. & Kaddoum, G. (2021c). URLLC-enabled by Laser Powered UAV Relay: A Quasi-Optimal Design of Resource Allocation, Trajectory Planning and Energy Harvesting. *published in IEEE Transactions on Vehicular Technology (early access)*.

Ranjha, A., Kaddoum, G. & Dev, K. (2021a). Facilitating URLLC in UAV-assisted Relay Systems with Multiple-Mobile Robots for 6G Networks. *published in IEEE Transactions on Industrial Informatics (early access)*.

Ranjha, A., Kaddoum, G., Rahim, M. & Dev, K. (2021b). URLLC in UAV-enabled Multicasting Systems: A Dual Time and Energy Minimization Problem using UAV Speed, Altitude and Beamwidth. *published in Elsevier Computer Communications (early access)*.

BIBLIOGRAPHY

(2016). International Business Times. Nokia and EE trial mobile base stations floating on drones to revolutionise rural 4G coverage. Consulted at http://www.ibtimes.co.uk/nokia-ee-trial-mobile-base-stationsfloating-drones-revolutionise-rural-4g-coverage-1575795.

(2018). Huawei. Connected Aerial Vehicle Live. Consulted at http://www.huawei.com/en/industry-insights/innovation/xlabs/usecases/mbbf2017-connected-aerial-vehicle-live.

Aceto, G., Persico, V. & Pescape, A. (2019). A survey on information and communication technologies for Industry 4.0: state-of-the-art, taxonomies, perspectives, and challenges. *IEEE Commun. Surveys Tuts.*, 21(4), 3467–3501.

Adeogun, R., Berardinelli, G., Mogensen, P. E., Rodriguez, I. & Razzaghpour, M. (2020). Towards 6G in-X Subnetworks With Sub-Millisecond Communication Cycles and Extreme Reliability. *IEEE Access*, 8, 110172-110188. doi: 10.1109/ACCESS.2020.3001625.

Adhikari, M., Munusamy, A., Hazra, A., Menon, V. G., Anavangot, V. & Puthal, D. (2021). Security and Privacy in Edge-centric Intelligent Internet of Vehicles: Issues and Remedies. *IEEE Consum. Electron. Mag.*

Aijaz, A. (2016, Apr.). Towards 5G-enabled tactile internet: Radio resource allocation for haptic communications. *IEEE WCNCW*, pp. 145–150.

Airod, F. E., Chafnaji, H. & Yanikomeroglu, H. (2021). HARQ in Full-Duplex Relay-Assisted Transmissions for URLLC. *IEEE Open J. Commun. Soc.*, 2, 409-422. doi: 10.1109/OJ-COMS.2021.3055073.

Al-Hourani, A., Kandeepan, S. & Jamalipour, A. (2014a). Modeling air-to-ground path loss for low altitude platforms in urban environments. *IEEE GLOBECOM*, pp. 2898–2904.

Al-Hourani, A., Kandeepan, S. & Lardner, S. (2014b). Optimal LAP altitude for maximum coverage. *IEEE Wirel. Commun. Lett.*, 3(6), 569–572.

Anand, A., De Veciana, G. & Shakkottai, S. (2018, Oct.). Joint scheduling of URLLC and eMBB traffic in 5G wireless networks. *IEEE INFOCOM*, pp. 1970–1978.

Andrews, J. G., Buzzi, S., Choi, W., Hanly, S. V., Lozano, A., Soong, A. C. & Zhang, J. C. (2014). What will 5G be? *IEEE J. Sel. Areas Commun.*, 32(6), 1065–1082.

Andrews, L. C. (1998). *Special functions of mathematics for engineers*. Spie Press.

Arribas, E., Mancuso, V. & Cholvi, V. (2019). Coverage Optimization with a Dynamic Network of Drone Relays. *IEEE Trans. Mobile Comput.* doi:10.1109/TMC.2019.2927335.

Awais, M. & Shah, M. A. (2017, Oct.). Information-centric networking: a review on futuristic networks. *Proc. IEEE 23rd Int. Conf. on Automation and Computing (ICAC)*, pp. 1–5.

Azari, M. M., Rosas, F., Chen, K.-C. & Pollin, S. (2017). Ultra reliable UAV communication using altitude and cooperation diversity. *IEEE Trans. Commun.*, 66(1), 330–344.

Bai, T., Pan, C., Deng, Y., Elkashlan, M., Nallanathan, A. & Hanzo, L. (2020). Latency Minimization for Intelligent Reflecting Surface Aided Mobile Edge Computing. *IEEE J. Sel. Areas Commun.*, 1-1.

Balanis, C. A. (2016). *Antenna theory: analysis and design*. John wiley & sons.

Bariah, L., Mohjazi, L., Muhaidat, S., Sofotasios, P. C., Kurt, G. K., Yanikomeroglu, H. & Dobre, O. A. (2020). A prospective look: Key enabling technologies, applications and open research topics in 6G networks. *IEEE Access*, 8, 174792–174820.

Basar, E., Di Renzo, M., De Rosny, J., Debbah, M., Alouini, M.-S. & Zhang, R. (2019). Wireless communications through reconfigurable intelligent surfaces. *IEEE Access*, 7, 116753–116773.

Bekmezci, I., Sahingoz, O. K. & Temel, Ş. (2013). Flying ad-hoc networks (FANETs): A survey. *Ad Hoc Networks*, 11(3), 1254–1270.

Bennis, M., Debbah, M. & Poor, H. V. (2018). Ultrareliable and low-latency wireless communication: Tail, risk, and scale. *Proc. of the IEEE*, 106(10), 1834–1853.

Berry, R. A. (2013). Optimal power-delay tradeoffs in fading channels—Small-delay asymptotics. *IEEE Trans. Inf. Theory*, 59(6), 3939–3952.

Beyene, Y. D., Jantti, R., Ruttik, K. & Iraji, S. (2017). On the performance of narrow-band Internet of Things (NB-IoT). *in Proc. IEEE 2017 Wireless Commun. and Netw. Conf.*, 1–6.

Boccardi, F., Heath, R. W., Lozano, A., Marzetta, T. L. & Popovski, P. (2014). Five disruptive technology directions for 5G. *IEEE Commun. Mag.*, 52(2), 74–80.

Bor-Yaliniz, R. I., El-Keyi, A. & Yanikomeroglu, H. (2016). Efficient 3-D placement of an aerial base station in next generation cellular networks. *IEEE ICC)*, pp. 1–5.

Boyd, S. & Vandenberghe, L. (2004). *Convex optimization*. Cambridge university press.

Braun, W. J. & Murdoch, D. J. (2016). *A first course in statistical programming with R*. Cambridge University Press.

Cai, Y., Wei, Z., Li, R., Ng, D. W. K. & Yuan, J. (2020). Joint trajectory and resource allocation design for energy-efficient secure UAV communication systems. *IEEE Trans. Commun.*, 68(7), 4536–4553.

Chan, C. (2016). It's Time to Lay the Groundwork for 5G Network Slicing. Consulted at https: //networkbuilders.intel.com/blog/its-time-to-lay-the-groundwork-for-5g-network-slicing.

Chang, B., Zhang, L., Li, L., Zhao, G. & Chen, Z. (2019a). Optimizing resource allocation in URLLC for real-time wireless control systems. *IEEE Trans. Veh. Technol*, 68(9), 8916–8927.

Chang, B., Zhao, G., Zhang, L., Imran, M. A., Chen, Z. & Li, L. (2019b). Dynamic Communication QoS Design for Real-Time Wireless Control Systems. *IEEE Sensors J.*

Chen, K., Wang, Y., Zhao, J., Wang, X. & Fei, Z. (2021). URLLC Oriented Joint Power Control and Resource Allocation in UAV-assisted Networks. *IEEE Internet Things J.*

Chen, N., Chen, Y., You, Y., Ling, H., Liang, P. & Zimmermann, R. (2016). Dynamic urban surveillance video stream processing using fog computing. *in Proc. IEEE 2016 2nd Int. Conf. on Multimedia Big Data*, 105–112.

Chen, W., Neely, M. J. & Mitra, U. (2007, May). Energy efficient scheduling with individual packet delay constraints: Offline and online results. *IEEE INFOCOM*, pp. 1136–1144.

Chen, W., Mitra, U. & Neely, M. J. (2009). Energy-efficient scheduling with individual packet delay constraints over a fading channel. *Wireless Netw.*, 15(5), 601–618.

Chen, Y., Feng, W. & Zheng, G. (2017). Optimum placement of UAV as relays. *IEEE Commun. Lett.*, 22(2), 248–251.

Chiaraviglio, L., D'Andreagiovanni, F., Liu, W., Gutierrez, J., Blefari-Melazzi, N., Choo, K.-K. R. & Alouini, M.-S. (2020). Multi-Area Throughput and Energy Optimization of UAV-aided Cellular Networks Powered by Solar Panels and Grid. *IEEE Trans. Mobile Comput.* doi:10.1109/TMC.2020.2980834.

Cui, X., Wang, W. & Fang, Z. (2005). Present situation and some problems analysis of small-size unmanned air vehicles. *Flight dynamics*, 23(1), 14–18.

Dai, H., Zhang, H., Hua, M., Li, C., Huang, Y. & Wang, B. (2019). How to deploy multiple UAVs for providing communication service in an unknown region? *IEEE Wirel. Commun. Lett.*, 8(4), 1276–1279.

Darwazeh, N. S., Al-Qassas, R. S., AlDosari, F. et al. (2015). A secure cloud computing model based on data classification. *Procedia Computer Science*, 52, 1153–1158.

Di Franco, C. & Buttazzo, G. (2015). Energy-aware coverage path planning of UAVs. *IEEE intl. conf. autonomous robot systems and competitions*, pp. 111–117.

Dogra, A., Jha, R. K. & Jain, S. (2021). A Survey on Beyond 5G Network With the Advent of 6G: Architecture and Emerging Technologies. *IEEE Access*, 9, 67512-67547. doi: 10.1109/ACCESS.2020.3031234.

Duffie, J. A. & Beckman, W. A. (2013). *Solar engineering of thermal processes*. John Wiley & Sons.

Durisi, G., Koch, T. & Popovski, P. (2015). Towards massive, ultra-reliable, and low-latency wireless: The art of sending short packets. *in Proc. IEEE*, 104(9), 1711–1726.

Elarabi, T., Deep, V. & Rai, C. K. (2015). Design and simulation of state-of-art ZigBee transmitter for IoT wireless devices. *in Proc. IEEE 2015 Int. Symp. on Signal Process. and Inf. Technol.*, 297–300.

Eom, S., Lee, H., Park, J. & Lee, I. (2019). UAV-aided wireless communication designs with propulsion energy limitations. *IEEE Trans. Veh. Technol.*, 69(1), 651–662.

Fotouhi, A., Qiang, H., Ding, M., Hassan, M., Giordano, L. G., Garcia-Rodriguez, A. & Yuan, J. (2019). Survey on uav cellular communications: Practical aspects, standardization advancements, regulation, and security challenges. *IEEE Commun. Surv. Tuts.*

Guo, H., Liang, Y., Chen, J. & Larsson, E. G. (2019, Dec.). Weighted Sum-Rate Maximization for Intelligent Reflecting Surface Enhanced Wireless Networks. *IEEE Global Commun. Conf. (GLOBECOM)*, pp. 1-6.

Guo, Y., Yin, S. & Hao, J. (2019). Resource allocation and 3-D trajectory design in wireless networks assisted by rechargeable UAV. *IEEE Wirel. Commun. Lett.*, 8(3), 781–784.

Guo, Y., Yin, S., Hao, J. & Du, Y. (2020). A Novel Trajectory Design Approach for UAV Based on Finite Fourier Series. *IEEE Wirel. Commun. Lett.*, 9(5), 671–674.

Gupta, L., Jain, R. & Vaszkun, G. (2015). Survey of important issues in UAV communication networks. *IEEE Commun. Surv. Tuts.*, 18(2), 1123–1152.

Hazra, A., Adhikari, M., Amgoth, T. & Srirama, S. N. (2020). Stackelberg game for service deployment of IoT-enabled applications in 6G-aware fog networks. *IEEE Internet Things J.*, 8(7), 5185–5193.

Hazra, A., Adhikari, M., Amgoth, T. & Srirama, S. N. (2021). Collaborative AI-enabled Intelligent Partial Service Provisioning in Green Industrial Fog Networks. *IEEE Internet Things J.*

He, H., Zhang, S., Zeng, Y. & Zhang, R. (2017). Joint altitude and beamwidth optimization for UAV-enabled multiuser communications. *IEEE Commun. Lett.*, 22(2), 344–347.

He, Z.-Q. & Yuan, X. (2019). Cascaded channel estimation for large intelligent metasurface assisted massive MIMO. *IEEE Wirel. Commun. Lett.*

Hiriart-Urruty, J.-B. & Lemaréchal, C. (2012). *Fundamentals of convex analysis*. Springer Science & Business Media.

Hu, S., Rusek, F. & Edfors, O. (2017, Jun.). The potential of using large antenna arrays on intelligent surfaces. *IEEE 85th Veh. Technol. Conf. (VTC Spring)*, pp. 1–6.

Hu, Y., Schmeink, A. & Gross, J. (2016). Blocklength-limited performance of relaying under quasi-static Rayleigh channels. *IEEE Trans. Wireless Commun.*, 15(7), 4548–4558.

Hu, Y., Zhu, Y., Gursoy, M. C. & Schmeink, A. (2018). SWIPT-enabled relaying in IoT networks operating with finite blocklength codes. *IEEE J. Sel. Areas Commun.*, 37(1), 74–88.

Huang, C., Zappone, A., Alexandropoulos, G. C., Debbah, M. & Yuen, C. (2019). Reconfigurable intelligent surfaces for energy efficiency in wireless communication. *IEEE Trans. Wireless Commun.*, 18(8), 4157–4170.

Jiang, F. & Swindlehurst, A. L. (2012). Optimization of UAV heading for the ground-to-air uplink. *IEEE J. Sel. Areas Commun.*, 30(5), 993–1005.

Jiang, X., Wu, Z., Yin, Z., Yang, W. & Yang, Z. (2019). Trajectory and Communication Design for UAV-Relayed Wireless Networks. *IEEE Wirel. Commun. Lett.*, 8(6), 1600–1603.

Jung, M., Saad, W. & Kong, G. (2019). Performance analysis of large intelligent surfaces (LISs): Uplink spectral efficiency and pilot training. *arXiv preprint arXiv:1904.00453*.

Jung, M., Saad, W., Jang, Y., Kong, G. & Choi, S. (2020). Performance analysis of large intelligent surfaces (LISs): Asymptotic data rate and channel hardening effects. *IEEE Trans. Wireless Commun.*, 19(3), 2052–2065.

Karlsson, K., Jiang, W., Wicker, S., Adams, D., Ma, E., van Renesse, R. & Weatherspoon, H. (2018). Vegvisir: A partition-tolerant blockchain for the internet-of-things. *in Proc. IEEE 38th Int. Conf. on Distrib. Comput. Syst.*, 1150–1158.

Khan, M., Heurtefeux, K., Mohamed, A., Harras, K. A. & Hassan, M. M. (2017a). Mobile target coverage and tracking on drone-be-gone uav cyber-physical testbed. *IEEE Syst. J.*, 12(4), 3485–3496.

Khan, T. A., Heath, R. W. & Popovski, P. (2017b). Wirelessly powered communication networks with short packets. *IEEE Trans. Commun.*, 65(12), 5529–5543.

Kulkarni, P. H., Kute, P. D. & More, V. (2016). IoT based data processing for automated industrial meter reader using Raspberry Pi. *in Proc. IEEE 2016 Int. Conf. on Internet of Things and Appl.*, 107–111.

Lahmeri, M.-A., Kishk, M. A. & Alouini, M.-S. (2019). Stochastic geometry-based analysis of airborne base stations with laser-powered UAVs. *IEEE Commun. Lett.*, 24(1), 173–177.

Lewis, R. M., Torczon, V. & Trosset, M. W. (2000). Direct search methods: then and now. *J. Comput. Appl. Math.*, 124(1-2), 191–207.

Li, S., Duo, B., Yuan, X., Liang, Y. & Di Renzo, M. (2020). Reconfigurable Intelligent Surface Assisted UAV Communication: Joint Trajectory Design and Passive Beamforming. *IEEE Wirel. Commun. Lett.*, 9(5), 716-720.

Li, X., Wang, Q., Liu, Y., Tsiftsis, T. A., Ding, Z. & Nallanathan, A. (2020). UAV-aided multi-way NOMA networks with residual hardware impairments. *IEEE Wireless Commun. Lett.*, 9(9), 1538–1542.

Li, Z., Uusitalo, M. A., Shariatmadari, H. & Singh, B. (2018, Aug.). 5g urllc: Design challenges and system concepts. *IEEE 15th Int. Symp. on Wireless Commun. Systems (ISWCS)*, pp. 1–6.

Liang, H., Gao, W., Nguyen, J. H., Orpilla, M. F. & Yu, W. (2019a). Internet of Things data collection using unmanned aerial vehicles in infrastructure free environments. *IEEE Access*, 8, 3932–3944.

Liang, Y.-C., Long, R., Zhang, Q., Chen, J., Cheng, H. V. & Guo, H. (2019b). Large intelligent surface/antennas (LISA): Making reflective radios smart. *J. Commun. Inf. Netw.*, 4(2), 40-50.

Lin, X., Mei, W. & Zhang, R. (2019). A New Store-then-Amplify-and-Forward Protocol for UAV Mobile Relaying. *IEEE Wirel. Commun. Lett.*, 9(5), 591–595.

Lin, X., Yajnanarayana, V., Muruganathan, S. D., Gao, S., Asplund, H., Maattanen, H.-L., Bergstrom, M., Euler, S. & Wang, Y.-P. E. (2018). The sky is not the limit: LTE for unmanned aerial vehicles. *IEEE Commun. Mag.*, 56(4), 204–210.

Liu, L., Zhang, S. & Zhang, R. (2019). Multi-beam UAV communication in cellular uplink: Cooperative interference cancellation and sum-rate maximization. *IEEE Trans. Wireless Commun.*, 18(10), 4679–4691.

Liu, Y., Ma, X., Shu, L., Hancke, G. P. & Abu-Mahfouz, A. M. (2020). From Industry 4.0 to Agriculture 4.0: Current Status, Enabling Technologies, and Research Challenges. *IEEE Trans. Ind. Informat.*

López, O. L. A., Alves, H., Souza, R. D. & Fernández, E. M. G. (2017). Ultrareliable short-packet communications with wireless energy transfer. *IEEE Signal Process. Lett.*, 24(4), 387–391.

Lyu, J., Zeng, Y. & Zhang, R. (2016). Cyclical multiple access in UAV-aided communications: A throughput-delay tradeoff. *IEEE Wirel. Commun. Lett.*, 5(6), 600–603.

Mahmood, N. H., Lopez, M., Laselva, D., Pedersen, K. & Berardinelli, G. (2018, Aug.). Reliability oriented dual connectivity for URLLC services in 5G New Radio. *Proc. IEEE 15th Int. Symp. on Wireless Commun. Systems (ISWCS)*, pp. 1–6.

Mahmood, N. H., López, O. A., Alves, H. & Latva-Aho, M. (2021). A Predictive Interference Management Algorithm for URLLC in Beyond 5G Networks. *IEEE Commun. Lett.*, 25(3), 995-999. doi: 10.1109/LCOMM.2020.3035111.

McMahan, B. & Ramage, D. (2017). Federated Learning: Collaborative Machine Learning without Centralized Training Data. Consulted at https://ai.googleblog.com/2017/04/federated-learning-collaborative.html.

Mei, W. & Zhang, R. (2020). UAV-Sensing-Assisted Cellular Interference Coordination: A Cognitive Radio Approach. *IEEE Wirel. Commun. Lett.*, 9(6), 799-803.

Mekki, K., Bajic, E., Chaxel, F. & Meyer, F. (2019). A comparative study of LPWAN technologies for large-scale IoT deployment. *ICT express*, 5(1), 1–7.

Meredith, J. M. (2017). *Study on enhanced LTE support for aerial vehicles*.

Mimoso, M. (2016). Operation and functioning of a self driving car and security vulnerabilities found in the firmware of the Bosch diagnostic dongle. Consulted at https://threatpost.com/patched-flaw-in-bosch-diagnostic-dongle-allowed-researchers-to-shut-off-engine/125061/.

Mozaffari, M., Saad, W., Bennis, M. & Debbah, M. (2017). Mobile unmanned aerial vehicles (UAVs) for energy-efficient internet of things communications. *IEEE Trans. Wireless Commun.*, 16(11), 7574–7589.

OrCAD. (2018). How Network Latency Affects the Future of Autonomous Vehicles? Consulted at https://www.orcad.com/jp/node/6591.

Ouyang, J., Che, Y., Xu, J. & Wu, K. (2018, Jul.). Throughput maximization for laser-powered UAV wireless communication systems. *2018 IEEE International Conference on Communications Workshops (ICC Workshops)*, pp. 1–6.

Pan, C., Ren, H., Wang, K., Elkashlan, M., Nallanathan, A., Wang, J. & Hanzo, L. (2020a). Intelligent Reflecting Surface Aided MIMO Broadcasting for Simultaneous Wireless Information and Power Transfer. *IEEE J. Sel. Areas Commun.*, 1-1.

Pan, C., Ren, H., Wang, K., Xu, W., Elkashlan, M., Nallanathan, A. & Hanzo, L. (2020b). Multicell MIMO Communications Relying on Intelligent Reflecting Surfaces. *IEEE Trans. Wireless Commun.*, 1-1.

Pan, C., Ren, H., Deng, Y., Elkashlan, M. & Nallanathan, A. (2019). Joint Blocklength and Location Optimization for URLLC-enabled UAV Relay Systems. *IEEE Commun. Lett.*

Park, J. & Popovski, P. (2017). Coverage and rate of downlink sequence transmissions with reliability guarantees. *IEEE Wireless Commun. Lett.*, 6(6), 722–725.

Parvez, I., Rahmati, A., Guvenc, I., Sarwat, A. & Dai, H. (2018). A survey on low latency towards 5G: RAN, core network and caching solutions. *IEEE Commun. Surveys Tuts.*, 20(4), 3098–3130.

Petrov, V., Gapeyenko, M., Moltchanov, D., Andreev, S. & Heath, R. W. (2020). Hover or Perch: Comparing Capacity of Airborne and Landed Millimeter-Wave UAV Cells. *IEEE Wirel. Commun. Lett.*, 1-1.

Polyanskiy, Y., Poor, H. V. & Verdú, S. (2010). Channel coding rate in the finite blocklength regime. *IEEE Trans. Inf. Theory*, 56(5), 2307.

Ranjha, A. & Kaddoum, G. (2020). Quasi-Optimization of Uplink Power for enabling Green URLLC in Mobile UAV-assisted IoT Networks: A Perturbation-based Approach. *IEEE Internet Things J.*, 1-1.

Ranjha, A. & Kaddoum, G. (2020a). Quasi-Optimization of Distance and Blocklength in URLLC aided Multi-Hop UAV Relay Links. *IEEE Wirel. Commun. Lett.*, 9(3), 306–310.

Ranjha, A. & Kaddoum, G. (2020b). Quasi-Optimization of Uplink Power for enabling Green URLLC in Mobile UAV-assisted IoT Networks: Perturbation-based Approach. *IEEE Internet Things J.*

Ranjha, A. & Kaddoum, G. (2020c). URLLC facilitated by mobile UAV relay and RIS: a joint design of passive beamforming, blocklength and UAV positioning. *IEEE Internet Things J.*

Rathore, M. M., Paul, A., Hong, W.-H., Seo, H., Awan, I. & Saeed, S. (2018). Exploiting IoT and big data analytics: Defining smart digital city using real-time urban data. *Sustainable cities and society*, 40, 600–610.

Ren, H., Pan, C., Deng, Y., Elkashlan, M. & Nallanathan, A. (2020a). Joint Pilot and Payload Power Allocation for Massive-MIMO-Enabled URLLC IIoT Networks. *IEEE J. Sel. Areas Commun.*, 38(5), 816-830.

Ren, H., Pan, C., Deng, Y., Elkashlan, M. & Nallanathan, A. (2020b). Resource Allocation for Secure URLLC in Mission-Critical IoT Scenarios (Early Access). *IEEE Trans. Commun.*, 1-1.

Ren, H., Pan, C., Wang, K., Deng, Y., Elkashlan, M. & Nallanathan, A. Achievable Data Rate for URLLC-Enabled UAV Systems with 3-D Channel Model. *IEEE Wirel. Commun. Lett.*

Ren, H., Pan, C., Deng, Y., Elkashlan, M. & Nallanathan, A. (2019, May). Resource Allocation for URLLC in 5G Mission-Critical IoT Networks. *IEEE ICC*, pp. 1–6.

Ren, H., Pan, C., Deng, Y., Elkashlan, M. & Nallanathan, A. (2020a). Joint Power and Blocklength Optimization for URLLC in a Factory Automation Scenario. *IEEE Trans. Wireless Commun.*, 19(3), 1786–1801.

Ren, H., Pan, C., Deng, Y., Elkashlan, M. & Nallanathan, A. (2020b). Joint Pilot and Payload Power Allocation for Massive-MIMO-Enabled URLLC IIoT Networks. *IEEE J. Sel. Areas Commun.*, 38(5), 816–830.

Ren, H., Pan, C., Wang, K., Xu, W., Elkashlan, M. & Nallanathan, A. (2020c). Joint Transmit Power and Placement Optimization for URLLC-enabled UAV Relay Systems. *IEEE Trans. Veh. Technol.*

Ren, H., Wang, K. & Pan, C. (2021). Intelligent Reflecting Surface-aided URLLC in a Factory Automation Scenario. *arXiv preprint arXiv:2103.09323*.

Russon, M. A. (2016a). Nokia and EE trial mobile base stations floating on drones to revolutionise rural 4G coverage. Consulted at https://www.ibtimes.co.uk/nokia-ee-trial-mobile-base-stations-floating-drones-revolutionise-rural-4g-coverage-1575795/.

Russon, M. A. (2016b). Nokia and EE trial for the mobile base stations floating on the drones to revolutionise the rural 4G coverage. Consulted at https://www.ibtimes.co.uk/nokia-ee-trial-mobile-base-stations-floating-drones-revolutionise-rural-4g-coverage-1575795/.

Salh, A., Audah, L., Shah, N. S. M., Alhammadi, A., Abdullah, Q., Kim, Y. H., Al-Gailani, S. A., Hamzah, S. A., Esmail, B. A. F. & Almohammedi, A. A. (2021). A Survey on Deep Learning for Ultra-Reliable and Low-Latency Communications Challenges on 6G Wireless Systems. *IEEE Access*, 9, 55098-55131. doi: 10.1109/ACCESS.2021.3069707.

Schulz, P., Matthe, M., Klessig, H., Simsek, M., Fettweis, G., Ansari, J., Ashraf, S. A., Almeroth, B., Voigt, J., Riedel, I., Puschmann, A., Mitschele-Thiel, A., Muller, M., Elste, T. & Windisch, M. (2017). Latency Critical IoT Applications in 5G: Perspective on the Design of Radio Interface and Network Architecture. *IEEE Commun. Mag.*, 55(2), 70-78.

Schulz, P., Matthe, M., Klessig, H., Simsek, M., Fettweis, G., Ansari, J., Ashraf, S. A., Almeroth, B., Voigt, J., Riedel, I. et al. (2017). Latency critical IoT applications in 5G: Perspective on the design of radio interface and network architecture. *IEEE Commun. Mag.*, 55(2), 70–78.

Sharma, S. K. & Wang, X. (2019). Towards massive machine type communications in ultra-dense cellular IoT networks: Current issues and machine learning-assisted solutions. *IEEE Commun. Surveys Tuts.*

Sharma, V., Sabatini, R. & Ramasamy, S. (2016). UAVs assisted delay optimization in heterogeneous wireless networks. *IEEE Commun. Lett.*, 20(12), 2526–2529.

She, C., Yang, C. & Quek, T. Q. (2017). Cross-layer optimization for ultra-reliable and low-latency radio access networks. *IEEE Trans. Wireless Commun.*, 17(1), 127–141.

She, C., Yang, C. & Quek, T. Q. (2018). Joint uplink and downlink resource configuration for ultra-reliable and low-latency communications. *IEEE Trans. Commun.*, 66(5), 2266–2280.

She, C., Liu, C., Quek, T. Q., Yang, C. & Li, Y. (2019). Ultra-reliable and low-latency communications in unmanned aerial vehicle communication systems. *IEEE Trans. Commun.*, 67(5), 3768–3781.

She, C., Sun, C., Gu, Z., Li, Y., Yang, C., Poor, H. V. & Vucetic, B. (2021a). A Tutorial on Ultrareliable and Low-Latency Communications in 6G: Integrating Domain Knowledge Into Deep Learning. *Proc. IEEE*, 109(3), 204-246. doi: 10.1109/JPROC.2021.3053601.

She, C., Sun, C., Gu, Z., Li, Y., Yang, C., Poor, H. V. & Vucetic, B. (2021b). A Tutorial on Ultrareliable and low-latency communications in 6G: integrating domain knowledge into deep learning. *Proc. IEEE*, 109(3), 204–246.

Sheng, Z., Mahapatra, C., Zhu, C. & Leung, V. C. (2015). Recent advances in industrial wireless sensor networks toward efficient management in IoT. *IEEE Access*, 3, 622–637.

Shiri, H., Park, J. & Bennis, M. (2020). Remote UAV Online Path Planning via Neural Network-Based Opportunistic Control. *IEEE Wirel. Commun. Lett.*, 9(6), 861-865.

Simsek, M., Aijaz, A., Dohler, M., Sachs, J. & Fettweis, G. (2016). 5G-enabled tactile internet. *IEEE J. Sel. Areas Commun.*, 34(3), 460–473.

Singer, S. (1999). Complexity Analysis of Nelder–Mead Search Iterations. 185-196.

Song, Q., Jin, S. & Zheng, F.-C. (2019). Completion time and energy consumption minimization for UAV-enabled multicasting. *IEEE Wireless Commun. Lett.*, 8(3), 821–824.

Spendley, W., Hext, G. R. & Himsworth, F. R. (1962). Sequential application of simplex designs in optimisation and evolutionary operation. *Technometrics*, 4(4), 441–461.

Strodthoff, N., Göktepe, B., Schierl, T., Hellge, C. & Samek, W. (2018). Enhanced machine learning techniques for early HARQ feedback prediction in 5G. *arXiv preprint arXiv:1807.10495*.

Sun, C., She, C., Yang, C., Quek, T. Q., Li, Y. & Vucetic, B. (2018a). Optimizing resource allocation in the short blocklength regime for ultra-reliable and low-latency communications. *IEEE Trans. Wireless Commun.*, 18(1), 402–415.

Sun, X., Yan, S., Yang, N., Ding, Z., Shen, C. & Zhong, Z. (2018b). Short-packet downlink transmission with non-orthogonal multiple access. *IEEE Trans. Wireless Commun.*, 17(7), 4550–4564.

Sun, Y., Xu, D., Ng, D. W. K., Dai, L. & Schober, R. (2019). Optimal 3D-trajectory design and resource allocation for solar-powered UAV communication systems. *IEEE Trans. Commun.*, 67(6), 4281–4298.

A. Ranjha and G. Kaddoum. (2020). URLLC Facilitated by Mobile UAV Relay and RIS: A Joint Design of Passive Beamforming, Blocklength and UAV Positioning. *IEEE Internet Things J.*, 1-1.

Uysal-Biyikoglu, E., Prabhakar, B. & El Gamal, A. (2002). Energy-efficient packet transmission over a wireless link. *IEEE/ACM Trans. Netw.*, 10(4), 487–499.

Wagner, D. (2018). Motion to Photon Latency in AR and VR. Consulted at https://medium.com/@DAQRI/motion-to-photon-latency-in-mobile-ar-and-vr-99f82c480926.

Wang, H., Wang, J., Ding, G., Wang, L., Tsiftsis, T. A. & Sharma, P. K. (2017). Resource allocation for energy harvesting-powered D2D communication underlaying UAV-assisted networks. *IEEE Trans. Green Commun. Netw.*, 2(1), 14–24.

Wang, K., Pan, C., Ren, H., Xu, W., Zhang, L. & Nallanathan, A. (2020a). Packet error probability and effective throughput for ultra-reliable and low-latency UAV communications. *IEEE Trans. Commun.*

Wang, L., Wang, K., Pan, C., Xu, W. & Aslam, N. (2020b). Joint Trajectory and Passive Beamforming Design for Intelligent Reflecting Surface-Aided UAV Communications: A Deep Reinforcement Learning Approach. *arXiv preprint arXiv:2007.08380*.

Wang, X. & Li, Z. (2013). Energy-efficient transmissions of bursty data packets with strict deadlines over time-varying wireless channels. *IEEE Trans. Wirel. Commun.*, 12(5), 2533–2543.

Wu, Q. & Zhang, R. (2020). Towards Smart and Reconfigurable Environment: Intelligent Reflecting Surface Aided Wireless Network. *IEEE Commun. Mag.*, 58(1), 106-112.

Wu, Q. & Zhang, R. (2019). Intelligent reflecting surface enhanced wireless network via joint active and passive beamforming. *IEEE Trans. Wireless Commun.*, 18(11), 5394–5409.

Xi, X., Cao, X., Yang, P., Chen, J., Quek, T. Q. & Wu, D. (2020). Network Resource Allocation for eMBB Payload and URLLC Control Information Communication Multiplexing in a Multi-UAV Relay Network. *IEEE Trans. Commun.*, 69(3), 1802–1817.

Xu, D., Sun, Y., Ng, D. W. K. & Schober, R. (2018). Robust resource allocation for UAV systems with UAV jittering and user location uncertainty. *2018 IEEE Globecom Workshops (GC Wkshps)*, pp. 1–6.

Xu, D., Sun, Y., Ng, D. W. K. & Schober, R. (2020). Multiuser MISO UAV communications in uncertain environments with no-fly zones: Robust trajectory and resource allocation design. *IEEE Trans. Commun.*, 68(5), 3153–3172.

Xu, L., Chen, M., Chen, M., Yang, Z., Chaccour, C., Saad, W. & Hong, C. S. (2021). Joint Location, Bandwidth and Power Optimization for THz-enabled UAV Communications. *IEEE Commun. Lett.*

Xu, S., Chang, T.-H., Lin, S.-C., Shen, C. & Zhu, G. (2016). Energy-efficient packet scheduling with finite blocklength codes: Convexity analysis and efficient algorithms. *IEEE Trans. Wirel. Commun.*, 15(8), 5527–5540.

Yan, C., Fu, L., Zhang, J. & Wang, J. (2019). A comprehensive survey on UAV communication channel modeling. *IEEE Access*, 7, 107769–107792.

Yang, Z., Pan, C., Shikh-Bahaei, M., Xu, W., Chen, M., Elkashlan, M. & Nallanathan, A. (2018). Joint altitude, beamwidth, location, and bandwidth optimization for uav-enabled communications. *IEEE Commun. Lett.*, 22(8), 1716–1719.

Ye, J., Zhang, C., Lei, H., Pan, G. & Ding, Z. (2018). Secure UAV-to-UAV systems with spatially random UAVs. *IEEE Wirel. Commun. Lett.*, 8(2), 564–567.

Yu, B., Guan, X. & Cai, Y. (2020). Joint Blocklength and Power Optimization for Half Duplex Unmanned Aerial Vehicle Relay System with Short Packet Communications. *Proc. IEEE WCSP*, pp. 981–986.

Yu, X., Xu, D. & Schober, R. (2019, Oct.). MISO Wireless Communication Systems via Intelligent Reflecting Surfaces : (Invited Paper). *IEEE/CIC Int. Conf. on Commun. in China (ICCC)*, pp. 735-740.

Yuan, W., Liu, C., Liu, F., Li, S. & Ng, D. W. K. (2020). Learning-based predictive beamforming for UAV communications with jittering. *IEEE Wirel. Commun. Lett.*, 1-1.

Zach. (2018a). Huawei connected aerial vehicle live demonstration at the Guangzhou grand world park. Consulted at https://www.huawei.com/en/industry-insights/outlook/mobile-broadband/xlabs/use-cases/mbbf2017-connected-aerial-vehicle-live/.

Zach. (2018b). Huawei. Connected Aerial Vehicle Live. Consulted at https://www.huawei.com/en/industry-insights/outlook/mobile-broadband/xlabs/use-cases/mbbf2017-connected-aerial-vehicle-live/.

Zafer, M. A. & Modiano, E. (2009). A calculus approach to energy-efficient data transmission with quality-of-service constraints. *IEEE/ACM Trans. Netw.*, 17(3), 898–911.

Zeng, Y. & Zhang, R. (2017). Energy-efficient UAV communication with trajectory optimization. *IEEE Trans. Wirel. Commun.*, 16(6), 3747–3760.

Zeng, Y., Zhang, R. & Lim, T. J. (2016a). Throughput maximization for UAV-enabled mobile relaying systems. *IEEE Trans. Wireless Commun.*, 64(12), 4983–4996.

Zeng, Y., Zhang, R. & Lim, T. J. (2016b). Wireless communications with unmanned aerial vehicles: Opportunities and challenges. *IEEE Commun. Mag.*, 54(5), 36–42.

Zeng, Y., Xu, X. & Zhang, R. (2018). Trajectory design for completion time minimization in UAV-enabled multicasting. *IEEE Trans. Wireless Commun.*, 17(4), 2233–2246.

Zhan, C. & Lai, H. (2019). Energy minimization in Internet-of-Things system based on rotary-wing UAV. *IEEE Wirel. Commun. Lett.*, 8(5), 1341–1344.

Zhang, G., Yan, H., Zeng, Y., Cui, M. & Liu, Y. (2018). Trajectory Optimization and Power Allocation for Multi-Hop UAV Relaying Communications. *IEEE Access*, 6, 48566–48576.

Zhang, J., Zeng, Y. & Zhang, R. (2019). Receding horizon optimization for energy-efficient UAV communication. *IEEE Wirel. Commun. Lett.*, 9(4), 490–494.

Zhao, M.-M., Shi, Q. & Zhao, M.-J. (2020). Efficiency maximization for UAV-enabled mobile relaying systems with laser charging. *IEEE Trans. Wirel. Commun.*, 19(5), 3257–3272.

Zhou, G., Pan, C., Ren, H., Wang, K., Di Renzo, M. & Nallanathan, A. (2020). Robust Beamforming Design for Intelligent Reflecting Surface Aided MISO Communication Systems. *IEEE Wirel. Commun. Lett.*, 1-1.

Zhou, G., Pan, C., Ren, H., Wang, K. & Nallanathan, A. (2020). A framework of robust transmission design for IRS-aided MISO communications with imperfect cascaded channels. *arXiv preprint arXiv:2001.07054*.

Zhu, Y., Zheng, G., Wong, K.-K. & Dagiuklas, T. (2020). Spectrum and Energy Efficiency in Dynamic UAV-Powered Millimeter Wave Networks. *IEEE Commun. Lett.*, 24(10), 2290–2294.